UNIVERSITAT
POLITÈCNICA
DE VALÈNCIA

PhD Thesis

Detailed modeling, simulation, and optimization of HVAC systems for electric buses in urban environments under real operating conditions

Author:

Joan Dídac Viana Fons

Supervisor:

Dr. Jorge Payá Herrero

València, December 2024

A mon pare, Dídac Viana Gómez,

a qui més m'haguera agradat que llegira aquesta tesi

Abstract

Urban buses are crucial for EU public transport, comprising more than half of all inland public transport journeys. Electric urban buses in the EU could reduce life-cycle emissions by 76% by 2030 compared to diesel. Although in 2024 only 1.4% of the EU's bus fleet is electric, all new urban buses must be zero-emission by 2035. This target highlights the pivotal role of electric buses in the transition to sustainable urban mobility.

The Heating, Ventilation, and Air Conditioning (HVAC) system is crucial for maintaining a safe and comfortable environment in vehicles but is also the primary auxiliary load, accounting for 1.5% of the global oil consumption. In urban electric buses, the driving range can be reduced by up to 50% in extreme weather. This emphasizes the need to model and optimize HVAC systems to reduce their energy impact and support the large-scale adoption of electric buses to mitigate urban pollution and emissions from urban transport.

Current literature reveals significant gaps in the development and application of detailed HVAC system models for electric buses operating in real-world urban environments. Specifically, there is a lack of comprehensive methodologies that integrate detailed models for accurate energy consumption assessments. Addressing these gaps is crucial to understanding energy flows and optimizing the use of resources while reducing costs and uncertainties.

In this thesis, a set of advanced models has been developed and integrated into a comprehensive global model to accurately simulate and optimize the HVAC system operation and energy consumption of

electric urban buses in real operating conditions.

The primary objective is to develop, validate and integrate a set of six advanced models. First, the spatial model creates a 3D city representation with buildings, trees, and a digital terrain model of the streets. The kinematic model then generates a year-long stochastic driving cycle using route data, street velocity limits, and traffic patterns. Next, the climate model calculates the external air temperature, humidity, visible horizon and radiation fluxes on all bus surfaces based on long-term climate data, the position and orientation of the bus and solar geometry. The thermal and HVAC coupled model computes, on the one hand, the thermal heat gains, node temperatures, moisture transfers, the thermal loads of mass and body nodes, and the latent loads of the indoor node using a system of ordinary differential equations, based on the bus optical and thermophysical properties, occupancy, air changes, auxiliary systems, and environmental conditions. On the other hand, the coupled model evaluates the HVAC operating mode and the operation points of each component of the equipment, their energy consumption and efficiency, and the outlet conditions of the air and condensate flowrate. Finally, the battery model estimates the overall bus energy consumption, including contributions from the motor, regenerative braking, HVAC, and other systems, as well as the impact of the battery efficiency.

The second objective is to implement this global model into a robust simulation tool, apply it to real urban bus routes and extract key insights from accurate disaggregated energy consumption results over extended periods. This includes the assessment of strategies to reduce the overall energy demand, analyzing the impact of different vehicle subsystems, supporting the optimization of the HVAC system components, and evaluating their impact on the total vehicle energy consumption.

The findings reveal the complexities of estimating the HVAC energy consumption due to numerous interacting factors, stochastic variables, and discrete control logic, requiring diverse models and extensive datasets. A model oversimplification can lead to significant errors, with direct solar irradiation inaccuracies exceeding 50% due to unaccounted

shading effects and notable variations in thermal gains across bus surfaces. The results highlight the critical role of transient thermal models, particularly when integrated with discrete control algorithms, and the significant impact of high occupancy stochasticity on the thermal load.

The simulations show that under representative conditions, the mean cooling demand on warm summer days is 12.1 kW, driven by solar and occupancy loads, while the heating demand on cold winter days averages 3.3 kW, mainly due to non-recirculated fresh air. The cooling mode is predominant (44.6% of the time), followed by ventilation (31.4%). The compressor consumes 69-75% of energy in summer and 58- 65% in mild months and winter. The HVAC consumption accounts for 5- 12% of the total bus energy use. This share is higher on higher frequency stops and lower speeds, reducing the driving range by 15-20% on warm days. Under extreme conditions, the HVAC consumption can rise by up to 165% on warm days and 181% on cold days. Insulation and optimized coatings can reduce the heating and cooling demand by 20- 31% while resizing the compressor by 25% offers cost savings without any efficiency loss.

Resumen

Los autobuses urbanos son fundamentales para el transporte público de la UE, representando más de la mitad de todos los viajes de transporte público terrestre. Los autobuses eléctricos urbanos en la UE podrían reducir las emisiones de ciclo de vida en un 76% para 2030 en comparación con los diésel. Aunque en 2024 solo el 1,4% de la flota de autobuses de la UE es eléctrica, todos los nuevos autobuses urbanos deberán ser de cero emisiones para 2035. Este objetivo resalta el papel fundamental de los autobuses eléctricos en la transición hacia una movilidad urbana sostenible.

El sistema de Calefacción, Ventilación y Aire Acondicionado (HVAC) es esencial para mantener un ambiente seguro y cómodo en los vehículos, pero también es la principal carga auxiliar, representando el 1,5% del consumo mundial de petróleo. En los autobuses eléctricos urbanos, la autonomía de conducción puede reducirse hasta un 50% en condiciones meteorológicas extremas. Esto resalta la necesidad de modelar y optimizar los sistemas HVAC para reducir su impacto energético y apoyar la adopción a gran escala de autobuses eléctricos para mitigar la contaminación urbana y las emisiones del transporte urbano.

La literatura actual revela importantes lagunas en el desarrollo y aplicación de modelos detallados de sistemas HVAC para autobuses eléctricos que operan en entornos urbanos reales. En concreto, existe una falta de metodologías que integren modelos detallados para evaluaciones precisas del consumo energético. Abordar estas lagunas es crucial para comprender los flujos de energía y optimizar el uso de los recursos, al tiempo que se reducen los costes y las incertidumbres.

En esta tesis, se ha desarrollado e integrado un conjunto de modelos avanzados en un modelo global completo para simular y optimizar con precisión la operación del sistema HVAC y el consumo de energía de los autobuses eléctricos urbanos en condiciones reales de operación.

El objetivo principal es desarrollar, validar e integrar un conjunto de seis modelos avanzados. Primero, el modelo espacial crea una representación 3D de la ciudad con edificios, árboles y un modelo digital del terreno de las calles. A continuación, el modelo cinemático genera un ciclo de conducción estocástico de un año utilizando datos de rutas, límites de velocidad en las calles y patrones de tráfico. Luego, el modelo climático calcula la temperatura del aire exterior, la humedad, el horizonte visible y los flujos de radiación en todas las superficies del autobús, basándose en datos climáticos a largo plazo, la posición y orientación del autobús y la geometría solar. El modelo térmico y acoplado con el HVAC calcula, por un lado, las ganancias de calor, las temperaturas de los nodos, las transferencias de humedad, las cargas térmicas de los nodos de masas internas y de la carcasa, y las cargas latentes del nodo interior utilizando un sistema de ecuaciones diferenciales ordinarias, basado en las propiedades ópticas y termofísicas del autobús, la ocupación, los cambios de aire, los sistemas auxiliares y las condiciones ambientales. Por otro lado, el modelo acoplado evalúa el modo de operación del HVAC y los puntos de operación de cada componente del equipo, su consumo de energía y eficiencia, y las condiciones de salida del aire y del flujo de condensado. Finalmente, el modelo de batería estima el consumo total de energía del autobús, incluyendo las contribuciones del motor, la frenada regenerativa, el HVAC y otros sistemas, así como el impacto de la eficiencia de la batería.

El segundo objetivo es implementar este modelo global en una herramienta de simulación robusta, aplicarla a rutas de autobuses urbanos reales y extraer conclusiones clave a partir de resultados precisos de consumo de energía desagregado durante períodos prolongados. Esto incluye la evaluación de estrategias para reducir la demanda total de energía, analizar el impacto de los diferentes subsistemas del vehículo, apoyar la optimización de los componentes del sistema HVAC y evaluar

su impacto en el consumo total de energía del vehículo.

Los hallazgos revelan las complejidades de estimar el consumo de energía del HVAC debido a numerosos factores interrelacionados, variables estocásticas y lógica de control discreta, lo que requiere modelos diversos y grandes conjuntos de datos. Una simplificación excesiva del modelo puede llevar a errores significativos, con imprecisiones en la irradiación solar directa superiores al 50% si no se consideran los efectos del sombreado y variaciones notables en las ganancias térmicas en las superficies del autobús. Los resultados destacan el papel crítico de los modelos térmicos transitorios, especialmente cuando se integran con algoritmos de control discreto, y el impacto significativo de la estocasticidad en la alta ocupación sobre la carga térmica.

Las simulaciones muestran que, en condiciones representativas, la demanda media de aire acondicionado en días cálidos de verano es de 12,1 kW, debido especialmente a las cargas solares y de ocupación, mientras que la demanda de calefacción en días fríos de invierno es de 3,3 kW, principalmente debido al aire fresco no recirculado. El modo de aire acondicionado es predominante (44,6% del tiempo), seguido por la ventilación (31,4%). El compresor consume entre el 69 y el 75% de la energía en verano y entre el 58 y el 65% en meses templados y en invierno. El consumo de HVAC representa entre el 5 y el 12% del uso total de energía del autobús. Esta proporción es mayor en paradas más frecuentes y a velocidades más bajas, reduciendo la autonomía de conducción en un 15-20% en días cálidos. En condiciones extremas, el consumo de HVAC puede aumentar hasta un 165% en días cálidos y un 181% en días fríos. El aislamiento y los recubrimientos optimizados pueden reducir la demanda de calefacción y aire acondicionado en un 20-31%, mientras que reducir la capacidad del compresor en un 25% ofrece ahorros de costes sin pérdida de eficiencia.

Resum

Els autobusos urbans són fonamentals per al transport públic de la UE, representant més de la meitat de tots els viatges de transport públic terrestre. Els autobusos elèctrics urbans a la UE podrien reduir les emissions de cicle de vida en un 76% per a 2030 en comparació amb els dièsel. Encara que en 2024 només l'1,4% de la flota d'autobusos de la UE és elèctrica, tots els nous autobusos urbans hauran de ser de zero emissions per a 2035. Aquest objectiu ressalta el paper fonamental dels autobusos elèctrics en la transició cap a una mobilitat urbana sostenible.

El sistema de Calefacció, Ventilació i Aire condicionat (HVAC) és essencial per a mantindre un ambient segur i còmode en els vehicles, però també és la principal càrrega auxiliar, representant l'1,5% del consum mundial de petroli. En els autobusos elèctrics urbans, l'autonomia de conducció pot reduir-se fins a un 50% en condicions meteorològiques extremes. Això ressalta la necessitat de modelar i optimitzar els sistemes HVAC per a reduir el seu impacte energètic i donar suport a l'adopció a gran escala d'autobusos elèctrics per a mitigar la contaminació urbana i les emissions del transport urbà.

La literatura actual revela importants llacunes en el desenvolupament i aplicació de models detallats de sistemes HVAC per a autobusos elèctrics que operen en entorns urbans reals. En concret, existeix una falta de metodologies que integren models detallats per a avaluacions precises del consum energètic. Abordar aquestes llacunes és crucial per a comprendre els fluxos d'energia i optimitzar l'ús dels recursos, al mateix temps que es redueixen els costos i les incerteses.

En aquesta tesi, s'ha desenvolupat i integrat un conjunt de models

avançats en un model global complet per a simular i optimitzar amb precisió l'operació del sistema HVAC i el consum d'energia dels autobusos elèctrics urbans en condicions reals d'operació.

L'objectiu principal és desenvolupar, validar i integrar un conjunt de sis models avançats. Primer, el model espacial crea una representació 3D de la ciutat amb edificis, arbres i un model digital del terreny dels carrers. A continuació, el model cinemàtic genera un cicle de conducció estocàstic d'un any utilitzant dades de rutes, límits de velocitat als carrers i patrons de trànsit. Després, el model climàtic calcula la temperatura de l'aire exterior, la humitat, l'horitzó visible i els fluxos de radiació en totes les superfícies de l'autobús, basant-se en dades climàtiques a llarg termini, la posició i orientació de l'autobús i la geometria solar. El model tèrmic i acoblat amb el HVAC calcula, d'una banda, els guanys de calor, les temperatures dels nodes, les transferències d'humitat, les càrregues tèrmiques dels nodes de masses internes i de la carcassa, i les càrregues latents del node interior utilitzant un sistema d'equacions diferencials ordinàries, basat en les propietats òptiques i termofísiques de l'autobús, l'ocupació, els bescanvis d'aire, els sistemes auxiliars i les condicions ambientals. D'altra banda, el model acoblat avalua el mode d'operació del HVAC i els punts d'operació de cada component de l'equip, el seu consum d'energia i eficiència, i les condicions d'eixida de l'aire i del flux de condensat. Finalment, el model de bateria estima el consum total d'energia de l'autobús, incloent-hi les contribucions del motor, la frenada regenerativa, el HVAC i altres sistemes, així com l'impacte de l'eficiència de la bateria.

El segon objectiu és implementar aquest model global en una eina de simulació robusta, aplicar-la a rutes d'autobusos urbans reals i extraure conclusions clau a partir de resultats precisos de consum d'energia desagregat durant períodes prolongats. Això inclou l'avaluació d'estratègies per a reduir la demanda total d'energia, analitzar l'impacte dels diferents subsistemes del vehicle, donar suport a l'optimització dels components del sistema HVAC i avaluar el seu impacte en el consum total d'energia del vehicle.

Els resultats revelen les complexitats d'estimar el consum d'energia del HVAC a causa de nombrosos factors interrelacionats, variables estocàstiques i lògica de control discreta, la qual cosa requereix models diversos i grans conjunts de dades. Una simplificació excessiva del model pot portar a errors significatius, amb imprecisions en la irradiació solar directa superiors al 50% si no es consideren els efectes de l'ombreig i variacions notables en els guanys tèrmics en les superfícies de l'autobús. Els resultats destaquen el paper crític dels models tèrmics transitoris, especialment quan s'integren amb algorismes de control discret, i l'impacte significatiu de la estocasticitat en l'alta ocupació sobre la càrrega tèrmica.

Les simulacions mostren que, en condicions representatives, la demanda mitjana d'aire condicionat en dies càlids d'estiu és de 12,1 kW, degut especialment a les càrregues solars i d'ocupació, mentre que la demanda de calefacció en dies freds d'hivern és de 3,3 kW, principalment a causa de l'aire fresc no recirculat. El mode d'aire condicionat és predominant (44,6% del temps), seguit per la ventilació (31,4%). El compressor consumeix entre el 69 i el 75% de l'energia a l'estiu i entre el 58 i el 65% en mesos temperats i a l'hivern. El consum de HVAC representa entre el 5 i el 12% de l'ús total d'energia de l'autobús. Aquesta proporció és major en parades més freqüents i a velocitats més baixes, reduint l'autonomia de conducció en un 15-20% en dies càlids. En condicions extremes, el consum de HVAC pot augmentar fins a un 165% en dies càlids i un 181% en dies freds. L'aïllament i els recobriments optimitzats poden reduir la demanda de calefacció i aire condicionat en un 20-31%, mentre que reduir la capacitat del compressor en un 25% ofereix estalvis de costos sense pèrdua d'eficiència.

Acknowledgments

I would like to express my sincere gratitude to all those who supported and guided me throughout this doctoral thesis.

Firstly, I am deeply thankful to my advisor, Professor Jorge Payá, for his continuous support, patience, and encouragement. His expertise and commitment were invaluable in helping me shape this thesis to its full potential.

To the members of the Energy Engineering University Research Institute (IIE), thank you for sharing your knowledge and commitment to academic excellence. I am also grateful to the UPV Urban Energy Transition Chair for broadening the mission and impact of my research.

I am profoundly grateful to the team of ImpactE for fostering my professional and personal growth over these past years. Thank you for allowing me to work alongside you on this meaningful project.

I am especially thankful to Aurora for her companionship and for bringing balance to my life. She made this journey possible, and this thesis belongs as much to her as it does to me.

I am deeply grateful to my family for their patience and unwavering support. Together, we have a team capable of facing any challenge.

Finally, to my friends, both near and far, thank you for your continuous encouragement. I have always felt your support.

This thesis reflects the contributions of many, and I am honored to share it with everyone involved. Thank you.

Contents

List of Figures

List of Tables

Chapter 1

Introduction

1.1 Motivation

1.1.1 Environmental impact and mitigation measures of transport in the EU

Transport is a basic need which helps integrate people into society and is recognized as one of the essential services under the European Pillar of Social Rights [1]. Transport systems have economic, environmental, and social impacts on the communities.

The transport sector represents the largest energy-consuming end-use sector in the European Union (EU), with more than a quarter of the total energy consumption and greenhouse gas emissions [2]. While other sectors have already lowered their emissions by 32% since 1990, the EU's transport emissions have increased by 33% and continue relying on oil products in more than 93% of the final energy [3].

Road transport is responsible for more than three-quarters of the total EU's transport greenhouse gas emissions [4] and is is one of the main contributors to air and noise pollution. This is especially important in urban areas, where over 70% of EU citizens live [5]. Air pollution is a significant health concern for European citizens. Currently, 96% of the urban population is exposed to air pollution levels above the recommendations of the World Health Organization, and around 300,000 people die every year due to air pollution in Europe [6]. Furthermore,

at least 20% of the urban population in the EU is exposed to levels of noise pollution which are harmful to health, and, in many cities, this percentage can reach 50% of the urban population [7]. Summing up, the environmental costs of road transport (including climate change, air pollution, noise, well-to-tank and habitat damage) are estimated at 270 billion euros per year in the EU, which corresponds to more than 1.8% of its GDP. This number increases up to 820 billion euros per year if accidents and congestion are included as external costs [8].

European citizens expect solutions clean mobility solutions to reduce congestion, gas emissions, noise and air pollution [9, 10]. The projected demand for passenger and goods could more than double by 2050, nearby increasing its negative impacts [11]. Paris commitments requires zero carbon transport before 2050, which is theoretically feasible but ambitious new policies and substantial investments need to be adopted [12].

In this context, the European Green Deal has committed to reducing the emissions by at least 55% before 2030. The objective is to become the first climate-neutral and zero-pollution continent by 2050 [13, 14]. The EU is focusing on further emission and pollution reductions in the transport sector, introducing new policy instruments for road transport. Within this scope, the two most important lines of action are, on the one hand, transforming the current transportation model based on personal motor vehicles to one focused on active mobility and clean public transport. On the other hand, it is important to reduce the impacts associated with private vehicles [15]. From 2027 onward, greenhouse gas emissions of the road transport sector will be covered by the new emission trading system [16] and all new cars and vans registered in Europe will be zero-emission by 2035 [17].

1.1.2 Situation and perspectives of urban electric buses in the EU

The buses belong to the heavy-duty vehicle sector, which are responsible for around 25% of total road emissions, despite constituting

only 2% of the vehicle fleet. To address this imbalance, the EU has established strict commitments to reduce emissions in this sector [18].

Currently, the EU has strengthened the regulation on the CO_2 emissions for new heavy-duty vehicles, requiring manufacturers to reduce the CO_2 emissions of new vehicles own to 30-45% by 2030, to 65% by 2035 and to 90% by 2040 [19].

Urban buses represent the most common form of public transportation in the EU, accounting for over half of all inland public transport journeys[20]. They also represent the most cost-efficient and flexible form of public transportation, requiring minimal investment to establish new routes or lines, and have a significant potential to reduce traffic congestion [21].

Urban buses contribute approximately to 3% of the total CO_2 emissions in the EU and are a major source of air pollution in urban environments [22]. Currently, only 2% of buses are battery-powered electric vehicles [23]. Nevertheless, the decarbonization of urban transport has already started and is expected to accelerate [24]. Market data supports this tendency, as more than one in three newly-registered urban buses in the EU was fully electric in 2023 [25].

Moreover, European regulations reinforce and aim to accelerate this trend by setting that all new urban buses registered in EU must be zero-emission by 2035, with a 90% emissions reduction target for new urban buses by 2030 [19].

Furthermore, battery-powered electric buses are the most effective solution for achieving net-zero emissions in urban environments [26, 27, 28]. Specifically, a battery electric urban bus in the EU could reduce life-cycle emissions by 76% by 2030, while a fuel-cell bus could reduce them by 57% [29]. These differences are mainly driven by the emissions associated with the fuel or electricity mix employed and the engine performance of each powertrain.

In light of the discussed points, it is evident that urban electric buses will play a pivotal role in transforming urban public transport in the

EU, representing a critical step towards sustainable, efficient, and clean urban mobility.

1.1.3 General challenges in the large-scale adoption of electrical buses

Despite the numerous advantages of electric buses, significant barriers still hinder their large-scale adoption. Addressing these challenges requires a dual approach to planning, encompassing both long-term strategic and operational approaches [30].

First, high financing costs present a substantial barrier, primarily driven by the expenses associated with batteries and the necessary charging infrastructure [31]. Although costs vary significantly across different regions, the total lifecycle cost of electric urban buses is generally comparable to that of internal combustion engines [32]. When considering externalized costs, such as environmental impacts, electric buses become considerably more advantageous. These challenges can be further addressed through policy support and public-private partnerships that formalize and implement long-term strategic frameworks to finance the life cycle of fleets and infrastructure, ensuring regulatory compliance and enhancing public accessibility and attractiveness [30].

Second, the lower operational flexibility of electric buses due to their limited driving range and related infrastructure presents additional challenges. Comprehensive operational planning is required to address these issues, including optimized routing and scheduling as well as electric grid stability [33]. Such planning is essential to ensure service and grid quality, reliability, and safety, thereby maximizing the benefits of the transition to electric buses, including increased energy efficiency and significant reductions in urban congestion, pollution, and emissions [34].

In both strategic and operational planning, bus energy consumption is a central parameter.

On the one hand, energy consumption is closely tied to the infras-

tructure requirements and battery sizing of the electric bus fleet. Proper battery sizing is a critical factor for operators, needing appropriate size to meet all energy needs without being excessively large and expensive. The bus energy demand influences the scale and distribution of charging infrastructure, the capacity of electrical grids, and the need for upgrades to existing facilities. Furthermore, energy consumption plays a vital role in environmental sustainability, which is a key driver behind the adoption of electric buses and their public support and acceptability. Lower energy consumption directly leads to with reduced costs, emissions, and pollution.

On the other hand, the bus energy consumption directly influences the operational efficiency of electric buses and charging infrastructure by determining their driving range and charging needs. Energy consumption is critical for the planning and optimization of routes and charging strategies to ensure the reliability of bus schedules and grid loads. Additionally, it helps reduce costs based on energy price fluctuations.

Simulation tools based on accurate and comprehensive models of electric buses are essential. These models can contribute to overcome the barriers by:

- Addressing knowledge gaps: Comprehensive models enable a deeper understanding of the electric bus performance, lifecycle costs, and externalized costs, which can act as an institutional and social barrier, helping in the definition, formalization, and dissemination of effective policies and action plans.
- Establishing specific environmental conditions: Bus manufacturers often provide performance range estimates under specific conditions, but real-world operational ranges are influenced by factors such as speed profiles, elevation changes, and solar radiation and temperature variations. These uncertainties can lead to operational issues, such as reduced battery life, poor service quality, and high electricity peak loads. Accurate modeling of these

dynamic factors in real operating conditions is therefore critical, especially in urban contexts where traffic and microclimate conditions, stop frequency, and passenger load variations significantly impact energy consumption.

- Optimizing infrastructure and battery sizing: Characterizing the energy demand under real operating conditions enables the correct sizing of the infrastructure and battery, making the transition to electric buses more feasible and cost-effective. Additionally, the optimal sizing improves the energy efficiency of bus systems by working within an appropriate operating range and reducing overall energy demands.

- Aligning the operational planning and infrastructure: Better predictions of energy demand can enhance the reliability of bus schedules and reduce the risk of overloads on the electric grid by aligning the range capabilities of electric buses with the availability, placement, and timing of charging.

- Providing strategic and decision-making framework: Accurate models enable the prioritization of investments, estimation of associated operational costs, and evaluation of new strategies or policies by supporting informed and cost-effective decision-making.

- Enabling subsystems optimization and integration of new solutions: These models facilitate detailed analysis of each subsystem's contribution, supporting optimization and the evaluation of new solutions within the overall system.

In conclusion, detailed and comprehensive energy consumption models help address the challenges in electric bus deployment, ensuring successful adoption by addressing knowledge gaps, minimizing costs and risks, optimizing resources, and reducing uncertainties.

1.1.4 Contribution and importance of HVAC in the field

Mobile Heating, Ventilation, and Air Conditioning (HVAC) systems are the main auxiliary energy load in vehicles [35], especially in urban contexts [36], and particularly in buses. The latter need larger and more energy-consuming systems, due to their design characteristics, such as higher volume, weight or transparent areas, and operation characteristics, as they run on fixed routes, move at slower speeds, and make frequent stops with high occupancy levels [37].

Furthermore, HVAC systems contribute to the most significant uncertainty in the overall energy consumption [38], due to their highly sensitive dependency to the different operating conditions and their nonlinear response.

This uncertainty is especially critical in electric buses, where the driving range is a significant operational challenge, since the HVAC also provides heating. Electrical motors do not generate sufficient exhaust heat whereas in internal combustion engines they can fulfill the entire heating demands. This results in a significant reduction in the range of electric buses by up to 50% in cold winter and warm summer days [37].

The primary function of HVAC systems is to maintain a healthy, safe, and comfortable thermal environment in the vehicle cabin by compensating for the thermal loads and ensuring a proper ventilation for fresh air and humidity control.

While these functions are essential to provide high-quality service, they currently have a substantial negative impact. HVAC systems consume 1.8 million barrels of oil equivalent per day, which represent more than 1.5% of the current global oil consumption [39]. Furthermore, they are responsible for more than 1% of the global energy-related CO_2 emissions, a combination of energy consumption (70%) and refrigerant leakage (30%). With no further policy action, energy use and emissions may almost triple by 2050.

This energy-intensive operation highlights the importance of optimizing HVAC systems, including refrigerant modifications and energy

efficiency improvements, to reduce their environmental impact.

According to the American Society of Heating, Refrigerating, and Air-Conditioning Engineers (ASHRAE), thermal comfort is defined as a "condition of mind that expresses satisfaction with the thermal environment" [40]. This subjective and complex concept depends on both personal and environmental factors. In line with this, the European Standard EN-14750 [41], pertaining to air conditioning for urban and suburban rolling stock, is the applicable standard in the EU, which establishes the thermal comfort specifications and HVAC requirements for urban bus cabins.

Current standards for HVAC system design are based on broad climate zones, leading to frequent oversizing and missed opportunities for optimization, as the lifecycle of most buses occurs in a single city. Energy models that simulate the real operating conditions in specific urban areas can help capitalize these opportunities by optimizing HVAC systems in this complex environment.

1.2 Background and research context

1.2.1 Overview of HVAC systems in urban electric buses

In internal combustion engine vehicles, the cabin thermal management is typically achieved with a vapor-compression system for cooling. For heating, the waste heat of the engine is used. However, the relatively low waste heat production by electric motors presents challenges for the cabin heating in electric vehicles. The most popular solution in electric vehicles is the use of a dedicated heater, such as Positive Temperature Coefficient (PTC). However, this solution, significantly reduces the driving range due to its high electricity demand, specially in electric buses, where the thermal demand is much higher than in light-duty electric vehicles.

The reversible vapor compression heat pump system is the most promising and cost-effective technology for electric buses, and provides both cooling and heating capacities with a higher energy efficiency. These systems feature an inverter-driven compressor and a four-way valve which can reverse the refrigerant flow direction, enabling the switch between heating and cooling modes. The Coefficient Of Performance (COP) is greater than one in most conditions.

The energy management of these systems consists in adjusting the speed of compressor and fans, effectively balancing the cabin's heat loads to maintain thermal comfort while minimizing the electricity consumption. Additionally, the control system regulates the ratio of recirculated air, ensuring a minimum fresh air flowrate per passenger.

In recent years, continuous innovations have been explored to boost the performance of these systems, and reduce their environmental impact.

For instance, Economized Vapor Injection (EVI) has been applied to improve the heating capacity and performance at low ambient temperatures [42].

Using two-phase ejector as an expansion valve can also improve the

system performance in cooling mode, while reducing the heat exchangers sizing [43].

The performance can be further improved by means of waste heat recovery from the electric motor, controller, inverters and batteries [44, 45] or from the cabin exhaust air [46]. The use of thermal energy storage based on Phase Change Materials (PCM) has also been studied to provide both heating and cooling with high energy density [47].

With respect to the refrigerant, R1234yf is considered as an interim option to replace R134a in the existing automotive HVAC systems. The thermophysical properties are similar, with a significantly lower Global Warming Potential (GWP). However, the environmental impacts of R1234yf and other Hydrofluoroolefin (HFO) become significant due to the formation of trifluoroacetic acid (TFA), which will affect the aquatic systems [48]. The hydrocarbon refrigerants are reported as promising alternatives to R134a due to its lower GWP and improved energy efficiency due to its good thermophysical properties compared to R134a. Among them, R290 can be good replacement for R134a, showing a better performance for both cooling and heating [49]. However, compressor modifications are required and secondary loop configurations are recommended. R744 is a feasible alternative in cold climates, offering better heating performance at low temperatures but lower cooling performance at high temperatures [50].

Also, other non-vapor compression systems have been explored, including magnetic heat pump systems [51] and thermoelectric systems [52].

However, most of these solutions are currently in research, development and testing stage in the automotive industry.

In this thesis, a hybrid system has been used to model the HVAC, which integrates a standard reversible vapor compression heat pump, and supplementary PTC heaters, used to support the heating capacity under very low ambient temperatures.

1.2.2 Main approaches to estimate the energy consumption of HVAC systems in urban electric buses

Calculating the energy consumption of HVAC systems of electric buses under real operating conditions can only be performed with a broader analysis that includes the examination of the main influencing factors. These factors are related with the cabin temperature, and include the outdoor temperature and humidity, solar radiation, air exchanges, long-wave radiation exchanges, bus geometry, thermophysical and optical properties, occupancy variation, and vehicle velocity.

To accurately model these elements in the complex and dynamic context of urban bus services, it is necessary to develop extensive models. To know the impact on the battery autonomy, the model should also calculate the consumption of the motor and all auxiliaries.

Current research on electric bus energy consumption are generally divided into three methodological approaches: empirical methods, data-driven methods and physical methods [53].

First, the empirical methods often assume the electric bus energy consumption per distance as a constant [54, 55]. This simplifying estimation helps focus on other complex areas such as large-scale bus scheduling or routing network optimization. However, these energy consumption estimates vary widely across different studies (1.24–2.48 kWh/km [54], 1.20–2.90 kWh/km [55]) and cannot be easily extrapolated to other conditions. This is because these estimations do not account for the specific operational conditions that can significantly influence the energy consumption.

Second, the data-driven methods, such as regression [56, 57], machine learning [53, 58, 59], or deep learning models [57, 60, 61], use algorithms to predict the energy consumption based on large volumes of experimental data, taking into account a variety of operational factors. On the one hand, regression-based models explicitly quantify cause-effect relationships, making them useful to develop control algorithms. However, they often show a poor fit due to the high dimensionality

and non-linearity of the problem. On the other hand, AI-based models can accurately capture these non-linear relationships and achieve a relatively high accuracy. However, the lack of explicit functional relationships between the influencing factors limits the understanding of these interactions and hinders the development of robust control algorithms. Nevertheless, large amounts of experimental or real-world operational data are needed to make the models representative and applicable to the wide range of potential operating conditions. This requires extensive data collection campaigns and subsequent data processing. Even with such efforts, it remains challenging to ensure that the models are truly representative, as they may not account for a full range of weather conditions.

Third, the physical-based methods [62, 63, 64, 65] calculate the instantaneous energy consumption using physical models and real-world parameters of the processes and components involved in the system. While this approach requires considerable effort in model development, it offers a comprehensible assessment by explicitly and thoroughly establishing cause-effect relationships between operating conditions and energy consumption. This allows for accurate predictions even in scenarios lacking prior data, thereby enhancing accuracy. Additionally, these models can provide valuable data to feed into data-driven methods to aid in their modeling. However, some issues are still challenging due to their stochastic nature (e.g., traffic, occupancy, temperature) or technical complexity (e.g., lack of data, shading, interaction of multiple physical systems). This often requires simplifications, which can sometimes be excessive.

In this thesis, a physical-based approach is used to develop a set of advanced models and integrate them into a comprehensive global model that enables the simulation of the energy consumed by HVAC systems in real operating conditions for an electric bus and its impact on the overall energy consumption requires the following submodels:

- A 3D model of the urban area, including buildings, trees, and streets, to establish shading, skyline, ground height, and slope at

every point along the route.

- A kinematic model, incorporating the speed profile of the actual urban route, consistent with the bus schedule and stochastic traffic conditions, to determine variables such as bus orientation, elapsed time, distance traveled, velocity, and acceleration at each discretized point along the route during the simulation period.
- A climate model, including the skyline and multicomponent radiation on all vehicle surfaces, to obtain temperature conditions, humidity, infrared sky irradiance, solar irradiance, and the skyline profile, enabling the assessment of long-wave and solar radiation at each bus surface at any position and time step of the driving route.
- A transient thermal model of the vehicle cabin, with multiple bus and external nodes, including heat gains, thermal loads, and moisture transfers at each time step.
- An HVAC model to evaluate the operating mode and points of each component, their energy consumption and efficiency, and the outlet conditions of air and condensate flowrate at each point along the route.
- A battery model of the bus to obtain overall energy consumption throughout the route, including motor, regenerative braking, HVAC, battery thermal management system, pneumatic, hydraulic, and auxiliary electrical systems, as well as the impact of battery efficiency.

As can be inferred from the previous list, calculating the HVAC consumption requires a comprehensible modeling which reproduces the main physical processes in a complex urban environment.

1.2.3 Detailed review of the modeling techniques employed in the present thesis

A comprehensive review has been performed within physical models. A special focus has been held on models which evaluate the energy consumption by HVAC systems in real operating conditions for an electric urban bus.

GIS model

Spatial models are crucial for the development of large-scale, high-resolution energy models in real-world contexts, particularly in extensive and heterogeneous environments such as urban areas [66]. These models provide not only real-world data but also enhance the scalability of energy models. This scalability is enabled by the availability of high-quality open data. When effectively abstracted (e.g., through discretization into points and systematic tabulation). The latter provides the essential inputs for the application of large-scale energy modeling [67].

In urban contexts, this approach involves shadow modeling, view factors, and street slopes, through geometric analysis. Traditional design-oriented software provides precise spatial definitions. However, this is computationally intensive and constrained to smaller scales due to the limited availability of extensive 3D-CAD data. For larger areas, Geographic Information Systems (GIS) models are commonly employed due to their flexibility, scalability, and the availability of standardized open data [68]. The GIS-based energy model enables the integration, analysis, interpretation, and visualization of detailed spatio-temporal multi-variable data at urban scale [69].

Most urban mobility studies use GIS due to the integration of city spatial transport network models with traffic, environmental, socioeconomic, and demographic data [70, 71]. This integration helps with the design, planning and management of transport networks and supports decision-making processes and policy development and evaluation [72, 73].

In energy studies related to mobility, researchers often use the spatial transport network model [74, 62, 75]. Some authors have employed spatial models to establish their kinematic models [76] and to determine the street slope [64, 62, 75, 77], which is a crucial input for the powertrain model. However, there is a notable lack of urban mobility studies which employ spatial models of the city (such as buildings or trees) to reproduce and analyze specific thermal conditions within this complex environment.

A 3D vector-based GIS model is proposed to accurately represent the urban environment, including buildings, trees, and streets separately. The buildings are created using a 3D vector model based on cadastral and LiDAR altimetry data [78]. The streets are characterized by a 2-meter resolution raster-based altimetric model or DTM, created from LiDAR ground points using spatial interpolation through the Delaunay triangulation method [79, 80]. Additionally, trees are depicted using a 3D vector model, providing the height and segmented canopy for each tree [81]. This city model allows to obtain the skyline or visible horizon of an specific point by means of a geometric analysis, determining the height, slope and orientation of any surface, such as streets. This is essential to predict whether a point is shaded or not at a given time.

Kinematic model

To accurately estimate the bus energy consumption in real-world conditions, a kinematic model representing the speed profile or driving cycle is essential [53]. While many authors use standard driving cycles [82, 83], models using synthetic driving cycles derived from real-world operations show significantly better results [58, 84, 85]. Recently, several methods and approaches have been developed to create synthetic driving cycles. Among these, the models based on stochastic techniques are the most suitable due to the non-deterministic nature of real-world traffic [58, 85]. Within the stochastic techniques, a distinction can be made between those relying on high-frequency data obtained from real-time data, which is not readily available and involves high collection costs [77, 86, 62, 87], and those using low-resolution data [75, 64, 76].

Based on this review, a driving route and a kinematic model have been developed for a year-long simulation based on the commercial schedule of the bus network. The model generates a synthetic driving cycle that represents the stochastic behavior of kinematic variables such as time, distance, velocity, and acceleration in real-world traffic conditions at each point along the route. The algorithm incorporates the generation of weighted stochastic stop points, known as traffic stops, using low-resolution open data (GTFS) and a mixed-integer nonlinear programming (MINLP) formulation is employed.

Climate model

To accurately estimate the urban bus energy consumption and to support in strategic and operational planning, it is crucial to work with a year representative series of real climate conditions. However, most studies only apply the models under specific fixed conditions [82, 64, 83] or in short periods [76, 77, 62, 86, 75]. Other researchers use annual periods [74] or representative year data [87] to describe the climate conditions. However, they do not account for the specific radiative and shading conditions of the urban environment, nor do they provide a detailed differentiation for each surface of the bus.

A year-long time series of hourly climate conditions has been developed for each point along the route and each side of the vehicle. Outdoor psychometric variables derived from Typical Meteorological Year (TMY) data are included. The model includes indoor temperature regulation, sky temperature calculation, and detailed skyline profiles to account for the urban impact on the radiation heat gain. The model computes direct, diffuse, and reflected irradiance on all bus surfaces, considering factors such as solar geometry, city surface reflectance, bus orientation, shadowing and view factors. This comprehensive approach enables an accurate modeling of heat transfer and energy consumption in urban bus operating conditions, accounting for real-world climate factors and providing a robust foundation for heat transfer analysis in electric urban buses.

Thermal model

To accurately estimate the thermal demand and the operating conditions of the HVAC, dynamic cabin thermal models are essential. Cabin thermal models have been extensively studied using several approaches. Advanced Computational Fluid Dynamics (CFD) techniques are employed to analyze thermal comfort and spatial temperature distribution within vehicle cabins [88, 89, 90]. Lumped parameter models offer a balance between accuracy and computational efficiency [91] and can be integrated with multiphysics software. However, many studies overlook the vehicle's driving profile and its impact on parameters such as external convection and shading [91, 92, 38]. Research often focuses on specific operational conditions or standard test cycles, neglecting real-world driving cycles and dynamic urban climates [93, 94, 95]. While some studies aim to integrate kinematic and thermal load models for a more comprehensive analysis of the energy demand, they often rely on steady-state models [64, 62, 75] or on simplified models [86, 96, 97]. Other researchers employ advanced models, similar to those developed in this thesis, using commercial simulation environments (e.g., DYMOLA [82, 83, 87], TRNSYS [98], or MATLAB [99]). However, none of these models incorporate input variables that account for detailed thermal conditions, such as the bus orientation in specific routes or critical factors like shadowing.

A transient dynamic thermal model has been created to predict the sensible thermal load in a bus cabin under variable ambient conditions, including shadowing and the vehicle orientation. The model uses a lumped-parameter approach with three nodes: indoor air, bus body envelope, and interior mass. A set of ordinary differential equations using the Heat Balance Method (HBM), has been solved at each time-step using an ode-solver to calculate the temperatures for each node. The model accounts for the energy and mass flows, including convective, solar radiative, and long-wave radiative heat gains. The total thermal load is analyzed by decomposing it into six components: solar load, external infrared load, air changes, occupancy load, auxiliary load, and convection, conduction, and internal infrared load. This provides an

overview of the energy requirements for an HVAC system, but also to analyze the origin, which are the individual load components.

HVAC model

To accurately simulate the response of a real HVAC system, a detailed heat pump components model has been employed. The model has to include a control and a coupling with the cabin thermal model.

The HVAC energy consumption is often assumed constant [76, 77, 64, 62]. In some cases, the efficiency is modeled as a function of the operating conditions [97, 100, 101, 102, 103, 104, 105, 74]. While some studies quantify the impact of each component of the vapor compression cycle, they frequently lack a detailed description or model of these components [105, 106, 107, 108]. Other investigations have developed component models based on conservation equations, using compressor efficiency curves derived from catalog data or from experimental data. However, they often rely on an average overall heat transfer coefficient to characterize the heat exchangers [109, 110, 111, 46, 112]. Only a few authors [113, 114, 115, 82, 83, 87] have developed highly accurate HVAC models that enable a robust numerical evaluation of the thermodynamic cycle, incorporating detailed physical models of each component. However, some of these models [113, 114, 115] have not been tested under real operating conditions in urban environments. Conversely, other studies [82, 83, 87] are limited by the omission of critical thermal load factors related to urban vehicle conditions, such as shading effects on vehicle surfaces, and lack a representative evaluation period that includes the kinematic conditions and the vehicle orientation. Additionally, no studies have addressed important operational modes such as frost/defrost, PTC elements, or the potential impact of window openings.

A physical model of a real HVAC system has been developed, component by component using the software IMST-ART [116]. The compressor was characterized using its catalog data across its frequency range. The fans were modeled based on their characteristic curves.

The heat exchangers, expansion device, and connecting lines were defined according to their geometric and thermophysical properties. The control system was faithfully modeled to include variables such as the compressor speed, the fan PWM (Pulse Width Modulation), recirculation ratios, the PTC heater power, and defrost activation. These controls were simulated across six operating modes: cooling, standard forced ventilation, open windows ventilation, standard heating, heating under frost/defrost conditions, and heating with PTCs. These models were integrated into the extended thermal model by adding moisture transfers, latent thermal loads, and the heat gain introduced by the HVAC fans. The resulting model is capable of evaluating the operating mode of the HVAC system, the operational points of each component, their respective energy consumption and efficiency, as well as the outlet conditions of the air and condensate flowrates.

Battery model

In order to predict the state of charge of the battery, and consequently the vehicle autonomy, it is important to evaluate the consumption of all other systems, not only the HVAC. This involves incorporating the powertrain consumption and other auxiliary systems, including the efficiency of the battery itself. Many researchers simplify the powertrain model and exclude regenerative braking [77, 75]. Other studies propose detailed powertrain models [62, 82, 76, 86, 74, 83, 82], but these models are limited in their estimation due to the lack of slope data [76, 86, 82] or dynamic route models [62, 74, 82, 83]. Regarding the consumption of auxiliaries, some authors assume it as constant [76, 77, 64, 75] or omit significant systems [62], while others develop detailed models of auxiliaries [82, 74, 83, 82], which have served as a foundation for the models employed in this thesis.

The model incorporates seven subsystems which act on the battery consumption. Motor consumption and regenerative braking energy are calculated using a powertrain model that considers the street slope, bus speed, acceleration, and road characteristics. The HVAC system's energy consumption is also accounted for. Hydraulic systems, focus-

ing on the steering pump and suspension, along with pneumatic systems, primarily the brakes, are modeled based on the bus speed and the frequency of the stops. The energy use of auxiliary electrical systems, including lighting, information, control, navigation, safety, and emergency systems, is incorporated as well. The battery thermal management system, which combines heating in cold weather and cooling on warm days, has a consumption modeled according to the external temperature. Additionally, the efficiency of the battery's charge and discharge processes is also included. The total battery consumption is determined by summing the energy contributions from all these subsystems.

Summary

Table 1.1 provides a summary of several physical models from literature which calculate the energy consumption of electric buses in urban areas. The selected models have thoroughly developed at least one of the submodels described before, including the HVAC consumption, and have simulated real-world operating conditions in urban environments.

Table 1.1: Summary of physical models employed in literature to evaluate the energy consumption of electric buses in urban environments.

Publication	Category	City	GIS	Kinematic	Climate	Thermal Load	HVAC	Powertrain	Auxiliary
Gallet et al. (2018) [76]	Network-wide estimation	Singapore	Bus network	Synthetic dynamic	Three months	-	Constant	No slope	Constant
Al-Ogaili et al. (2020) [77]	Model validation	Kuala Lumpur, Malaysia	Bus network and slope	Empirical	A day	-	Constant	No regenerative braking	Constant
El-Taweel et al. (2021) [64]	Sensitivity	Brampton, Canada	Bus network and slope	Synthetic stochastic dynamic	Parametric	Steady	Constant	Detailed	Constant
Hjelkrem et al. (2021) [62]	Model validation	China & Norway	Empirical	Microtrip mean values	Specific days	Steady	Constant	No detailed speed profile	Constant
Basma et al. (2022) [74]	Comparative bus service	Paris, France	Bus network	Trip mean values	A year	Simplified	Regression	No detailed speed profile	Constant
Broatch et al. (2023) [86]	Modeling and simulation	València, Spain	Bus network	Empirical	Specific days	Simplified	Not specified	No slope	Simplified
Dougier et al. (2023) [75]	Charging strategies	Compiègne, France	Bus network and slope	Synthetic dynamic	Specific days	Steady	Constant	No regenerative braking	Constant
Basma et al. (2023) [87]	Battery sizing & charging strategy	Paris, France	Bus network	Empirical	Typical year	No detailed radiative	No detailed control	No slope	Detailed

As observed in the table 1.1, none of the published models combines all the necessary features to calculate accurately the energy consumption in real-world urban environments. Most models either simplify the problem or omit some submodels, including significant simplifications in the HVAC submodel and the thermal load calculations. Very often, there is no 3D city model to calculate the shading and visibility factors for radiative calculations. Only one author [64] has developed a stochastic kinematic model that incorporates detailed traffic data. Nevertheless, one of the most comprehensive models is described in reference [87]. Although this model is detailed in most submodels, including HVAC, and applies these models over a representative period, it does not address detailed kinematic modeling and lacks advanced HVAC control for factors such as defrost conditions, the consumption of PTCs, or the possibility of window ventilation.

1.3 Identified gaps and research questions

Based on the previous literature review, two main gaps and limitations have been identified.

Firstly, there is a research gap in the development of coupled vehicle and HVAC system models which can evaluate their impact on the overall energy consumption of electric buses, in real-world urban environments. Current literature lacks integration of the detailed models necessary to fully capture the factors with an impact in these complex operational conditions. For instance, previous studies overlook GIS models that are essential for providing the inputs for detailed radiative and shadow models. This can lead to substantial inaccuracies in energy consumption estimations. Furthermore, there is limited literature regarding the integration of dynamic thermal models with physical HVAC models, including their operational modes and control logic, which is crucial to determine the overall energy consumption and efficiency in variable operating conditions.

Secondly, the energy consumption of electric buses has slightly been studied in real driving cycles over long periods. The implementation of this methodology into an efficient simulation tool enables disaggregated results over annual periods, even with low time resolution. This tool helps obtain the breakdown of the energy consumption of each individual component, as well as sensitivity analyses and optimization studies based on a substantial datasets within a simulation environment. This is crucial for strategic and operational planning in the large-scale deployment of electric bus fleets.

To address these gaps, this thesis attempts to answer to the following main questions:

- **How can a comprehensive and detailed overall energy model of electric buses be constructed to accurately represent the dynamics of real operating conditions within a urban environments?**
  - Which factors and models are necessary to calculate the de-

mand and the vehicle consumption?

- How can the cabin model be coupled with the HVAC model for an accurate prediction of the consumption?

- As an application of the previous global model, **which is the energy demand and consumption in real operating conditions of urban electric buses of Mediterranean cities, and what measures can be implemented to reduce them?**
  - What is the impact of the different thermal loads, and what strategies can be employed to reduce them?
  - What is the energy consumption of the HVAC system and its impact on the overall consumption in real conditions in a city?
  - What is the frequency of the different operational modes of the HVAC system and their corresponding energy consumption and efficiency?
  - If the compressor is sized according to the specific climatic conditions at a given location, is it very different from a conventional compressor in the automotive industry?

1.4 Objectives

To address the research questions mentioned before, the primary objective of this thesis is to **develop a set of advanced models and integrate them into a comprehensive global model that enables obtaining the operation point and energy consumption of HVAC systems in electric urban buses under real driving conditions**.

As an application, the second objective is to **analyze the disaggregated energy consumption and operating conditions to obtain an insight on the current impact of the HVAC and potential improvements**.

The following specific objectives were established to achieve these goals:

1. Development and validation of a 3D city model based on Geographic Information Systems (GIS), incorporating a robust vector model of buildings and trees, and a Digital Elevation Model (DEM) for streets.

2. Development and validation of a kinematic vehicle model that generates a representative driving cycle using a stochastic approach, employing low-resolution GTFS route data, street speed limits, and traffic stops at street intersections.

3. Development of a climatic model that captures outdoor air temperature and humidity, multi-component radiation flows on the bus surfaces and their visible horizons from a shading model. The climatic model will use the city's long-term climatic data (TMY), solar geometry, and the outcomes from the previous models.

4. Development and validation of a transient thermal load model for the bus cabin. A set of ordinary differential equations will enable the calculation of the heat gains, node temperatures, moisture transfers, internal mass and shell node thermal loads, and interior latent loads. This is based on optical and thermophysical properties of the bus, occupancy, air exchanges, auxiliary systems, and environmental conditions.

5. Development of a physical model of a mobile reversible heat pump using IMST-ART, represented by detailed performance map. This model includes the compressor and fan speeds and recirculation ratios. The control includes six operating modes, encompassing cooling, standard forced ventilation, open windows ventilation, standard heating, heating in frost/defrost conditions, and heating with Positive Temperature Coefficient (PTC) heaters.

6. Integration of the thermal load and HVAC model to evaluate the equipment operating mode and the working points of each component, their energy consumption and efficiency, as well as the output conditions of the airflow and condensate.

7. Development of a bus battery model to determine the total vehicle energy consumption, including the engine, regenerative braking, air conditioning, battery thermal management system, auxiliary pneumatic, hydraulic, and electrical systems.

8. Integration of the previously developed models into a global model which obtains the operating conditions, modes, and performance points of the different system components.

9. Development of an efficient simulation tool, capable of obtaining accurate disaggregated results over annual periods with a low time resolution.

10. Simulation and evaluation of the energy demand and consumption under real operating conditions of urban electric buses in a representative Mediterranean city, considering both typical annual conditions and extreme days of winter and summer.

11. Perform a sensitivity analysis to evaluate the impact of different parameters and conditions on the thermal load, and propose effective strategies to reduce the thermal demand.

12. HVAC design application by optimizing compressor sizing for both representative and extreme conditions.

Specific objectives 1 to 8 align with the first main objective, whereas objectives 9 to 12 correspond to the second main objective.

The thesis contributes to several Sustainable Development Goals (SDGs). It enhances the understanding and assessment of the energy impact of HVAC systems in electric buses, promoting innovation in sustainable transportation (SDG 9). It also supports the development of more efficient urban public transport (SDG 11) and aids climate change mitigation by identifying potential improvements in energy consumption and emissions (SDG 13).

1.5 Scope and boundaries of the thesis

Given the complexity of the overall simulation tool, some hypothesis have been assumed, and the models has also been conceived for some specific situations. In summary:

- The research primarily focuses on the characteristics and needs of urban buses in a Mediterranean climate. However, the proposed models have been developed using available open data from most cities worldwide and the model can be applied to many other cities.
- The study has been applied to battery-powered electric buses, although fuel cell electric buses could be used with all models except the powertrain.
- The vehicle and HVAC system characteristics and control, are based on real data provided by the bus company EMT in Valencia and from the HVAC manufacturer. The results represent a standard 12-meter electric bus.
- Operating conditions (such as occupancy and schedules) are based on real data, while kinematic and climatic data are derived from statistically representative open data.
- A single air node within the cabin has been used, and the driver's air conditioning unit has not been included in the model due to the small temperature difference between the two thermal zones as in previous studies from literature [99, 113].
- The modeling of external wind speed and direction has not been considered. However, the external convection coefficient and infiltrations have been calculated based on the bus speed.
- A representative climate file of Valencia has been employed. However, the spatial variations of the urban heat island effects and specific humidity within the urban environment were not considered.

- Although the cabin humidity has been modeled, neither dehumidification nor defrosting modes have been considered, and no control mechanisms based on these parameters have been established.

- A hybrid system has been used to model the HVAC. The latter includes a standard reversible vapor compression heat pump system, which is the most common technology in the EU. Supplementary PTC heaters have been used used to support the heating under very low ambient temperatures.

- Regarding the methodology, a through monitoring campaign was proposed to the urban bus fleet of Valencia. Unfortunately, due to funding issues this was not possible and the global model validation was performed against published data. As future work, it would be very convenient to validate the integrated global model within the urban context, and to compare the energy consumption against real dynamic experimental tests. Nevertheless, all the main sub-models have been validated independently. On the one hand, the GIS and shadow model have been validated using real CAD elevation views of the buildings and the SketchUp shadow tool, while the consistency of the kinematic model has been validated using real GTFS data of bus schedule routes. On the other hand, the cabin thermal model was validated with experimental tests, while the HVAC model was validated with the manufacturer's data and using the IMST-ART tool, which has already been extensively validated in the literature with experimental data from heating and cooling systems.

1.6 Structure

The research has been organized as presented in Figure 1.1. The background colors refers to chapters, shaded areas indicate overlapping chapters, and the colors of the outline borders represent the objectives.

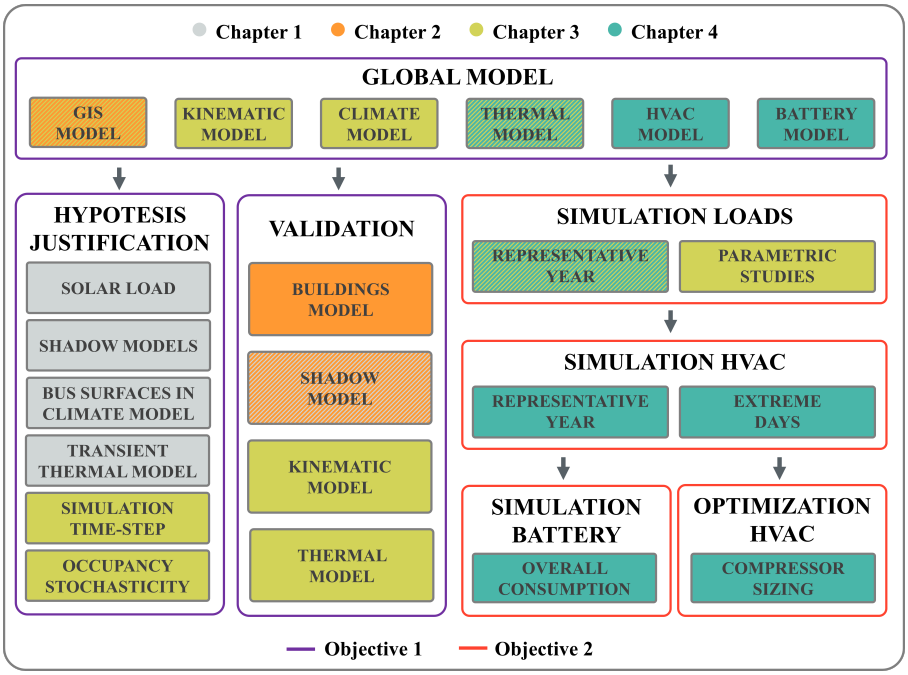

Figure 1.1: Structure of the thesis.

Chapter 1 provides an **introduction** to the motivation, the background and research context, the identified gaps and research questions, the objectives, and the scope of the thesis.

Chapters 2 to 4 align with the **three peer-reviewed articles** published as part of this thesis. A detailed description and contextualization of the articles is provided below:

- **Chapter 2: Development and validation in a 2D-GIS environment**

of a 3D shadow cast vector-based model on arbitrarily orientated and tilted surfaces. The main objective of this article is the development of a systematic GIS-based methodology. The latter has helped generate a 3D vector-based city model of existing buildings and their shadow-cast profiles on arbitrarily oriented and tilted planar surfaces, using a 2D-GIS approach. The methodology involves building the 3D city model with robust statistical estimators and applying an analytical shadow model to calculate shadow profiles on any arbitrarily oriented and tilted 3D surface at any time of the year. The models have been thoroughly validated, demonstrating a building height error of less than 1% for the city model and less than 2% in the overall methodology, including both 3D and shadow model. The primary contribution of this chapter is the development of an efficient and accurate GIS model for the urban buildings and a highly accurate analytical shadow-cast model. These models will serve as a foundation to create tailored models in the context of urban mobility.

- **Chapter 3: Dynamic cabin model of an urban bus in real driving condition**. This research presents the development and integration of a comprehensive dynamic thermal model of a bus within real urban driving route. The tool incorporates a 3D urban model, including buildings, trees and streets. Regarding the bus position, a weighted stochastic kinematic model has been employed, including the bus route consistent with the bus schedule, the actual speed limits of the route and the traffic. A climate model has been developed, considering all bus surfaces and environmental factors. The latter includes a detailed long-wave and short-wave radiative model, and a transient thermal model of the cabin, considering the different heat gains and thermal loads. The model was validated against dynamic experimental tests and two important hypotheses have been studied in detail: the time-step and the stochasticity of the occupancy. Additionally, a sensitivity analysis was conducted to measure and understand the influence of different parameters and conditions on the thermal load. The main

contribution of this chapter is the development of comprehensible models to analyze the thermal conditions of an urban bus under real-world operating conditions. To this end, the GIS model was enhanced by incorporating trees and streets. A more efficient shading model was developed for urban mobility context, along with a kinematic model that simulates the bus movement along its driving route. Additionally, a climate model was established to characterize the specific thermal conditions encountered by the bus, and a thermal load model was proposed to quantify the energy required to maintain cabin comfort. These models were integrated and used to simulate a representative year, yielding results that facilitate the validation, justification, and understanding of the thermal performance of these vehicles in practical operating conditions.

- **Chapter 4: HVAC system operation, consumption and compressor size optimization in urban buses of Mediterranean cities**. This chapter is an example of the potential application of the global model in multiple urban routes. As Chapter 3 focuses more on the load analysis, Chapter 4 is complementary since it focuses on the final target, which is the HVAC system energy consumption. The latter has been analyzed in a representative year and also in extreme weather conditions. The study introduces an HVAC system based on component-based physical model, incorporating a control model with six operating modes. This HVAC model is integrated with an extended thermal model that captures the contributions of the HVAC system to both energy and moisture mass balances within the cabin's air node. Additionally, a comprehensive battery model evaluates the impact of the HVAC on the overall energy consumption, taking into account factors such as the motor powertrain, regenerative braking, HVAC, battery thermal management, pneumatic and hydraulic systems, auxiliary electrical systems, and battery efficiency. The study also includes a dual-approach optimization for the compressor sizing, addressing both representative and extreme weather conditions. This chap-

ter contributes to the thesis by consolidating and integrating all the developed models.

Chapter 5 contains a **discussion of the results** presented in the previous chapters, placing them within the broader context of the thesis.

Finally, **Chapter 6** summarizes the main **conclusions** and contributions of this research, identifying potential future research directions and challenges.

1.7 References

[1] European Commission. The European pillar of social rights action plan. Publications Office of the European Union, 2021. https://doi.org/doi/10.2767/89.

[2] European Environment Agency. Transport and Environment Report 2022: Digitalisation in the Mobility System: Challenges and Opportunities. Technical report. 2022. https://doi.org/10.2800/47438.

[3] European Environment Agency. EEA greenhouse gases. Data viewer on Total greenhouse gas emissions and removals of the EU, based on data reported by EU Member States under the EU Governance Regulation.

[4] European Environment Agency. Greenhouse gas emissions from transport in Europe. 2023.

[5] Eurostat. Eurostat regional yearbook. Publications Office of the European Union, 2022. https://doi.org/doi/10.2785/915176.

[6] European Environment Agency. Europe's air quality status 2024. Technical report. 2024. https://doi.org/doi/10.2800/5970.

[7] European Environment Agency. Environmental noise in Europe — 2020. Technical report. 2020. https://doi.org/doi/10.2800/686249.

[8] European Commission. Handbook on the external costs of transport. Publications Office of the European Union, 2020. https://doi.org/doi/10.2832/51388.

[9] European Commission. Attitudes of Europeans towards Urban Mobility. Technical report. 2013.

[10] European Commission. Attitudes of Europeans towards Air Quality. Technical report. 2022.

[11] European Commission. Transport in the European Union - Current Trends and Issues. Technical report. 2019.

[12] P. Plötz, J. Wachsmuth, T. Gnann, F. Neuner, D. Speth, and S. Link. Net-zero-carbon transport in europe until 2050—targets, technologies and policies for a long-term eu strategy. In: *Karlsruhe: Fraunhofer Institute for Systems and Innovation Research ISI* (2021).

[13] European Commission. Regulation EU 2021/1119 of the European Parliament and of the Council of 30 June 2021 establishing the framework for achieving climate neutrality and amending Regulations (EC) No 401/2009 and EU 2018/1999 ('European Climate Law'). In: *Brussels: European Commission* (2021).

[14] European Commission. COM/2021/400 final - Pathway to a Healthy Planet for All. EU Action Plan: 'Towards Zero Pollution for Air, Water and Soil'. 2021.

[15] European Commission. COM/2021/811 final - The New EU Urban Mobility Framework. 2021.

[16] European Commission. C/2023/6783 - Commission Implementing Regulation EU 2023/2122 of 17 October 2023 amending Implementing Regulation EU 2018/2066 as regards updating the monitoring and reporting of greenhouse gas emissions pursuant to Directive 2003/87/EC of the European Parliament and of the Council. 2023.

[17] European Commission. PE/66/2022/REV/1 - Regulation EU 2023/851 of the European Parliament and of the Council of 19 April 2023 amending Regulation EU 2019/631 as regards strengthening the CO2 emission performance standards for new passenger cars and new light commercial vehicles in line with the Union's increased climate ambition (Text with EEA relevance). 2022.

[18] E. Mulholland. The revised CO2 standards for heavy-duty vehicles in the European Union. Technical report. 2024.

[19] European Commission. PE/29/2024/REV/1 - Regulation EU 2024/1610 of the European Parliament and of the Council of 14 May 2024 amending Regulation EU 2019/1242 as regards

strengthening the CO2 emission performance standards for new heavy-duty vehicles and integrating reporting obligations, amending Regulation EU 2018/858 and repealing Regulation EU 2018/956 (Text with EEA relevance). 2024.

[20] Eurostat. Modal split of inland passenger transport. 2024. https://doi.org/10.2908/TRAN_HV_PSMOD.

[21] European Automobile Manufacturers' Association. Buses - Fact sheet. 2023.

[22] European Commission. The Expert Group on Clean Buses - Procurement and Operation. Publications Office of the European Union, 2019.

[23] European Automobile Manufacturers' Association. Vehicles on European roads. 2024.

[24] Bloomberg. Electric Vehicle Outlook 2024. Technical report. 2024.

[25] M. Molliere. Battery-electric is now the most popular for new city buses in the EU. 2024.

[26] K. G. Logan, J. D. Nelson, and A. Hastings. Electric and hydrogen buses: Shifting from conventionally fuelled cars in the UK. In: *Transportation Research Part D: Transport and Environment* 85 (2020), 102350. https://doi.org/10.1016/j.trd.2020.102350.

[27] M. Mahmoud, R. Garnett, M. Ferguson, and P. Kanaroglou. Electric buses: A review of alternative powertrains. In: *Renewable and Sustainable Energy Reviews* 62 (2016), 673–684. https://doi.org/10.1016/j.rser.2016.05.019.

[28] H. Kim, N. Hartmann, M. Zeller, R. Luise, and T. Soylu. Comparative TCO Analysis of Battery Electric and Hydrogen Fuel Cell Buses for Public Transport System in Small to Midsize Cities. In: *Energies* 14.(14) (2021). https://doi.org/10.3390/en14144384.

[29] European Commission. TDetermining the environmental impacts of conventional and alternatively fuelled vehicles through LCA. Publications Office of the European Union, 2020.

[30] World Resources Institute. Barriers to adopting electric buses. 2019.

[31] M. Sadrani, R. Mirqasemi, A. Tirachini, and C. Antoniou. Barriers to electrification of bus systems: A fuzzy multi-criteria analysis in developed and developing countries. In: *Energy Conversion and Management* 314 (2024), 118700. https://doi.org/10.1016/j.enconman.2024.118700.

[32] A. Avenali, G. Catalano, M. Giagnorio, and G. Matteucci. Assessing cost-effectiveness of alternative bus technologies: Evidence from US transit agencies. In: *Transportation Research Part D: Transport and Environment* 117 (2023), 103648. https://doi.org/10.1016/j.trd.2023.103648.

[33] A. L. Rodrigues and S. R. Seixas. Battery-electric buses and their implementation barriers: Analysis and prospects for sustainability. In: *Sustainable Energy Technologies and Assessments* 51 (2022), 101896. https://doi.org/10.1016/j.seta.2021.101896.

[34] R. J. Thorne, I. B. Hovi, E. Figenbaum, D. R. Pinchasik, A. H. Amundsen, and R. Hagman. Facilitating adoption of electric buses through policy: Learnings from a trial in Norway. In: *Energy Policy* 155 (2021), 112310. https://doi.org/10.1016/j.enpol.2021.112310.

[35] Z. Zhang, J. Wang, X. Feng, L. Chang, Y. Chen, and X. Wang. The solutions to electric vehicle air conditioning systems: A review. In: *Renewable and Sustainable Energy Reviews* 91 (2018), 443–463. https://doi.org/10.1016/J.RSER.2018.04.005.

[36] M. B. B. de Moura and A. Tribess. Climate control system improvements for better cabin environmental conditions and reduction of fuel consumption. In: *SAE Technical Papers*. 2007. https://doi.org/10.4271/2007-01-2673.

[37] Asian Development Bank. Sustainable Transport Solutions: Low-Carbon Buses in the People's Republic of China. 2018. https://doi.org/10.22617/TCS189646-2.

[38] J. Vepsäläinen, K. Otto, A. Lajunen, and K. Tammi. Computationally efficient model for energy demand prediction of electric city bus in varying operating conditions. In: *Energy* 169 (2019), 433–443. https://doi.org/10.1016/J.ENERGY.2018.12.064.

[39] International Energy Agency. Cooling on the Move. The future of air conditioning in vehicles. https://www.iea.org/reports/cooling-on-the-move. 2019.

[40] ASHRAE American Society of Heating Refrigerating and A.-C. Engineers. ASHRAE Handbook - Fundamentals. Atlanta, GA: ASHRAE, 2017.

[41] Asociación Española de Normalización (UNE). Railway applications - Air conditioning for urban, suburban and regional rolling stock (UNE-EN Standard No. 14750). 2007.

[42] Y. Guo, J. Guo, W. Yang, P. Zhao, Y. Zhou, R. Deng, and Z. Jin. Experimental investigation on the heating performance of a R410A vapor-injection heat pump of an electric bus in cold regions. In: *Applied Thermal Engineering* 222 (2023), 119938. https://doi.org/10.1016/j.applthermaleng.2022.119938.

[43] Ş. Ünal, M. T. Erdinç, and Ç. Kutlu. Optimal thermodynamic parameters of two-phase ejector refrigeration system for buses. In: *Applied Thermal Engineering* 124 (2017), 1354–1367. https://doi.org/10.1016/j.applthermaleng.2017.06.115.

[44] X. Han, H. Zou, J. Wu, C. Tian, M. Tang, and G. Huang. Investigation on the heating performance of the heat pump with waste heat recovery for the electric bus. In: *Renew Energy* 152 (2020), 835–848. https://doi.org/10.1016/J.RENENE.2020.01.075.

[45] D.-Y. Lee, C.-W. Cho, J.-P. Won, Y. C. Park, and M.-Y. Lee. Performance characteristics of mobile heat pump for a large passenger electric vehicle. In: *Applied Thermal Engineer-*

ing 50.(1) (2013), 660–669. https://doi.org/10.1016/j.applthermaleng.2012.07.001.

[46] E. Afrasiabian, R. Douglas, M. Geron, and G. Cunningham. A numerical evaluation of a novel recovery fresh air heat pump concept for a generic electric bus. In: *Appl Therm Eng* 209 (2022), 118181. https://doi.org/10.1016/J.APPLTHERMALENG.2022.118181.

[47] P. Xie, L. Jin, G. Qiao, C. Lin, C. Barreneche, and Y. Ding. Thermal energy storage for electric vehicles at low temperatures: Concepts, systems, devices and materials. In: *Renewable and Sustainable Energy Reviews* 160 (2022), 112263. https://doi.org/10.1016/j.rser.2022.112263.

[48] M. Mohanraj and J. D. P. Abraham. Environment friendly refrigerant options for automobile air conditioners: a review. In: *Journal of Thermal Analysis and Calorimetry* 147 (1 2022), 47–72. https://doi.org/10.1007/S10973-020-10286-W/TABLES/10.

[49] E. Navarro, I. Martínez-Galvan, J. Nohales, and J. Gonzálvez-Maciá. Comparative experimental study of an open piston compressor working with R-1234yf, R-134a and R-290. In: *International Journal of Refrigeration* 36.(3) (2013), 768–775. https://doi.org/10.1016/j.ijrefrig.2012.11.017.

[50] Y. Song, H. Wang, Y. Ma, X. Yin, and F. Cao. Energetic, economic, environmental investigation of carbon dioxide as the refrigeration alternative in new energy bus/railway vehicles' air conditioning systems. In: *Applied Energy* 305 (2022), 117830. https://doi.org/10.1016/j.apenergy.2021.117830.

[51] B. Torregrosa-Jaime, J. Corberán, C. Vasile, C. Muller, M. Risser, and J. Payá. Sizing of a reversible magnetic heat pump for the automotive industry. In: *International Journal of Refrigeration* 37 (2014). New Developments in Magnetic Refrigeration, 156–164. https://doi.org/10.1016/j.ijrefrig.2013.06.018.

[52] N. Muralidhar, M. Himabindu, and R. Ravikrishna. Modeling of a hybrid electric heavy duty vehicle to assess energy recovery using a thermoelectric generator. In: *Energy* 148 (2018), 1046–1059. https://doi.org/10.1016/j.energy.2018.02.023.

[53] P. Li, Y. Zhang, K. Zhang, and M. Jiang. The effects of dynamic traffic conditions, route characteristics and environmental conditions on trip-based electricity consumption prediction of electric bus. In: *Energy* 218 (2021), 119437. https://doi.org/10.1016/J.ENERGY.2020.119437.

[54] Z. Gao, Z. Lin, T. J. LaClair, C. Liu, J.-M. Li, A. K. Birky, and J. Ward. Battery capacity and recharging needs for electric buses in city transit service. In: *Energy* 122 (2017), 588–600. https://doi.org/10.1016/J.ENERGY.2017.01.101.

[55] X. He, S. Zhang, W. Ke, Y. Zheng, B. Zhou, X. Liang, and Y. Wu. Energy consumption and well-to-wheels air pollutant emissions of battery electric buses under complex operating conditions and implications on fleet electrification. In: *Journal of Cleaner Production* 171 (2018), 714–722. https://doi.org/10.1016/j.jclepro.2017.10.017.

[56] J. Vepsäläinen, A. Ritari, A. Lajunen, K. Kivekäs, and K. Tammi. Energy Uncertainty Analysis of Electric Buses. In: *Energies* 11.(12) (2018). https://doi.org/10.3390/en11123267.

[57] H. Abdelaty and M. Mohamed. A Prediction Model for Battery Electric Bus Energy Consumption in Transit. In: *Energies* 14.(10) (2021). https://doi.org/10.3390/en14102824.

[58] P. Li, Y. Zhang, Y. Zhang, and K. Zhang. Prediction of electric bus energy consumption with stochastic speed profile generation modelling and data driven method based on real-world big data. In: *Appl Energy* 298 (2021), 117204. https://doi.org/10.1016/J.APENERGY.2021.117204.

[59] H. Abdelaty, A. Al-Obaidi, M. Mohamed, and H. E. Farag. Machine learning prediction models for battery-electric bus energy consumption in transit. In: *Transportation Research*

Part D: Transport and Environment 96 (2021), 102868. https://doi.org/10.1016/j.trd.2021.102868.

[60] Y. Gao, S. Guo, J. Ren, Z. Zhao, A. Ehsan, and Y. Zheng. An Electric Bus Power Consumption Model and Optimization of Charging Scheduling Concerning Multi-External Factors. In: *Energies* 11.(8) (2018). https://doi.org/10.3390/en11082060.

[61] Y. Chen, Y. Zhang, and R. Sun. Data-driven estimation of energy consumption for electric bus under real-world driving conditions. In: *Transportation Research Part D: Transport and Environment* 98 (2021), 102969. https://doi.org/10.1016/j.trd.2021.102969.

[62] O. A. Hjelkrem, K. Y. Lervåg, S. Babri, C. Lu, and C. J. Södersten. A battery electric bus energy consumption model for strategic purposes: Validation of a proposed model structure with data from bus fleets in China and Norway. In: *Transp Res D Transp Environ* 94 (2021), 102804. https://doi.org/10.1016/J.TRD.2021.102804.

[63] K. Kivekas, J. Vepsalainen, and K. Tammi. Stochastic Driving Cycle Synthesis for Analyzing the Energy Consumption of a Battery Electric Bus. In: *IEEE Access* 6 (2018), 55586–55598. https://doi.org/10.1109/ACCESS.2018.2871574.

[64] N. A. El-Taweel, A. Zidan, and H. E. Z. Farag. Novel Electric Bus Energy Consumption Model Based on Probabilistic Synthetic Speed Profile Integrated with HVAC. In: *IEEE Transactions on Intelligent Transportation Systems* 22.(3) (2021), 1517–1531. https://doi.org/10.1109/TITS.2020.2971686.

[65] C. Fiori and V. Marzano. Modelling energy consumption of electric freight vehicles in urban pickup/delivery operations: analysis and estimation on a real-world dataset. In: *Transp Res D Transp Environ* 65 (2018), 658–673. https://doi.org/10.1016/J.TRD.2018.09.020.

[66] A. Sola, C. Corchero, J. Salom, and M. Sanmarti. Multi-domain urban-scale energy modelling tools: A review. In: *Sustainable Cities and Society* 54 (2020), 101872. https://doi.org/10.1016/j.scs.2019.101872.

[67] A. Anand and C. Deb. The potential of remote sensing and GIS in urban building energy modelling. In: *Energy and Built Environment* 5.(6) (2024), 957–969. https://doi.org/10.1016/j.enbenv.2023.07.008.

[68] C. Li. 2.09 - GIS for Urban Energy Analysis. In: *Comprehensive Geographic Information Systems*. Edited by B. Huang. Oxford: Elsevier, 2018, 187–195. https://doi.org/10.1016/B978-0-12-409548-9.09652-4.

[69] N. Abbasabadi and M. Ashayeri. Urban energy use modeling methods and tools: A review and an outlook. In: *Building and Environment* 161 (2019), 106270. https://doi.org/10.1016/j.buildenv.2019.106270.

[70] G. Droj, L. Droj, and A.-C. Badea. GIS-Based Survey over the Public Transport Strategy: An Instrument for Economic and Sustainable Urban Traffic Planning. In: *ISPRS International Journal of Geo-Information* 11.(1) (2022). https://doi.org/10.3390/ijgi11010016.

[71] M. Zhang. The Use and Value of Geographic Information Systems in Transportation Modeling. In: *International Encyclopedia of Transportation*. Edited by R. Vickerman. Oxford: Elsevier, 2021, 440–447. https://doi.org/10.1016/B978-0-08-102671-7.10364-1.

[72] X. Liu, P. Payakkamas, M. Dijk, and J. de Kraker. GIS Models for Sustainable Urban Mobility Planning: Current Use, Future Needs and Potentials. In: *Future Transportation* 3.(1) (2023), 384–402. https://doi.org/10.3390/futuretransp3010023.

[73] K. Jetlund and B. Neuhäuser. Geographic Information Systems for Transportation. In: *Springer Handbook of Geographic Information*. Edited by W. Kresse and D. Danko. Cham: Springer

International Publishing, 2022, 707–727. https://doi.org/10.1007/978-3-030-53125-6_26.

[74] H. Basma, C. Mansour, M. Haddad, M. Nemer, and P. Stabat. Energy consumption and battery sizing for different types of electric bus service. In: *Energy* 239 (2022), 122454. https://doi.org/10.1016/J.ENERGY.2021.122454.

[75] N. Dougier, B. Celik, S.-K. Chabi-Sika, M. Sechilariu, F. Locment, and J. Emery. Modelling of Electric Bus Operation and Charging Process: Potential Contribution of Local Photovoltaic Production. In: *Applied Sciences* 13.(7) (2023), 4372. https://doi.org/10.3390/app13074372.

[76] M. Gallet, T. Massier, and T. Hamacher. Estimation of the energy demand of electric buses based on real-world data for large-scale public transport networks. In: *Appl Energy* 230 (2018), 344–356. https://doi.org/10.1016/J.APENERGY.2018.08.086.

[77] A. Saadon Al-Ogaili, A. Ramasamy, T. Juhana Tengku Hashim, A. N. Al-Masri, Y. Hoon, M. Neamah Jebur, R. Verayiah, and M. Marsadek. Estimation of the energy consumption of battery driven electric buses by integrating digital elevation and longitudinal dynamic models: Malaysia as a case study. In: *Applied Energy* 280 (2020), 115873. https://doi.org/10.1016/j.apenergy.2020.115873.

[78] J. D. Viana-Fons, J. Gonzálvez-Maciá, and J. Payá. Development and validation in a 2D-GIS environment of a 3D shadow cast vector-based model on arbitrarily orientated and tilted surfaces. In: *Energy Build* 224 (2020). https://doi.org/10.1016/j.enbuild.2020.110258.

[79] J.-R. Roussel and D. Auty. Airborne LiDAR Data Manipulation and Visualization for Forestry Applications. https://cran.r-project.org/package=lidR. 2023.

[80] J.-R. Roussel, D. Auty, N. C. Coops, P. Tompalski, T. R. Goodbody, A. S. Meador, J.-F. Bourdon, F. de Boissieu, and A.

Achim. lidR: An R package for analysis of Airborne Laser Scanning (ALS) data. In: *Remote Sensing of Environment* 251 (2020), 112061. https://doi.org/10.1016/j.rse.2020.112061.

[81] M. Dalponte and D. A. Coomes. Tree-centric mapping of forest carbon density from airborne laser scanning and hyperspectral data. In: *Methods Ecol Evol* 7.(10) (2016), 1236–1245. https://doi.org/10.1111/2041-210X.12575.

[82] H. Basma, C. Mansour, M. Haddad, M. Nemer, and P. Stabat. Comprehensive energy modeling methodology for battery electric buses. In: *Energy* 207 (2020), 118241. https://doi.org/10.1016/J.ENERGY.2020.118241.

[83] R. A. Haddad, H. Basma, and C. Mansour. Modeling and control of heat pump system for battery electric buses. In: *Proceedings of the Institution of Mechanical Engineers, Part D: Journal of Automobile Engineering* 236.(14) (2022), 3201–3220. https://doi.org/10.1177/09544070211069465.

[84] R. Günther, T. Wenzel, M. Wegner, and R. Rettig. Big data driven dynamic driving cycle development for busses in urban public transportation. In: *Transp Res D Transp Environ* 51 (2017), 276–289. https://doi.org/10.1016/J.TRD.2017.01.009.

[85] H. Gong, Y. Zou, Q. Yang, J. Fan, F. Sun, and D. Goehlich. Generation of a driving cycle for battery electric vehicles: A case study of Beijing. In: *Energy* 150 (2018), 901–912. https://doi.org/10.1016/J.ENERGY.2018.02.092.

[86] A. Broatch, P. Olmeda, P. Bares, and S. Aceros. Integral Thermal Management Studies in Winter Conditions with a Global Model of a Battery-Powered Electric Bus. In: *Energies (Basel)* 16.(1) (2023). https://doi.org/10.3390/en16010168.

[87] H. Basma, C. Mansour, M. Haddad, M. Nemer, and P. Stabat. A novel method for co-optimizing battery sizing and charging strategy of battery electric bus fleets: An application to the city

of Paris. In: *Energy* 285 (2023), 129459. https://doi.org/10.1016/j.energy.2023.129459.

[88] S. Chen, B. Du, Q. Li, and D. Xue. The influence of different orientations and ventilation cases on temperature distribution of the car cabin in the hot soak. In: *Case Studies in Thermal Engineering* 39 (2022), 102401. https://doi.org/10.1016/J.CSITE.2022.102401.

[89] M. A. Alam, R. Kumar, D. Banoriya, A. S. Yadav, G. Goga, K. K. Saxena, D. Buddhi, and R. Mohan. Design and development of thermal comfort analysis for air-conditioned compartment. In: *International Journal on Interactive Design and Manufacturing* (2022), 1–11. https://doi.org/10.1007/S12008-022-01015-8/METRICS.

[90] P. Bandi, N. P. Manelil, M. P. Maiya, S. Tiwari, A. Thangamani, and J. L. Tamalapakula. Influence of flow and thermal characteristics on thermal comfort inside an automobile cabin under the effect of solar radiation. In: *Appl Therm Eng* 203 (2022), 117946. https://doi.org/10.1016/J.APPLTHERMALENG.2021.117946.

[91] V. Lemort, G. Olivier, and C. De Pelsemaker. Thermal Energy Management in Vehicles. https://www.wiley.com/en-us/Thermal+Energy+Management+in+Vehicles-p-9781119251750. 2023, 320.

[92] Y. Bie, Y. Liu, S. Li, and L. Wang. HVAC operation planning for electric bus trips based on chance-constrained programming. In: *Energy* 258 (2022), 124807. https://doi.org/10.1016/J.ENERGY.2022.124807.

[93] D. Ramsey, L. Boulon, and A. Bouscayrol. Modeling of an EV air conditioning system for energetic studies in summer. In: *2021 IEEE Vehicle Power and Propulsion Conference, VPPC 2021 - Proceedings*. 2021. https://doi.org/10.1109/VPPC53923.2021.9699119.

[94] F. Lan, H. Chen, J. Chen, and W. Li. Effect of urban microclimates on dynamic thermal characteristics of a vehicle cabin. In: *Case Studies in Thermal Engineering* (2023), 103162. https://doi.org/10.1016/J.CSITE.2023.103162.

[95] Z. Shuofeng, M. R. Amini, J. Sun, and C. Mi. A Two-Layer Real-Time Optimization Control Strategy for Integrated Battery Thermal Management and HVAC System in Connected and Automated HEVs. In: *IEEE Trans Veh Technol* 70.(7) (2021), 6567–6576. https://doi.org/10.1109/TVT.2021.3085938.

[96] J. Jiang, Y. Yu, H. Min, Q. Cao, W. Sun, Z. Zhang, and C. Luo. Trip-level energy consumption prediction model for electric bus combining Markov-based speed profile generation and Gaussian processing regression. In: *Energy* 263 (2023), 125866. https://doi.org/10.1016/J.ENERGY.2022.125866.

[97] H. He, M. Yan, C. Sun, J. Peng, M. Li, and H. Jia. Predictive air-conditioner control for electric buses with passenger amount variation forecast. In: *Appl Energy* 227 (2018), 249–261. https://doi.org/10.1016/J.APENERGY.2017.08.181.

[98] D. C. Vásconez Núñez. Desarrollo de un modelo para el cálculo del consumo de climatización en vehículos de pasajeros urbanos. PhD thesis. Valencia (Spain): Universitat Politècnica de València, 2019. https://doi.org/10.4995/Thesis/10251/121133.

[99] B. Torregrosa-Jaime, F. Bjurling, J. M. Corberán, F. Di Sciullo, and J. Payá. Transient thermal model of a vehicle's cabin validated under variable ambient conditions. In: *Appl Therm Eng* 75 (2015), 45–53. https://doi.org/10.1016/J.APPLTHERMALENG.2014.05.074.

[100] D. Ramsey, A. Bouscayrol, L. Boulon, A. Desreveaux, and A. Vaudrey. Flexible Simulation of an Electric Vehicle to Estimate the Impact of Thermal Comfort on the Energy Consumption. In: *IEEE Transactions on Transportation Electrification* 8.(2) (2022), 2288–2298. https://doi.org/10.1109/TTE.2022.3144526.

[101] D. Ramsey, A. Bouscayrol, and L. Boulon. Energy Consumption of a Battery Electric Vehicle in Winter Considering Preheating: Tradeoff between Improved Performance and Total Energy Consumption. In: *IEEE Vehicular Technology Magazine* 17.(3) (2022), 104–112. https://doi.org/10.1109/MVT.2022.3158043.

[102] M. A. Fayazbakhsh and M. Bahrami. Comprehensive Modeling of Vehicle Air Conditioning Loads Using Heat Balance Method. In: *SAE Technical Papers* 2 (2013). https://doi.org/10.4271/2013-01-1507.

[103] H. Khayyam, J. Abawajy, and R. N. Jazar. Intelligent energy management control of vehicle air conditioning system coupled with engine. In: *Appl Therm Eng* 48 (2012), 211–224. https://doi.org/10.1016/J.APPLTHERMALENG.2012.04.050.

[104] M. Direk, M. S. Mert, F. Yüksel, and A. Keleşoğlu. Exergetic Investigation of a R1234yf Automotive Air Conditioning System with Internal Heat Exchanger. In: *International Journal of Thermodynamics* 21.(2) (2018), 103–109. https://doi.org/10.5541/IJOT.357232.

[105] C. Dullinger, W. Struckl, and M. Kozek. A modular thermal simulation tool for computing energy consumption of HVAC units in rail vehicles. In: *Appl Therm Eng* 78 (2015), 616–629. https://doi.org/10.1016/J.APPLTHERMALENG.2014.11.065.

[106] E. Tosun, M. Bilgili, G. Tuccar, A. Yasar, and K. Aydin. Exergy analysis of an inter-city bus air-conditioning system. In: *International Journal of Exergy* 20.(4) (2016), 445–464. https://doi.org/10.1504/IJEX.2016.078094.

[107] R. Prabakaran and D. Mohan Lal. A novel exergy based charge optimisation for a mobile air conditioning system: An experimental study. In: *J Therm Anal Calorim* 132.(2) (2018), 1241–1252. https://doi.org/10.1007/S10973-018-6998-0/METRICS.

[108] E. B. Ratts and J. S. Brown. An experimental analysis of cycling in an automotive air conditioning system. In: *Appl Therm Eng* 20.(11) (2000), 1039–1058. https://doi.org/10.1016/S1359-4311(99)00080-0.

[109] J. Jabardo, W. Mamani, and M. R. Ianella. Modeling and experimental evaluation of an automotive air conditioning system with a variable capacity compressor. In: *International Journal of Refrigeration* 25.(8) (2002), 1157–1172. https://doi.org/10.1016/S0140-7007(02)00002-6.

[110] G. H. Lee and J. Y. Yoo. Performance analysis and simulation of automobile air conditioning system. In: *International Journal of Refrigeration* 23.(3) (2000), 243–254. https://doi.org/10.1016/S0140-7007(99)00047-X.

[111] D. Di Battista and R. Cipollone. High efficiency air conditioning model based analysis for the automotive sector. In: *International Journal of Refrigeration* 64 (2016), 108–122. https://doi.org/10.1016/J.IJREFRIG.2015.12.014.

[112] J.-M. Corberán, S. Martínez-Ballester, J. Gonzálvez-Maciá, and C. La-Barbera. Error estimation of single phase effectiveness and LMTD methodologies when applied to heat exchangers with phase change. In: *Journal of Physics: Conference Series* 745.(3) (2016), 032125. https://doi.org/10.1088/1742-6596/745/3/032125.

[113] D. C. Vásconez-Núñez, J. Gonzálvez-Maciá, J. M. Corberán, and J. Payá. Development and validation of a dynamic thermal model of a minibus using TRNSYS. In: *International Journal of Vehicle Design* 77.(1–2) (2018), 87–107. https://doi.org/10.1504/IJVD.2018.098272.

[114] R. Mastrullo, A. W. Mauro, and C. Vellucci. Refrigerant Alternatives for High Speed Train A/C Systems: Energy Savings and Environmental Emissions Evaluation under Variable Ambient Conditions. In: *Energy Procedia* 101 (2016), 280–287. https://doi.org/10.1016/J.EGYPRO.2016.11.036.

[115] B. Torregrosa-Jaime, J. Payá, and J. Corberan. Design of efficient air-conditioning systems for electric vehicles. In: *SAE International Journal of Alternative Powertrains* 2.(2) (2013), 291–303. https://doi.org/10.4271/2013-01-0864.

[116] Universitat Politècnica de Valéncia, Instituto de Ingenieria Energética, Spain. IMST-ART v4.0 - Simulation tool to assist the selection, design and optimization of refrigerator equipment and components. http://www.imst-art.com. 2022.

Chapter 2

Development and validation in a 2D-GIS environment of a 3D shadow cast vector-based model on arbitrarily orientated and tilted surfaces

Chapter adapted from the paper:

Joan Dídac Viana-Fons, José María Gonzálvez-Maciá, Jorge Payá. *Development and validation in a 2D-GIS environment of a 3D shadow cast vector-based model on arbitrarily orientated and tilted surfaces.* In: *Energy & Buildings* (2020), Vol. 224, p. 110258.
DOI: https://doi.org/10.1016/j.enbuild.2020.110258.

Instituto Universitario de Investigación en Ingeniería Energética, Universitat Politècnica de València, Camí de Vera s/n, Valencia, Spain.

Abstract:

This paper presents a systematic GIS-based methodology to obtain the shadow cast profile of a group of buildings on arbitrarily orientated and tilted surfaces. The model is integrated in the widely-employed 2D-GIS environment. Given its scalability, the methodology can be easily applied from a local level up to a district, city or even regional level. This work is of interest for a wide range of applications such as for instance in Solar Resource Assessments (SRA) in urban environments. The starting point is to use cadastral cartography and LiDAR altimetric data to obtain a 3D vector-based model of the buildings using high robust mode estimators. Once the geometry of the buildings is defined, analytical models are applied to calculate the shadow-cast profile on any arbitrarily orientated and tilted surface of the surroundings. The model has been implemented in the R programming language. An extensive validation has been carried out for several buildings of Valencia (Spain) using CAD elevation views of the buildings and the SketchUp's shadow tool. The error of the vector-based city model is lower than 1% in all LiDAR datasets. The maximum error of the overall methodology, including both height and shadow models, is lower than 2%.

Keywords: Urban shadow model; Urban solar irradiation; 3D city model; Daylight simulation; Model validation, GIS.

Nomenclature

LiDAR: Light Detection and Ranging.

CAD: Computer-Aided Design.

SoI: Surface of Interest.

LoD: Level of Detail.

GIS: Geographic Information Systems.

DEM: Digital Elevation Model.

EDFM: Empirical Probability Density Function mode.

HRM: Half-Range mode.

HSM: Half-Sample mode.

SM: Shorth mode.

LMSM: Least Median of Squares mode.

RPM: Robust Parametric mode.

MAE: Maximum Relative Error.

RMSE: Root-Mean-Square Error.

Z: Height.

α: Plane azimuth or aspect.

G: Centroid of a polygon.

K: Kernel function.

h: Bandwidth.

μ: Mean.

B_0: Building footprint.

B_n: SoI on its plane.

S_0: Shadow footprint.

S_n: Shadow profile on its plane.

p_0: Vertex of S_0.

p_n: Vertex of S_n.

π_h: Horizontal plane.

π_r: Non-vertical rotated plane.

$\hat{n}$: Direction vector of the π_n.

$\hat{u}$: Axis of rotation.

XY: Ground coordinate.

β: Plane elevation or slope.

SF: Shadow factor.

f: Probability density function.

λ: Power parameter of transformation.

ω: Standard deviation.

B_h: SoI projection on π_h.

B_r: SoI projection on π_r.

S_h: Shadow profile projection on π_h.

S_r: Shadow profile projection on π_r.

p_h: Vertex of S_h.

p_r: Vertex of S_r.

π_n: Plane of the SoI.

$\hat{h}$: Direction vector of the π_h.

$\hat{s}$: Direction vector of the sun.

θ: Angle of rotation.

2.1 Introduction

Urban areas currently concentrate around half of the world's population but consume over two-thirds of the world's energy and account for around the same share of CO_2 emissions [1]. This situation can be seen as an opportunity since cities could potentially cut their carbon emissions by 90 percent by 2050 [2] using current technologies and policies. This change in the paradigm of the cities has motivated the development and enrichment of 3D city models extending their functionality and usability in a perspective of sustainability [3]. Many of these applications are energy-related [4, 5, 6] and these 3D city models are the starting point in building or urban scales for assessing the urban solar resource [7]. In these applications, a correct shadow model is essential to make a suitable solar assessment, especially in urban contexts, where complex geometries cast very large and variable shadows resulting in a dramatic decrease of the incident solar radiation [8, 9]. Accurate shadow models are essential in many research areas such as in urban daylight analysis, in urban building energy modeling or even for the analysis of solar thermal and photovoltaic potential on urban scale. Such areas require calculating accurately the specific shadow cast profile by nearby obstructions throughout each day and season.

A shadow cast model must address multiple requirements, as the accuracy of the results, the adaptability to the different building shapes and orientations and finally, the scalability. Although there are many algorithms to obtain shadow profiles in urban environments, there is still no methodology which fulfills simultaneously the three above-mentioned requirements. Therefore, the primary goal of the present study was to perform and validate a simple solution for shadow profile cast calculation achieving:

- A good accuracy by applying analytical vector-based models.
- An adaptable model based on robust statistical estimators and able to calculate cast shadows on arbitrary sloped and orientated surfaces.

- A scalable methodology starting from open and available data in most countries and integrating the model into widely used 2D-GIS environments.

Nowadays, the most common way to perform shading calculations is usually with design-oriented software. Design-oriented models of buildings can predict their shadows with great precision. This software includes specialized applications such as Radiance [10] TOWNSCOPE II [11] or SOLENE [12] and general 3D-CAD or BIM applications such as SketchUp [13], Rhinoceros [14] or Autodesk Revit [15]. Although design-oriented software has a high accuracy and provides advanced visualization capabilities, the high computational cost in the specialized software and the lack of availability of 3D-CAD data at large scale or a city level, the use of these tools is usually limited to a local or architectural scale [7, 16]. In order to model and analyze entire cities, non-analytical approaches have also been proposed, such as Machine Learning [17, 18], which is a computationally efficient alternative to analytical methods. However, those approaches cannot completely replace analytical models, especially in environments with complex geometries such as the urban landscape. Among the analytical methods and for areas up to some square kilometers, shadow calculations and other spatial analysis are usually performed using Geographic Information Systems (GIS) models, which have proved to be the most powerful method to estimate the solar potential [8]. In these environments, shadow calculations have been commonly performed with a raster-based approach based on a digital elevation model (DEM) employing common open-source tools such as r.sun model [19] in GRASS GIS, the doshade command in the insol R package [20] or using proprietary software as the Solar Analyst extension [21] in ArcGIS. These tools have specific routines for the calculation of shadows using ray-tracing algorithms based on a DEM whereby a whereby the sunlight obstruction is evaluated for every grid cell for a given timestamp or solar position. This approach has the advantage of simplicity and high-speed processing, although this is at the expense of accuracy and large file size, both of which depend on the grid resolution [22]. Additionally, raster-based models are appro-

priate for modeling data changes continuously across a region, as the natural terrain, where the grid resolution is not critical. Furthermore, raster models cannot be employed in areas of differing relief complexity nor for the modeling of vertical surfaces since they would present discontinuities. Different strategies have been developed recently to assess the solar potential on vertical surfaces which significantly contribute to the overall solar potential of modern cities [23] due their high areas. These include models based on hyperpoints [24, 25], 2D triangular mesh [26, 27] and 3D-voxel [28, 29]. The latter are all grid-based models that discretize the space in basic computational elements such as hyperpoints, triangles or voxels, and apply the ray-tracing algorithm to the planar-mid-point of the element. However, the previous approaches are usually not available or not implemented in common GIS software. Furthermore, only some of these publications [25, 27] have validated the radiation results and none of them have been experimentally validated the shadow results separately from the solar radiation. The other type of data in common GIS environments is vector data. Vector data in GIS is formed by one or more interconnected vertices or points which generate spatial entities representing real-world features, such as buildings. The accuracy of this approach depends on scale and the desired level of detail [30]. Vector-based models are more appropriate to automatically model [31, 32] and analyze fine-scale urban spaces, characterized by a highly variable and discontinuous relief, and common available data, such as LiDAR and building footprints datasets. The degree of complexity of a 3D model in GIS environments is categorized according to the level of detail (LoD) concept of the standard CityGML [33]. Although there are many models and strategies to obtain a vector-based 3D city models from LiDAR data, usually these methods are sensitive to the local point density as well as to the noise, outliers and missing data [34]. The higher the LoD the higher the density of required points. Furthermore, the use of high LoDs for analytic purposes increases substantially the computational cost or limits the scale of the model to be processed. In contrast, calculation errors due to the use of a low granularity (LoD) could be high [35]. Therefore, the LoD must be carefully selected according to the shape of the buildings, the accuracy and the

extension of the study. Furthermore, the LoD should be coherent with the quality and availability of the LiDAR datasets. Wang et al. [34] stated that the prismatic modeling (LoD1) is suitable for multilevel flat buildings which prevail in cities. In parallel, the open and available sources in most countries are usually low-density airborne LiDAR data ($<$1 pts/m^2) which are coherent with the different variants of LoD1 proposed by Biljecki et al. [36]. Then, the prismatic modeling, which is the simplest LoD, thoroughly models the real-world features in an urban context and can be applied to large areas using low computation resources. Assuming a given fine footprint of the buildings (i.e. cadastral map), the critical parameter to model accurately in LoD1 is the building height which, as the geometric reference of the model, could have higher influence on the results than the granularity (LoD) of the model according to Biljecki et al. [35]. This is a key point particularly in shadow analysis, where an error in the geometric model may involve much larger errors in the shadow cast [37]. As a consequence and giving the considerable level of contamination of LiDAR datasets, statistical estimators with high robustness to outliers are essential to obtain correct height values of each building and therefore, to enable accurate shadow calculations. Vector-based shadow algorithms are based on the search for the intersections between the sun rays and the surface of interest [38, 39]. Recent publications contribute to their advance in GIS environments [29, 40, 41, 42, 43]. Among the previous literature, the shadow model used by Vulkan et al. [42] and implemented in the shadow R package [44], allows the calculation of shadow profiles on horizontal planes based on a 2.5D vector-based model through trigonometric relations. The present work tries to move a step beyond the previous shadow model of Vulkan et al. [42] by adding the possibility to calculate shadows on tilted surfaces, and by including a quantitative validation of the model. This paper proposes and validates a simple solution for shadow modeling in cities from open and available data in most countries and using widely used 2D-GIS environments. Given the previous literature review, the present model includes the following novelties:

- Analytical vector-based shadow model to obtain a non-discretized shadow profile cast in arbitrary sloped and orientated surfaces integrated in the widely used 2D-GIS environment.
- Quantitative experimental validation of the shadow model for five-hour interval of two representative days in three surfaces of different slopes.
- Analysis and discussion on the best robust mode estimators to calculate the height of the buildings using LiDAR data.

2.2 Model Description

The developed methodology is able to obtain a 3D vector-based city model of the existing buildings and their cast shadow profiles over any arbitrarily orientated and tilted planar surface in a 2D-GIS environment (scheme in Figure 2.1). The methodology consists in building a 3D city model (steps 1 to 3) in a 2D-GIS environment, using high robust statistic estimators. After this, an analytical shadow model is applied (steps 5 to 9) to calculate the shadow profile on any arbitrarily orientated and tilted 3D surface for any time of the year. The modeling approach

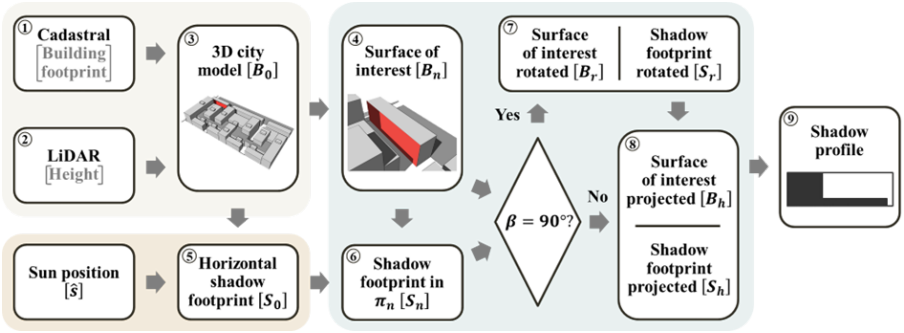

Figure 2.1: Workflow of the proposed methodology.

starts with the use of the cadastral map (1) and the contained LiDAR data (2) to build the 3D city model (3) by the vertical extruding of the buildings' footprint with their estimated height value. Once it has been obtained and given the sun position, the shadow model starts by calculating the horizontal shadow footprint (5). The latter, combined with the plane equations of the shaded surface (4), is projected onto the plane of the surface of interest SoI (6). Finally, depending on the slope β of the SoI the model processes differently these results in a 2D-GIS environment. In non-vertical surfaces (8), the shadow profile (9) is obtained as the intersection of the horizontal projection of the SoI and the shadow footprint, while in vertical surfaces (7) a previous rotation of the two polygons in the horizontal plane is required.

2.2.1 City Model

First, a model of the desired buildings, district or city is developed. The starting point is the flat footprint of the buildings included in the cadastral cartography and the associated LiDAR point cloud dataset, which contains the height value Z of a XY regular grid.

A vector-based 3D model of the buildings is then obtained following a similar procedure to Ledoux and Meijers [45]. The latter is based on the vertical extruding of the 2D building footprint, with a height value Z obtained by a statistic estimator of the LiDAR points contained in each polygon.

These height values of each building can be assumed as a sample drawn from a unimodal, continuous distribution. Because of the nature of the data (e.g. presence of obstacles or clouds, planimetric and altimetric uncertainties or disparity between the footprints) these samples may contain a very significant presence of outliers or data from outside the population which is sampled. As a consequence, the height values of the LiDAR data enclosed within a building footprint are a potentially highly skewed and kurtotic sample [46]. For this reason, a proper measure of the central tendency, with low bias and high efficiency and robustness to outliers, is essential to obtain accurate and reliable information from these datasets.

In this paper, the seven high robust statistic estimators studied by Bickel [47] and Bickel and Frühwirth [48] have been considered to measure the central tendency. Furthermore, the arithmetic mean or central value, used in many cases in the generation of LiDAR-based city models [45, 49], has been included in the comparative study. As indicated in the results, the latter has shown that the mean value is not a proper estimator of the building height due to its inherent outlier sensitivity. The robust statistics correspond to the median and the six mode estimators studied in Bickel and Frühwirth [48] which can be classified into three groups:

(1) Kernel density estimation: non-parametric method to estimate

a smoothed empirical probability density function of a random variable. Considering a Gaussian kernel K, the density function f of a random variable x based on a finite data sample $\{x_i\}_{i=1}^{n}$ is given in Eq. 2.1:

$$f(x) = \frac{1}{nh}\sum_{i=1}^{n} K\left(\frac{x - x_i}{h}\right) = \frac{1}{nh\sqrt{2\pi}}\sum_{i=1}^{n} \exp\left[-\frac{1}{2}\left(\frac{x - x_i}{h}\right)^2\right] \quad (2.1)$$

where $h > 0$ is the smoothing parameter called the bandwidth which balances the trade-off between bias and noise, hence the choice of h is crucial for the performance of its estimator. Then, the bandwidth selection is based on the optimal properties of f by using the Sheather & Jones (1991) procedure [50] implemented in the `stats` R package [51]. Once the function f is obtained, the empirical probability density function mode (EDFM) is defined as the value for which f reaches a maximum.

(2) Direct estimation: this set of methods does not involve density estimation. Four different mode estimators have been considered: the half-range mode (HRM) which is based on finding iteratively the half-range modal interval, defined as the interval of fixed range that contains the maximum number of observations. The half-sample mode (HSM) is also based on the iterative calculation of the modal interval, in this case using half-samples instead of half-ranges. Finally, the last two estimators are non-iterative and use only the first shortest half-sample to estimate the mode. These estimators are the short mode (SM), defined as the mean of these points, and the least median of squares mode (LMSM), defined as the midpoint.

(3) Parametric estimation: this estimation is based on the data transformation into a normal distribution and then an analytical calculation of the mode of this transformed data. Within this group of procedures, the strategy proposed by Bickel [47] has been considered. In this case, a power transformation $y = x^{\lambda}$ with respect to the power parameter λ is applied and the mean μ and standard deviation σ of the transformed data y is estimated using the sample median and the standardized median absolute deviation. The robust parametric mode

(RPM) can be estimated according to the Eq. 2.2:

$$\mathrm{RPM} = \frac{1}{2}\left[\mu + \sqrt{\mu^2 + \frac{4\sigma^2(\lambda - 1)}{\lambda}}\right] \tag{2.2}$$

The previous statistical estimators have all been compared with CAD elevation views in order to determine which estimator is the best estimate for the actual building height. As a result, an LoD1 block model of the city is obtained according to the level of detail (LoD) concept of the standard CityGML [33], which indicates the complexity and the degree of abstraction of a 3D city model. This 3D city model, also known as 2.5D model, is easily integrated in 2D-GIS environments by saving the height value of each 2D building polygon as an attribute in the associated database.

2.2.2 Shadow Model

The shadow model consists in an analytical procedure, applied and integrated in 2D-GIS environments, to obtain the shadow profile on any arbitrarily orientated and tilted surface for any point in time. Once the buildings are defined, in order to implement the shadow model, a distinction is established between the shading objects (which cast shadows) and the shaded objects or surface of interest (SoI) which receive such shadows. The shading objects are fully defined by the 3D block city model. For the shaded objects, the associated database contains the centroid G height value of each polygon, its inclination (β) and orientation (α) of the plane π_n. The shadow profile is represented in a 2D-GIS environment given its projection S_h on the horizontal plane π_h. The shadow factor SF is defined as the ratio of the shaded area S_n with respect to the total surface B_n. The shadow factor is consequently equal to the ratio of their horizontal projections, as indicated in Eq. 2.3:

$$SF = \frac{S_n}{B_n} = \frac{S_h}{B_h} \tag{2.3}$$

The shadow model starts from the shadow footprint S_0 on a horizontal plane π_h by means of the model developed by Vulkan et al. [42]. This

model consists in shifting the contour of the buildings in the opposite direction to sun azimuth by a distance depending on the building height and the sun elevation. Once the corresponding polygon S_0 is obtained, the model applies the operation of projection onto a plane along the direction of a given vector for each vertex p_0 of the polygon S_0. Specifically, the model calculates its projection S_n onto the plane π_n in the direction of the sun $\hat{s}$ by applying vector equations to each point p_0. The projected point p_n of point p_0 onto the plane π_n in the specified direction $\hat{s}$ is given in Eq. 2.4:

$$p_n = p_0 - t \cdot \hat{s} \qquad t = \frac{n \cdot v_1}{n \cdot \hat{s}} v_1 = G - p_0 \qquad (2.4)$$
$$p_0 \in \pi_h \qquad p_n, G \in \pi_n |n| = \|\hat{s}\| = 1$$

Once the projection p_n of each vertex p_0 is obtained, the polygon S_n is assembled. In order to integrate the results in a 2D-GIS environment and to use the corresponding tools, the model distinguishes between vertical and non-vertical shadowed surfaces (Figure 2.2). For non-vertical surfaces, the representation of the shadow profile in a 2D-GIS environment is obtained as the intersection between the horizontal projection of the surface of interest B_h, which is usually equivalent to the given footprint, and the shadow footprint S_h, obtained by projecting each vertex p_n of the polygon S_n on the horizontal plane π_h, i.e., setting the height of each vertex p_n. to zero. For vertical surfaces, it is not possible

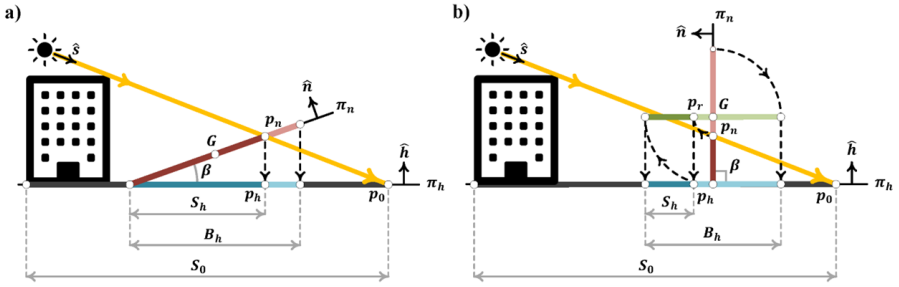

Figure 2.2: Shadow model for a) non-vertical and b) vertical surfaces.

to apply the previous approach given that, on a horizontal 2D environment, the vertical surfaces are represented as lines and not as polygons.

For this reason, a rotation is applied to the surface of interest B_n and the shadow footprint S_n on a plane π_r, which is not vertical. Thus, the rotated surface of interest B_r and the shadow footprint S_r is obtained using a same angle θ and rotation axis $\hat{u}$ for both polygons. Although any non-vertical plane pr could be considered, the horizontal plane at G point (p_r in Fig. 2.2) is recommended, because in this way the real magnitude of the shadow profile is obtained. The angle h and the axis of rotation for this operation is given in Eq.2.5:

$$\begin{aligned} p_r &= G + v_2 \cdot \cos(\theta) + (v_2 \cdot \hat{u}) \cdot \hat{u} \cdot (1 - \cos(\theta)) + (\hat{u} \times v_2) \cdot \sin(\theta) \\ v_2 &= p_n - G \\ \|\hat{u}\| &= 1 \end{aligned} \tag{2.5}$$

When the angle and axis has been considered, the resulting rotation of such polygons on a horizontal plane is achieved by applying the Rodrigues' rotation formula [52] to every vertex p_n of the polygons B_n and S_n. Eq. 2.6 defines the calculation, according to the right-hand rule, of the rotated point p_r of point p_n by an angle θ, rotation axis $\hat{u}$ and using G as a center of rotation:

$$\begin{aligned} \theta &= \arccos\left(\frac{n \cdot h}{\|n\| \cdot \|h\|}\right) \\ \hat{u} &= \frac{n \times h}{\|n \times h\|} \end{aligned} \tag{2.6}$$

Once the non-vertical rotation pr of each vertex p_n is obtained, the polygons S_r and B_r are assembled. Finally, the shadow profile in a 2D-GIS environment is obtained by applying the same procedure than for non-vertical shadowed surfaces, i.e., which is intersecting their horizontal projection.

2.3 Results, Model Validation, and Discussion

The methodology has been applied to several buildings of the Polytechnic City of Innovation (CPI) of the Universitat Politècnica de València (39°28′12″N, 0°22′35″O), which is located in the east of Spain (Figure 2.3). Such buildings present two significant points of interest for the validation which are that the detailed CAD drawings are available, and that the buildings cast shadows on horizontal, vertical, and tilted surfaces of the surroundings. The methodology has been implemented in the R programming language [51] and has been validated using CAD software.

The CPI consists of 30 multilevel flat buildings. The total building footprint area is of around 12,700 m^2, placed in a 190x90m land, with building height values in the range from 14 m to 29 m with respect to the ground level, with a footprint area between 50 m^2 and 2,150 m^2. Along the west side of the CPI, there is a 6° tilted garden over 20 m width, approximately.

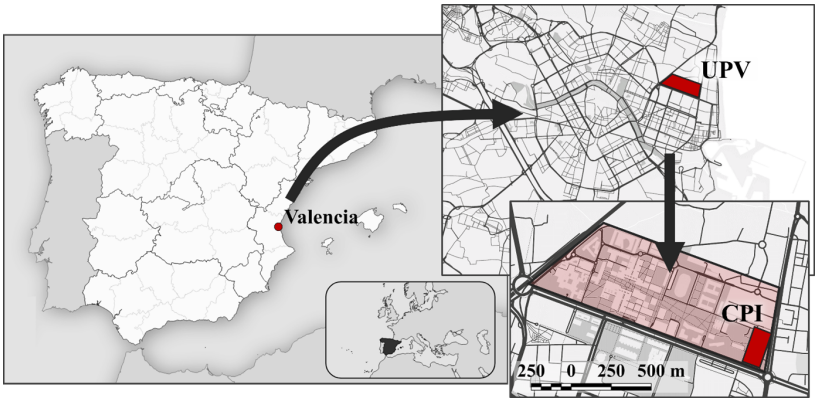

Figure 2.3: Location of the case study in València, Spain.

2.3.1 City Model

In order to validate the city model, the height of each building was obtained using the statistic estimators of central tendency explained

in Section 2.1 compared to the mean, as evidence of their robustness towards outliers, and two open government LiDAR datasets of low-density (0.5pts/m^2), which correspond to the years 2009 and 2015 [53]. The accuracy of each statistic applied to each dataset has been evaluated by comparing the results obtained with the heights defined in the CAD elevation views. Two error estimators have been calculated for each case: the root-mean-square error (RMSE) and the mean absolute error (MAE), as given in Eq. 2.7:

$$\begin{aligned} \mathrm{RMSE} &= \sqrt{\frac{\sum_{i=1}^{n}(x_{\mathrm{CAD},i} - x_{\mathrm{model},i})^2}{n}} \\ \mathrm{MAE} &= \frac{\sum_{i=1}^{n}|x_{\mathrm{CAD},i} - x_{\mathrm{model},i}|}{n} \end{aligned} \tag{2.7}$$

Both error metrics are used together to measure the model performance. The MAE is used to evaluate the average magnitude of the error while the RMSE, compared with the prior, is employed to diagnose the presence of large errors. The RMSE and MAE of each estimator and LiDAR dataset for all the buildings has been obtained in meters. The results are shown in Table 2.1, where the final row "total" has been calculated by running estimators over the merged LiDAR datasets. Very similar

Table 2.1: Root-mean-square error and mean absolute error of city models in two LiDAR datasets.

	RMSE [m]							
	SM	LMSM	HSM	HRM	EDFM	RPM	Median	Mean
LiDAR 2009	0.061	0.060	0.064	0.063	0.063	0.065	0.065	1.423
LiDAR 2015	0.061	0.061	0.059	0.063	0.056	0.062	0.062	1.306
Total	0.061	0.061	0.061	0.063	0.060	0.064	0.063	1.366
	MAE [m]							
	SM	LMSM	HSM	HRM	EDFM	RPM	Median	Mean
LiDAR 2009	0.061	0.060	0.064	0.063	0.063	0.065	0.065	1.423
LiDAR 2015	0.061	0.061	0.059	0.063	0.056	0.062	0.062	1.306
Total	0.061	0.061	0.061	0.063	0.060	0.064	0.063	1.366

results can be observed for the seven high robust statistics studied by Bickel and Frühwirth [48]. These measures of central tendency show

mean errors lower than 0.1 m and no significant differences between the two datasets are observed. Such results are consistent with the employed LiDAR datasets, which present a maximum RMSE in the Z coordinate of 0.20 m [53]. Despite the high level of similarity between the different statistical estimators, the estimator which provides the best fitting with the real height, according to the results of the most recent (2015) and the total set of LiDAR data, is the empirical probability density function mode (EDFM) based on a normal kernel function and using the bandwidth according to the Sheather and Jones [50] procedure. In contrast, the mean value is not a proper estimator of the building height, since it presents a high error due to its high sensitivity to outliers. Figure 2.4 shows a comparison between the actual building

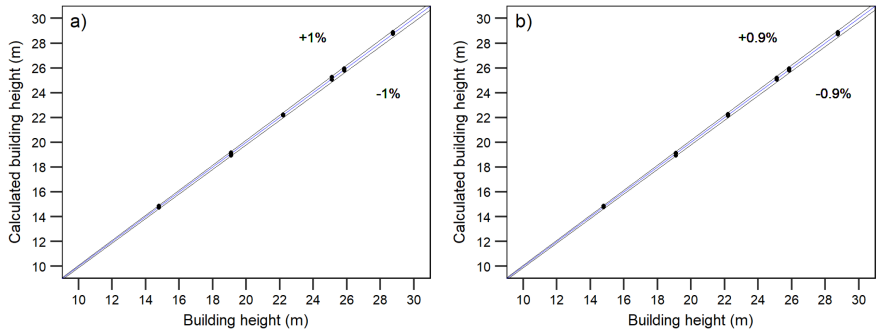

Figure 2.4: City model fit using the empirical probability density function mode (EDFM) for two LiDAR datasets: a) 2009 and b) 2015.

height, extracted from the CAD drawings, and the height obtained by the proposed model, using the EDFM with both LiDAR datasets. The maximum relative error is smaller than 1% in all cases.

2.3.2 Shadow Model

In order to apply and validate the shadow model, the best building height estimator and LiDAR dataset have been taken, which corresponds to the EDFM of 2015 data. For such model, the shadow profile has been calculated in three surfaces (Figure 2.5) with different β incli-

nation (A-horizontal, B-vertical, and C-tilted) for five hours (from 10 to 14 local time) at both solstices to test both short and long shadows for the location. In order to have a reference, the set of buildings has

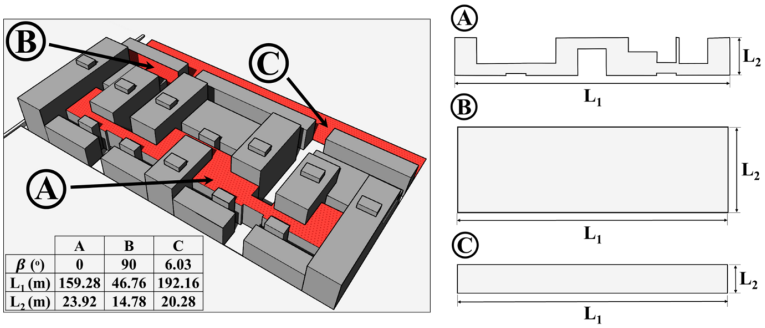

	A	B	C
β (°)	0	90	6.03
L_1 (m)	159.28	46.76	192.16
L_2 (m)	23.92	14.78	20.28

Figure 2.5: Studied surfaces A, B, and C of the Polytechnic City of Innovation (CPI).

been modeled in SketchUp using their detailed architectural 2D-CAD views. The shadow profile has been obtained for each surface and hour (Figure 2.6) by using the SketchUp's shadow tool developed by Yezioro and Shaviv [54].

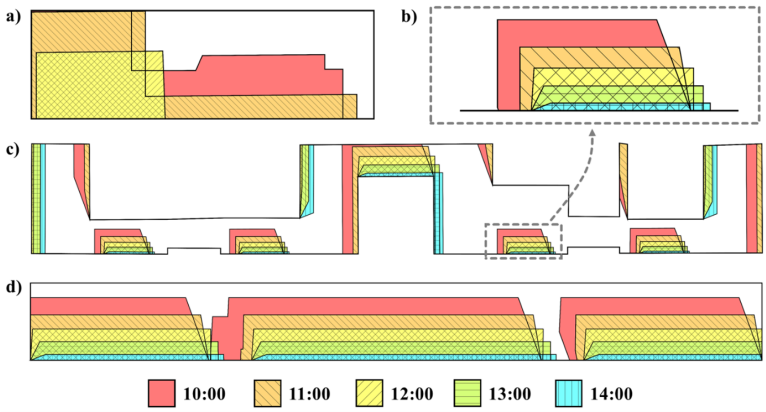

Figure 2.6: Shadow profiles on different surfaces and hours on June 21st for a) vertical surface, b) details of horizontal surface, c) horizontal surface, and d) tilted surface.

Following the procedure explained in the Section 2.2, the shadow factor and the relative error series have been obtained for the five-hour interval of each representative day in the studied surfaces.

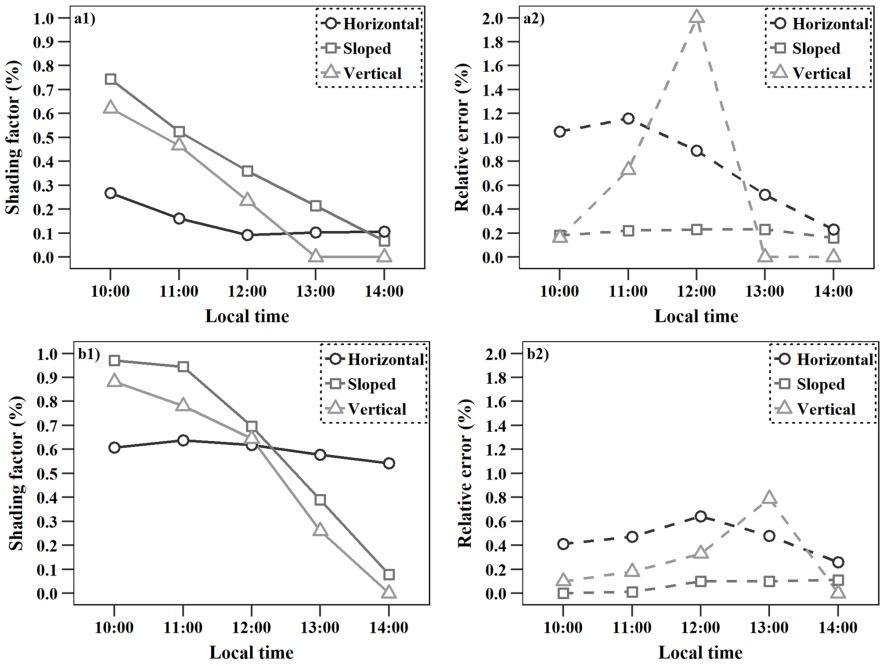

Figure 2.7: Hourly shadow factor (1) and relative error (2) for a) June 21st and b) December 22nd.

Figure 2.7 plots the shadow factor SF series and their relative error (RE) against the CAD (SketchUp) results as given in Eq. 2.8.

$$RE = \frac{|SF_{CAD} - SF_{model}|}{SF_{CAD}} \tag{2.8}$$

On the one hand, the time series of the shadow factor SF show that the shadow is significantly greater in the early hours of the morning than in the early afternoon on the inclined and vertical surfaces, while for the horizontal surface, the inter-daily fluctuations are not so variable. These

results are explained taking into account that the two non-horizontal surfaces are oriented to the southeast ($\alpha = 288.6°$, counterclockwise convention measuring from the south), so the shadows are null in this orientation at 14:26 local time for June 21st and 14:14 local time for December 22nd. There are taller buildings in the southeast and southwest direction, which explains the small variation of the shadow factor on the horizontal surface. Regarding the annual variation of the shadow factor, the results show that the shadow is much greater in the winter solstice than in the summer solstice, mainly because the solar elevation in winter is much lower in the site latitude.

On the other hand, the series of the relative error show higher accuracy on the sloped surface than on the horizontal, while for the vertical surface, this precision is variable over time, showing maximums at certain time points. The two primary elements influencing the model accuracy are:

1. The city model error propagation, since the errors in the geometric model could lead to greater errors in the shadow cast. The height of the buildings that cast shadows on the sloped surface has an average error of 3 cm, similar to the values of the other surfaces, which are 5 cm for the horizontal and 6 cm for the vertical surface. However, the shadow on the vertical surface presents the maximum relative error on June 21st at 12:00 local time when the shadow cast is only due to a building whose height error is 10 cm.

2. The shadow and surface size, since the shadow factor SF is a relative measure of the shaded area with respect to the total surface area. For this reason, the accuracy is logically greater in larger areas.

Therefore, the greater precision of the model in the sloped surface is due to the combination of a greater precision in the city model and to a large area and shadow size (Fig. 2.6). However, despite these

differences between the results obtained, the most notable aspect of the series of the relative error is the very low error which is obtained.

For the validation of the overall methodology, including both height and shadow models, the shadow profiles were also obtained in the SketchUp's shadow tool and the shadow factor SF was calculated in each case. Table 2.2 presents the RMSE and the MAE of the overall methodology by the shadow factor obtained against the SketchUp results of each surface and day.

Table 2.2: Root-mean-square error (RMSE) and mean absolute error (MAE) of the overall methodology measured by the shadow factor obtained against the SketchUp's shadow tool for different days and surfaces.

Surface	June 21st	December 22nd	Total
Sloped	0.09 (0.08)	0.04 (0.03)	0.07 (0.05)
Vertical	0.26 (0.18)	0.15 (0.13)	0.21 (0.16)
Horizontal	0.16 (0.13)	0.29 (0.27)	0.23 (0.20)
Total	0.18 (0.13)	0.19 (0.14)	0.19 (0.14)

The results show that the average accuracy of the shadow factor on the sloped surface is significantly higher than in the other two surfaces according to the relative errors shown in Figure 2.7. In contrast, the results show no significant differences between the total values of the two selected days. However, there are significant and complementary differences between the vertical and horizontal surface at both solstices, because the surfaces are perpendicularly oriented.

Finally, Figure 2.8 summarizes the validation of the overall methodology for the three surfaces on the two representative days. The hourly results of the model have been compared with respect to the reference SketchUp's shadow tool results.

The results show that the average accuracy of the shadow factor on the sloped surface is significantly higher than in the other two surfaces according to the relative errors shown in Figure 2.7. In contrast, the results show no significant differences between the total values of the

two selected days. However, there are significant differences between the values of the two days both for the vertical and horizontal surface. This aspect can be explained by the size differences of the shaded surface between the two days.

Finally, Figure 2.8 summarizes the validation of the global model for the three surfaces on the two representative days. The hourly results of the model have been compared with respect to the SketchUp results.

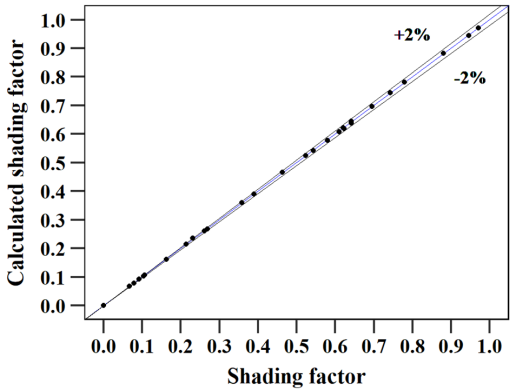

Figure 2.8: Global model fitting for all surfaces through the shadow factor evaluation.

2.4 Conclusions

An accurate estimation of shadow profiles is essential for several downstream applications on urban scale. In these applications, a shadow cast model must be accurate, adaptable to the geometric complexity of the buildings and scalable.

The present article presents an accurate and systematic GIS-based methodology which has been developed to obtain the shadow cast by a group of buildings on arbitrarily orientated and tilted surfaces. The methodology is integrated into the scalable and widely used 2D-GIS environment and can be useful for the solar resource assessment in fine-scale urban environments of most countries using open access data.

The starting point of the model is to employ cadastral cartography and LiDAR altimetric data to obtain a 3D vector-based model of the existing buildings, by means of robust statistical estimators. Analytical models are finally applied for the calculation of the shadow cast on any surrounding surface.

The above-mentioned methodology has been validated on 30 buildings of the Universitat Politècnica de València (UPV, Spain). The validation has been performed using the CAD elevation views of the buildings and 3D-CAD software. Different LiDAR point cloud datasets have been employed and evaluated for the 3D model validation, while the shadow model has been validated for both different surface orientations and points in time. The following conclusions have been drawn:

- The error obtained in the validation of the vector-based 3D model of the buildings is lower than 1% with all robust mode estimators.
- The mean value is not a proper estimator of the building height because of its inherent high sensitivity to outliers. The authors recommend to use robust estimators such as the EDFM.
- The maximum relative error of the overall methodology, including both 3D and shadow model, is lower than 2% for the shadow factor calculations.

- The accuracy of the model is not dependent on the day of the year or hour of the day but the shadow factor calculation is particularly sensitive to propagation of the height model errors of the involved buildings and, to a lesser degree, to the size of the shadow and the surface.

As future work, the presented methodology will be used to calculate the direct solar irradiation in buildings, including facades and tilted roofs. For a full solar resource assessment, the diffuse component will be considered by using the sky view factor (SVF) of the surfaces of interest. The methodology will be further improved by including a 3D city model that estimates the inclination and orientation of building roofs and a shadow model that uses them as shading objects.

2.5 Acknowledgments

This work has been supported by the Generalitat Valenciana under the program “Subvencions per a la contractació de personal investigador de caràcter predoctoral (ACIF/2019/239)”.

2.6 References

[1] United Nations. World Urbanization Prospects: The 2018 Revision. 2019. https://doi.org/10.18356/b9e995fe-en.

[2] Coalition for Urban Transitions. Climate Emergency, Urban Opportunity. 2019.

[3] R. Billen, A.-F. Cutting-Decelle, O. Marina, J.-P. de Almeida, C. M., G. Falquet, T. Leduc, C. Métral, G. Moreau, J. Perret, G. Rabin, R. S. Jose, I. Yatskiv, and S. Zlatanova. 3D City Models and urban information: Current issues and perspectives. In: *EDP Sciences* (2014), I–118. https://doi.org/10.1051/tu0801/201400001.

[4] F. Biljecki, J. Stoter, H. Ledoux, S. Zlatanova, and A. Çöltekin. Applications of 3D city models: State of the art review. In: *ISPRS International Journal of Geo-Information* 4 (2015), 2842–2889. https://doi.org/10.3390/ijgi4042842.

[5] C. Reinhart and C. C. Davila. Urban building energy modeling - A review of a nascent field. In: *Building and Environment* 97 (2016), 196–202. https://doi.org/10.1016/j.buildenv.2015.12.001.

[6] X. Oregi, N. Hermoso, I. Prieto, J. Izkara, L. Mabe, and P. Sismanidis. Automatised and georeferenced energy assessment of an Antwerp district based on cadastral data. In: *Energy and Buildings* 173 (2018), 176–194. https://doi.org/10.1016/j.enbuild.2018.05.018.

[7] S. Freitas, C. Catita, P. Redweik, and M. Brito. Modelling solar potential in the urban environment: State-of-the-art review. In: *Renewable and Sustainable Energy Reviews* 41 (2015), 915–931. https://doi.org/10.1016/j.rser.2014.08.060.

[8] R. Machete, A. Falcão, M. Gomes, and A. M. Rodrigues. The use of 3D GIS to analyse the influence of urban context on buildings' solar energy potential. In: *Energy and Buildings* 177 (2018), 290–302. https://doi.org/10.1016/J.ENBUILD.2018.07.064.

[9] I. Lima, V. Scalco, and R. Lamberts. Estimating the impact of urban densification on high-rise office building cooling loads in a hot and humid climate. In: *Energy and Buildings* 182 (2019), 30–44. https://doi.org/10.1016/j.enbuild.2018.10.019.

[10] G. W. Larson and R. A. Shakespeare. Rendering with Radiance: The Art and Science of Lighting Visualization. Morgan Kaufman, 1998.

[11] J. Teller and S. Azar. Townscope II—A computer system to support solar access decision-making. In: *Solar Energy* 70.(3) (2001). Urban Environment, 187–200. https://doi.org/10.1016/S0038-092X(00)00097-9.

[12] F. Miguet and D. Groleau. A daylight simulation tool for urban and architectural spaces—application to transmitted direct and diffuse light through glazing. In: *Building and Environment* 37.(8) (2002), 833–843. https://doi.org/10.1016/S0360-1323(02)00049-5.

[13] Trimble Inc. SketchUp. 2019. https://doi.org/https://www.sketchup.com.

[14] Robert McNeel and Associates. Rhinoceros. 2019.

[15] Autodesk Inc. Autodesk Revit. 2020. https://doi.org/https://www.autodesk.com/products/revit/overview.

[16] G. Desthieux, C. Carneiro, R. Camponovo, P. Ineichen, E. Morello, A. Boulmier, N. Abdennadher, S. Dervey, and C. Ellert. Solar energy potential assessment on rooftops and facades in large built environments based on lidar data, image processing, and cloud computing. Methodological background, application, and validation in geneva (solar cadaster). In: *Frontiers in Built Environment* 4 (2018), 331553. https://doi.org/10.3389/FBUIL.2018.00014/BIBTEX.

[17] A. Vartholomaios. A machine learning approach to modelling solar irradiation of urban and terrain 3D models. In: *Computers, Environment and Urban Systems* 78 (2019), 101387. https://doi.org/10.1016/j.compenvurbsys.2019.101387.

[18] D. Assouline, N. Mohajeri, and J.-L. Scartezzini. Quantifying rooftop photovoltaic solar energy potential: A machine learning approach. In: *Solar Energy* 141 (2017), 278–296. https://doi.org/10.1016/j.solener.2016.11.045.

[19] J. Hofierka and M. Súri. The solar radiation model for Open source GIS: implementation and applications. In: *Open Source GIS - GRASS Users Conference*. 2002.

[20] J. Corripio. insol: Solar Radiation. 2019. https://doi.org/https://cran.r-project.org/package=insol.

[21] P. Fu and P. Rich. Design and Implementation of the Solar Analyst: an ArcView Extension for Modeling Solar Radiation at Landscape Scales. In: *19th Annual ESRI User Conference*. 1999, 1–24.

[22] Esri. What is raster data? - Help | ArcGIS Desktop. 2020. https://doi.org/https://desktop.arcgis.com/en/arcmap/latest/manage-data/raster-and-images/what-is-raster-data.htm.

[23] M. Brito, S. Freitas, S. Guimarães, C. Catita, and P. Redweik. The importance of facades for the solar PV potential of a Mediterranean city using LiDAR data. In: *Renewable Energy* 111 (2017), 85–94. https://doi.org/10.1016/J.RENENE.2017.03.085.

[24] C. Catita, P. Redweik, J. Pereira, and M. Brito. Extending solar potential analysis in buildings to vertical facades. In: *Computers and Geosciences* 66 (2014), 1–12. https://doi.org/10.1016/j.cageo.2014.01.002.

[25] M. Brito, P. Redweik, C. Catita, S. Freitas, and M. Santos. 3D Solar Potential in the Urban Environment: A Case Study in Lisbon. In: *Energies* 12 (2019), 3457. https://doi.org/10.3390/en12183457.

[26] S. Kaynak, B. Kaynak, and A. Özmen. A software tool development study for solar energy potential analysis. In: *Energy and Buildings* 162 (2018), 134–143. https://doi.org/10.1016/J.ENBUILD.2017.12.033.

[27] J. Liang, J. Gong, J. Zhou, A. Ibrahim, and M. Li. An open-source 3D solar radiation model integrated with a 3D Geographic Information System. In: *Environmental Modelling and Software* 64 (2015), 94–101. https://doi.org/10.1016/j.envsoft.2014.11.019.

[28] J. Liang and J. Gong. A Sparse Voxel Octree-Based Framework for Computing Solar Radiation Using 3D City Models. In: *ISPRS International Journal of Geo-Information* 6 (2017), 106. https://doi.org/10.3390/ijgi6040106.

[29] J. Hofierka and M. Zlocha. A New 3-D Solar Radiation Model for 3-D City Models. In: *Transactions in GIS* 16 (2012), 681–690. https://doi.org/10.1111/j.1467-9671.2012.01337.x.

[30] QGIS Development Team. Vector Data - Documentation for QGIS 3.4. 2020. https://doi.org/https://docs.qgis.org/3.4/en/docs/gentle_gis_introduction/vector_data.html.

[31] Q. Zhou and U. Neumann. Fast and extensible building modeling from airborne LiDAR data. In: *GIS: Proceedings of the ACM International Symposium on Advances in Geographic Information Systems*. 2008, 43–50. https://doi.org/10.1145/1463434.1463444.

[32] J. Yan, K. Zhang, C. Zhang, S. Chen, and G. Narasimhan. Automatic construction of 3-D building model from airborne LIDAR data through 2-D snake algorithm. In: *IEEE Transactions on Geoscience and Remote Sensing* 53 (2015), 3–14. https://doi.org/10.1109/TGRS.2014.2312393.

[33] G. Gröger and L. Plümer. CityGML - Interoperable semantic 3D city models. In: *ISPRS Journal of Photogrammetry and Remote Sensing* 71 (2012), 12–33. https://doi.org/10.1016/j.isprsjprs.2012.04.004.

[34] R. Wang, J. Peethambaran, and D. Chen. LiDAR Point Clouds to 3-D Urban Models: A Review. In: *IEEE Journal of Selected Topics in Applied Earth Observations and Remote Sensing* 11 (2018), 606–627. https://doi.org/10.1109/JSTARS.2017.2781132.

[35] F. Biljecki, H. Ledoux, J. Stoter, and G. Vosselman. The variants of an LOD of a 3D building model and their influence on spatial analyses. In: *ISPRS Journal of Photogrammetry and Remote Sensing* 116 (2016), 42–54. https://doi.org/10.1016/j.isprsjprs.2016.03.003.

[36] F. Biljecki, H. Ledoux, and J. Stoter. An improved LOD specification for 3D building models. In: *Computers, Environment and Urban Systems* 59 (2016), 25–37. https://doi.org/10.1016/j.compenvurbsys.2016.04.005.

[37] F. Biljecki, G. Heuvelink, H. Ledoux, and J. Stoter. Propagation of positional error in 3D GIS: estimation of the solar irradiation of building roofs. In: *International Journal of Geographical Information Science* 29 (2015), 2269–2294. https://doi.org/10.1080/13658816.2015.1073292.

[38] W. Newman, I. Sutherland, and G. Hodgman. Graphics and Reentrant Polygon Clipping. In: 1974.

[39] K. Weiler and P. Atherton. Hidden surface removal using polygon area sorting. In: *ACM SIGGRAPH Computer Graphics* 11 (1977), 214–222. https://doi.org/10.1145/965141.563896.

[40] A. Strzalka, N. Alam, E. Duminil, V. Coors, and U. Eicker. Large scale integration of photovoltaics in cities. In: *Applied Energy* 93 (2012), 413–421. https://doi.org/10.1016/j.apenergy.2011.12.033.

[41] M. Weisthal. Assessment of potential energy savings in Israel through climate-aware residential building design. PhD thesis. Ben Gurion University of the Negev, 2014.

[42] A. Vulkan, I. Kloog, M. Dorman, and E. Erell. Modeling the potential for PV installation in residential buildings in dense urban areas. In: *Energy and Buildings* 169 (2018), 97–109. https://doi.org/10.1016/j.enbuild.2018.03.052.

[43] S. Pili, G. Desogus, and D. Melis. A GIS tool for the calculation of solar irradiation on buildings at the urban scale, based on Italian standards. In: *Energy and Buildings* 158 (2018), 629–646. https://doi.org/10.1016/j.enbuild.2017.10.027.

[44] M. Dorman and E. Erell. A shadow: R Package for Geometric Shadow Calculations in an Urban Environment. In: *The R Journal* 11 (2019), 287. https://doi.org/10.32614/rj-2019-024.

[45] H. Ledoux and M. Meijers. Topologically consistent 3D city models obtained by extrusion. In: *International Journal of Geographical Information Science* 25 (2011), 557–574. https://doi.org/10.1080/13658811003623277.

[46] M. Bartels, H. Wei, and D. Mason. DTM generation from LIDAR data using skewness balancing. In: *Proceedings - International Conference on Pattern Recognition*. 2006, 566–569. https://doi.org/10.1109/ICPR.2006.463.

[47] D. Bickel. Robust and efficient estimation of the mode of continuous data: the mode as a viable measure of central tendency. In: *Journal of Statistical Computation and Simulation* 73 (2003), 899–912. https://doi.org/10.1080/0094965031000097809.

[48] D. Bickel and R. Frühwirth. On a fast, robust estimator of the mode: Comparisons to other robust estimators with applications. In: *Computational Statistics and Data Analysis* 50 (2006), 3500–3530. https://doi.org/10.1016/j.csda.2005.07.011.

[49] Esri. Obtaining elevation information for building footprints - Help | ArcGIS Desktop. 2020. https://doi.org/https://desktop.arcgis.com/en/arcmap/latest/extensions/3d-analyst/3d-buildings-obtaining-elevation-information-for-building-footprints.htm.

[50] S. Sheather and M. Jones. A Reliable Data-Based Bandwidth Selection Method for Kernel Density Estimation. In: *Journal of the Royal Statistical Society. Series B (Methodological)* 53 (1991), 683–690. https://doi.org/http://www.jstor.org/stable/2345597.

[51] R Core Team. R: A Language and Environment for Statistical Computing. https://www.R-project.org/. 2022.

[52] H. Cheng and K. Gupta. An historical note on finite rotations. In: *Journal of Applied Mechanics, Transactions ASME* 56 (1989), 139–145. https://doi.org/10.1115/1.3176034.

[53] Instituto Geográfico Nacional. Plan Nacional de Ortofotografía Aérea. 2020. https://doi.org/https://pnoa.ign.es.

[54] A. Yezioro and E. Shaviv. Shading: A design tool for analyzing mutual shading between buildings. In: *Solar Energy* 52.(1) (1994). Solar Buildings, 27–37. https://doi.org/10.1016/0038-092X(94)90078-G.

Chapter 3

Dynamic cabin model of an urban bus in real driving conditions

Chapter adapted from the paper:

Joan Dídac Viana-Fons [a,b], Jorge Payá [a]. *Dynamic cabin model of an urban bus in real driving conditions.* In: *Energy* (2024), Vol. 288, p. 129769.
DOI: https://doi.org/10.1016/j.energy.2023.129769.

[a] Instituto Universitario de Investigación en Ingeniería Energética, Universitat Politècnica de València, Camí de Vera s/n, Valencia, Spain.

[b] ImpactE, C/ Joan Verdeguer nº 16, Valencia, 46024, Spain.

Abstract:

The transport sector is a key sector to reduce the emission reduction targets. The main auxiliary load, the HVAC system, contributes significantly to the energy consumption and affects the driving range in electric vehicles. Accurate and dynamic models are needed to optimize these systems in urban environments. This research presents a dynamic thermal model of a cabin, including a detailed 3D urban model, a consistent weighted stochastic kinematic model, a climate model accounting for all bus surfaces and environment, and a transient thermal model of the cabin. A validation was performed against dynamic experimental tests. The most demanding mode is for cooling, with a mean cooling demand of 105 kWh/100km in a warm summer day. The heating demand on a cold winter day is around 22 kWh/100km. The components analysis reveals that the occupancy contributes to 33-45% of the cooling demand in summer and the solar components account for 20-42%. Air changes contribute to 20% of the heating demand in winter, and conduction, convection, and internal infrared components represent 40% of the negative load, except for summer when they account for 10-20% of the positive load. A sensitivity analysis has also been performed to quantify the impact of different strategies.

Keywords: Modeling; Thermal load; Electric vehicle; Urban; Bus; Air conditioning.

Nomenclature

GIS: Geographic Information Systems.

HVAC: Heating, Ventilation and Air Conditioning.

CFD: Computational Fluid Dynamics.

GTFS: General Transit Feed Specification.

HBM: Heat Balance Method.

SVF: Sky View Factor.

VF: Radiative View Factor.

TMY: Typical Meteorological Year.

MAPD: Mean Absolute Percentage Deviation.

DTM: Digital Terrain Model.

MINLP: Mixed Integer Nonlinear Programming.

T: temperature.

V: volume.

$\dot{v}$ volumetric flowrate.

H: height.

A: area.

U: heat transfer coefficient.

m: mass.

ρ: density.

c_p: specific heat capacity.

t_{CPU}: computational cost.

n: count.

g: gravity acceleration.

$\dot{n}$ rate.

θ: solar angle of incidence.

α: absorptance.

τ: transmittance.

ϵ: emittance.

G: global irradiance.

B: direct irradiance.

D: diffuse irradiance.

R: reflected irradiance.

IG: infrared irradiance.

$\dot{Q}$ sensible load power.

Q: sensible load energy.

$\dot{I}$ solar radiative heat gain.

$\dot{E}$ long-wave radiative heat gain.

ω: Stefan-Boltzmann constant.

t: elapsed time.

d: distance traveled.

v: velocity.

a: acceleration.

sd: standard deviation.

e: external, outdoor node (subindex).

i: internal, indoor node (subindex).

m: mass node (subindex).

b: body node (subindex).

sky: sky node (subindex).

o: occupancy node (subindex).

a: auxiliary node (subindex).

s: sun node (subindex).

n: normal (subindex).

d: diffuse (subindex).

0: horizontal (subindex).

win: windows (subindex).

wal: walls (subindex).

sol: solar (subindex).

inf: infrared external (subindex).

ach: air changes (subindex).

occ: occupancy (subindex).

aux: auxiliary (subindex).

cci: convection, conduction and internal infrared (subindex).

tot: total (subindex).

p: route point (subindex).

ţ: microtrip (subindex).

$trip$: trip (subindex).

BS: bus stop (subindex).

TS: trip stop (subindex).

lim: limit (subindex).

$door$: bus door (subindex).

$cand$: candidate (superindex).

j: bus surface (superindex).

$+$: positive (superindex).

$-$: negative (superindex).

3.1 Introduction

Transport represents the largest energy-consuming end-use sector in the European Union (EU), with more than a quarter of the total energy consumption and greenhouse gas emissions [1]. The European Green Deal has committed to reduce the emissions before 2050 by at least 90% [2]. While other sectors have already lowered their emissions by 32% since 1990, the EU's transport emissions have increased by 33% [3]. Therefore, the transport sector faces a significant challenge in the coming decades.

Within the transport sector, mobile Heating, Ventilation and Air Conditioning systems (HVAC) represent the main auxiliary load on the battery [4], especially in urban transport [5]. In vehicles with an internal combustion engine, mobile HVAC can have a peak consumption of 40% in warm climates and congested traffic while for electric vehicles, they can reduce the driving range by up to 50% in hot and humid days [6] or by 50-70% under extreme cold conditions [7].

In buses, the thermal requirements are bigger due to the higher volume, transparent area surfaces and occupancy. Thus, bigger HVAC systems are required, which demand a higher energy consumption and reduce the range of electric buses by 30-50% [8].

The main function of the mobile HVAC is to ensure a safe and comfortable thermal environment in the cabin by compensating the heat loads of the vehicle. Accurate, dynamic, low-computational models of cabin heat loads are required to design, simulate, and optimize these systems [9]. These models should cover the following key sub-models:

- A 3D model of the urban area, including buildings, trees and streets.
- A kinematic model, including the speed profile of the real urban route consistent with the bus schedule and the stochastic traffic conditions.
- A climate model, including the skyline and multicomponent radi-

ation in all surfaces of the vehicle.

- A transient thermal model of the vehicle cabin, including the different heat gains and thermal loads.

During the last decades, different analysis and methods have been applied in urban environments to evaluate the energy consumption of vehicles in real driving conditions. For an accurate estimation of the bus consumption in real conditions, a kinematic model that represents the speed profile or driving cycle is essential [10, 11]. Many authors use standard driving cycles, but models that employ synthetic driving cycles derived from real-world operations demonstrate significantly better results [11, 12, 13]. In recent times, several methods and approaches have been developed to build synthetic driving cycles but models based on stochastic techniques are the most suitable due to the non-deterministic nature of real-world traffic [11, 13]. Among the latter, a distinction can be made between those that rely on high-frequency data obtained from real-time data acquisition equipment, which is not readily available and involves high collection costs [12, 14, 15] and those that use low-resolution data [11, 16, 17]. In some of these studies, the authors only focus on the generation of the synthetic driving cycle [12, 13]. Other authors estimate the impact on consumption, although they exclusively model the powertrain [11] or consider other factors such as occupancy, traffic, environmental and route conditions [10, 14]. The previous studies do not model the thermal loads and assume a constant impact on the consumption. In contrast, many studies incorporate thermal load models, but do not consider a driving profile [17, 18] or assume a fixed driving pattern between all bus stops [19]. However, most of these studies have a high-level approach and use excessively simplified climate demand models. In some cases, they do not consider the solar radiation [20, 17, 18], they use models based on a steady state balance [15] or they assume a constant value [16]. Other authors implement a more detailed transient thermal model, but only using one node of air with no walls nor internal mass inertia and without considering the variation the solar radiation due to the shadow casting or the route's orientation [19].

Currently, there are two main approaches to model the vehicle's cabin. On the one hand, Computational Fluid Dynamics (CFD) models are commonly used to calculate in detail the heat transfer, the spatial temperature distribution and the internal airflow [21, 22, 23], or to analyze the occupants' thermal comfort [24, 25, 26, 27]. On the other hand, lumped parameter models are often employed, assuming that the air properties are uniformly distributed in the cabin space. Such models help determine the evolution of the internal temperature or to calculate the heat which has to be removed to maintain the cabin in thermal comfort conditions. Lumped parameter models offer an appropriate balance between accuracy and computational cost and ease the integration with other systems and their control, such as HVAC, vehicle traction or energy management. Furthermore, lumped parameter models have been implemented in flexible and thoroughly validated software such as AMESim [28], Modelica [29], Dymola [30], TRNSYS [31] or MATLAB [32, 33, 34, 35, 36, 37] or in vehicle simulators such as GT-Suite [38], AUTONOMIE [39] or ADVISOR [40]. However, most of these studies have been applied to specific operational conditions or standard test cycles to focus on model validation or calibration [31, 36], sensitivity or parametric analysis [28, 30], energy management strategies [34] or component design [29]. Other authors have used the models in real-world driving cycles [28, 32, 34, 37], but without incorporating spatial models of the route or buildings, nor modeling the climate conditions. Some of these authors have used recorded climate data during the driving route using sensors for model validation [32] or HVAC analysis [37] while others exclusively gather data on real routes for the traction model [28, 34]. Finally, only one study [31] was found for a given interurban vehicle journey and none of them have conducted under real driving conditions in an urban environment.

In conclusion, many studies have been found in literature considering urban environments and cabin thermal models. However, no study has been found integrating both accurate dynamic models to calculate, under real driving conditions in urban environments, the thermal energy demands to help to assist design and optimization of the full HVAC

system, for a given urban route.

Given the previous literature review, the present model includes the following novelties:

1. Integration in a global simulation model over a period of one year, with a time-step of 1 min, a detailed real vector-based 3D urban and route model, a climate conditions model and a transient thermal cabin model.

2. Development of a detailed long-wave and short-wave radiative model including shadowing, view factors, angular-dependent and multicomponent transmittance of windows and multicomponent radiation on the different surfaces of the vehicle over a vehicle routing model based on the real urban service route.

3. Development of a one-year period weighted stochastic urban driving cycle based on low-resolution data consistent with the bus schedule, the actual speed limits of the route and the traffic.

4. Evaluation and justification of hypothesis, including the time-step and the stochasticity of the occupancy.

3.2 Methodology

The modeling approach consists in integrating four models (Fig. 3.1) which are applied sequentially in every time-step. Firstly, the geographic information system or GIS model (Section 3.2.3) is applied to obtain, on the one hand, a vectorial-based 3D model of the city, including buildings and trees and, on the other hand, a raster-based digital terrain model (DTM) of the streets. Secondly, the kinematic model (Section 3.2.4) is developed to construct a weighted stochastic driving cycle for one-year period based on low-resolution open data of the route (GTFS), the velocity limits of the streets and the generation of weighted stochastic traffic stop points using the intersections of the street network. Thirdly, the climate model (Section 3.2.5) is performed to obtain, on the one hand and for each time-step, the air nodes temperature (external and internal) and the multicomponent radiation fluxes and skyline on each surface of the bus, both based on representative long-term climate data of the city (TMV), the solar geometry and the previous model outputs. The thermal capacitances and heat transfer coefficients of each node and surface are obtained, based on the bus geometry and on the thermophysical properties of the different materials. Fourthly, the thermal model (Section 3.2.6) is used to calculate, using a system of ordinary differential equations, the different heat gains, the mass and body node temperatures and the thermal loads and its components, based on the bus optical properties, the model parameters for occupancy, air changes and auxiliary and the conditions model outputs. All the models have been developed in R [41] and are integrated in a global model, which allows simulating the vehicle under the dynamic and complex conditions of the urban environment within a 1-min time-series along a representative year.

3.2.1 Location and climate conditions

The present study has been performed in Valencia, Spain (12 masl, 39°28′12″N, 0°22′35″O), which is characterized by a hot-summer Mediterranean climate or Csa, according to the Köppen-Geiger climate

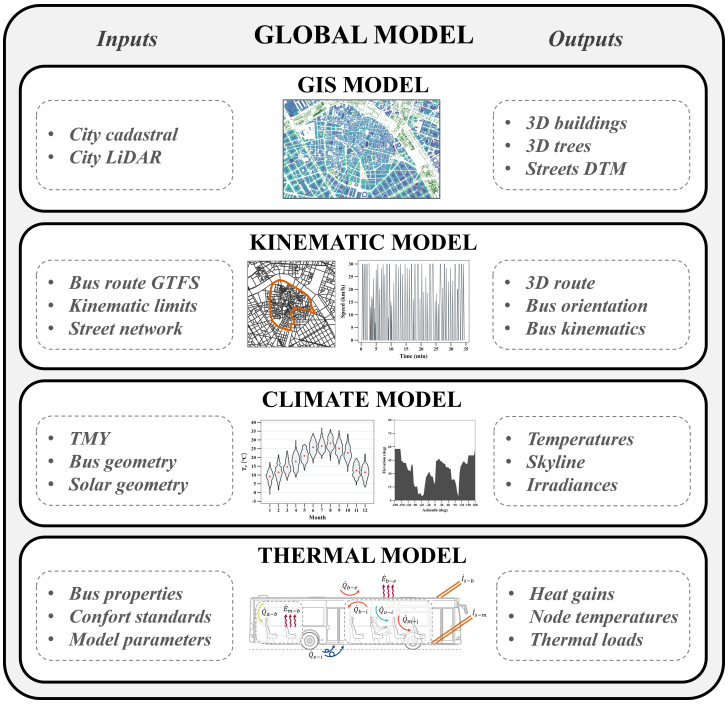

Figure 3.1: Scheme of the methodology.

classification system [42]. Valencia can be taken as an example of a Mediterranean city [43].

Figure 3.2 represents the diurnal hourly global horizontal irradiance distribution for each month in TMY3 dataset of the period 2005-2020 from satellite-based PVGIS-SARAH2 database [44] with a mean value ranging from $235\,\mathrm{W\,m^{-2}}$ in January to $516\,\mathrm{W\,m^{-2}}$ in August. The hourly dry bulb temperature distribution within the driving cycle and its schedule is in the mean range of 9.6 °C, with an annual minimum of −1 °C and a maximum of 37 °C.

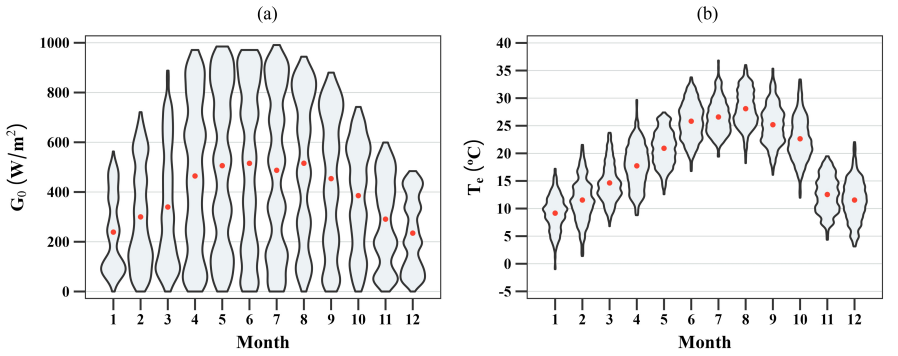

Figure 3.2: (a) Diurnal hourly global horizontal irradiance G_0 distribution and (b) hourly dry bulb temperature T_e distribution in the operation range time for each month in TMY dataset.

3.2.2 Route and vehicle description

This study is based on real data from the bus and the driving route. Among the different driving routes of the urban service fleet [45], the route which has been selected has an electric bus (Irizar model i2e). Route C1 is circular, with a total length of 4.99 km through the city town (Fig. 3.3). The vehicle is a 12 m standard bus, with dimensions 2.99 m height x 2.55 m width x 11.95 m longitude and standard geometric and thermophysical characteristics of an urban bus with 80 passenger capacity. The characterization of the vehicle is summarized in Table 3.1. The data has been obtained from the detailed geometry of the vehicle, and from the thermophysical and optical properties of the different materials. All windows are one-pane 6 mm thick with 15 kg m^{-3} density [46], 1 W m^{-1} K^{-1} thermal resistivity [47] and glass k value of 0.8 W m^{-1} K^{-1} thermal resistivity [48] and 1,400 J kg^{-1} K^{-1} specific heat capacity [49]. The frontal unit is a laminated glass with anti-reflective coatings while the other windows are tempered body-tinted glazing. The walls are multilayer bodies with a red paint exterior coating with 0.88 of thermal emittance and 0.57 α solar absortance [49]. The convective coefficients used for both walls and windows are 5 W m^{-2} K^{-1} for the indoor surfaces [50] while for outdoor surfaces are

calculated according to the bus speed.

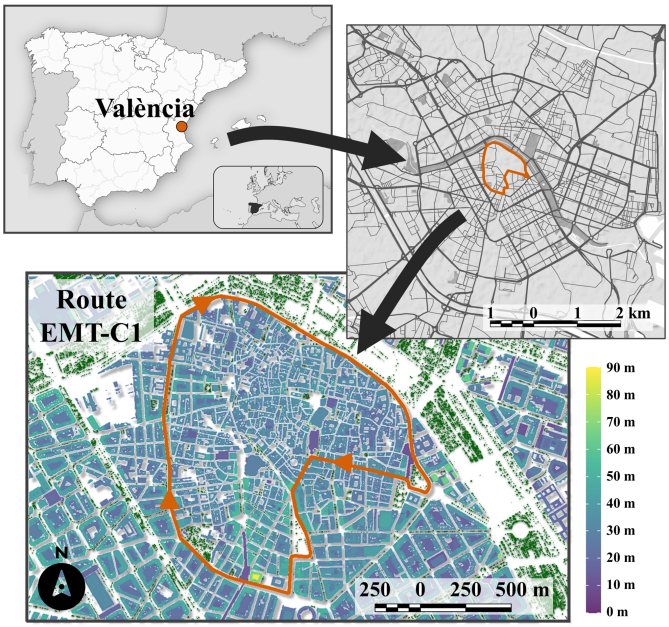

Figure 3.3: Location, 3D vectorial model and bus route of the case study in València, Spain.

3.2.3 GIS model

This model generates a 3D spatial representation of the city, distinguishing between buildings, trees, and streets. The buildings have been modeled using a 3D vector-based model based on cadastral and altimetric information of the LIDAR point cloud using the methodology explained in Ref. [50]. To represent the streets, a digital terrain model (DTM) or raster-based altimetric model of 2 m of resolution has been generated. This DTM was built from ground points of the LIDAR dataset employing a spatial interpolation based on a Delaunay triangulation approach [51, 52]. To represent the trees, a 3D vector-based model has been employed based on [53], which yields the height and

Table 3.1: Geometry of windows and walls, thermophysical and optical properties for each bus surface.

	Front	Left	Right	Back	Roof	Floor
				Windows		
A_{win} (m^2) [45]	3.0	11.2	16.5	1.2	0.0	0.0
τ_{win} [46]	0.69	0.45	0.45	0.45	0.45	0.45
q_{win} [46]	0.28	0.50	0.50	0.50	0.50	0.50
ϵ_{win} [48]	0.84	0.84	0.84	0.84	0.84	0.84
				Walls		
A_{wal} (m^2) [45]	4.6	24.7	19.5	6.3	31.1	31.1
ρ_{wal} ($\text{kg}\,\text{m}^{-3}$) [31]	55.3	55.3	55.3	55.3	45.6	19.0
$c_{p,\text{wal}}$ ($\text{J}\,\text{kg}^{-1}\,\text{K}^{-1}$) [31]	1402	1402	1402	1402	1402	1337
R_{wal} (kW) [31]	0.690	0.690	0.690	0.690	0.235	0.690

segmented crown of each individual tree.

3.2.4 Kinematic model

Once the 3D model of the city is obtained, the driving route and the kinematic model are obtained for a year of simulation period in a daily range from 06:00h to 24:00h according to the commercial schedule of the Valencia bus network [45]. First, the spatial information of the simulated route and bus stops have been extracted from the public transport feeds (GTFS) [54] and discretized into points every 1 m, where the azimuth or direction of the route has been obtained. Second, the ground height and slope have been calculated from the DTM.

The objective of the kinematic model is to construct a synthetic driving cycle that characterizes the stochastic behavior of the kinematic variables such as elapsed time t, distance traveled d, velocity v, and acceleration a in the real-world traffic conditions, at each discretized point along the route during the simulation period. To accomplish this goal, an algorithm has been developed for the construction of a weighted stochastic driving cycle, starting from the microtrips approach and incorporating a generation of weighted stochastic stop points (referred to as traffic stops) using low-resolution open data (GTFS), and applying

a mixed-integer nonlinear programming (MINLP) formulation.

A microtrip μ is defined as a section of a driving route between two consecutive time points at which the bus has zero speed (Figure 3.4). These stop points could be bus stops as well as traffic stops, which may include instances such as traffic lights, stop signs, pedestrian crosswalks, or pauses prompted by congested traffic conditions. A trip is the journey between two bus stops, which is composed of one or more microtrips and the time spent at the stops. To construct the model,

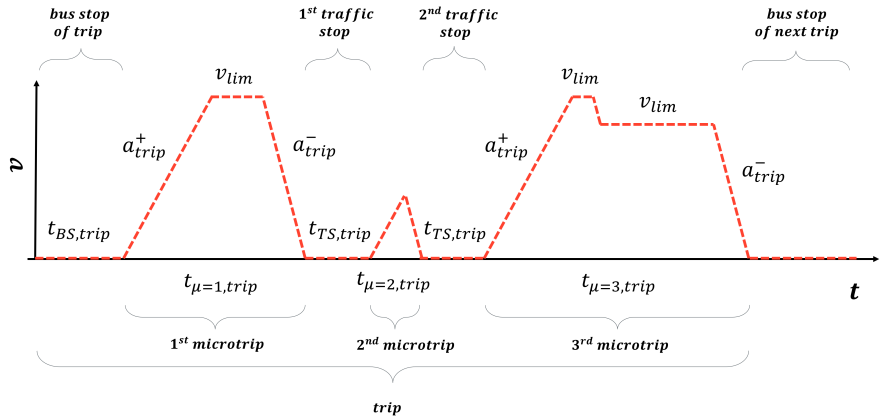

Figure 3.4: Synthetic speed profile. In this example, a trip is composed of the bus stop of duration t_{BS}, three microtrips of duration t_{μ}, and two traffic stops of duration t_{TS}. Other elements are the acceleration, which can be positive a^+ or negative a^-, as well as the velocity limit v_{lim} at each discretized point of the trip.

two open data sources are available: the GTFS dataset and the city's street network, including the speed limits. On the one hand, the GTFS dataset provides the trip duration t_{trip} and the distance traveled d_{trip} for each bus line and day of the year. These values inherently contain the real-world traffic conditions. On the other hand, from the city's street network, the associated speed limit $v_{lim,p}$ at each point p along the trip and the intersections of the route with the remaining streets are collected. In this study, these intersections have been considered as

potential candidates for traffic stops in the stochastic generation of stop points.

To obtain the kinematic variables at each discretized point p, a MINLP problem has been formulated for each trip. The objective function is defined as the minimization of the absolute deviation between the sum of times for the microtrips and stops of the trip and the total trip time t_{trip}. This problem is individually defined and solved for each trip, being subjected to multiple constraints: spatial (traveled distance), temporal (duration of microtrips and stops), velocity (specific street speed limits), acceleration (bus, comfort and safety limits), and their interrelations in accordance with Eq. 3.1.

$$
\begin{aligned}
&\min \left| t_{BS,trip} + n_{TS,trip} \cdot t_{TS,trip} + \sum_{\mu} t_{\mu,trip} - t_{trip} \right| \\
&\text{s.t.:} \\
&a_{p,\mu} = \frac{v_{p+1,\mu}^2 - v_{p,\mu}^2}{2 \cdot d_{p,\mu}} \qquad a_{p,\mu} \in \{a_{trip}^-, 0, a_{trip}^+\} \\
&t_{p,\mu} = \frac{2 \cdot d_{p,\mu}}{v_{p+1,\mu} - v_{p,\mu}} \qquad \sum_{p} t_{p,\mu} = t_{\mu,trip} \\
&\sum_{\mu} d_{\mu,trip} = d_{trip} \qquad \sum_{p} d_{p,\mu} = d_{\mu,trip} \\
&t_{BS,trip}, t_{TS,trip}, n_{TS,trip} \geq 0 \qquad 0 \leq v_{p,\mu} \leq v_{p,\mathrm{lim}} \\
&t_{p,\mu}, t_{\mu,trip}, t_{trip} \geq 0 \qquad d_{p,\mu}, d_{\mu,trip}, d_{trip} \geq 0
\end{aligned}
\tag{3.1}
$$

where $a_{p,\mu}$, $v_{p,\mu}$, $d_{p,\mu}$, $t_{p,\mu}$ denote the acceleration, velocity, traveled distance, and elapsed time at point p in the microtrip μ, and $d_{\mu,\mathrm{trip}}$, $t_{\mu,\mathrm{trip}}$ the total traveled distance and elapsed time of the microtrip μ in a certain trip.

To address this, the genetic algorithm developed in [55] has been applied. Through this approach, five variables have been obtained for each trip: the duration of the bus stop $t_{\mathrm{BS,trip}}$, the number of traffic stops $n_{\mathrm{TS,trip}}$, their respective duration $t_{\mathrm{TS,trip}}$, and the positive a_{trip}^+ and negative a_{trip}^- accelerations. Table 3.2 shows the initial values,

upper, and lower limits defined to solve the problem. For the weighted

Table 3.2: Initial values (IV), upper (UL) and lower (LL) limits for the MINLP problem.

	$n_{TS,trip}$	$t_{BS,trip}$ (s)	$t_{TS,trip}$ (s)	a^{+}_{trip} (m/s^2)	a^{-}_{trip} (m/s^2)
IV	0	15	20	0.9	-0.7
LL	0	0	5	0.4	-0.4
UL	$n^{\text{cand}}_{TS,trip}$	25	30	1.5	-2

stochastic selection of traffic stops within each trip, a set of candidate points denoted as $n^{\text{cand}}_{\text{TS,trip}}$ are obtained from the intersections of the trip with other streets. The algorithm then selects combinations of these candidates using random weighted sampling. The probability weights for each candidate are assigned based on the speed limit of the respective candidate in comparison to the rest of the candidates within the trip. Consequently, intersections with streets featuring higher speed limits have a greater likelihood of being chosen as traffic stops.

Furthermore, two convergence strategies are applied to the algorithm when it exceeds a certain number of iterations, depending on the sign of the objective function. If the objective function is positive, indicating that the microtrip and stop times exceed the trip duration, the speed limits are increased by multiplying $v_{\text{lim,p}}$ by a factor greater than one. On the other hand, if the objective function is negative, the number of candidate traffic stops is increased using random weighted sampling to the non-stop trip points and by assigning its probability weights based on the distance from other traffic stop candidates. Then, points that are farther away from other candidates are more likely to be selected.

Figure 3.5, as an illustrative example, the speed profile and orientation obtained for a complete bus journey of the studied route is presented.

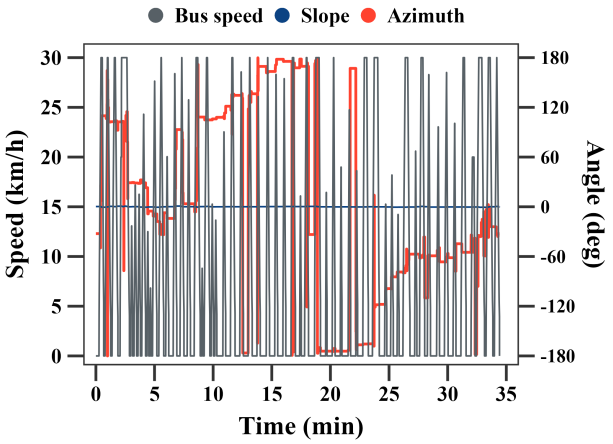

Figure 3.5: Speed profile obtained for a complete bus journey.

3.2.5 Climate Model

This model obtains the climate conditions at each bus surface in any position and time step of the driving route. The starting point is a year time series of hourly meteorological variables (TMY). The variables obtained from TMY are the external outdoor temperature T_e, the horizontal infrared irradiance from sky IG_0, the direct normal irradiance B_n, and the global horizontal irradiance G_0.

The indoor temperature T_i is determined in every time step using the regulation curve described in the UNE-EN 14750 standard [56] as a function of the TMY external outdoor temperature T_e. The sky temperature T_{sky} is obtained from the TMY horizontal infrared irradiance from the sky $IG_{0-\text{sky}}$ according to [57].

Lastly, the skyline or horizon profile has been calculated for each point of the route and each side of the vehicle. The use of the skyline is important to model the impact of the real city environment on both long-wave and solar radiation heat gain components. Firstly, the skyline helps to determine whether the surface is shadowed when the sun is behind its horizon profile at a specific time, which impacts on the

direct solar irradiance component. Secondly, the skyline allows to measure the Sky View Factor (SVF), defined as the proportion of the sky which is visible. The SVF has an impact on the diffuse and reflected solar irradiance components and also helps define the radiative view factors used in the long-wave radiation heat exchanges between the bus surfaces, the sky, and the surrounding city surfaces.

Finally, the direct B^j, diffuse D^j, and reflected R^j irradiance components on each of the six j bus surfaces are obtained in each time step using the TMY solar radiation variables, the solar geometry [58], the city surfaces reflectance [59], the slope and orientation of each bus surface, and the shadow effects obtained from the skyline.

3.2.6 Thermal Model of the Cabin

A transient dynamic thermal model has been developed to predict the sensible thermal load (from now onward, thermal load) in the cabin of the bus Q_i under variable ambient conditions, including shadowing and the orientation and slope of the vehicle during the route. This model is based on a lumped-parameter approach, with three bus nodes, assuming that the temperature is uniform in each node: the indoor air node i, the bus body envelope b, representing all internal and external window and wall surfaces of the bus enclosure, and the interior mass m, representing the seats, dashboard and other thermal masses of the vehicle. The thermal model is implemented as a system of ordinary differential equations, using the Heat Balance Method (HBM) [48]. The heat transfer between seven nodes enables the calculation of the mean temperature of the indoor air T_i, the bus body T_b, and the bus mass T_m. The external nodes are the external air node e, the surrounding city surfaces, the sky, and the sun. The thermal load depends on multiple energy and mass flows (Figure 3.6), conceptualized as heat gains or contributions, which can be convective $\dot{Q}$, solar radiative $\dot{I}$, or long-wave radiative $\dot{E}$.

Eq. 3.2 represents the energy balance of the indoor air. The total mass of air has been assumed to be constant.

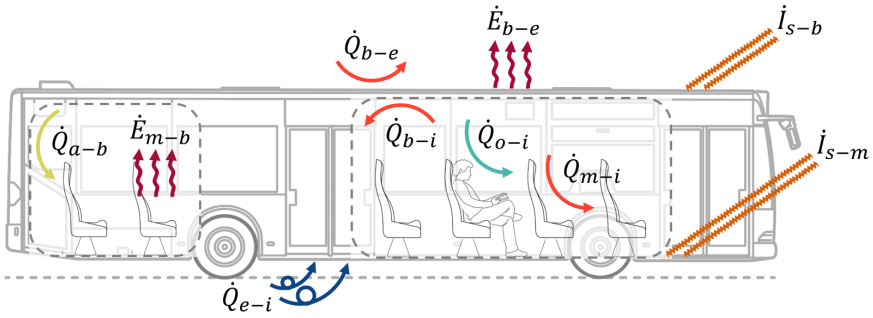

Figure 3.6: Heat gains of the thermal model. $\dot{Q}_{b-i}$ is the heat transfer from the body to the indoor air, $\dot{Q}_{m-i}$ from the mass to the indoor air, $\dot{Q}_{o-i}$ is the occupancy heat gain, $\dot{Q}_{e-i}$ is the heat gain by air changes, $\dot{Q}_{e-b}$ the heat transfer from external to body, $\dot{Q}_{a-b}$ is the heat gain from auxiliaries to body, $\dot{E}_{e-b}$ the long-wave radiation exchange between the exterior and the body, $\dot{E}_{m-b}$ the long-wave radiation exchange between the mass and the body, $\dot{I}_{s-b}$ the solar radiation heat gain to the body and $\dot{I}_{s-m}$ the solar radiation heat gain to the mass.

$$\frac{dQ_i}{dt} = V_i \cdot \rho_i \cdot c_{p,i} \frac{dT_i}{dt} = \dot{Q}_{b-i} + \dot{Q}_{m-i} + \dot{Q}_{o-i} + \dot{Q}_{e-i} \tag{3.2}$$

where Q_i represents the thermal load, i.e., the power to add to or remove from the cabin to have the comfort temperature. The occupancy $\dot{Q}_{o-i}$ heat gain, which includes the heat losses from the occupants, has been modeled using the hourly occupancy schedule of a mean day as a long-term representative time series, provided by the city bus service [45] and the sensible heat load of a seated person in accordance with the UNE-EN 14750 standard [56]. The heat gain by air changes $\dot{Q}_{e-i}$ includes the infiltrations of external air into the vehicle due to doorway openings and by leakage due to faulty sealing. The mean air changes by infiltrations are calculated in $4.34\,\mathrm{h}^{-1}$ considering the impact of the bus speed as in [60]. Equation 3.3 describes the volumetric flowrate due to doorway openings $v_{e-i,trip}$ in a certain trip taking into account the air exchange through the doors orifice and the passage airflow which occur when the

passengers come in or out of the bus [61].

$$v_{e-i,trip} = \frac{t_{BS,trip}}{t_{trip}} \left(\frac{A_{door}}{6} \cdot \sqrt{g \cdot \left| \frac{T_e - T_i}{T_e} \right| \cdot H_{door}} + n_{occ} \cdot V_{occ} \right) \quad (3.3)$$

where $\frac{t_{BS,trip}}{t_{trip}}$ is the ratio of time that the doors are opened in the bus stop in a given trip, A_{door} and H_{door} are the area and height of the opened doors [45], g is the acceleration of gravity, $V_{occ} = 0.25\,\mathrm{m}^3$ is the exchanged volume due to each occupant's passage according to [61], and n_{occ} is the occupant's passage rate at which passengers leave or enter the bus, assumed as $\frac{1}{10}$ of the stayed occupancy boarding or alighting through the doors during the bus stop in a given trip. As previously explained, the two last heat gain models ($\dot{Q}_{o-i}$ and $\dot{Q}_{e-i}$) are related to the occupancy, which exhibits an important stochastic tendency. In section 3.2.2, a comprehensive evaluation of adopting a stochastic model is conducted.

The heat gain from masses to indoor air $\dot{Q}_{m-i}$ represents the convective heat exchange between both nodes, expressed in Equation 3.4.

$$\dot{Q}_{m-i} = U_{m-i} \cdot A_m \cdot (T_m - T_i) \quad (3.4)$$

where $U_{m-i} = 12\,\mathrm{W\,m^{-2}\,K^{-1}}$ is the heat transfer coefficient between the mass and the indoor air according [36] and A_m the area of the interior mass assumed $100\,\mathrm{m}^2$, consistent with [36] considering the size differences.

The heat gain $\dot{Q}_{b-i}$ represents the convective heat exchange from the body node to the indoor air, described in Equation 3.5.

$$\dot{Q}_{b-i} = U_{b-i} \cdot A_b \cdot (T_b - T_i) \quad (3.5)$$

where $U_{b-i} = 2.75\,\mathrm{W\,m^{-2}\,K^{-1}}$ is the heat transfer coefficient between the body and the indoor air and A_b the body area, both obtained from values of each surface of the bus, including windows and walls.

Equation 3.6 is the energy balance of the vehicle body.

$$m_b \cdot c_{p,b} \frac{dT_b}{dt} = -\dot{Q}_{b-i} + \dot{Q}_{e-b} + \dot{Q}_{a-b} + \dot{E}_{e-b} + \dot{E}_{m-b} + \dot{I}_{s-b} \quad (3.6)$$

where $m_b = 5{,}534\,\mathrm{kg}$ is the body mass and $c_{p,b} = 1{,}193\,\mathrm{J\,kg^{-1}\,K^{-1}}$ is the specific heat capacity calculated from volumes and densities of windows and the multilayered walls.

The long-wave radiation exchange between the exterior and the body $\dot{E}_{e-b}$ can be estimated according to Equation 3.7, obtained as the result of the heat transfer between the body surfaces j, both walls and windows, and the independent contributions of the sky and the surrounding city surfaces. The temperature of the surrounding city surfaces is considered uniform and equal to the external temperature T_e and the radiative view factors are obtained using the sky view factor.

$$\dot{E}_{e-b} = \sigma \cdot \sum_j \Big((\epsilon^j_{wal} \cdot A^j_{wal} + \epsilon^j_{win} \cdot A^j_{win}) \cdot \Big(SVF^j \cdot (T^4_{sky} - T^4_b) + (1 - SVF^j) \cdot (T^4_e - T^4_b) \Big) \Big) \quad (3.7)$$

where σ is the Stefan-Boltzmann constant.

The long-wave radiation exchange between the masses and the body $\dot{E}_{m-b}$ is obtained through Equation 3.8, where $\epsilon_m = 0.95$ [62] is the emittance of the interior mass and $\mathrm{VF}_{m-b} = 1$ [36] is the view factor from the interior mass towards the body.

$$\dot{E}_{m-b} = \sigma \cdot \epsilon_m \cdot \mathrm{VF}_{m-b} \cdot A_m \cdot (T^4_m - T^4_b) \quad (3.8)$$

The solar radiation absorbed by the body $\dot{I}_{s-b}$ is obtained according to Equation 3.9, based on the global irradiance on each surface G^j calculated in the climate model.

$$\dot{I}_{s-b} = \sum_j (\alpha^j_{wal} \cdot A^j_{wal} + \alpha^j_{win} \cdot A^j_{win}) \cdot G^j \quad (3.9)$$

The convective heat gain from external air to body $\dot{Q}_{e-b}$ is obtained through Equation 3.10.

$$\dot{Q}_{e-b} = U_{e-b} \cdot A_b \cdot (T_e - T_b) \quad (3.10)$$

where U_{e-b} is the heat transfer coefficient between the body and the external air, obtained from the geometry and thermophysical properties

for each bus surface and calculating the convective coefficient through Equation 3.11, as a function of the bus speed v according to [63].

$$h_{e-b} = 9 + 3.5 \cdot v^{0.66} \tag{3.11}$$

The heat gains due to auxiliaries $\dot{Q}_{a-b}$ is fixed to 600 W, as 10% of the waste heat of electric motor, motor controller, battery, and inverters [64].

Equation 3.12 is the energy balance of interior mass node. The thermal energy of the masses is calculated as the product of their thermal mass, considered constant, and the variation of their temperature, considered uniform.

$$m_m \cdot c_{p,m} \cdot \frac{dQ_i}{dt} = -\dot{Q}_{m-i} - \dot{E}_{m-b} + \dot{I}_{s-m} \tag{3.12}$$

where $m_m = 1{,}500\,\mathrm{kg}$ are the mass and $c_{p,m} = 750\,\mathrm{J\,kg^{-1}\,K^{-1}}$ the specific heat capacity according to [30].

The solar radiation absorbed by the mass $\dot{I}_{s-m}$ is obtained according to Equation 3.13, starting from the direct B^j, diffuse D^j, and reflected R^j irradiance on each surface j obtained from the climate model and considering the angular behavior of the solar energy transmittance of windows. Then, the direct radiation transmittance of each window $\tau^j_{n,win}$ is calculated for each time-step depending on the solar angle of incidence θ^j according to Ref. [65], who address an accurate model of the solar transmittance at angle of incidence given the normal incidence transmittance, the number of panes in the window and the type of coating. For the diffuse and reflected radiation transmittance $\tau^j_{d,win} = \tau^j_{n,win}(60\circ)$ has been assumed in all windows, according to Ref. [58].

$$\dot{I}_{s-m} = \sum_j \left(B^j \cdot \tau^j_{n,win}(\theta^j) + (D^j + R^j) \cdot \tau^j_{d,win} \right) \cdot A^j_{win} \tag{3.13}$$

The system of differential equations is solved every time-step with an ode-solver. The cabin is pre-conditioned, as a common and recommended strategy [66]. The different components of the total cabin load

are calculated in order to quantify the different contributions and to help obtain more effective optimization strategies. The total load has been divided into six components:

- Solar $\dot{Q}_{\text{sol}}$, which measures the impact of $\dot{I}_{s-b}$ and $\dot{I}_{s-m}$.
- External infrared $\dot{Q}_{\text{inf}}$, which quantify the impact of $\dot{E}_{e-b}$.
- Air changes $\dot{Q}_{\text{ach}}$, which addresses the impact of $\dot{Q}_{e-i}$.
- Occupancy $\dot{Q}_{\text{occ}}$, corresponding to $\dot{Q}_{o-i}$.
- Auxiliary $\dot{Q}_{\text{aux}}$, due to $\dot{Q}_{a-b}$.
- Convection, conduction, and internal infrared $\dot{Q}_{\text{cci}}$ that groups the rest of thermal gains corresponding to exchanges between the three bus nodes and the conduction-convection between these and the external air node.

The values of the load components are obtained in each time step as the difference of the total load and the ode result obtained when the corresponding thermal gains have been set to zero.

3.3 Validation and Justification of Hypotheses

3.3.1 Validation

Kinematic model

In this section, the validation of the consistency of the kinematic model is performed. Figure 3.7 shows the comparison of the normalized trip elapsed time t_{trip} between the low-resolution GTFS data and the prediction obtained by solving the MINLP of Eq. 3.1 in all simulated trips. The synthetic driving cycle is accurate and consistent with the bus schedule along the year since the maximum annual error is only 1%.

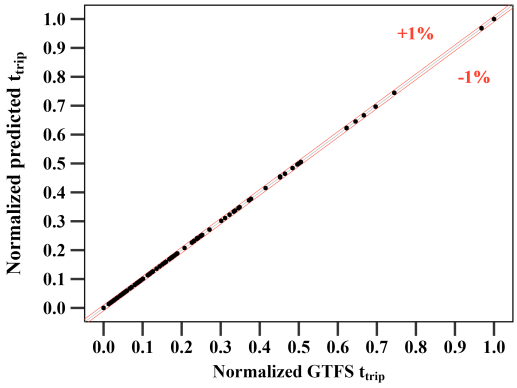

Figure 3.7: Normalized trip time comparison.

Thermal model

The thermal model was firstly validated against a warm-up with an air heater and the following cool-down and secondly was validated parking the vehicle under real outdoor conditions during several days of summer, both using the same data and boundary conditions reported in the study [36]. Figure 3.8 shows a comparison of measured and simulated cabin air temperature and the mean absolute percentage deviation

or MAPD=$\frac{1}{n}\sum_t^n \left|\frac{\hat{y}(t)-y(t)}{y(t)}\right|$, where $\hat{y}$ is the prediction and y is the actual value. As can be observed in Figure 3.8, the model reproduces accu-

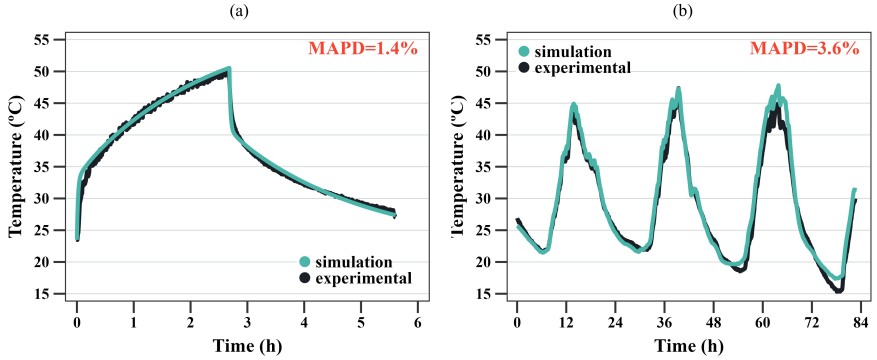

Figure 3.8: Comparison of experimental and simulation indoor cabin temperatures.

rately the experimental data, with a mean absolute percentage error of 1.4% and 3.6%. With these results, the thermal model and its ability to reproduce dynamic evolution are considered validated.

3.3.2 Justification of Hypotheses

Two important hypotheses have been studied in this section: the time-step and the stochasticity of the occupancy. As the main objective of the model is to predict the total thermal load within a trip, the load has been selected as the target variable, and its sensitivity has been analyzed depending on the assumptions.

Simulation time-step and computational cost

The present section explores the impact of the simulation time-step in both the accuracy and the computational cost. 14 different time-steps have been studied. For every month, a representative day has been simulated, more particularly, the 15th of each month. Figure 3.9 shows the MAPD of mean daily cumulative total thermal loads,

both for positive Q^{+}_{tot} and negative Q^{-}_{tot} contributions with respect to the smallest time-step (1 second). The total computational cost per trip t_{CPU} in seconds is also represented on the second y-axis. For the evaluation of the computational cost, all simulations used the same computer with the following specifications: Processor Intel©Core$^{\text{TM}}$ i5-7300U CPU@2.60GHz, RAM: 8.0 GB and OS Windows 10, 64 bit. The

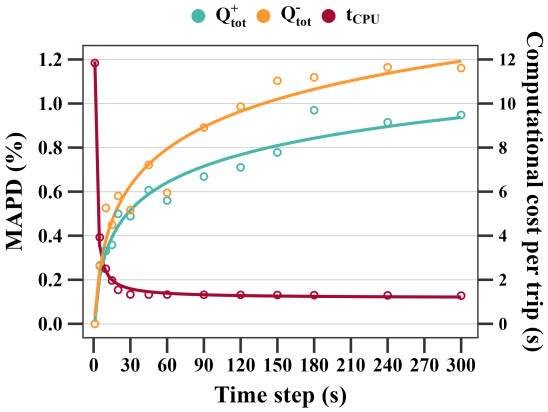

Figure 3.9: Impact of the time-step on the MAPD of the mean daily cumulative total thermal loads and computational cost per trip

MAPD of both positive and negative thermal loads increase almost logarithmically with increasing time-steps while the computational cost decreases substantially when increasing the time-step from 1 to 20s. The MAPD for a 1-min time-step is lower than 1% and the computational cost is lower than 2 seconds. Thus, a time-step of 1 min has been selected in the remaining part of the study, as a compromise between good accuracy and an affordable computational cost.

Stochasticity of the occupancy

This section studies the impact on the thermal load of adopting a stochastic model for two parameters associated with the occupancy. The occupancy has been modeled in the thermal model using the mean day hourly schedule as a long-term representative time series, while the

rate at which passengers leave or enter the bus is assumed to be 1/10 of the occupancy in each bus stop. However, it is widely known that passenger behavior exhibits a stochastic nature.

In order to evaluate the influence of the stochasticity of these parameters on the thermal load, a total of 20 samples for each variable are generated. The samples are generated multiplying the original values by a random factor for the normal distribution with a mean equal to 1 and two cases of standard deviation sd, a moderate dispersion (sd = 0.1) and a high dispersion (sd = 0.2). The evaluation of each variable has been conducted independently, while using the deterministic model of the other variable, in order to evaluate the individual influence of each parameter. Figure 3.10 (a) shows the distribution, boxplot and mean (red point) of the original occupancy and the samples of each dispersion case. The simulations have been carried out and the impact on both

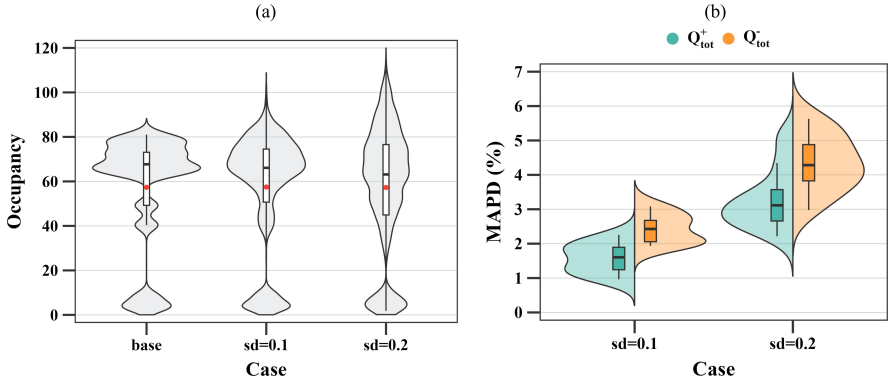

Figure 3.10: Stochasticity of the occupancy.

the total daily cumulative positive and negative thermal load has been evaluated. Figure 3.10 (b) shows the distribution and boxplot of the MAPD for both positive and negative thermal load for the occupancy stochastic model.

The impact of a moderate dispersion is not significant, with a frequent MAPD of 2% and generally below 4%. In contrast, the influence of a high dispersion can reach a non-negligible magnitude, with a max-

imum MAPD of 6-7%.

Since actual dispersion data of occupancy is not available, the deterministic has been retained for the remaining studies.

In the case of the ratio of passengers boarding or leaving at each bus stop, the findings indicate that there is no influence on the thermal load for any level of dispersion, as the maximum MAPD is less than 0.1%.

3.3.3 Simulation Results

Figure 3.11 shows the node temperatures for a representative day of a cold month (January), a mild weather month (March), and a warm month (July). Figure 3.12 represents the inter-daily distribution of the thermal load. The range of indoor air temperatures is (19 °C,

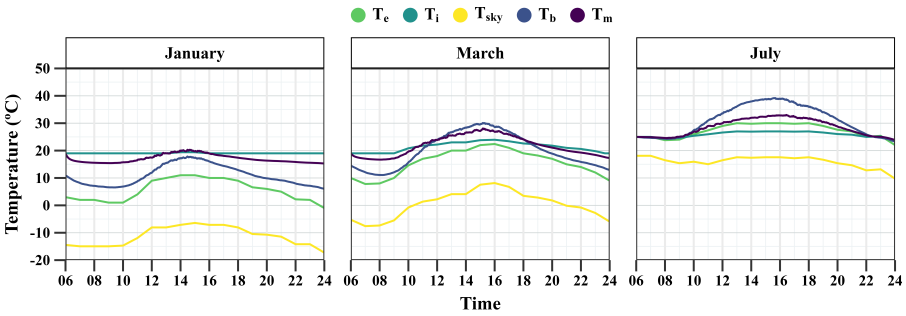

Figure 3.11: Temperatures of the external node T_e, indoor air node T_i, sky T_{sky}, body node T_b, and mass node T_m in a representative day of January, March, and July.

29 °C), based on the outdoor external temperature range according to the regulation curve described in the UNE-EN 14750 standard [56]. The body temperature is highly influenced by solar radiation, reaching around 10 °C compared to the outdoor air temperature in summer. The mass node temperature is also influenced by solar radiation, but even more by the indoor air temperature and remains within a relatively

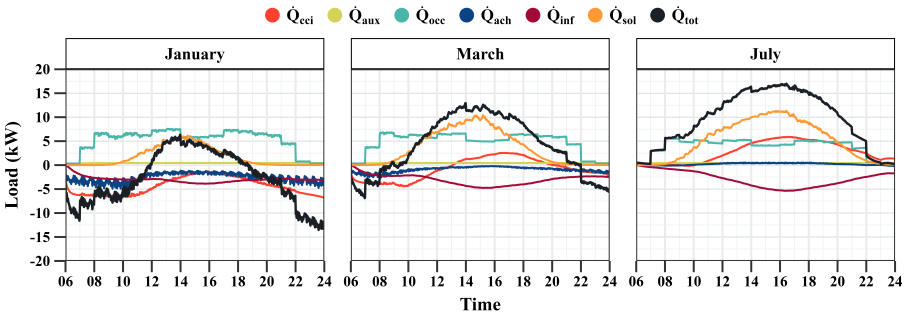

Figure 3.12: Instantaneous thermal load components in a representative day of January, March, and July. Components: conduction, convection, and internal infrared (Q_{cci}), auxiliary (Q_{aux}), occupancy (Q_{occ}), air changes (Q_{ach}), external infrared (Q_{inf}), solar radiation (Q_{sol}), and total (Q_{tot}).

small range of around $\pm 5\,\mathrm{K}$, except for the summer midday, when it reaches $+7\,\mathrm{K}$.

In winter, the most important negative load component is the conduction, convection, and internal infrared, mainly due to low external temperatures, yielding a peak of $-6.8\,\mathrm{kW}$. This component is closely related to infrared external exchanges, and both of them being linked to the body temperature. If the body temperature does not exceed the interior temperature, both components remove heat from the cabin, with conduction, convection, and internal infrared playing a predominant role. However, shortly after the body temperature surpasses the interior temperature, this component becomes positive due to heat transfer into the cabin, while the infrared external component becomes predominant in heat extraction, with a peak of $-5.4\,\mathrm{kW}$ in summer when the body temperature reaches $40\,^{\circ}\mathrm{C}$. Both components effectively reflect the thermal inertia of the body node, which transfers the absorbed heat, mainly through solar radiation, but with some delay and damping. Another significant component during winter is the air exchanges, which reach $-4.8\,\mathrm{kW}$ when the outdoor temperature is lower. This component exhibits pronounced fluctuations, exceeding $2\,\mathrm{kW}$, due to the opening of doors at bus stops.

In summer and spring, the most important component is the solar radiation positive load, with a peak of 11.3 kW in summer and 10.4 kW in spring.

Occupation has a significant positive contribution along the year, between 4.1 kW and 7.4 kW, from 8:00 to 21:00. The contribution of auxiliaries over the year and the contribution of the air changes in summer are nearly negligible.

Figure 3.13 shows the mean daily cumulative thermal loads for each month, stacked in their different components (bars) and the totals (points), both positive and negative. It is important to note that the sum of the cumulative components does not correspond to the cumulative totals since, in each time-step, the total values are the net balance of positive and negative contributions. Therefore, there are components with both signs on the same day, which means that its contribution has cooled (negative) and heated (positive) the vehicle in different moments of the day. This provides an overview of the energy requirements for an HVAC system (totals) and their origin (load components). The cooling demand for a warm summer day is around 162 kWh, while the heating demand for a cold winter day is around 34 kWh. On the one hand, the cooling demand is higher than 115 kWh between May and September and the heating demand is higher than 20 kWh between December and March. On the other hand, the heating demand is lower than 10 kWh between June and October and the cooling demand is lower than 40 kWh in January and December. These results are in accordance with the International Council on Clean Transportation [67], International Energy Agency [68], or an extensive campaign of urban buses in Italy [69].

The cumulative occupancy component is nearly constant over the year, being 65-73% of total cumulative positive in winter and 33-45% in summer. The cumulative external infrared component is also almost constant, accounting for 35-44% of total cumulative negative in winter and 67-91% in summer. The cumulative solar component has a relative weight of 20-42% of the total cumulative positive load throughout the year, reaching more than 40% between April and August. The

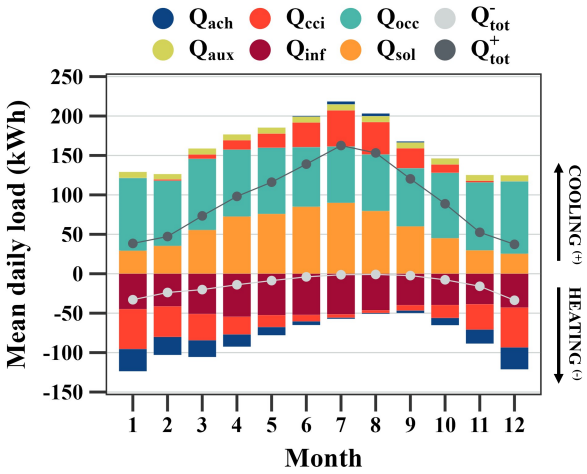

Figure 3.13: Cumulative mean daily thermal loads of the air changes component Q_{ach}, conduction, convection, and internal infrared component Q_{cci}, occupancy component Q_{occ}, auxiliary component Q_{aux}, external infrared component Q_{inf}, and solar radiation component Q_{sol}. Bars are the thermal load components and points the total load.

cumulative air changes component is only important in the heating demand with a contribution exceeding 20% between November and March. Lastly, the conduction, convection, and internal infrared component play a significant role in the negative load during winter, contributing to around 40%. On the contrary, in summer, this component contributes to the positive load but with a slightly lower percentage, ranging from 10-20%.

Based on these findings, as the occupation and external infrared load are almost constant over the year, the variability of the cooling and heating demand is mainly dependent on the positive solar load component, the negative air changes load component, and on conduction, convection, and internal infrared components (with a positive or negative sign depending on the season).

3.3.4 Sensitivity Analysis

In this section, a sensitivity analysis has been performed to understand and quantify the influence of different parameters and conditions on the thermal load. Table 3.3 describes the parameters addressed in the study. Figure 3.14 shows the mean daily cumulative total thermal

Table 3.3: Cases of the sensitivity analysis. B = Base case.

Category	Case	Description
External wall color [49]	B	Red: $\varepsilon_{\text{wall}} = 0.88$, $\alpha_{\text{wall}} = 0.57$
	C.1	Black: $\varepsilon_{\text{wall}} = 0.86$, $\alpha_{\text{wall}} = 0.56$
	C.2	White: $\varepsilon_{\text{wall}} = 0.76$, $\alpha_{\text{wall}} = 0.27$
	C.3	Clear: $\varepsilon_{\text{wall}} = 0.90$, $\alpha_{\text{wall}} = 0.09$
Wall insulation [31]	B	Polyurethane: 5 mm roof, 15 mm other surfaces
	W.1	Polyurethane: 5 mm all surfaces
	W.2	Polyurethane: 15 mm all surfaces
	W.3	Polyurethane: 15 mm roof, 30 mm other surfaces
Window glass [46]	B	6mm one-pane: front clear, others gray-tinted
	G.1	6mm one-pane: all-clear
	G.2	12mm one-pane: front clear, others gray-tinted
	G.3	6+12+6mm two-pane: front clear, others gray-tinted
Air changes [60]	B	Leakage $4.34\,\text{h}^{-1}$ and opens variable
	A.1	Leakage $10 \cdot$ B (windows open)
	A.2	Leakage $0.5 \cdot$ B (better sealing)
	A.3	Leakage $0.1 \cdot$ B & $0.1 \cdot$ Opens (air curtain)
Occupancy [45]	B	Hourly schedule 80 passengers max
	O.1	$0.50 \cdot$ B
	O.2	$0.75 \cdot$ B
	O.3	$1.25 \cdot$ B
Outdoor convective coefficient [63]	B	Function of the bus speed
	H.1	$0.50 \cdot$ B
	H.2	$0.75 \cdot$ B
	H.3	$1.25 \cdot$ B

load (with dots) and the different components (with bars). Two dotted horizontal lines represent the total load variation with respect to the base case (B). In practically all cases, reducing the cooling load implies increasing the heating load, and vice versa. In case G.2, the cooling demand decreases by 3% without increasing the heating needs, although the impact of the 12 mm one-pane is small. In both G.1 and G.3 cases, the cooling demand grows, and the heating demand drops. In G.1 just

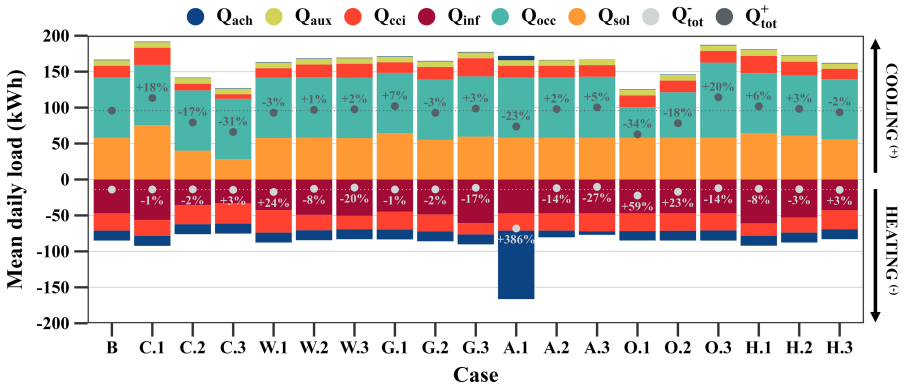

Figure 3.14: Mean daily cumulative total thermal load for the different cases of the sensitivity analysis. Cases: base B, external wall color C, wall insulation W, window glass G, air changes A, occupancy O, outdoor convective coefficient H. Bars are the mean daily cumulative thermal load components and points the total load. Components: air changes Q_{ach}, auxiliary Q_{aux}, conduction, convection, and internal infrared Q_{cci}, external infrared Q_{inf}, occupancy Q_{occ}, solar radiation Q_{sol}.

the solar contribution is affected, significantly increasing the cooling demand. In G.3 the changes in the window insulation and their thermal mass significantly reduce the heating demand.

The increase in the heating demand stands out in case A.1, where a significant increase in infiltrations, for example due to the window openings when there are no occupants [60]. This could reduce the cooling demand by 23% but it would increase the heating demand by 386%. In both A.2 and A.3 cases, the heating demand grows, and the cooling needs are reduced. A.2 demonstrates that infiltrations caused by openings have a more significant impact compared to infiltrations caused by leakage (around 73% in the base case). This is evident as a 50% reduction in leakage infiltrations only results in a 14% decrease in heating demand. In contrast, case A.3 shows a very significant reduction of the heating demand, around 27%, through an action such as an air curtain, which can minimize the air changes both for openings and leakage. This action could be used exclusively in winter.

The occupation has a linear impact on the thermal load, increasing the heating demand in winter and reducing the cooling demand in summer.

The influence of the wall insulation on the cooling demand is almost negligible, but it significantly affects the heating demand. Using the same thickness of polyurethane in the roof as in the other sides reduces the heating demand by 8% and if the current thickness is doubled the reduction would be 20%. In contrast, the importance of the external wall color and coating in the cooling demand is clear. The use of very dark or very clear colors yields a variation in the mean daily cooling demand between 66 kWh and 113 kWh. With white walls, the current cooling demand would be reduced by 31%.

3.4 Conclusions

The present research involves the development and integration of a set of advanced models that simulate the thermal cabin load of a vehicle in the dynamic and complex conditions of the urban environment. A detailed real 3D urban model have been developed and combined with a kinematic model, which generates a consistent stochastic speed profile. A climate conditions model calculates the radiation through each wall and the shadows induced by the urban environment. A transient model of the cabin enables the calculation of the thermal load. The model has been validated experimentally.

For the rest of the analysis, the vehicle under study is a bus from the urban fleet of València (Spain). The simulations have been performed for one year with a time-step of 1-min. The model has helped to obtain the thermal loads. This is essential to understand the impact of different optimization strategies.

Before carrying out a sensitivity analysis, two important hypotheses have been studied in detail: the time-step and the stochasticity of the occupancy. A time-step of 1 min was finally fixed as a compromise between accuracy and a low computational cost.

The results revealed that cooling load is the most demanding mode, especially in July and August. The mean daily cooling demand per distance covered for a warm summer day is around 105 kWh/100km. The mean daily heating demand per distance covered for a cold winter day is around 22 kWh/100km.

The occupation load is almost constant over the year, contributing to 33–45% in positive loads in summer. The solar gain accounts for approximately 20–42% of the positive load throughout the year, reaching over 40% from April to August. The significance of air changes is mainly observed during the colder months, contributing to more than 20% of the heating demand between November and March. The conduction, convection and internal infrared component is important (40 %) in negative loads.

Finally, a sensibility analysis has been performed to comprehend and measure the impact on the thermal load of 6 strategies, with 3 cases each. Window changing could affect the cooling (3%) and heating (17%) demand depending on the number of panes and their thickness. As the occupancy level rises, the cooling demand also increases in a nearly proportional manner, whereas the heating demand decreases. The impact of wall insulation on the cooling demand is very low but has a significant influence on the heating demand (20%). The impact of air changes on the thermal load can be important and could be managed through devices and control systems to minimize the demand on the HVAC system. Thus, the cooling demand could be reduced by 23% by opening the windows when there are no occupants. In contrast, if an action is employed to minimize air changes, the heating demand can be reduced by 27%. The results also indicate that the external wall color and coating has a relevant impact on the heating demand. With white walls, the current cooling demand could be reduced by 31%.

As next steps, the model will be integrated into an HVAC system, a powertrain and battery model, to analyze the energy consumption in several routes of the city.

3.5 Acknowledgments

This work has been supported by the Generalitat Valenciana under the program "Subvencions per a la contractació de personal investigador de caràcter predoctoral (ACIF/2019/239)". The authors gratefully acknowledge the support of Angel Navarro and EMT València for providing the data of the bus and the route.

3.6 References

[1] European Commission. EU reference scenario 2020. Energy, transport and GHG emissions: trends to 2050. 2021. https://doi.org/doi/10.2833/35750.

[2] European Commission. COM/2019/640 final - The European Green Deal. 2019.

[3] European Environment Agency. EEA greenhouse gases. Data viewer on Total greenhouse gas emissions and removals of the EU, based on data reported by EU Member States under the EU Governance Regulation.

[4] Z. Zhang, J. Wang, X. Feng, L. Chang, Y. Chen, and X. Wang. The solutions to electric vehicle air conditioning systems: A review. In: *Renewable and Sustainable Energy Reviews* 91 (2018), 443–463. https://doi.org/10.1016/J.RSER.2018.04.005.

[5] M. B. B. de Moura and A. Tribess. Climate control system improvements for better cabin environmental conditions and reduction of fuel consumption. In: *SAE Technical Papers*. 2007. https://doi.org/10.4271/2007-01-2673.

[6] International Energy Agency. Cooling on the Move. The future of air conditioning in vehicles. https://www.iea.org/reports/cooling-on-the-move. 2019.

[7] J. R. M. Delos Reyes, R. v. Parsons, and R. Hoemsen. Winter Happens: The Effect of Ambient Temperature on the Travel Range of Electric Vehicles. In: *IEEE Trans Veh Technol* 65.(6) (2016), 4016–4022. https://doi.org/10.1109/TVT.2016.2544178.

[8] Asian Development Bank. Sustainable Transport Solutions: Low-Carbon Buses in the People's Republic of China. 2018. https://doi.org/10.22617/TCS189646-2.

[9] A. Lajunen, Y. Yang, and A. Emadi. Review of Cabin Thermal Management for Electrified Passenger Vehicles. In: *IEEE Trans Veh Technol* 69.(6) (2020), 6025–6040. https://doi.org/10.1109/TVT.2020.2988468.

[10] P. Li, Y. Zhang, K. Zhang, and M. Jiang. The effects of dynamic traffic conditions, route characteristics and environmental conditions on trip-based electricity consumption prediction of electric bus. In: *Energy* 218 (2021), 119437. https://doi.org/10.1016/J.ENERGY.2020.119437.

[11] P. Li, Y. Zhang, Y. Zhang, and K. Zhang. Prediction of electric bus energy consumption with stochastic speed profile generation modelling and data driven method based on real-world big data. In: *Appl Energy* 298 (2021), 117204. https://doi.org/10.1016/J.APENERGY.2021.117204.

[12] R. Günther, T. Wenzel, M. Wegner, and R. Rettig. Big data driven dynamic driving cycle development for busses in urban public transportation. In: *Transp Res D Transp Environ* 51 (2017), 276–289. https://doi.org/10.1016/J.TRD.2017.01.009.

[13] H. Gong, Y. Zou, Q. Yang, J. Fan, F. Sun, and D. Goehlich. Generation of a driving cycle for battery electric vehicles: A case study of Beijing. In: *Energy* 150 (2018), 901–912. https://doi.org/10.1016/J.ENERGY.2018.02.092.

[14] K. Kivekas, J. Vepsalainen, and K. Tammi. Stochastic Driving Cycle Synthesis for Analyzing the Energy Consumption of a Battery Electric Bus. In: *IEEE Access* 6 (2018), 55586–55598. https://doi.org/10.1109/ACCESS.2018.2871574.

[15] N. A. El-Taweel, A. Zidan, and H. E. Z. Farag. Novel Electric Bus Energy Consumption Model Based on Probabilistic Synthetic Speed Profile Integrated with HVAC. In: *IEEE Transactions on Intelligent Transportation Systems* 22.(3) (2021), 1517–1531. https://doi.org/10.1109/TITS.2020.2971686.

[16] M. Gallet, T. Massier, and T. Hamacher. Estimation of the energy demand of electric buses based on real-world data for large-scale public transport networks. In: *Appl Energy* 230 (2018), 344–356. https://doi.org/10.1016/J.APENERGY.2018.08.086.

[17] Y. Bie, Y. Liu, S. Li, and L. Wang. HVAC operation planning for electric bus trips based on chance-constrained programming. In: *Energy* 258 (2022), 124807. https://doi.org/10.1016/J.ENERGY.2022.124807.

[18] J. Vepsäläinen, K. Otto, A. Lajunen, and K. Tammi. Computationally efficient model for energy demand prediction of electric city bus in varying operating conditions. In: *Energy* 169 (2019), 433–443. https://doi.org/10.1016/J.ENERGY.2018.12.064.

[19] H. He, M. Yan, C. Sun, J. Peng, M. Li, and H. Jia. Predictive air-conditioner control for electric buses with passenger amount variation forecast. In: *Appl Energy* 227 (2018), 249–261. https://doi.org/10.1016/J.APENERGY.2017.08.181.

[20] J. Jiang, Y. Yu, H. Min, Q. Cao, W. Sun, Z. Zhang, and C. Luo. Trip-level energy consumption prediction model for electric bus combining Markov-based speed profile generation and Gaussian processing regression. In: *Energy* 263 (2023), 125866. https://doi.org/10.1016/J.ENERGY.2022.125866.

[21] Y. Mao, J. Wang, and J. Li. Experimental and numerical study of air flow and temperature variations in an electric vehicle cabin during cooling and heating. In: *Appl Therm Eng* 137 (2018), 356–367. https://doi.org/10.1016/J.APPLTHERMALENG.2018.03.099.

[22] S. Chen, B. Du, Q. Li, and D. Xue. The influence of different orientations and ventilation cases on temperature distribution of the car cabin in the hot soak. In: *Case Studies in Thermal Engineering* 39 (2022), 102401. https://doi.org/10.1016/J.CSITE.2022.102401.

[23] M. Aliahmadipour, M. Abdolzadeh, and K. Lari. Air flow simulation of HVAC system in compartment of a passenger coach. In: *Appl Therm Eng* 123 (2017), 973–990. https://doi.org/10.1016/J.APPLTHERMALENG.2017.05.086.

[24] M. A. Alam, R. Kumar, D. Banoriya, A. S. Yadav, G. Goga, K. K. Saxena, D. Buddhi, and R. Mohan. Design and development of thermal comfort analysis for air-conditioned compartment. In: *International Journal on Interactive Design and Manufacturing* (2022), 1–11. https://doi.org/10.1007/S12008-022-01015-8/METRICS.

[25] M. S. Oh, J. H. Ahn, D. W. Kim, D. S. Jang, and Y. Kim. Thermal comfort and energy saving in a vehicle compartment using a localized air-conditioning system. In: *Appl Energy* 133 (2014), 14–21. https://doi.org/10.1016/J.APENERGY.2014.07.089.

[26] J. H. Moon, J. W. Lee, C. H. Jeong, and S. H. Lee. Thermal comfort analysis in a passenger compartment considering the solar radiation effect. In: *International Journal of Thermal Sciences* 107 (2016), 77–88. https://doi.org/10.1016/J.IJTHERMALSCI.2016.03.013.

[27] P. Bandi, N. P. Manelil, M. P. Maiya, S. Tiwari, A. Thangamani, and J. L. Tamalapakula. Influence of flow and thermal characteristics on thermal comfort inside an automobile cabin under the effect of solar radiation. In: *Appl Therm Eng* 203 (2022), 117946. https://doi.org/10.1016/J.APPLTHERMALENG.2021.117946.

[28] A. Lajunen. Energy Efficiency and Performance of Cabin Thermal Management in Electric Vehicles. In: *SAE Technical Papers*. Volume 2017-March. March. 2017. https://doi.org/10.4271/2017-01-0192.

[29] S. Bellocchi, G. L. Guizzi, M. Manno, M. Salvatori, and A. Zaccagnini. Reversible heat pump HVAC system with regenerative heat exchanger for electric vehicles: Analysis of its impact on

driving range. In: *Appl Therm Eng* 129 (2018), 290–305. https://doi.org/10.1016/J.APPLTHERMALENG.2017.10.020.

[30] C. Os'Boyle, R. Douglas, R. Best, and M. Geron. Vehicle Thermal Modelling for Improved Drive Cycle Analysis of a Generic City Bus. In: *2020 5th International Conference on Smart and Sustainable Technologies, SpliTech 2020*. 2020. https://doi.org/10.23919/SPLITECH49282.2020.9243725.

[31] D. C. Vásconez Núñez. Desarrollo de un modelo para el cálculo del consumo de climatización en vehículos de pasajeros urbanos. PhD thesis. Valencia (Spain): Universitat Politècnica de València, 2019. https://doi.org/10.4995/Thesis/10251/121133.

[32] D. Ramsey, A. Bouscayrol, L. Boulon, A. Desreveaux, and A. Vaudrey. Flexible Simulation of an Electric Vehicle to Estimate the Impact of Thermal Comfort on the Energy Consumption. In: *IEEE Transactions on Transportation Electrification* 8.(2) (2022), 2288–2298. https://doi.org/10.1109/TTE.2022.3144526.

[33] E. Afrasiabian, R. Douglas, M. Geron, and G. Cunningham. A numerical evaluation of a novel recovery fresh air heat pump concept for a generic electric bus. In: *Appl Therm Eng* 209 (2022), 118181. https://doi.org/10.1016/J.APPLTHERMALENG.2022.118181.

[34] D. Ramsey, L. Boulon, and A. Bouscayrol. Modeling of an EV air conditioning system for energetic studies in summer. In: *2021 IEEE Vehicle Power and Propulsion Conference, VPPC 2021 - Proceedings*. 2021. https://doi.org/10.1109/VPPC53923.2021.9699119.

[35] D. Ramsey, A. Bouscayrol, and L. Boulon. Energy Consumption of a Battery Electric Vehicle in Winter Considering Preheating: Tradeoff between Improved Performance and Total Energy Consumption. In: *IEEE Vehicular Technology Magazine* 17.(3) (2022), 104–112. https://doi.org/10.1109/MVT.2022.3158043.

[36] B. Torregrosa-Jaime, F. Bjurling, J. M. Corberán, F. Di Sciullo, and J. Payá. Transient thermal model of a vehicle's cabin validated under variable ambient conditions. In: *Appl Therm Eng* 75 (2015), 45–53. https://doi.org/10.1016/J.APPLTHERMALENG.2014.05.074.

[37] F. Lan, H. Chen, J. Chen, and W. Li. Effect of urban microclimates on dynamic thermal characteristics of a vehicle cabin. In: *Case Studies in Thermal Engineering* (2023), 103162. https://doi.org/10.1016/J.CSITE.2023.103162.

[38] A. Broatch, P. Olmeda, P. Bares, and S. Aceros. Integral Thermal Management Studies in Winter Conditions with a Global Model of a Battery-Powered Electric Bus. In: *Energies (Basel)* 16.(1) (2023). https://doi.org/10.3390/en16010168.

[39] Z. Shuofeng, M. R. Amini, J. Sun, and C. Mi. A Two-Layer Real-Time Optimization Control Strategy for Integrated Battery Thermal Management and HVAC System in Connected and Automated HEVs. In: *IEEE Trans Veh Technol* 70.(7) (2021), 6567–6576. https://doi.org/10.1109/TVT.2021.3085938.

[40] A. A. Abulifa, A. B. C. Soh, M. K. Hassan, R. M. K. R. Ahmad, and M. A. M. Radzi. Energy Management System in Battery Electric Vehicle Based on Fuzzy Logic Control to Optimize the Energy Consumption in HVAC System. In: *International Journal of Integrated Engineering* 11.(4) (2019), 11–20. https://doi.org/10.30880/ijie.2019.11.04.002.

[41] R Core Team. R: A Language and Environment for Statistical Computing. https://www.R-project.org/. 2022.

[42] M. Kottek, J. Grieser, C. Beck, B. Rudolf, and F. Rubel. World Map of the Köppen-Geiger climate classification updated. In: *Meteorologische Zeitschrift* 15.(3) (2006), 259–263. https://doi.org/10.1127/0941-2948/2006/0130.

[43] F. Gómez, N. Tamarit, and J. Jabaloyes. Green zones, bioclimatics studies and human comfort in the future development of

urban planning. In: *Landsc Urban Plan* 55.(3) (2001), 151–161. https://doi.org/10.1016/S0169-2046(01)00150-5.

[44] T. Huld, E. Paietta, P. Zangheri, and I. P. Pascua. Assembling Typical Meteorological Year Data Sets for Building Energy Performance Using Reanalysis and Satellite-Based Data. In: *Atmosphere 2018, Vol. 9, Page 53* 9.(2) (2018), 53. https://doi.org/10.3390/ATMOS9020053.

[45] Empresa Municipal de Transportes de Valencia. https://www.emtvalencia.es. 2023.

[46] NSG Group. Pilkington catalogue.

[47] Asociación Española de Normalización (UNE). Glass in building - Determination of thermal transmittance (U value) - Calculation method (UNE-EN Standard No. 673). 2011.

[48] ASHRAE American Society of Heating Refrigerating and A.-C. Engineers. ASHRAE Handbook - Fundamentals. Atlanta, GA: ASHRAE, 2017.

[49] L. Kauder. NASA Technical Publication. Spacecraft Thermal Control Coatings References. Technical report. 2005.

[50] R. Prabakaran, D. M. Lal, and S. C. Kim. A state of art review on future low global warming potential refrigerants and performance augmentation methods for vapour compression based mobile air conditioning system. In: *Journal of Thermal Analysis and Calorimetry 2022 148:2* 148.(2) (2022), 417–449. https://doi.org/10.1007/S10973-022-11485-3.

[51] J.-R. Roussel, D. Auty, N. C. Coops, P. Tompalski, T. R. Goodbody, A. S. Meador, J.-F. Bourdon, F. de Boissieu, and A. Achim. lidR: An R package for analysis of Airborne Laser Scanning (ALS) data. In: *Remote Sensing of Environment* 251 (2020), 112061. https://doi.org/10.1016/j.rse.2020.112061.

[52] J.-R. Roussel and D. Auty. Airborne LiDAR Data Manipulation and Visualization for Forestry Applications. https://cran.r-project.org/package=lidR. 2023.

[53] M. Dalponte and D. A. Coomes. Tree-centric mapping of forest carbon density from airborne laser scanning and hyperspectral data. In: *Methods Ecol Evol* 7.(10) (2016), 1236–1245. https://doi.org/10.1111/2041-210X.12575.

[54] Google Inc. General Transit Feed Specification. https://developers.google.com/transit/gtfs/reference. 2022.

[55] W. R. Mebane and J. S. Sekhon. Genetic Optimization Using Derivatives: The rgenoud Package for R. In: *J Stat Softw* 42.(11) (2011), 1–26. https://doi.org/10.18637/JSS.V042.I11.

[56] Asociación Española de Normalización (UNE). Railway applications - Air conditioning for urban, suburban and regional rolling stock (UNE-EN Standard No. 14750). 2007.

[57] U.S. Department of Energy. EnergyPlusTM Version 22.1.0 - Engineering Reference. 2022.

[58] J. A. Duffie and W. A. Beckman. Solar Engineering of Thermal Processes: Fourth Edition. Solar Engineering of Thermal Processes: Fourth Edition, 2013. https://doi.org/10.1002/9781118671603.

[59] T. R. Oke, G. Mills, A. Christen, and J. A. Voogt. Urban Climates. Cambridge University Press, 2017. https://doi.org/10.1017/9781139016476.

[60] S. K. Chaudhry and S. P. Elumalai. The influence of school bus ventilation scenarios over in-cabin PM number concentration and air exchange rates. In: *Atmos Pollut Res* 11.(8) (2020), 1396–1407. https://doi.org/10.1016/J.APR.2020.05.021.

[61] O. A. Hjelkrem, K. Y. Lervåg, S. Babri, C. Lu, and C. J. Södersten. A battery electric bus energy consumption model for strategic purposes: Validation of a proposed model structure with data from bus fleets in China and Norway. In: *Transp Res D Transp Environ* 94 (2021), 102804. https://doi.org/10.1016/J.TRD.2021.102804.

[62] J. W. Lee, E. Y. Jang, S. H. Lee, H. S. Ryou, S. Choi, and Y. Kim. Influence of the spectral solar radiation on the air flow and temperature distributions in a passenger compartment. In: *International Journal of Thermal Sciences* 75 (2014), 36–44. https://doi.org/10.1016/J.IJTHERMALSCI.2013.07.018.

[63] W. Li and J. Sun. Numerical simulation and analysis of transport air conditioning system integrated with passenger compartment. In: *Appl Therm Eng* 50.(1) (2013), 37–45. https://doi.org/10.1016/J.APPLTHERMALENG.2012.05.030.

[64] X. Han, H. Zou, J. Wu, C. Tian, M. Tang, and G. Huang. Investigation on the heating performance of the heat pump with waste heat recovery for the electric bus. In: *Renew Energy* 152 (2020), 835–848. https://doi.org/10.1016/J.RENENE.2020.01.075.

[65] J. Karlsson and A. Roos. Modelling the angular behaviour of the total solar energy transmittance of windows. In: *Solar Energy* 69.(4) (2000), 321–329. https://doi.org/10.1016/S0038-092X(00)00083-9.

[66] M. Tozzi, M. V. Corazza, U. Guida, and A. Musso. Testing innovations for increased energy efficiency of electric buses: Evidence from the EBSF-2 project. In: *Transportation Research Procedia* 48 (2020), 2166–2175. https://doi.org/10.1016/J.TRPRO.2020.08.273.

[67] International Council on Clean Transportation. Strategies for deploying zero-emission bus fleets: Route-level energy consumption and driving range analysis. 2021.

[68] International Energy Agency. Global EV Outlook 2023. Paris, 2023.

[69] M. Corazza, V. Conti, A. Genovese, F. Ortenzi, and M. P. Valentini. A Procedure to Estimate Air Conditioning Consumption of Urban Buses Related to Climate and Main Operational Characteristics. In: *World Electric Vehicle Journal 2021, Vol. 12, Page 29* 12.(1) (2021), 29. https://doi.org/10.3390/WEVJ12010029.

Chapter 4

HVAC system operation, consumption and compressor size optimization in urban buses of Mediterranean cities

Chapter adapted from the paper:

Joan Dídac Viana-Fons [a,b], Jorge Payá [a]. *HVAC system operation, consumption and compressor size optimization in urban buses of Mediterranean cities.* In: *Energy* (2024), Vol. 296, p. 131151.
DOI: https://doi.org/10.1016/j.energy.2024.131151

[a] Instituto Universitario de Investigación en Ingeniería Energética, Universitat Politècnica de València, Camí de Vera s/n, Valencia, Spain.

[b] ImpactE, C/ Joan Verdeguer nº 16, Valencia, 46024, Spain.

Abstract:

Electric buses are a key element in the transition to sustainable urban mobility. The HVAC system is the primary auxiliary load and significantly affects the efficiency and the driving range. In this work, advanced dynamic models have been developed to simulate accurately and optimize the urban bus energy consumption under real operating and extreme conditions, with a particular emphasis on HVAC systems. This study integrates a 3D city model, a weighted stochastic driving cycle, a climate model, a transient thermal model coupled with a physical HVAC system model using IMST-ART and a battery model. Different bus lines and urban typologies have been analyzed in the city of València. The results indicate that the overall consumption is similar across the different bus lines, around 2.10 $\mathrm{Wh\,km^{-1}}$. The HVAC is the second largest contributor, after the powertrain, and can reduce the driving range by 15-20% on mild and hot summer days, respectively. Finally, the size of the compressor has been optimized, revealing that a scale factor of 75% is more convenient, since the energy consumption can be reduced by 3% with lower costs in the compressor.

Keywords: Modeling; HVAC; Electric vehicle; Urban; Bus; Optimization

Nomenclature

GIS: Geographic Information Systems.

HVAC: Heating, Ventilation and Air Conditioning.

CFD: Computational Fluid Dynamics.

GTFS: General Transit Feed Specification.

LCZ: Local Climate Zone.

SVF: Sky View Factor.

PWM: Pulse Width Modulation.

TMY: Typical Meteorological Year.

MAPD: Mean Absolute Percentage Deviation.

DTM: Digital Terrain Model.

MINLP: Mixed Integer Nonlinear Programming.

PTC: Positive Temperature Coefficient.

COP: Coefficient of Performance.

C: cooling mode.

H: heating mode.

V: ventilation mode.

T: temperature.

RH: relative humidity.

$\dot{V}$: volumetric flowrate.

m: mass.

t: elapsed time.

l: length.

v: velocity.

n: angular speed.

a: acceleration.

z: building height.

z_0: ground height.

n_{BS}: number of bus stops.

$\dot{I}$: solar radiative heat gain.

$\dot{E}$: long-wave radiative heat gain.

$\dot{Q}$: convective load power.

Q: convective load energy.

$\dot{V}$: Power.

W: Energy.

$\dot{\omega}$: moisture transfer.

ω: humidity ratio.

Δh_{vap}: heat of vaporization.

λ_{ice}: frost/defrost control parameter.

p_r: pressure ratio.

p: absolute pressure.

r: ratio.

δ: recirculation ratio.

e: external, outdoor node (subindex).

i: internal, indoor node (subindex).

m: mass node (subindex).

b: body node (subindex).

sky: sky node (subindex).

o: occupancy node (subindex).

a: auxiliary node (subindex).

s: sun node (subindex).

x: HVAC node (subindex).

D: demand (subindex).

ice: frost/defrost conditions (subindex).

f: non-recirculated fresh air (subindex).

$hvac$: HVAC system (subindex).

out: exfiltrations (subindex).

fan: fan (subindex).

$comp$: compressor (subindex).

ptc: PTC (subindex).

tot: total (subindex).

wo: window open (subindex).

$cndnst$: condensate (subindex).

mot: motor (subindex).

reg: regenerative breaking (subindex).

hyd: hydraulic (subindex).

pne: pneumatic (subindex).

ele: electric auxiliaries (subindex).

eff: efficiency (subindex).

$btms$: battery thermal management system (subindex).

$batt$: battery (subindex).

U: unmet (subindex).

$cond$: condensing (subindex).

$evap$: evaporating (subindex).

dis: discharge (subindex).

suc: suction (subindex).

L: latent (superindex).

S: sensible (superindex).

$+$: positive (superindex).

$-$: negative (superindex).

N: nominal (superindex).

max: maximum (superindex).

min: minimum (superindex).

4.1 Introduction

The electrification of urban buses is a key point for the transition towards sustainable urban mobility. Currently, over 3% of all operational buses globally are electric, with perspectives of up to 10% by 2030 [1]. By 2030 only zero-emission city buses can be presumably sold in the European Union [2]. The main auxiliary load on the battery is the Heating, Ventilation, and Air Conditioning system (HVAC), which can reduce the range of electric buses to 50% in cold winter or hot summer days [3]. Thus, a correct modeling and sizing of HVAC systems is crucial in electric mobility to extend the vehicle range and to reduce the environmental impact. The operation and sizing of the HVAC system is based on standards [4] which only differentiate large climate areas and do not size the systems for the specific working conditions. This means that HVAC systems are often oversized and present significant room for optimization. Dynamic, accurate and computationally efficient models are required [5], but the rest of the vehicle models should also be thorough enough to have a good prediction of the HVAC impact on the driving range. In recent years, significant advancements have been performed in the prediction of the energy consumption of vehicles in urban environments. The number of articles with the keywords thermal comfort, air conditioning and automobile has increased steadily since the year 2000, reaching in 2022 four times the value of year 2000. These studies focus on multiple factors which impact the energy consumption, such as driving cycles or route characteristics, climate or environmental effects, HVAC systems, energy management or control strategies. Many studies focus on examining the vehicle's speed profile or driving cycle. Recent research employs synthetic driving cycles derived from real-world data and stochastic techniques for more accurate results, [6, 7]. However, the research is often limited to either the generation of these driving cycles or to the modeling of the powertrain consumption, without fully incorporating the complexities and energy impact of dynamic environmental conditions. Cabin thermal models have also been well explored. One approach is with advanced Computational Fluid Dynamics (CFD) which help analyze thermal comfort and the spatial

temperature distribution in vehicle cabins [8, 9, 10]. Another approach is with lumped parameter models, which offer a compromise between accuracy and computational efficiency [11], and can be easily integrated with other systems using multiphysics software. However, most existing studies fail to consider the vehicle's driving profile and its impact on important parameters, such as the external convection or shading [12, 13]. They also focus on specific operational conditions or standard test cycles, often overlooking real-world driving cycles and the dynamic urban climate [14, 15, 16]. Some studies attempt to combine kinematic and thermal load models for a more comprehensive analysis of energy demand [17, 18, 19, 20]. However, oversimplified models are often employed, lacking the consideration of critical factors such as the solar radiation, transient thermal effects, or latent heat gains [12, 13, 19, 20]. Regarding the estimation of the HVAC consumption, a constant energy consumption or efficiency is frequently assumed. In some cases, the efficiency is introduced as a function of the operation conditions [20, 21, 22, 23, 24, 25, 26]. Some studies quantify the influence of each component of the vapor compression cycle, but do not present their description nor their detailed model [26, 27, 28, 29]. Other investigations develop models of each component according to the conservation equations, with compressor efficiency curves obtained from catalog databases or experiments, but they assume an average overall heat transfer coefficient to characterize the heat exchangers [30, 31, 32, 33, 34]. Finally, other authors [35, 36, 37] develop an accurate HVAC model using the IMST-ART software [38], which allows high numerical robustness evaluation of refrigeration equipment performance, including a detailed physical model of each component. However, only one work [35] was found considering the operation of the HVAC system during a given interurban vehicle journey and none of them have been conducted under real operating conditions in an urban environment. Finally, other authors investigate the overall energy consumption of buses in urban areas. Many of these studies focus on the operation, sizing, or selection of the battery [39], on auxiliary systems [40], or the integration of thermal systems [41], while others concentrate on planning charging stations [42] or fleet management [43]. The models often oversimplify

part of the sub-systems, and none focus specially on modeling a real HVAC system, nor on modeling thermal loads in a dynamic and complex urban environment. Concerning the optimization of mobile HVAC systems, different studies explore changes in architecture, refrigerant, or control strategies [44, 45, 46]. However, very few authors address the sizing of the compressor, which is the most energy-consuming component. For instance, some researchers focus on specific operating points and conditions [47, 48], but not on the size of the compressor for real driving conditions. The final objective of our work is to develop a detailed HVAC simulation tool which can assist in the selection of the size of the compressor, given the real conditions in which the vehicle will work. Consequently, a detailed thermal model of the cabin is also required, and the simulation tool has to provide information on the energy consumption of the system for all the necessary HVAC modes. The present research extends the study of thermal loads presented in Ref. [49] by coupling the models from this study with the humidity transfer model, the HVAC system model and the energy consumption models of the other bus systems, including the battery and the powertrain. The integration of these models enables comprehensive simulations of the HVAC system's operation across typical annual and extreme weather conditions, as well as the strategic optimization of the compressor size. To the author's knowledge, the present HVAC system model, which combines detailed operational simulations with a compressor optimization, is the most detailed found in literature up to date. This work introduces the following novelties:

- Integration in a global simulation model of a detailed real 3D urban model, a weighted stochastic urban driving cycle, a climate conditions model, a coupled transient thermal cabin and HVAC model, and an overall bus consumption or battery model.
- Development of a physical model of a real mobile reversible heat pump. This model includes the compressor and fans' speeds and recirculation ratios within the control model of six operating modes, encompassing cooling, standard forced ventilation, open

windows ventilation, standard heating, heating in frost/defrost conditions, and heating with PTCs.

- Demonstration that the compressor size can be reduced by a factor of 25% by maintaining or even reducing the energy consumption.

4.2 Methodology

The methodology integrates six models (Figure 4.1) applied sequentially in every time step.

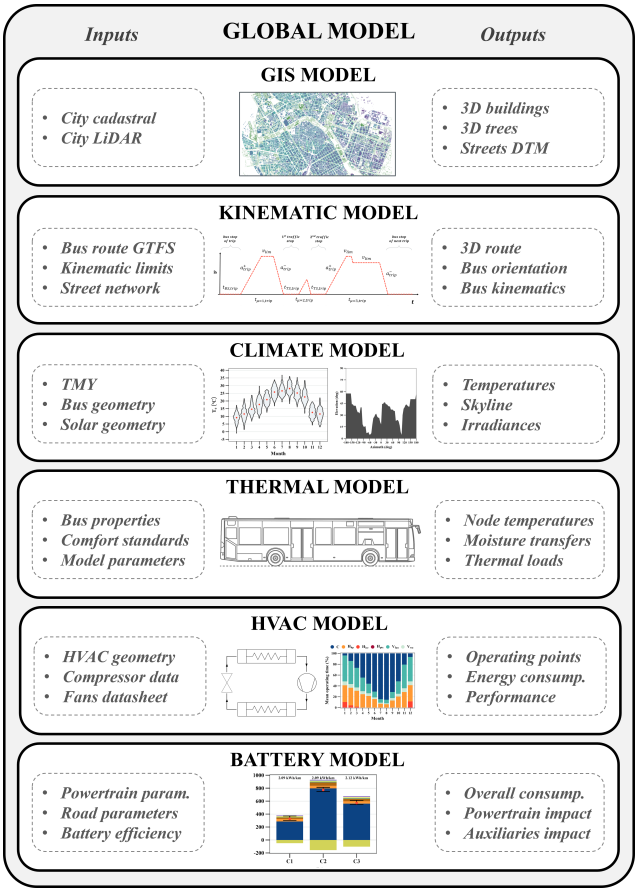

Figure 4.1: Scheme of the methodology.

Initially, the geographic information system (GIS) model (Section 4.2.3) constructs a vector-based 3D city model with buildings and trees, and a raster-based digital terrain model (DTM) for streets. Next, the kinematic model (Section 4.2.4) creates a year-long weighted stochas-

tic driving cycle using low-resolution GTFS route data, street velocity limits, and stochastic traffic stops at street intersections. The climate model (Section 4.2.5) obtains the external air temperature and humidity, the multicomponent radiation fluxes on the bus surfaces and their skylines, for each time step, using the long-term city climate data (TMY), solar geometry, and outputs from the previous models. The thermal capacitances and heat transfer coefficients for each node and surface are based on the bus geometry and material properties. The thermal and HVAC coupled model (Section 4.2.6) computes, on the one hand, the thermal heat gains, node temperatures, moisture transfers, the thermal loads of mass and body nodes, and the latent loads of the indoor node using a system of ordinary differential equations, based on the bus optical and thermophysical properties, occupancy, air changes, auxiliary systems, and environmental conditions. On the other hand, the coupled model evaluates the HVAC operating mode and the operation points of each component of the equipment, their energy consumption and efficiency, and the outlet conditions of the air and condensate flowrate. Lastly, the battery model of the bus (Section 4.2.7) is developed to obtain the overall bus energy consumption, including motor, regenerative braking, HVAC, battery thermal management system, the pneumatic, hydraulic, and auxiliary electrical systems, as well as the impact of the battery efficiency. All the models have been developed in R [50] and the overall model has been solved with 1-minute time series for a representative year (Section 4.3.1) and under extreme weather conditions (Section 4.3.2). The optimal compressor size is discussed in Section 4.4.

4.2.1 Location and climate conditions

This study has been applied in València, Spain (39°28′12″N, 0°22′35″O, 12 masl), which has a hot-summer Mediterranean climate [51]. València serves as an example of a Mediterranean city [52], since the weather is similar to other cities such as Barcelona (Spain), Rome (Italy), Lisbon (Portugal), or Marseille (France). The study uses a representative year-long time series of hourly meteorological variables

from the TMY dataset spanning 2005-2020 from the PVGIS-SARAH2 satellite-based database [53]. The hourly distribution of dry bulb temperature during the driving cycle typically varies between 9-29 °C, with yearly extremes of -1 °C and 37 °C. The median monthly value of the relative humidity during the operating period varies from 80% in January to 53.6% in June.

4.2.2 Route and vehicle description

This study uses real data from a specific electric bus and multiple lines from the urban service fleet [54]. The selected bus is an Irizar i2e electric bus, a standard 12-meter vehicle, with an 80-passenger capacity. Three circular urban routes (Figure 4.2) have been simulated, covering different urban typologies (Table 4.1). First, the C1 bus line covers a 4.99 km circular city center route, with a mean speed of 8.77 km/h and 3.4 bus-stops/km, predominantly in a compact-midrise urban area (Local Climate Zone or LCZ 2 [55]) with a Sky View Factor (SVF) or ratio of visible sky of 0.68. Second, the C2 bus line is an 8.55 km circular route through a ring road, with wider and faster streets, with a mean speed of 20.51 km/h, 3.0 bus-stops/km, in an open-midrise urban landscape (LCZ 4) and SVF 0.76. Third, the C3 line is a 15.14 km circular route through a more external traffic ring, where the buildings are taller and streets narrower than the C2 route, with a mean speed of 15.14 km/h, 2.9 bus-stops/km and a predominant LCZ 2.

Table 4.1: Characterization of the bus lines in the study.

line	n_BS	l (km)	v (km/h)	SVF	z (m)	z_0 (m)	LCZ
C1	17	4.99	8.77	0.68	21±9	14±2	2
C2	26	8.55	20.51	0.76	22±9	15±5	5
C3	36	12.46	15.14	0.67	24±10	14±3	2

4.2.3 GIS model

The GIS model creates a 3D spatial layout of the city, identifying buildings, trees, and streets separately. The buildings have been

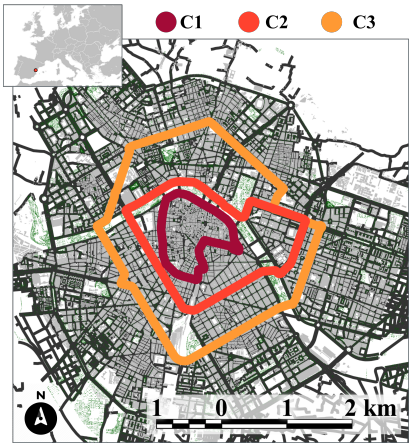

Figure 4.2: Location, 3D vectorial model, and bus lines of the case study in València, Spain.

generated using a 3D vector model derived from cadastral and LiDAR altimetry data, as detailed in [56]. For streets, a 2-meter resolution raster-based altimetric model or digital terrain model (DTM) is developed. This DTM is constructed from LiDAR ground points using spatial interpolation through a Delaunay triangulation method [57, 58]. Trees are depicted with a 3D vector model based on the technique described in [59], which provides the height and segmented canopy of each tree. Using this city model, it is feasible to determine if a specific point is shaded at a given moment, to calculate its skyline or visible horizon, or to determine the street slope.

4.2.4 Kinematic model

This model, explained in detail in [49], generates a real-world representative synthetic driving cycle that determines the kinematic variables at each simulated point considering real-world traffic conditions. The model integrates the city network, driving route, and bus stop spatial data, with a weighted stochastic traffic stop generation and applying a microtrip approach to define the driving cycle in a mixed-integer nonlinear programming (MINLP) formulation. The MINLP problem is

applied for each trip, defined as the journey between two bus stops, and minimizes the deviation between the GTFS's empirical trip duration data [60] and the calculated value of the constructed driving cycle, subject to spatial, temporal, and other kinematic related constraints. The genetic algorithm from Ref. [61] has been applied to solve the problem, obtaining the bus stop duration, the number and duration of traffic stops, the kinematic variables, and the bus direction and ground slope at each route point.

4.2.5 Climate model

This model calculates the climate conditions on each bus surface for every route position and time step. The model provides external temperature, horizontal infrared sky irradiance, direct normal irradiance, and global horizontal irradiance. The sky temperature is derived from TMY's infrared sky irradiance [62]. A skyline profile has been obtained for each route point to assess long-wave and solar radiation effects in urban environments. This includes determining surface shadowing and calculating the SVF, which has an impact on the diffuse and reflected solar components and long-wave radiative exchanges. The direct, diffuse, and reflected solar irradiance on each bus surface is calculated using the TMY data, the solar geometry [63], the city reflectance [55], the slope and orientation of each bus surface, and the shadow effects from the skyline.

4.2.6 Coupled dynamic thermal and HVAC model

Description of the bus thermal load

An advanced dynamic thermal model has been developed to estimate both the sensible and latent thermal load in real operation conditions. This present model extends the model detailed in Ref. [49] by adding the moisture transfers, the latent thermal loads and the heat gain introduced by the fans of the HVAC system. The model is based on a lumped-parameter approach, with three bus nodes (the indoor air

i, the bus body envelope b, and the internal masses m) and four external nodes (the external air e, the surrounding urban surfaces, the sky, and the sun s), considering the variable environmental factors such as the shading, vehicle orientation, and road slope during the route. The thermal load is influenced by multiple energy and mass flows (Fig. 4.3). These are abstracted as convective heat transfers $\dot{Q}$, solar radiative heat gains $\dot{I}$, long-wave radiative heat exchanges $\dot{E}$ and moisture transfers $\dot{\omega}$. This thermal load model has been coupled with the HVAC model into a system of differential ordinary equations (ODE), as detailed in Section 4.2.6.

Description of the HVAC system

The HVAC system is the standard equipment of the municipal bus fleet in València. An integrated rooftop HVAC system is used with a conventional heat pump containing R134A as the refrigerant. The compressor is a Bock model HGX34P/315-2A, a semi-hermetic four-cylinder reciprocating compressor with variable speed. All heat exchangers are modeled using their geometry and their thermo-physical characteristics (i.e., materials, tube surface finish). The external unit has two fans of 205 W, and the internal unit has four centrifugal fans of 394 W. A thermostatic expansion valve ensures constant superheating at the evaporator outlet of 8.6 K. The geometric characteristics (diameters and lengths) and thermo-physical characteristics (pipe and insulation materials and heat exchanges) of the refrigerant lines have also been introduced. The HVAC system has a liquid receiver at the condenser outlet. Finally, a set of PTCs (Positive Temperature Coefficient) thermistors with a nominal power of 9 kW are integrated at the output of the internal heat exchanger as an electrical auxiliary air heater. These are used as back-up of the heat pump if its capacity is lower than the thermal load.

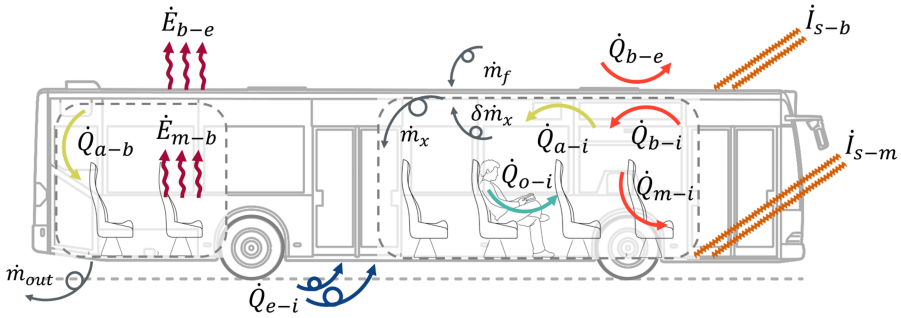

Figure 4.3: Heat gains and mass transfers of the thermal model. $\dot{Q}_{b-i}$ is the heat transfer from the body to the indoor air, $\dot{Q}_{m-i}$ from the mass to the indoor air, $\dot{Q}_{o-i}$ is the occupancy heat gain, $\dot{Q}_{a-i}$ is the heat gain from auxiliaries to the indoor air, $\dot{Q}_{e-i}$ is the heat gain by air changes, $\dot{Q}_{e-b}$ the heat transfer from external to the body, $\dot{Q}_{a-b}$ is the heat gain from auxiliaries to the body, $\dot{E}_{e-b}$ the long-wave radiation exchange between the exterior and the body, $\dot{E}_{m-b}$ the long-wave radiation exchange between the mass and the body, $\dot{I}_{s-b}$ the solar radiation heat gain to the body and $\dot{I}_{s-m}$ the solar radiation heat gain to the mass, $\dot{m}_x$ is the interior HVAC exchanger outlet mass flowrate, $\dot{m}_f$ is non-recirculated external fresh air mass flowrate, δ is the recirculation ratio and $\dot{m}_{out}$ is the exfiltrations mass flowrate.

IMST-ART performance maps of the HVAC system

The HVAC system has been modeled component by component with IMST-ART, which assists in the selection, design, and optimization of HVAC systems [64]. This software contains the geometric design of each component, as well as its thermo-physical characteristics, and the thermodynamic cycle described by the refrigerant. This professional tool has undergone extensive experimental validation [38, 65, 66, 67] with differences between measured and predicted values lower than 5%. In this study, the compressor is defined through its catalog data for different frequencies (15-50 Hz), the fans through their characteristic curve, and the heat exchangers, expansion device, and lines through the geometric and thermo-physical characteristics. Performance maps are obtained through parametric studies, where the variables of interest (compressor speed and energy consumption, capacity of the heat

exchangers, refrigerant pressures and temperatures, outlet conditions of the airflow and condensate flowrate) as a function of the input values (thermal demand, fans' operating points and inlet conditions of the airflow).

Coupled system of differential ordinary equations

In Eq.4.1-4.4, the energy and moisture mass balances of the coupled dynamic thermal and HVAC model are established as a system of differential ordinary equations.

$$m_i \cdot c_{p,i} \cdot \frac{dT_i}{dt} = \dot{Q}_{b-i} + \dot{Q}_{m-i} + \dot{Q}^S_{o-i} + \dot{Q}_{a-i} + \dot{Q}^S_{e-i} + \dot{Q}^S_{x-i} \quad (4.1)$$

$$m_b \cdot c_{p,b} \cdot \frac{dT_b}{dt} = -\dot{Q}_{b-i} + \dot{Q}_{e-b} + \dot{Q}_{a-b} + \dot{E}_{e-b} + \dot{E}_{m-b} + \dot{I}_{s-b} \quad (4.2)$$

$$m_m \cdot c_{p,m} \frac{dT_m}{dt} = -\dot{Q}_{m-i} - \dot{E}_{m-b} + \dot{I}_{s-m} \quad (4.3)$$

$$m_i \cdot \frac{d\omega_i}{dt} = \dot{\omega}_{o-i} + \dot{\omega}_{e-i} + \dot{\omega}_{x-i} \quad (4.4)$$

This model extends the thermal load model explained in Ref. [49] by adding the HVAC system contributions, both for energy and moisture mass balances in the cabin's air node. In Eq.4.1, the sensible heat from climate control system $\dot{Q}^S_{x-i}$ and the auxiliaries heat gain $\dot{Q}_a$, from the HVAC internal fans is added to the energy balance in the cabin's air node energy balance to ensure that the temperature T_i is in comfort conditions. Eq.4.4 represents the mass balance of moisture on the indoor cabin node as a function of three sources: the moisture transfer from the occupancy to the cabin $\dot{\omega}_{o-i}$, obtained using the hourly occupancy, the latent heat load of a seated person according to UNE-EN 14750 standard [4], and the enthalpy of vaporization at the indoor psychrometric conditions $\Delta h_{\nu ap,i}$. The moisture transfer from the external air node to the cabin due to leakages and openings $\dot{\omega}_{e-i}$. The moisture transfer from the climate control system $\dot{\omega}_{x-i}$, obtained from the coupled HVAC model.

The HVAC contributions of the balances, both the thermal gain $\dot{Q}^S_{x-i}$ and the moisture transfer $\dot{\omega}_{x-i}$ is calculated in accordance with

Eq.4.5.

$$\begin{aligned} \dot{Q}^S_{x-i} &= \rho_x \dot{V}_{x-i} c_{p,x} (T_x - T_i) \\ \dot{\omega}_{x-i} &= \rho_x \dot{V}_{x-i} (\omega_x - \omega_i) \end{aligned} \tag{4.5}$$

where x depends on the mode. In cooling mode (C), the cabin's air intake is the outlet airflow of the evaporator. In heating mode (H) the air comes from the condenser. In ventilation mode (V), fresh air is directly supplied from outdoors. In all cases, the cabin's exfiltration mass flowrate ($\dot{m}_{out}$) due to overpressure is assumed to be equivalent to the non-recirculated cabin's inlet mass flowrate.

The differential equation system is solved every time step using an ode-solver. The initial conditions include cabin pre-conditioning at the start of the day, which is a common strategy [68] to enhance early passenger comfort and reduce the consumption of the battery.

Control and operation model of the HVAC system

The HVAC control strategy sets the indoor operating temperature T_i according to a control curve [4] based on the external temperature T_e, while ω_i is left unrestricted, ensuring it is within the acceptable values of the standard [4]. The objective of the coupled model is to obtain the operating point of the HVAC that compensates this specific thermal load. If compensation is not possible, the indoor temperature is iteratively adjusted to meet the net balance.

To determine the HVAC mode, the sensible thermal load $\dot{Q}^S_i$ is assessed for ventilation (V) suitability. In this case, $\dot{V}_{x-i}$ combines non-recirculated external fresh air from the internal fans $\dot{V}_{fan-i}$ and, if needed and conditions are favorable, the air intake through the windows $\dot{V}_{wo-i}$. The first is calculated using a regulation coefficient r_{fan-i}, relative to its nominal flowrate $\dot{V}^N_{fan-i}$, conducted with the recirculation ratio or through its PWM of the fans. The second is obtained with a regulation coefficient r_{wo-i} of the maximum airflow capacity when opening all windows $\dot{V}^N_{wo-i}$, considered to be 14.46 air changes per hour

[69]. As a result, if ventilation compensates the load, $x = V$ is fixed. Otherwise, the mode is C for positive $\dot{Q}_i^S$ and H for negative.

Once the mode is known, the total HVAC demand $\dot{Q}_D$ is calculated using Eq.4.6. Only the latent load in mode C has been considered due to its significant impact on the consumption [70]. The impact of frost/defrost operation has also been considered (in H mode).

$$\dot{Q}_D = \begin{cases} \dot{Q}_i^S + \dot{Q}_f^S + \dot{Q}_i^L + \dot{Q}_f^L & , x = C \\ \dot{Q}_i^S + \dot{Q}_f^S + \lambda_{ice} \cdot \dot{Q}_{ice} & , x = H \end{cases} \tag{4.6}$$

where $\dot{Q}_i^L = \Delta h_{vap,i} \cdot \omega_{o-i} + \Delta h_{vap,e} \cdot \omega_{e-i}$ is the latent load of the indoor air node, obtained from the moisture contributions of the occupants and the external node due to infiltrations and openings. $\dot{Q}_f^S = \rho_e \cdot \dot{V}_{x-i} \cdot (1-\delta) \cdot c_{p,e} \cdot (T_e - T_i)$ is the energy required by the HVAC to heat or cool the non-recirculated external fresh air, and $\dot{Q}_f^L = \rho_e \cdot \dot{V}_{x-i} \cdot (1-\delta) \cdot \Delta h_{vap,e} \cdot (\omega_e - \omega_i)$ its latent load. λ_{ice} is a control parameter for frost/defrost conditions, activated when the mode is H and $T_e < 5°C$ [62], and $\dot{Q}_{ice}$ accounts for the loss of efficiency due to frost formation and the extra load that must be compensated for the defrost, according to the model described in [62], which also defines the extra power that the compressor and fans must supply $\dot{W}_{ice}$ in these conditions.

The recirculation ratio δ, defined as the ratio of the recirculated mass airflow to the total mass airflow, is fixed for each mode (0% in V, 64% in H, 90% in C) according to the standard system operation. The internal fan air flowrates $\dot{V}_{x-i}$ are set for each mode (PWM 60% in H, PWM 80% in C, PWM 100% in V), while the PWM of the external axial fans depends on the external temperature in the H and C modes (Table 4.2), and is turned off for ventilation. Once the demand is determined, the psychrometric conditions of the airflow entering the internal heat exchanger are calculated as a mixture of the recirculated and non-recirculated airflow.

The compressor speed is calculated by multidimensional linear interpolation using the HVAC system's performance map from IMST-ART, based on the operating model, thermal demand, flowrates and tem-

Table 4.2: PWM of external fans depending on the external temperature T_e and mode.

Mode C	PWM (%)	Mode H	PWM (%)
$T_e \leq 15°C$	60	$T_e \leq 5°C$	90
$15°C < T_e \leq 20°C$	70	$5°C < T_e \leq 10°C$	80
$20°C < T_e \leq 25°C$	80	$10°C < T_e \leq 15°C$	70
$25°C < T_e \leq 30°C$	90	$T_e > 15°C$	60
$T_e > 30°C$	100		

peratures and relative humidities. As a result, this map provides the fan energy consumption, refrigerant pressures and temperatures, airflow outlet conditions and condensate flowrate.

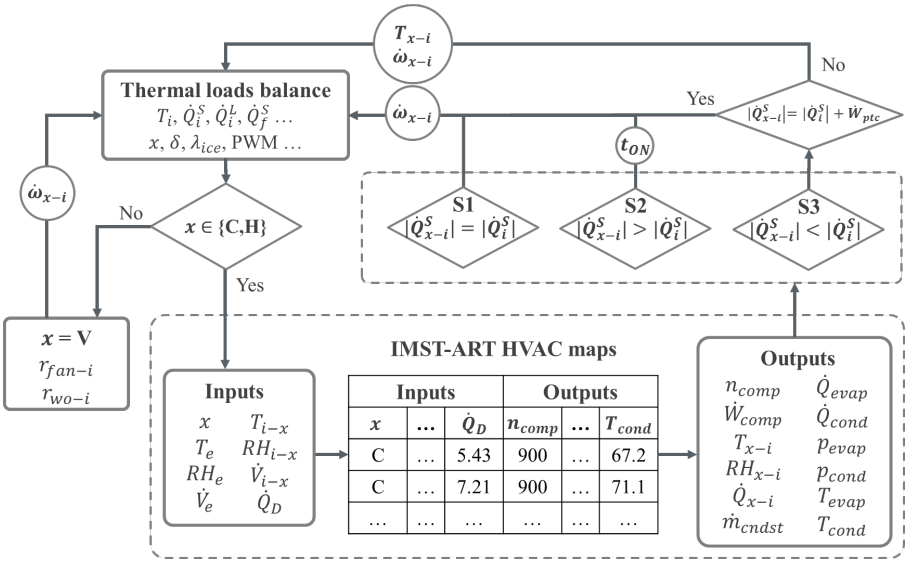

Figure 4.4: Methodology diagram for the coupled thermal load and HVAC model.

Once the operating point of the HVAC system is obtained, the sensible heat flow output from the internal exchanger is assessed for three scenarios (Figure 4.4). The first involves the compressor speed falling

within the manufacturer's specified range and matching the sensible demand, using the IMST-ART map interpolation for the desired outlet temperature T_x. In the second situation, with the minimum compressor speed (15 Hz) and excess sensible output, the equipment's on-time ratio t_{ON} is calculated for adjusted capacity and consumption. The third case, at maximum compressor speed (50 Hz) with insufficient sensible output, involves activating PTCs for heating and, if needed, iteratively adjusting the indoor air temperature and HVAC inlet airflow to balance the ODE.

Once the balances are resolved, the performance results such as the compressor's COP_{comp}, the overall COP_{hvac}, and the pressure ratio p_r are obtained, according to Eq.4.7.

$$\begin{aligned} \dot{W}_{hvac} &= t_{ON} \cdot (W_{comp} + W_{fan.i} + W_{fan,e} + W_{ptc} + \lambda_{ice} \cdot W_{ice}) \\ COP_{comp} &= \frac{Q_{hvac}}{t_{ON} \cdot (W_{comp} + \lambda_{ice} \cdot W_{ice,comp})} \\ COP_{hvac} &= \frac{Q_{hvac}}{W_{hvac}} \\ p_r &= \frac{p_{dis}}{p_{suc}} \end{aligned} \tag{4.7}$$

where Q_{hvac} is the heat delivered by the equipment during the time-step, $W_{ice,comp}$ is the extra power that the compressor must supply in frost/defrost conditions during the time step, p_{dis} is the absolute discharge pressure and p_{suc} is the absolute suction pressure.

4.2.7 Battery model

To determine the total bus energy consumption, the different power flows at the components of the electric bus have been modeled. Seven sub-systems are considered given their impact on the battery consumption $\dot{W}_{bat}$:

- The motor consumption $\dot{W}_{mot}$ and regenerative braking energy $\dot{W}_{reg}$ are derived from the powertrain model explained in Refs.

[71, 72], using the street slope from the 3D model, bus speed and acceleration from the kinematic model, and bus and road characteristics from Refs. [41, 54].

- The obtained HVAC system consumption $\dot{W}_{hvac}$.
- The consumption of hydraulic systems $\dot{W}_{hyd}$ (primarily the steering pump and the suspension system) is modeled using a linear approach [40]. A regression determines the consumption per distance as a function of the average speed and the number of stops per distance.
- The consumption of pneumatic systems $\dot{W}_{pne}$ (mainly for the brakes) is also modeled using a linear model [40].
- The consumption of auxiliary electrical systems $\dot{W}_{ele}$ includes multiple sources such as the lighting systems, the information, control and navigation systems, or the safety and emergency systems. Their overall consumption is assumed to be equal to 0.5 kW in all lines.
- The battery thermal management system consumption $\dot{W}_{bms}$ includes heating on cold winter days and cooling during normal operation, especially on hot days. This consumption has been obtained as a function of the external temperature, by Ref. [40].
- The impact on consumption from the battery's charge/discharge efficiency $\dot{W}_{eff}$ has been modeled assuming an overall charging and discharging efficiency of 0.93 [72].

Eq.4.8 encompasses the total battery consumption from the mentioned power flow components.

$$\dot{W}_{bat} = \dot{W}_{mot} - \dot{W}_{reg} + \dot{W}_{hvac} + \dot{W}_{hyd} + \dot{W}_{pne} + \dot{W}_{ele} + \dot{W}_{bms} + \dot{W}_{eff} \quad (4.8)$$

4.3 Simulation results

4.3.1 Representative year

The present section shows the results of a one-year simulation with a one-minute time step. The results focus on the HVAC system and the total battery consumption for the three bus lines. Table 4.3 shows the Mean Absolute Percentage Deviation (MAPD) for the different lines, as calculated by MAPD $= \frac{1}{n}\sum_t^n \left|\frac{\hat{y}(t)-y(t)}{y(t)}\right|$, where $\hat{y}$ is the prediction and y is the reference value. The results reveal a very small difference between the three lines, for all the main performance indicators of the HVAC system. For this reason, the rest of the HVAC results focus mainly on one single line (C1). Figure 4.5 shows the instantaneous thermal HVAC

Table 4.3: Mean absolute percentage deviation (MAPD) between lines C2 and C3 with respect to C1 for the main daily indicators.

line	Q_i	W_{comp}	W_{hvac}	COP_{comp}	COP_{hvac}	W_{mot}
C2	3.4%	5.3%	3.7%	0.3%	0.8%	18.4%
C3	2.0%	2.1%	1.7%	0.1%	0.3%	14.3%

demand contributions (sensible and latent) on a typical cold winter day (January), a mild day (March), and a hot summer day (July). The two contributions to the total demand $\dot{Q}_D$, according to Eq.4.6, are the thermal load of the cabin $\dot{Q}_i$, and the thermal load due to the non-recirculated fresh airflow from outside $\dot{Q}_f$. Above, the operating modes are represented: cooling (C), standard heating (H_{hp}), heating under frost/defrost conditions (H_{ice}), and heating with PTCs activated (H_{ptc}), ventilation mode with only internal blowers (V_{fan}), and ventilation where windows are also opened (V_{wo}). Figure 4.6 displays the series of temperature T and relative humidity RH inside the cabin i, outside e, and at the HVAC output x in the days discussed. Figure 4.7 shows the instantaneous consumptions of each HVAC component and the total consumption $\dot{W}_{hvac}$ on the same representative days. The consumptions of the compressor $\dot{W}_{comp}$, internal blowers $\dot{W}_{fan,i}$, external fans $\dot{W}_{fan,e}$, and PTCs $\dot{W}_{ptc}$ have been differentiated. In January, due to low external temperatures, the thermal demand remains nega-

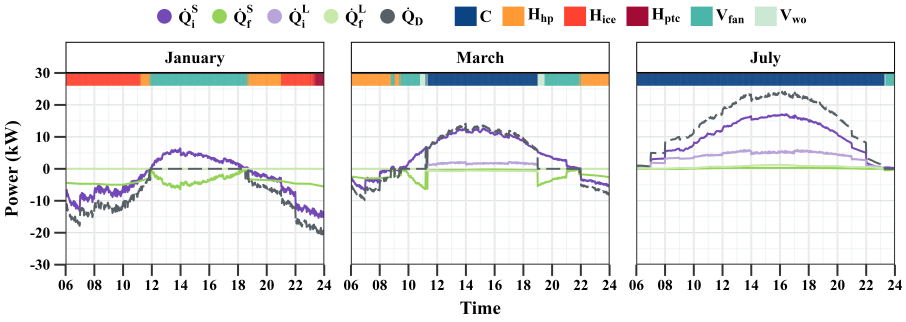

Figure 4.5: Instantaneous thermal demand contributions to the HVAC demand and the corresponding modes throughout a typical day in three different months of the year.

tive and the indoor temperature stays at the minimum setpoint value (19 °C), except during the midday. The system operates in heating mode until 11:45, primarily to warm the non-recirculated fresh airflow and compensate for the cabin conduction and convection losses. Until 11:15, under frost/defrost cycle conditions, the total absolute demand is of 3.2-17.8 kW, the compressor consumption fluctuates between 0.8 and 7.0 kW and the fans consume 0.4 kW each. During the 30 minutes of the standard H_{hp} operation, the absolute demand decreases from 3.2 kW to null and the temperature at the condenser outlet is between 1.0-8.9 °C, with a relative humidity between 41.1-63.0 %. The indoor relative humidity, starting from 49.0 %, gradually increases throughout the morning, mainly due to the moisture accumulation from occupants because of the 64 % recirculation rate in this mode. Between 11:45 and 18:45, the cabin's thermal demand becomes positive, primarily due to occupancy and solar radiation, peaking at 6.4 kW. This demand is compensated with ventilation, meeting the HVAC output to exterior conditions, and the internal fan is the only consumption of the system, with around 0.5 kW. The indoor relative humidity stays within 26.0-46.9 %, where the occupants' contribution compensates for the dehumidification by the exterior airflow. From 18:45 onward, the cabin's demand becomes negative again, almost symmetrically to the morning,

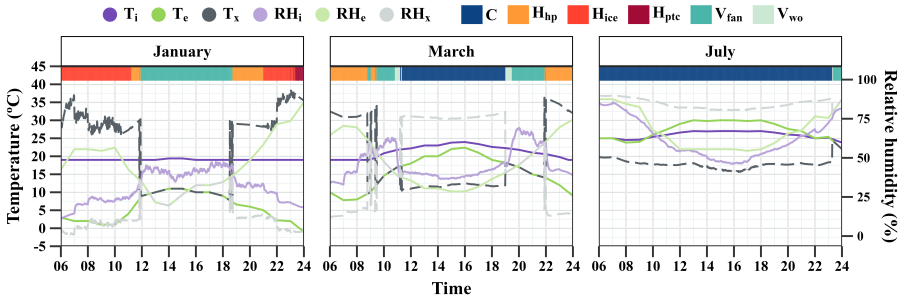

Figure 4.6: Series of temperature T and relative humidity RH inside the cabin i, outside e, and at the HVAC output x throughout a typical day in three different months of the year.

until 23:00. At a total thermal absolute demand of 17.9 kW, the heat pump cannot maintain the cabin temperature, and hereby the PTCs are activated with a peak of 2.8 kW at 24:00, leading to a total consumption of 10.2 kW to supply an absolute demand of 20.5 kW.

In March, the external temperature below 15 °C during early and late hours activates the heating mode, with a total thermal absolute demand ranging 2.0-9.8 kW, a compressor consumption around 0.5-2.4 kW and total consumption, including fans, reaching up to 3 kW. From 9:00, the cabin's demand turns positive and is initially met by ventilation using internal blowers, consuming up to 0.8 kW to compensate for a peak load of 14.1 kW. When this is insufficient, the windows are opened for 15 minutes, as the external conditions are favorable for load compensation, but the airflow from the internal blowers is not high enough. When still insufficient, the cooling mode is activated and the windows are closed until 19:00. The thermal demand in the cabin reaches a maximum of 13.0 kW with a compressor consumption between 1.1-3.1 kW and a total consumption, including fans, of maximum 4.0 kW. When the cooling mode is activated, the cabin's latent load reaches 2.2 kW which is partially compensated by the non-recirculated fresh air, but mainly by the condensation of moist air from the recirculated airflow (90 %) in the evaporator. Consequently, the relative humidity in the

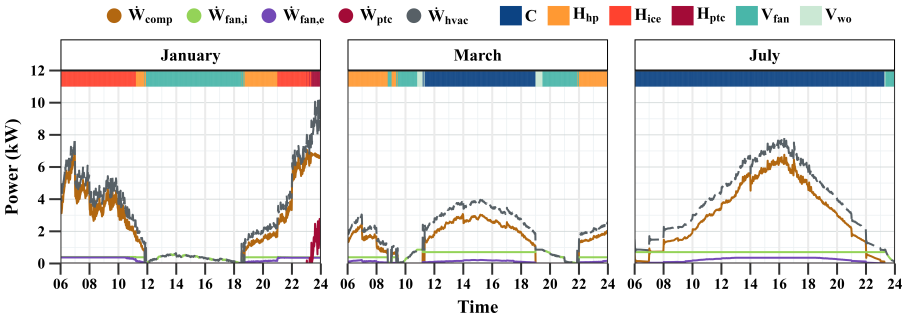

Figure 4.7: Instantaneous HVAC consumptions of each component and the corresponding modes throughout a typical day in three different months of the year.

cabin drops drastically from 77.0 % to 37.0 %. From this hour onward, the behavior is almost symmetric to the morning.

In July, the external temperature and relative humidity are high, even early (25 °C/94 %). Thus, the cooling mode is activated to meet the load requirements from occupancy and solar radiation. As the external temperature increases, the cabin's thermal demand and the compressor consumption rise, peaking at 30 °C with a compressor consumption of 6.8 kW and a total of 7.8 kW to compensate for a total demand of 24.1 kW with the 29.4 % of the latent component. The relative humidity decreases until 61.0 %, mainly because the condensation in the evaporator compensates for the indoor accumulation of moisture. After the peak, the operation is symmetric to the morning. However, in this case, at the end of the day, the load can be compensated just with ventilation.

Finally, the results have been compared with other reference publications [73, 74], achieving very similar outcomes for a comparable bus under similar load conditions, both for cooling and heating modes. Figure 4.8 represents the average daily cumulative sensible and latent thermal HVAC demand contributions, using stacked bars for contributions, and lines with points for the total accumulated demand Q_D, including both positive and negative values. The cooling demand for a

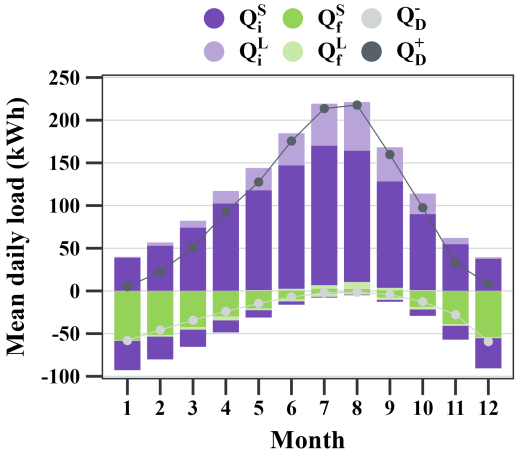

Figure 4.8: Average daily cumulative sensible and latent thermal HVAC demand contributions.

warm summer day is around 218 kWh, while the heating demand for a cold winter day is around 59 kWh. The cumulative cabin sensible heat load contribution is the predominant factor in the cooling demand (70-98%), while the sensible heat load from non-recirculated fresh airflow is the main contributor to the heating demand (43-68%), compensating for the cabin's positive contributions. The latent loads of both contributions compensate each other on cold and mild days, whereas on hot days, they contribute significantly to the cooling demand, exceeding 20% from June to October.

Figure 4.9 represents the mean operation time percentage of each mode. Since the thermal demand is compensated all year long, the percentage of uncompensated time has not been represented. Cooling mode is the most frequently operating mode throughout the year (44.6%), followed by ventilation (31.4%) and heating (24.0%). Cooling exceeds 50% from May to October, while heating is activated scarcely, except from December to March, with operating times ranging 31-41%. Ventilation is dominant from November to March (42-55)%, often sufficient to compensate for the positive cabin's thermal loads in these months.

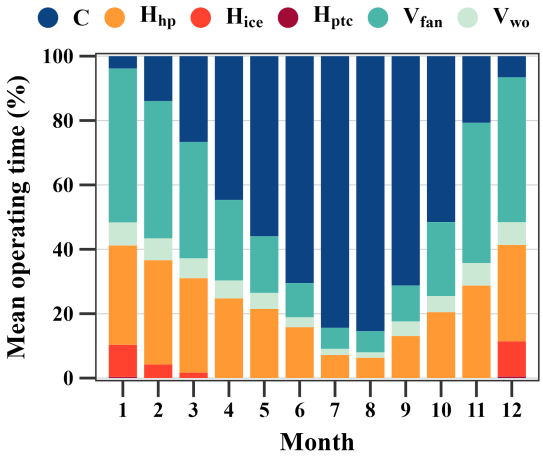

Figure 4.9: Mean operation time of each HVAC mode.

However, during peak load hours in these months, especially in the middle of the day with high occupancy, cooling is still necessary. Similarly, in summer, heating is still needed in the early or late hours of the day with low occupancy to warm the fresh airflow. Between December and March, the system operates 2-11% of the time under frost/defrost cycle conditions due to the low external temperatures, representing 26% of December's heating operation. On the coldest winter days, in January and December, brief PTC activation is needed (0.4%). The ventilation mode, combining window opening with maximum fan airflow, is active for about 5% annually when conditions are favorable and the airflow of the internal blowers is insufficient, serving as an intermediary strategy between fan-driven ventilation and active cooling.

Figure 4.10 shows the daily cumulative energy consumption of the HVAC components, with stacked bars for the compressor $\dot{W}_{comp}$, internal fans $\dot{W}_{fan,i}$, external fans $\dot{W}_{fan,e}$, and PTCs $\dot{W}_{ptc}$, and points and lines showing total consumption $\dot{W}_{hvac}$.

The peak total consumption reaches 63.9 kWh in hot summer days, with a minimum of 22.8 kWh on mild-cold days (November) and around

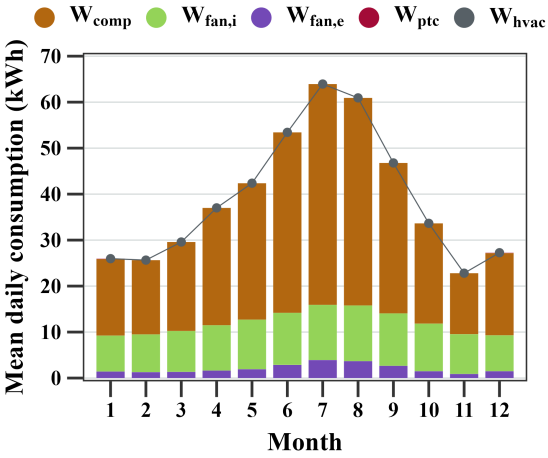

Figure 4.10: Daily cumulative energy consumption of the HVAC components.

26.6 kWh in cold winter days (January and December). The compressor is the largest consumer, accounting for 69-75% between April and September, in cooling-dominated periods, and 58-65% in other months when ventilation is the primary mode. The next major impact comes from the internal fans (19-38%) with more impact in moderately warm days where they are often the only operational device (ventilation mode). The consumption of the external fans is low all throughout the year (4-6% of the total). Lastly, the consumption of PTCs occurs only on the coldest days and is low even in these days (0.4%).

Figure 4.11 illustrates the yearly distribution of compressor and fan speeds (internal and external), across operating modes, using violin diagrams and a scatter plot to represent speed probability density and operational points. The fan speed depends on the mode, with the scatter plot showing the values and the violin diagram indicating the frequency. Ventilation modes set the internal blowers to their maximum speed (65 Hz) while deactivating the compressor and the external fans. Internal blowers are fixed in heating and cooling, with external fans (38-52 Hz) adjusted for external temperatures. The compressor usually runs at minimum speed (15 Hz), staying below 35 Hz in cooling and

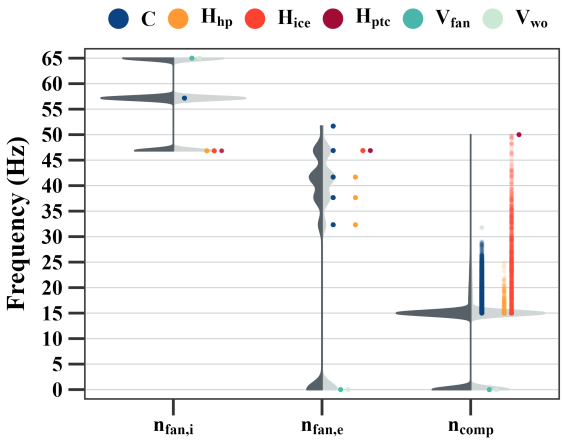

Figure 4.11: Yearly distribution of compressor and fan speeds (internal and external) across operating modes.

rarely exceeding it in heating (0.3% of the time, less than 0.1% annually). In heating, the on-time ratio is mostly below one (91.7% of the time), while in cooling, it is 83.5%, highlighting the system's oversizing and optimization potential.

Figure 4.12 presents the yearly distribution of three key system parameters across different modes: global COP_{hvac} for overall system efficiency, compressor COP_{comp} for the efficiency of the most energy-consuming component, and pressure ratio p_r for operational range of the system. Violin diagrams for each mode show the probability density of these parameters, while a scatter plot illustrates their range of values. In cooling and standard heating, the COP_{comp} are similar with the most probable value is around 4, while the COP_{hvac} is 2.9-3.1, respectively. Under frost/defrost conditions COP_{comp} falls to 3.7 and COP_{hvac} to 2.8. In PTC mode COP_{comp} drops below 2.5 and COP_{hvac} to 2.2. The pressure ratio ranges within 2.6-2.8 in cooling, 3.6-3.7 in standard heating, and 3.6-6.7 under frost/defrost conditions, and reaches up to 6.8 in PTC mode. Table 4.4 displays the annual summary of the most relevant indicators in each operating mode (m). Energy values per dis-

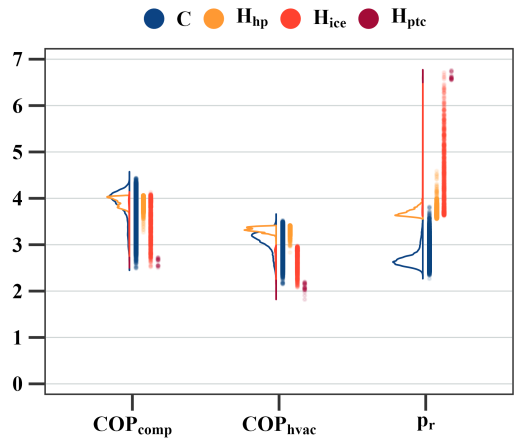

Figure 4.12: Yearly distribution of the global COP_{hvac}, compressor COP_{comp}, and pressure ratio p_r across different modes.

tance covered, their operating time percentage in each mode (ot), and performance and operation parameters have been obtained.

The cooling mode is active 44.8% of the time throughout the year, compensating for 72% of the thermal load in the cabin using the same percentage of the total annual consumption. The average annual consumption is $400\,\mathrm{Wh\,km^{-1}}$, distributed among the compressor (74%), internal fans (20%), and external fans (6%). The average COP_{comp} is 3.88, while the global is 2.71, with an average pressure ratio of 2.69. The average on-time ratio is below 65%, showing that the HVAC system is clearly oversized.

Ventilation is active 31.2% of the time but only compensates 15% of the cabin load. Ventilation is used to compensate low-intensity positive loads, consuming only 7% of the annual consumption, with an average consumption of $53\,\mathrm{Wh\,km^{-1}}$ from the internal blowers.

Heating modes operate 23.9% of the time, compensating 13% of the cabin load with an average consumption of $227\,\mathrm{Wh\,km^{-1}}$, accounting for 21% of the annual consumption.

Table 4.4: Annual summary of the most important indicators for each operating mode.

m	ot (%)	t_{ON} (%)	Q_i ($\frac{\text{Wh}}{\text{km}}$)	Q_D ($\frac{\text{Wh}}{\text{km}}$)	$\dot{W}_{comp}$ ($\frac{\text{Wh}}{\text{km}}$)	$\dot{W}_{fan,i}$ ($\frac{\text{Wh}}{\text{km}}$)	$\dot{W}_{fan,e}$ ($\frac{\text{Wh}}{\text{km}}$)	$\dot{W}_{ptc}$ ($\frac{\text{Wh}}{\text{km}}$)	$\dot{W}_{hvac}$ ($\frac{\text{Wh}}{\text{km}}$)	COP_{comp}	COP_{hvac}	p_r
C	44.8	64.4	1131	1113	297	81	22	-	400	3.88	2.71	2.70
V_{fan}	26.2	0.0	299	-	-	44	-	-	44	-	-	-
V_{wo}	5.0	0.0	601	-	-	99	-	-	99	-	-	-
H_{hp}	21.6	39.8	327	563	143	44	10	-	197	3.92	2.69	3.70
H_{ice}	2.2	94.6	886	1381	402	45	39	-	487	3.29	2.66	4.36
H_{ptc}	0.1	100	1529	2149	764	45	42	146	997	2.53	2.09	6.63

Table 4.5: HVAC performance, energy consumption and unmet load ratio Q_U on Line C1 under extreme conditions for six cases: peak TMY cooling (C+0.0K) and heating days (H-0.0K), plus ambient temperature variations (+2.5K, +5.0K for cooling; -2.5K, -5.0K for heating).

case	T_e^{max} (°C)	T_e^{min} (°C)	W_{comp} ($\frac{\text{Wh}}{\text{km}}$)	W_{ptc} ($\frac{\text{Wh}}{\text{km}}$)	W_{hvac} ($\frac{\text{Wh}}{\text{km}}$)	COP_{comp}	COP_{hvac}	n_{comp} (Hz)	Q_U (%)	p_r	T_{cond} (°C)	T_{evap} (°C)	T_{dis} (°C)
C+0.0K	37.0	21.0	360	0	469	3.4	2.3	17	0.0	3.1	47.2	9.5	76.8
C+2.5K	39.5	23.5	422	0	534	3.2	2.2	19	0.0	3.2	49.7	10.3	79.7
C+5.0K	42.0	26.0	523	0	638	3.1	2.1	22	0.0	3.4	52.2	10.7	83.0
H-0.0K	9.0	-1.0	267	11	337	3.2	2.5	29	0.0	5.0	35.5	-9.1	77.6
H-2.5K	6.5	-3.5	333	84	478	3.0	2.3	32	0.0	5.3	34.9	-10.6	79.3
H-5.0K	4.0	-6.0	415	211	677	2.9	2.3	33	1.1	5.7	33.8	-11.8	79.3

The average consumption is lower, but the average pressure ratio increases to 3.77 due to the temperature and pressure differences between evaporation and condensation. Among the three heating modes, the standard heating mode is the least demanding, consuming on average less than 50% of the cooling mode, as it operates under less demanding conditions. The heating mode under frost/defrost conditions is much more demanding, significantly reducing the efficiency of the evaporator and compressor during frost and increasing the cabin load during defrost. As a result, the average pressure ratio increases by 18%, and the average consumption rises to $487\,\mathrm{Wh\,km^{-1}}$, reducing the compressor COP_{comp}. Finally, the heating mode with PTC is the most demanding, always operating under frost/defrost conditions, the compressor working at nominal speed (3,000 rpm) and adding the consumption of PTCs. Consequently, the average pressure ratio increases to 6.63, the consumption rises to $997\,\mathrm{Wh\,km^{-1}}$, and the global COP_{hvac} drops down to 2.09. The HVAC system is perfectly capable of covering the heating demand. However, considering that the average on-time ratio in the standard heating mode is below 40%, the size of the heat pump can be potentially reduced, and the capacity of the PTC heaters increased to meet the heating demand requirements during, for example, 2.3% of the time represented by frost/defrost conditions and the current PTC usage.

The results suggest a significant potential for optimization due to the oversizing of the HVAC system. The mean on-time ratio in heating and cooling is below 57%, and the thermal demand is never higher than the system's capacity. Some potential strategies could be downsizing the HVAC system or introducing a thermal energy storage system. This would result in higher operating times and depending on the compressor and the control strategies, there is also room for a small improvement in the overall system's efficiency.

Figure 4.13 presents the average daily total cumulative energy consumption of the bus that the battery needs to supply for the three analyzed bus lines. The different contributions are represented with stacked bars, the net battery consumption in a red circle, and the daily

range net consumption with an error bar. Line C2 shows the high-

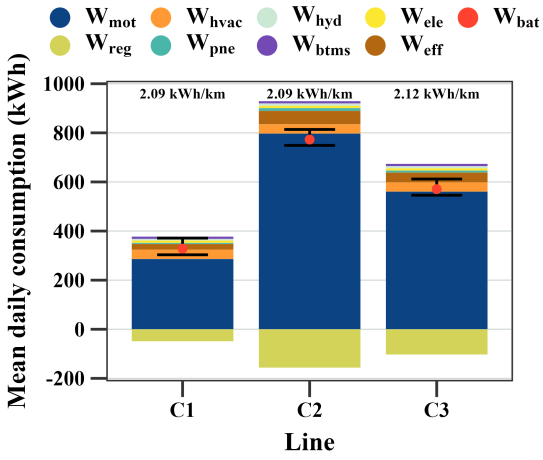

Figure 4.13: Average daily total cumulative energy consumption of the bus.

est average daily energy consumption (773 kWh), followed by C3 (571 kWh) and C1 (329 kWh), all of them with a daily range around (-25,42 kWh) concerning the annual mean. The variances between them are primarily due to the different distances traveled, which is a result of the mean speed, and to a lesser extent, the impact of acceleration, number of stops, shading, and topographical factors of each route. However, the energy consumption per unit of distance traveled remains remarkably consistent across all three cases, registering at 2.09 $\mathrm{Wh\,km^{-1}}$ for lines C1 and C2, and 2.12 $\mathrm{Wh\,km^{-1}}$ for line C3. This similarity is due to the compensatory effect of the different consumption components involved. In all lines, the powertrain consumption W_{mot} is the largest component, being 76% in C1, 86% in C2 and 83% in C3, although a significant portion of this (17% in C1, 20% in C2 and 18% in C3) is recovered through regenerative braking W_{reg}, standing for a net impact of 72% in C1, 83% in C2 and 80% in C3. The next highest consuming component is the HVAC W_{hvac} (12% in C1, 5% in C2 and 7% in C3), followed the consumption due to the battery charge and discharge efficiency W_{eff} (7% in all lines), auxiliary electrical systems W_{ele} and

battery thermal management W_{btms} (3% in C1, 1% in C2 and 2% in C3), hydraulic systems W_{hyd} (2% in C1, 1% in C2 and 2% in C3) and pneumatic systems W_{pne} (2% in C1, 2% in C2 and 1% in C3).

The annual average HVAC consumption per km is $0.24\,\mathrm{Wh\,km^{-1}}$ for C1, $0.10\,\mathrm{Wh\,km^{-1}}$ for C2, and $0.14\,\mathrm{Wh\,km^{-1}}$ for C3. The impact of the HVAC consumption on an average day of each month varies among the lines, with C1 ranging 7-20% (0.13-$0.47\,\mathrm{Wh\,km^{-1}}$), C2 between 3-10% ($0.06$-$0.20\,\mathrm{Wh\,km^{-1}}$), and C3 in 4-12% ($0.08$-$0.27\,\mathrm{Wh\,km^{-1}}$). The highest value occurs on a cooling-dominant day (July), and the lowest on a ventilation-dominant day (February).

The overall consumption per distance traveled is comparable to other publications, such as 2 - $4.6\,\mathrm{Wh\,km^{-1}}$ [39], 1.24 – $2.48\,\mathrm{Wh\,km^{-1}}$ [75], and 0.955 - $2.20\,\mathrm{Wh\,km^{-1}}$ [76].

4.3.2 Extreme weather conditions

This section analyzes the HVAC system's performance under severe weather conditions. For this purpose, the day with the highest cooling demand and the day with the highest heating demand from the TMY dataset were selected. To simulate extreme weather scenarios, the outdoor temperatures were adjusted by adding +2.5K and +5K in the peak cooling day and by reducing the temperature (-2.5K and -5K) in the peak heating day.

Table 4.5 presents the simulation results for the six cases of Line C1, by encompassing the modified TMY days with elevated and reduced temperatures. The most relevant indicators are reported in Table 4.5, for instance the operational performance variables (mean pressure ratio p_r, mean compressor speed n_{comp}, mean compressor and global COP, condensing T_{cond}, evaporating T_{evap} and discharge T_{dis} temperatures), the energy consumption (compressor, PTC and total HVAC system) and the unmet load ratio (Q_U).

The analysis reveals significant variations in the HVAC system's energy consumption under extreme weather conditions compared to the

annual TMY mean. In very warm days, the HVAC system can consume up to 90% more energy on the warmest peak TMY day or up to 165% more in the +5K case. In very cold days, the heating demand increases the energy consumption by 40% on the coldest TMY day or up to 182% in the -5K case. In these severe days, higher compressor speeds and higher refrigerant pressures and temperatures are obtained, hereby reducing the COP. In the heating scenarios, there is a significant increase in the use of the PTCs.

4.4 Optimization of the compressor size

Since the previous results indicate that the compressor is oversized, a parametric study has been performed to assess the impact of the compressor size on the energy consumption and on the load coverage. The IMST-ART performance maps of the compressor have been scaled with a factor of 100% (original scale), 87.5%, 75%, 62.5%, and 50%. These maps were first employed to identify an optimal compressor size that maximizes energy efficiency and meets the thermal load demands, both in real and in extreme weather conditions, while ensuring that internal operational limits, including refrigerant pressures and temperatures, are not exceeded. For each compressor size, a representative year simulation for line C1 was performed.

Figure 4.14 illustrates the impact of the compressor scale on the compressor COP_{comp}, the compressor speed n_{comp} and the unmet load ratio Q_u. In order to consider the impact of more severe weather conditions, in heating mode the impact of lower ambient temperatures (down to -5°C) has been represented in the x-axis. In cooling mode, the impact of +5°C in the ambient temperature has also been addressed. The

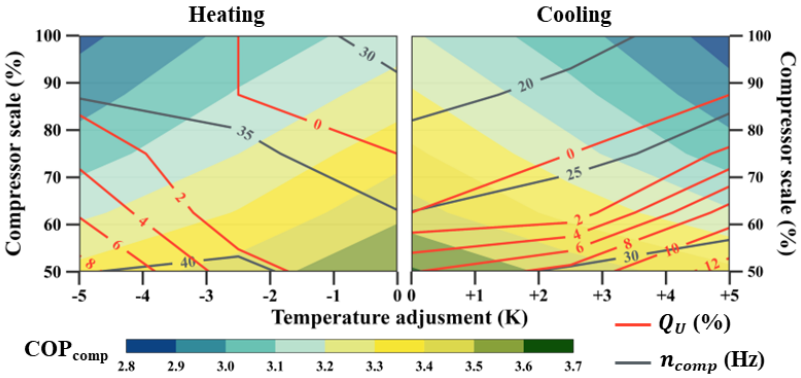

Figure 4.14: COP_{comp}, compressor speed (n_{comp}), and unmet load ratio (Q_U) for different compressor scales under ±5K on the ambient temperature.

results clearly indicate that the current compressor is oversized, a scale of 80% can adequately meet the thermal load during the peak demand

days of the TMY. In winter, 5K lower ambient temperatures would lead to 8% of unmet load. This number is higher for 5K higher temperatures in summer (12% unmet load). For compressor scales below 75% the system does not fully meet the cooling load.

Table 4.6 presents the full-year simulation results in terms of operating time, performance, energy consumption, and unmet load (Q_U) for different compressor scales. The results demonstrate that the system

Table 4.6: Main performance indicators obtained in Line C1 for different compressor scales in a full year simulation.

Scale (%)	ot (%)	W_{comp} ($\frac{\text{Wh}}{\text{km}}$)	W_{ptc} ($\frac{\text{Wh}}{\text{km}}$)	W_{hvac} ($\frac{\text{Wh}}{\text{km}}$)	COP_{comp}	COP_{hvac}	n_{comp} (Hz)	Q_U (%)
50.0	53	153	3	234	4.7	2.9	22	3.3
62.5	48	156	1	234	4.5	2.9	19	0.5
75.0	45	159	1	236	4.2	2.8	17	0.0
87.5	42	163	0	239	4.1	2.8	16	0.0
100	40	168	0	243	3.9	2.7	16	0.0

enhances its operation at lower scales. When the scale factor is 50%, the operating time increases by 13%. The mean compressor speed is reduced by 38% with a 23% decrease in the pressure ratio, a 4% reduction in average daily consumption, and a 7% improvement in the global COP.

Considering the outcomes from extreme cases and the annual simulation across different scales, a 75% scale is optimal to maximize operational efficiency and energy savings, while ensuring a full load compensation for a representative year. This achieves a 3% reduction in the annual energy consumption and a 4% enhancement in the COP, equivalent to an annual saving of over 200 MWh when applied across a fleet of 500 buses. Following the ASHRAE Standard [77] criterion, which recommends a maximum annual Q_U of 3.4% to ensure adequate thermal coverage, the optimal compressor scale could be reduced to 50% of the current size. However, considering the expected temperature increase due to climate change, a more conservative approach is to adopt

a scale of 75%. With this scale, even under an extreme +5K scenario, the uncompensated load would only exceed 2% of the time.

4.5 Conclusions

The shift towards electric urban buses is key for sustainable transportation, with HVAC systems playing a crucial role in extending the range of batteries.

The present study introduces advanced dynamic models for simulating urban bus energy consumption under real conditions, emphasizing HVAC consumption and its impact on overall energy consumption. This study includes a 3D city model, a stochastic driving cycle for traffic realism, and a climate model for environmental factors. The thermal and HVAC model analyzes thermal loads and moisture, while a detailed HVAC model covers multiple operating modes. A comprehensive battery model evaluates overall energy usage, including the motor and auxiliary systems, allowing precise simulations in complex urban environments. The model has been applied to a bus from the urban fleet of València, Spain. The simulations involve a one-year period at 1-min intervals on three lines, covering different urban typologies. The mean daily results for the main HVAC indicators across the three lines are similar, with maximum deviations of 3.4% in cabin load, 3.7% in total energy consumption, and 0.8% in global COP.

The results of the full-year simulation show that cooling is the dominant mode (44.6% of the time), followed by ventilation (31.4%), and heating (24.0%). The average annual consumption in cooling mode is $0.40\,\mathrm{Wh\,km^{-1}}$, for ventilation $0.05\,\mathrm{Wh\,km^{-1}}$, and the average for the heating modes is $0.23\,\mathrm{Wh\,km^{-1}}$. The compressor generally operates at a minimum speed (15 Hz) and only reaches its maximum speed (50 Hz) in heating mode for less than 0.1% of the total operational time. Cooling mode speeds do not exceed 35 Hz, and heating mode rarely does. Regarding the main performance indicators, in cooling and standard heating modes, the compressor's COP averages around 4, while the overall system's COP is approximately 3. Under frost/defrost conditions, these figures drop to 3.7 and 2.8, respectively, and decrease further in PTC mode to below 2.5 and 2.2. Pressure ratios vary with each mode, ranging from 2.6-2.8 in cooling, 3.6-3.7 in standard heating,

3.6-6.7 under frost/defrost conditions, and up to 6.8 in PTC mode.

The impact of more severe weather conditions has also been analyzed. The energy consumption increased substantially, up to 165% more in the +5K scenario compared to the TMY annual mean. These conditions forced the HVAC system to operate under higher pressures and temperatures.

The study suggests that the HVAC system could be potentially downsized, given that the on-time ratio is always below 65% in cooling mode and below 40% in standard heating mode (no defrost). Potential optimizations include increasing PTC heater capacity for occasional frost/defrost conditions and introducing a thermal energy storage buffer. Regarding the overall energy consumption for each line, line C2 has the highest average daily energy use at 773 kWh, followed by C3 (571 kWh) and C1 (329 kWh), with a daily variance of around (-25.42 kWh) from the annual mean. Consumption differences are mainly due to the traveled distance. The energy use per km is similar across lines: $2.09\,\mathrm{Wh\,km^{-1}}$ for C1 and C2, and $2.12\,\mathrm{Wh\,km^{-1}}$ for C3. The powertrain is the major consumer, with a significant part offset by regenerative braking, with a mean annual net contribution of 76-86%. The HVAC is the second largest contributor, with a mean annual ratio between 5 and 12%. The HVAC system's annual average energy consumption varies by bus line: $0.24\,\mathrm{Wh\,km^{-1}}$ for line C1, $0.10\,\mathrm{Wh\,km^{-1}}$ for line C2, and $0.14\,\mathrm{Wh\,km^{-1}}$ for line C3. As a conclusion, the impact of HVAC on urban electric bus consumption is notably higher on routes with lower speeds and more stops per kilometer. In these cases, the driving range in cooling mode, which is the most demanding mode in València, can be reduced by the HVAC by up to 15% to 20% in mild summer days with hot summer days, respectively.

Lastly, an optimization study has demonstrated that a scale factor of 75% is more convenient for the compressor. The annual energy consumption can be potentially reduced by 3%, with a 4% improvement in the COP. The impact on the performance is relatively small, but a 25% reduction of the size is not negligible with respect to its cost.

The findings of this study underscore the importance of adapting and optimizing HVAC systems given real operational conditions. This can only be addressed with sufficiently detailed models on the thermal model of the vehicle, of the thermal loads, or of the HVAC system.

4.6 Acknowledgments

This work has been supported by the Generalitat Valenciana inside the program "Subvencions per a la contractació de personal investigador de caràcter predoctoral (ACIF/2019/239)". The authors gratefully acknowledge the support of Angel Navarro and EMT València for providing the bus and route data.

4.7 References

[1] International Energy Agency. Global EV Outlook 2023. Paris, 2023.

[2] European Commission. Proposal for amending Regulation EU 2019/1242 as regards strengthening the CO2 emission performance standards for new heavy-duty vehicles and integrating reporting obligations, and repealing Regulation EU 2018/956. 2023.

[3] Asian Development Bank. Sustainable Transport Solutions: Low-Carbon Buses in the People's Republic of China. 2018. https://doi.org/10.22617/TCS189646-2.

[4] Asociación Española de Normalización (UNE). Railway applications - Air conditioning for urban, suburban and regional rolling stock (UNE-EN Standard No. 14750). 2007.

[5] A. Lajunen, Y. Yang, and A. Emadi. Review of Cabin Thermal Management for Electrified Passenger Vehicles. In: *IEEE Trans Veh Technol* 69.(6) (2020), 6025–6040. https://doi.org/10.1109/TVT.2020.2988468.

[6] P. Li, Y. Zhang, K. Zhang, and M. Jiang. The effects of dynamic traffic conditions, route characteristics and environmental conditions on trip-based electricity consumption prediction of electric bus. In: *Energy* 218 (2021), 119437. https://doi.org/10.1016/J.ENERGY.2020.119437.

[7] P. Li, Y. Zhang, Y. Zhang, and K. Zhang. Prediction of electric bus energy consumption with stochastic speed profile generation modelling and data driven method based on real-world big data. In: *Appl Energy* 298 (2021), 117204. https://doi.org/10.1016/J.APENERGY.2021.117204.

[8] S. Chen, B. Du, Q. Li, and D. Xue. The influence of different orientations and ventilation cases on temperature distribution of the car cabin in the hot soak. In: *Case Studies in Thermal*

Engineering 39 (2022), 102401. https://doi.org/10.1016/J.CSITE.2022.102401.

[9] M. A. Alam, R. Kumar, D. Banoriya, A. S. Yadav, G. Goga, K. K. Saxena, D. Buddhi, and R. Mohan. Design and development of thermal comfort analysis for air-conditioned compartment. In: *International Journal on Interactive Design and Manufacturing* (2022), 1–11. https://doi.org/10.1007/S12008-022-01015-8/METRICS.

[10] P. Bandi, N. P. Manelil, M. P. Maiya, S. Tiwari, A. Thangamani, and J. L. Tamalapakula. Influence of flow and thermal characteristics on thermal comfort inside an automobile cabin under the effect of solar radiation. In: *Appl Therm Eng* 203 (2022), 117946. https://doi.org/10.1016/J.APPLTHERMALENG.2021.117946.

[11] V. Lemort, G. Olivier, and C. De Pelsemaker. Thermal Energy Management in Vehicles. https://www.wiley.com/en-us/Thermal+Energy+Management+in+Vehicles-p-9781119251750. 2023, 320.

[12] Y. Bie, Y. Liu, S. Li, and L. Wang. HVAC operation planning for electric bus trips based on chance-constrained programming. In: *Energy* 258 (2022), 124807. https://doi.org/10.1016/J.ENERGY.2022.124807.

[13] J. Vepsäläinen, K. Otto, A. Lajunen, and K. Tammi. Computationally efficient model for energy demand prediction of electric city bus in varying operating conditions. In: *Energy* 169 (2019), 433–443. https://doi.org/10.1016/J.ENERGY.2018.12.064.

[14] D. Ramsey, L. Boulon, and A. Bouscayrol. Modeling of an EV air conditioning system for energetic studies in summer. In: *2021 IEEE Vehicle Power and Propulsion Conference, VPPC 2021 - Proceedings*. 2021. https://doi.org/10.1109/VPPC53923.2021.9699119.

[15] F. Lan, H. Chen, J. Chen, and W. Li. Effect of urban microclimates on dynamic thermal characteristics of a vehicle cabin. In:

Case Studies in Thermal Engineering (2023), 103162. https://doi.org/10.1016/J.CSITE.2023.103162.

[16] Z. Shuofeng, M. R. Amini, J. Sun, and C. Mi. A Two-Layer Real-Time Optimization Control Strategy for Integrated Battery Thermal Management and HVAC System in Connected and Automated HEVs. In: *IEEE Trans Veh Technol* 70.(7) (2021), 6567–6576. https://doi.org/10.1109/TVT.2021.3085938.

[17] N. A. El-Taweel, A. Zidan, and H. E. Z. Farag. Novel Electric Bus Energy Consumption Model Based on Probabilistic Synthetic Speed Profile Integrated with HVAC. In: *IEEE Transactions on Intelligent Transportation Systems* 22.(3) (2021), 1517–1531. https://doi.org/10.1109/TITS.2020.2971686.

[18] M. Gallet, T. Massier, and T. Hamacher. Estimation of the energy demand of electric buses based on real-world data for large-scale public transport networks. In: *Appl Energy* 230 (2018), 344–356. https://doi.org/10.1016/J.APENERGY.2018.08.086.

[19] J. Jiang, Y. Yu, H. Min, Q. Cao, W. Sun, Z. Zhang, and C. Luo. Trip-level energy consumption prediction model for electric bus combining Markov-based speed profile generation and Gaussian processing regression. In: *Energy* 263 (2023), 125866. https://doi.org/10.1016/J.ENERGY.2022.125866.

[20] H. He, M. Yan, C. Sun, J. Peng, M. Li, and H. Jia. Predictive air-conditioner control for electric buses with passenger amount variation forecast. In: *Appl Energy* 227 (2018), 249–261. https://doi.org/10.1016/J.APENERGY.2017.08.181.

[21] D. Ramsey, A. Bouscayrol, L. Boulon, A. Desreveaux, and A. Vaudrey. Flexible Simulation of an Electric Vehicle to Estimate the Impact of Thermal Comfort on the Energy Consumption. In: *IEEE Transactions on Transportation Electrification* 8.(2) (2022), 2288–2298. https://doi.org/10.1109/TTE.2022.3144526.

[22] D. Ramsey, A. Bouscayrol, and L. Boulon. Energy Consumption of a Battery Electric Vehicle in Winter Considering Preheating: Tradeoff between Improved Performance and Total Energy Consumption. In: *IEEE Vehicular Technology Magazine* 17.(3) (2022), 104–112. https://doi.org/10.1109/MVT.2022.3158043.

[23] M. A. Fayazbakhsh and M. Bahrami. Comprehensive Modeling of Vehicle Air Conditioning Loads Using Heat Balance Method. In: *SAE Technical Papers* 2 (2013). https://doi.org/10.4271/2013-01-1507.

[24] H. Khayyam, J. Abawajy, and R. N. Jazar. Intelligent energy management control of vehicle air conditioning system coupled with engine. In: *Appl Therm Eng* 48 (2012), 211–224. https://doi.org/10.1016/J.APPLTHERMALENG.2012.04.050.

[25] M. Direk, M. S. Mert, F. Yüksel, and A. Keleşoğlu. Exergetic Investigation of a R1234yf Automotive Air Conditioning System with Internal Heat Exchanger. In: *International Journal of Thermodynamics* 21.(2) (2018), 103–109. https://doi.org/10.5541/IJOT.357232.

[26] C. Dullinger, W. Struckl, and M. Kozek. A modular thermal simulation tool for computing energy consumption of HVAC units in rail vehicles. In: *Appl Therm Eng* 78 (2015), 616–629. https://doi.org/10.1016/J.APPLTHERMALENG.2014.11.065.

[27] E. Tosun, M. Bilgili, G. Tuccar, A. Yasar, and K. Aydin. Exergy analysis of an inter-city bus air-conditioning system. In: *International Journal of Exergy* 20.(4) (2016), 445–464. https://doi.org/10.1504/IJEX.2016.078094.

[28] R. Prabakaran and D. Mohan Lal. A novel exergy based charge optimisation for a mobile air conditioning system: An experimental study. In: *J Therm Anal Calorim* 132.(2) (2018), 1241–1252. https://doi.org/10.1007/S10973-018-6998-0/METRICS.

[29] E. B. Ratts and J. S. Brown. An experimental analysis of cycling in an automotive air conditioning system. In: *Appl Therm Eng* 20.(11) (2000), 1039–1058. https://doi.org/10.1016/S1359-4311(99)00080-0.

[30] J. Jabardo, W. Mamani, and M. R. Ianella. Modeling and experimental evaluation of an automotive air conditioning system with a variable capacity compressor. In: *International Journal of Refrigeration* 25.(8) (2002), 1157–1172. https://doi.org/10.1016/S0140-7007(02)00002-6.

[31] G. H. Lee and J. Y. Yoo. Performance analysis and simulation of automobile air conditioning system. In: *International Journal of Refrigeration* 23.(3) (2000), 243–254. https://doi.org/10.1016/S0140-7007(99)00047-X.

[32] D. Di Battista and R. Cipollone. High efficiency air conditioning model based analysis for the automotive sector. In: *International Journal of Refrigeration* 64 (2016), 108–122. https://doi.org/10.1016/J.IJREFRIG.2015.12.014.

[33] E. Afrasiabian, R. Douglas, M. Geron, and G. Cunningham. A numerical evaluation of a novel recovery fresh air heat pump concept for a generic electric bus. In: *Appl Therm Eng* 209 (2022), 118181. https://doi.org/10.1016/J.APPLTHERMALENG.2022.118181.

[34] J.-M. Corberán, S. Martínez-Ballester, J. Gonzálvez-Maciá, and C. La-Barbera. Error estimation of single phase effectiveness and LMTD methodologies when applied to heat exchangers with phase change. In: *Journal of Physics: Conference Series* 745.(3) (2016), 032125. https://doi.org/10.1088/1742-6596/745/3/032125.

[35] D. C. Vásconez-Núñez, J. Gonzálvez-Maciá, J. M. Corberán, and J. Payá. Development and validation of a dynamic thermal model of a minibus using TRNSYS. In: *International Journal of Vehicle Design* 77.(1–2) (2018), 87–107. https://doi.org/10.1504/IJVD.2018.098272.

[36] R. Mastrullo, A. W. Mauro, and C. Vellucci. Refrigerant Alternatives for High Speed Train A/C Systems: Energy Savings and Environmental Emissions Evaluation under Variable Ambient Conditions. In: *Energy Procedia* 101 (2016), 280–287. https://doi.org/10.1016/J.EGYPRO.2016.11.036.

[37] B. Torregrosa-Jaime, J. Payá, and J. Corberan. Design of efficient air-conditioning systems for electric vehicles. In: *SAE International Journal of Alternative Powertrains* 2.(2) (2013), 291–303. https://doi.org/10.4271/2013-01-0864.

[38] J. Corberan, J. Gonzalvez, P. Montes, and R. Blasco. 'ART' A Computer Code To Assist The Design Of Refrigeration and A/C Equipment. In: *International Refrigeration and Air Conditioning Conference*. https://docs.lib.purdue.edu/iracc/570. 2002.

[39] H. Basma, C. Mansour, M. Haddad, M. Nemer, and P. Stabat. Energy consumption and battery sizing for different types of electric bus service. In: *Energy* 239 (2022), 122454. https://doi.org/10.1016/J.ENERGY.2021.122454.

[40] H. Basma, C. Mansour, M. Haddad, M. Nemer, and P. Stabat. Comprehensive energy modeling methodology for battery electric buses. In: *Energy* 207 (2020), 118241. https://doi.org/10.1016/J.ENERGY.2020.118241.

[41] A. Broatch, P. Olmeda, P. Bares, and S. Aceros. Integral Thermal Management Studies in Winter Conditions with a Global Model of a Battery-Powered Electric Bus. In: *Energies (Basel)* 16.(1) (2023). https://doi.org/10.3390/en16010168.

[42] D. Nicolaides, D. Cebon, and J. Miles. An Urban Charging Infrastructure for Electric Road Freight Operations: A Case Study for Cambridge UK. In: *IEEE Syst J* 13.(2) (2019), 2057–2068. https://doi.org/10.1109/JSYST.2018.2864693.

[43] O. A. Hjelkrem, K. Y. Lervåg, S. Babri, C. Lu, and C. J. Södersten. A battery electric bus energy consumption model for strategic purposes: Validation of a proposed model structure with data from bus fleets in China and Norway. In: *Transp Res D Transp*

Environ 94 (2021), 102804. https://doi.org/10.1016/J.TRD.2021.102804.

[44] D. Nam, P. Lee, G. Lee, Y. Kwon, and J. Lee. Optimization of an oil charge amount on electric driven scroll compressor for eco-friendly vehicle. In: *International Journal of Refrigeration* 57 (2015), 54–61. https://doi.org/10.1016/J.IJREFRIG.2015.05.009.

[45] L. He, P. Li, Y. Zhang, H. Jing, and Z. Gu. Control strategy analysis of multistage speed compressor for vehicle air conditioning based on particle swarm optimization. In: *Case Studies in Thermal Engineering* 47 (2023), 103033. https://doi.org/10.1016/J.CSITE.2023.103033.

[46] R. Prabakaran, D. M. Lal, and S. C. Kim. A state of art review on future low global warming potential refrigerants and performance augmentation methods for vapour compression based mobile air conditioning system. In: *Journal of Thermal Analysis and Calorimetry 2022 148:2* 148.(2) (2022), 417–449. https://doi.org/10.1007/S10973-022-11485-3.

[47] T. Lee, K. H. Shin, J. Kim, D. Jung, and J. H. Kim. Design optimization of external variable displacement compressor with R1234yf for vehicle air conditioning system. In: *Appl Therm Eng* 198 (2021), 117493. https://doi.org/10.1016/J.APPLTHERMALENG.2021.117493.

[48] D. Srinivasan and P. Phadke. Reducing AC Power Consumption By Compressor Downsizing on a Sports Utility Vehicle. In: *International Refrigeration and Air Conditioning Conference*. https://docs.lib.purdue.edu/iracc/844. 2006.

[49] J. D. Viana-Fons and J. Payá. Dynamic cabin model of an urban bus in real driving conditions. In: *Energy* (2023), 129769. https://doi.org/10.1016/J.ENERGY.2023.129769.

[50] R Core Team. R: A Language and Environment for Statistical Computing. https://www.R-project.org/. 2022.

[51] M. Kottek, J. Grieser, C. Beck, B. Rudolf, and F. Rubel. World Map of the Köppen-Geiger climate classification updated. In: *Meteorologische Zeitschrift* 15.(3) (2006), 259–263. https://doi.org/10.1127/0941-2948/2006/0130.

[52] F. Gómez, N. Tamarit, and J. Jabaloyes. Green zones, bioclimatics studies and human comfort in the future development of urban planning. In: *Landsc Urban Plan* 55.(3) (2001), 151–161. https://doi.org/10.1016/S0169-2046(01)00150-5.

[53] T. Huld, E. Paietta, P. Zangheri, and I. P. Pascua. Assembling Typical Meteorological Year Data Sets for Building Energy Performance Using Reanalysis and Satellite-Based Data. In: *Atmosphere 2018, Vol. 9, Page 53* 9.(2) (2018), 53. https://doi.org/10.3390/ATMOS9020053.

[54] Empresa Municipal de Transportes de Valencia. https://www.emtvalencia.es. 2023.

[55] T. R. Oke, G. Mills, A. Christen, and J. A. Voogt. Urban Climates. Cambridge University Press, 2017. https://doi.org/10.1017/9781139016476.

[56] J. D. Viana-Fons, J. Gonzálvez-Maciá, and J. Payá. Development and validation in a 2D-GIS environment of a 3D shadow cast vector-based model on arbitrarily orientated and tilted surfaces. In: *Energy Build* 224 (2020). https://doi.org/10.1016/j.enbuild.2020.110258.

[57] J.-R. Roussel and D. Auty. Airborne LiDAR Data Manipulation and Visualization for Forestry Applications. https://cran.r-project.org/package=lidR. 2023.

[58] J.-R. Roussel, D. Auty, N. C. Coops, P. Tompalski, T. R. Goodbody, A. S. Meador, J.-F. Bourdon, F. de Boissieu, and A. Achim. lidR: An R package for analysis of Airborne Laser Scanning (ALS) data. In: *Remote Sensing of Environment* 251 (2020), 112061. https://doi.org/10.1016/j.rse.2020.112061.

[59] M. Dalponte and D. A. Coomes. Tree-centric mapping of forest carbon density from airborne laser scanning and hyperspectral data. In: *Methods Ecol Evol* 7.(10) (2016), 1236–1245. https://doi.org/10.1111/2041-210X.12575.

[60] Google Inc. General Transit Feed Specification. https://developers.google.com/transit/gtfs/reference. 2022.

[61] W. R. Mebane and J. S. Sekhon. Genetic Optimization Using Derivatives: The rgenoud Package for R. In: *J Stat Softw* 42.(11) (2011), 1–26. https://doi.org/10.18637/JSS.V042.I11.

[62] U.S. Department of Energy. EnergyPlusTM Version 22.1.0 - Engineering Reference. 2022.

[63] J. A. Duffie and W. A. Beckman. Solar Engineering of Thermal Processes: Fourth Edition. Solar Engineering of Thermal Processes: Fourth Edition, 2013. https://doi.org/10.1002/9781118671603.

[64] Universitat Politècnica de Valéncia, Instituto de Ingenieria Energética, Spain. IMST-ART v4.0 - Simulation tool to assist the selection, design and optimization of refrigerator equipment and components. http://www.imst-art.com. 2022.

[65] F. Vera-García, J. R. García-Cascales, J. M. Corberán-Salvador, J. Gonzálvez-Maciá, and D. Fuentes-Díaz. Assessment of condensation heat transfer correlations in the modelling of fin and tube heat exchangers. In: *International Journal of Refrigeration* 30.(6) (2007), 1018–1028. https://doi.org/10.1016/J.IJREFRIG.2007.01.005.

[66] J. R. García-Cascales, F. Vera-García, J. M. Corberán-Salvador, J. Gonzálvez-Maciá, and D. Fuentes-Díaz. Assessment of boiling heat transfer correlations in the modelling of fin and tube heat exchangers. In: *International Journal of Refrigeration* 30.(6) (2007), 1004–1017. https://doi.org/10.1016/J.IJREFRIG.2007.01.006.

[67] A. Pisano, S. Martinez-Ballester, J. M. Corberán, F. H. Monpeán, F. I. Gómez, and J.-R. G. Cascales. A Discussion about the Methodology to Validate the Correlations of Heat Transfer Coefficients and Pressure Drop during the Condensation in a Finned-Tube Heat Exchanger. https://docs.lib.purdue.edu/iracc/1405. 2014.

[68] M. Tozzi, M. V. Corazza, U. Guida, and A. Musso. Testing innovations for increased energy efficiency of electric buses: Evidence from the EBSF-2 project. In: *Transportation Research Procedia* 48 (2020), 2166–2175. https://doi.org/10.1016/J.TRPRO.2020.08.273.

[69] S. K. Chaudhry and S. P. Elumalai. The influence of school bus ventilation scenarios over in-cabin PM number concentration and air exchange rates. In: *Atmos Pollut Res* 11.(8) (2020), 1396–1407. https://doi.org/10.1016/J.APR.2020.05.021.

[70] N. S. Raman, K. Devaprasad, B. Chen, H. A. Ingley, and P. Barooah. Model predictive control for energy-efficient HVAC operation with humidity and latent heat considerations. In: *Appl Energy* 279 (2020), 115765. https://doi.org/10.1016/J.APENERGY.2020.115765.

[71] C. Gaete-Morales, H. Kramer, W. P. Schill, and A. Zerrahn. An open tool for creating battery-electric vehicle time series from empirical data, emobpy. In: *Scientific Data 2021 8:1* 8.(1) (2021), 1–18. https://doi.org/10.1038/s41597-021-00932-9.

[72] C. Fiori and V. Marzano. Modelling energy consumption of electric freight vehicles in urban pickup/delivery operations: analysis and estimation on a real-world dataset. In: *Transp Res D Transp Environ* 65 (2018), 658–673. https://doi.org/10.1016/J.TRD.2018.09.020.

[73] E. Afrasiabian, R. Douglas, and R. Best. Real-Time modelling of a two-unit baseline air conditioning system for a generic bus subjected to different levels of occupancy. In: *2020 15th In-*

ternational Conference on Ecological Vehicles and Renewable Energies, EVER 2020. 2020. https://doi.org/10.1109/EVER48776.2020.9243013.

[74] C. Os'Boyle, R. Douglas, R. Best, and M. Geron. Vehicle Thermal Modelling for Improved Drive Cycle Analysis of a Generic City Bus. In: *2020 5th International Conference on Smart and Sustainable Technologies, SpliTech 2020*. 2020. https://doi.org/10.23919/SPLITECH49282.2020.9243725.

[75] Z. Gao, Z. Lin, T. J. LaClair, C. Liu, J.-M. Li, A. K. Birky, and J. Ward. Battery capacity and recharging needs for electric buses in city transit service. In: *Energy* 122 (2017), 588–600. https://doi.org/10.1016/J.ENERGY.2017.01.101.

[76] S. Doulgeris, A. Zafeiriadis, N. Athanasopoulos, N. Tzivelou, M. Michali, S. Papagianni, and Z. Samaras. Evaluation of energy consumption and electric range of battery electric busses for application to public transportation. In: *Transportation Engineering* 15 (2024), 100223. https://doi.org/10.1016/J.TRENG.2023.100223.

[77] ASHRAE American Society of Heating Refrigerating and A.-C. Engineers. ASHRAE Handbook - Fundamentals. Atlanta, GA: ASHRAE, 2017.

Chapter 5

Discussion of the main results

This chapter presents a comprehensive overview of the findings and insights from the PhD thesis. The discussion is organized into two sections:

- Discussion and justification of the modeling approach: This section offers a general discussion on the methodology.
- Results overview: This section provides a comprehensive summary of the results, aligning them with the primary objectives and identified research gaps in the literature.

5.1 Discussion and justification of the modeling approach

This section justifies the level of detail and complexity adopted in part of the submodels. This discussion is not included in the three published articles, since it is a general perspective of the entire simulation tool. This section discusses:

- The variability of the total instantaneous HVAC consumption is analyzed, as well as its relationship with the external temperature and the solar radiation.
- Exploring whether the global solar horizontal radiation from TMY could determine the solar heat gain of the bus.
- Two potential approaches to shading models are discussed, as well as the importance of employing a shading model in urban environments.
- The effect of modeling each bus surface individually on the overall thermal dynamics is evaluated.
- The differences between using a transient thermal model or a steady-state model are compared.

5.1.1 The total instantaneous HVAC consumption

The operating conditions and their impact on the HVAC system consumption in buses operating within an urban environment are complex. On the one hand, these conditions are influenced by stochastic variables such as weather, traffic, and passenger occupancy. On the other hand, the HVAC system's response and energy consumption are nonlinear with respect to these conditions, and its control logic results in discrete operational modes.

Figure 5.1 illustrates the density distribution of the HVAC instantaneous energy consumption over a representative year. The opera-

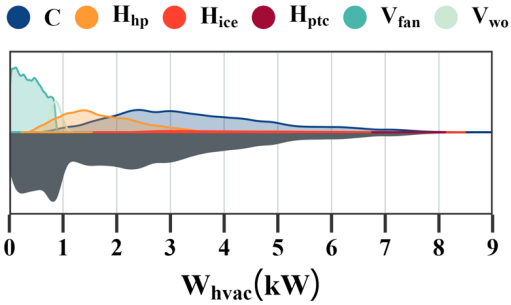

Figure 5.1: Distribution density of the HVAC system's consumption W_{hvac} over a representative year in the different operational modes (above) and total (below).

tional modes are: cooling (C), standard heating (H_{hp}), heating under frost/defrost conditions (H_{ice}), and heating with PTCs activated (H_{ptc}), ventilation mode with only internal blowers (V_{fan}), and ventilation where windows are also open (H_{wo}).

The results show the high variability of HVAC instantaneous consumption, both in total and within each operational mode. This highlights that each operating mode is different, and yet all are necessary to estimate the total HVAC consumption. It also underscores the potential errors from oversimplification, particularly when assuming a uniform behavior.

Figure 5.2 illustrates the relationship between the total equipment consumption and both the exterior temperature and the horizontal radiation for the different operating modes over a representative year.

The results reveal the HVAC consumption depends strongly on the exterior temperature and solar radiation. These factors clearly affect the consumption, but deriving a robust approximation based only on these variables only is not straightforward. Other factors, including stochastic variables, such as occupancy and traffic, also significantly affect the thermal load and need to be integrated and consistently considered. For instance, occupancy levels are related to bus stop waiting times

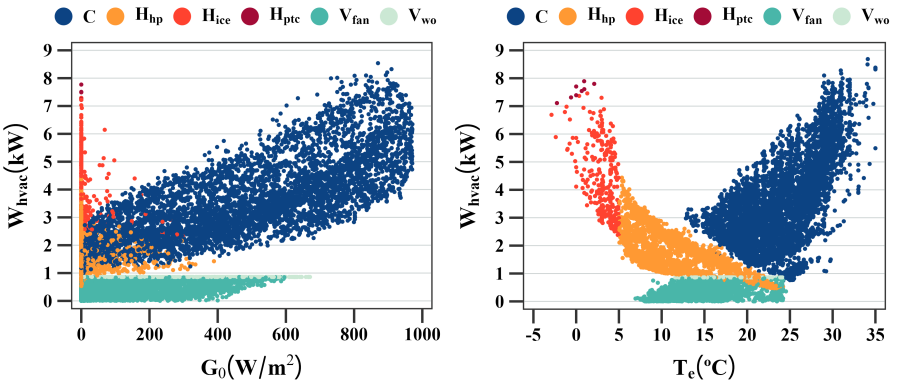

Figure 5.2: Relationship between the total HVAC system's consumption W_{hvac}, the exterior temperature T_e and the horizontal radiation G_0 differentiating between operational modes.

and air exchanges due to the door opening and passenger flow. The bus speed also affects on the external convection coefficients and on the infiltration rates.

5.1.2 Solar heat gain

Solar radiation is identified as a major component of the total thermal load, particularly during the summer months. This hypothesis was confirmed in Chapter 3, which demonstrates that the solar load (20-42%) of the total cumulative positive load over the year, exceeding 40% between April and August. Consequently, a correct modeling of the solar radiation is crucial for the estimation of the HVAC system consumption.

In urban vehicles, solar radiation is highly variable due to dynamic factors such as shadows and the orientation of the bus. Consequently, accurate modeling of the city and bus route is crucial to precisely estimate the HVAC system consumption.

Figure 5.3 illustrates the total solar heat gain of the bus in relation to horizontal global radiation, distinguishing between scenarios where the

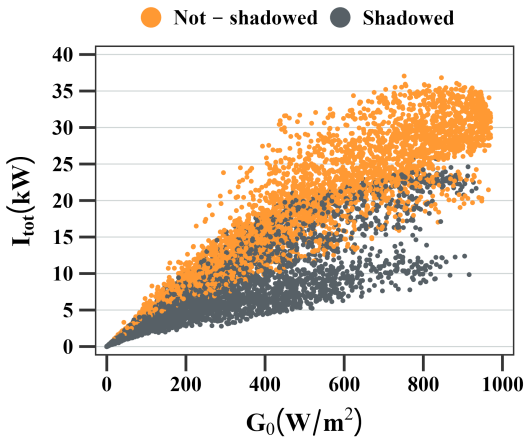

Figure 5.3: Relationship between the total solar heat gain I_{tot} and the horizontal global radiation G_0, when the vehicle is shaded or unshaded.

vehicle is shaded or unshaded. The horizontal solar radiation does not precisely determine the solar heat gain. Detailed models are necessary to capture the specific solar gain of the bus at any given time.

5.1.3 Shadow models

In Chapter 2, a cast-based shadow model was developed to determine the spatial distribution of shading or partial shading on each surface of the bus. This model is highly valuable in situations of partial shading, for instance in the nonlinear response of photovoltaic systems or in building surfaces where the duration of partial shading leads to substantial variations in the building load. However, in the context of urban buses, where the system is in motion, shading is intermittent and its spatial distribution is less critical compared to the previous cases. Consequently, there is an opportunity to simplify the shadow model to one based on representative points on each surface of the bus. This approach involves evaluating whether each point is shaded or not, assuming that if a point is shaded, the entire surface is considered to be shaded. Based on this hypothesis, the model can be adapted to a

skyline-based model, which assesses the visible horizon of these representative points, thus making it more scalable.

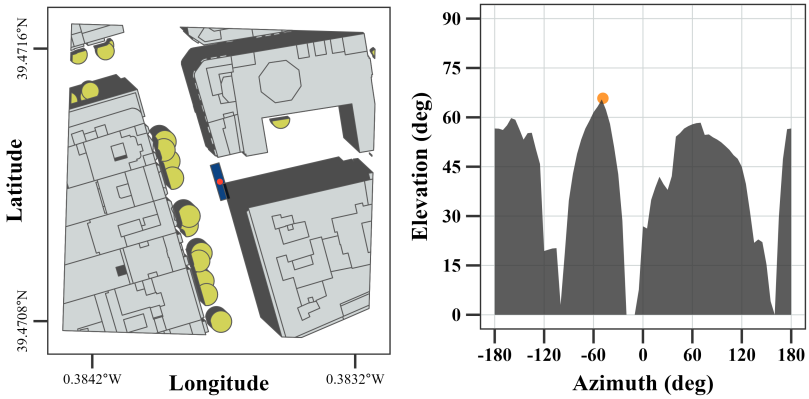

(a) (b)

Figure 5.4: Comparison of shadow models on the 15-06-2023 12:50:00 CEST in a partial shaded scenario where 12.25% of the roof surface is shadowed. (a) Cast-based model: Shadow cast (dark gray) from buildings (light gray) and trees (green) over a bus roof surface (blue). Red point represents the centroid of the roof bus surface. (b) Skyline-based model: Visible skyline (dark gray) and sun position (orange) from the centroid of the bus surface.

The cast-based model calculates, at each time step, the projection of shadows from all surrounding elements onto a surface using a ray-tracing algorithm and polygon closure methods (see Figure 5.4b). The calculations are performed in every time step. In contrast, the skyline-based model determines the visible skyline or horizon for a spatial point (see Figure 5.4a), which remains constant regardless of time or the solar position. In each time step the model determines if the sun is "hidden" behind the skyline. This approach allows for the spatial discretization of the route and the evaluation of consistent points across different time steps, enabling the skyline to be computed once per point (valid for any time step) and only checking at each time step whether the sun intersects the skyline. Additionally, the skyline-based model provides results for visible sky or view factors for diffuse and reflected solar radi-

ation, as well as for long-wave radiative heat exchanges. Furthermore, with this simplification of the model, additional surfaces can be incorporated without significantly increasing the overall computational cost. For instance, trees, which are crucial for shading in urban spaces, can be included. The scalability advantages of the skyline-based model are diminished if multiple points on each surface need to be evaluated, as a 2D grid. The impact of using a single representative point was assessed. Moreover, the skyline-based model simplifies the process by eliminating the need to model partial shading on the bus surface and avoids the complexity of solving 2D or 3D heat transfer equations with a large number of interacting bus nodes.

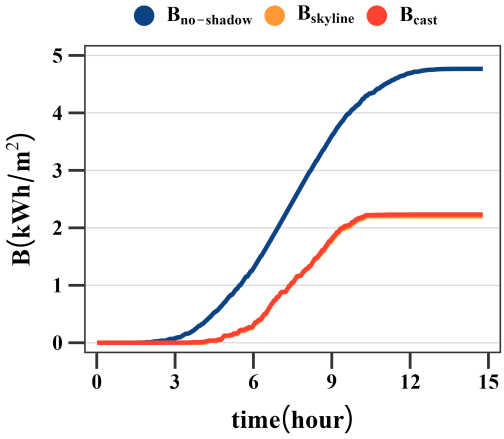

Figure 5.5: Difference in accumulated direct solar radiation on the bus roof throughout a day of June for the cast-based shadow model B_{cast}, the skyline-based shadow model $B_{skyline}$ and for the non-shadowed model $B_{no-shadow}$.

Figure 5.5 illustrates the variation in accumulated direct solar radiation on the bus roof over a day in June across three models, comparing the direct component of radiation with and without shadow effects. The difference between the shadow models is very small, with an accumulated difference of 1.3%. This finding leads to the conclusion that the skyline-based model effectively balances accuracy and computational cost, enabling scalable results without compromising the

accuracy. However, if the shadows are not considered, the impact is very high, with a daily cumulative increase of over 53%. This clearly underscores the importance of employing a shading model in urban environments.

5.1.4 Bus surfaces in climate model

Table 5.1 shows the annual mean percentage of radiation fluxes distributed across different bus surfaces. The radiation includes the solar irradiance absorbed by opaque surfaces and windows, the irradiance transmitted through windows, and the long-wave irradiance exchanges between bus surfaces, the sky, and the urban surroundings.

Table 5.1: Annual mean percentage of radiation in each bus surface, including the solar irradiance absorbed by opaque surfaces $I_{wal,abs}$, absorbed by windows $I_{win,abs}$ and transmitted by windows $I_{win,tra}$, and the long-wave irradiance exchanges with sky E_{sky} and urban surrounding surfaces E_{sur}.

	front	left	right	back	roof	floor
$I_{wal,abs}$ (%)	4.4	22.5	17.8	6.1	49.2	0.0
$I_{win,abs}$ (%)	5.9	37.1	52.5	4.5	0.0	0.0
$I_{win,tra}$ (%)	14.7	33.4	47.6	4.3	0.0	0.0
E_{sky} (%)	5.0	25.0	22.9	5.0	42.1	0.0
E_{sur} (%)	5.0	23.5	24.3	5.1	9.7	32.4

The results show significant variations depending on the bus surface, which supports the importance of modeling a bus with distinct surface properties. The roof accounts for nearly half (49.2%) of the total solar irradiance absorbed by opaque surfaces, followed by the left and right sides, while the front and rear surfaces receive only a minimal share. Additionally, the left and right sides are primarily responsible for both the absorption and transmission of solar irradiance through windows, as the roof and floor lack windows. The roof also demonstrates the highest level of radiative exchange with the sky (42.1%), whereas the floor predominantly engages in exchanges with urban surroundings (32.4%). Furthermore, the differences in thermal capacities and conductances due to the different materials of each surface must be also

considered, as discussed in Chapter 3. These variations highlight the necessity of modeling each surface individually to accurately capture the overall thermal dynamics.

5.1.5 Transient thermal model

Figure 5.6 presents a comparison, for a typical day of June, of the instantaneous total solar heat gain, the thermal load, and the thermal load assuming no thermal capacity.

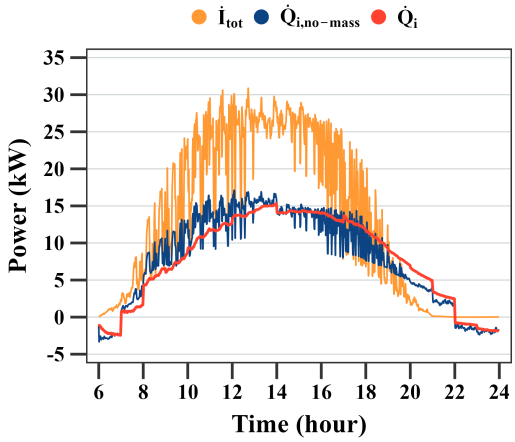

Figure 5.6: Comparison between instantaneous total solar heat gain $\dot{I}_{tot}$, thermal load $\dot{Q}_i$ and thermal load with null (10^{-6}J/K) thermal capacity $\dot{Q}_{i,no-mass}$ in a day of June.

The results highlight the critical role of the thermal inertia in dampering the effects of the heat gains on the thermal load. The thermal load with no inertia shows results very similar to the heat gain. This indicates that, in the absence of thermal masses, the vehicle responds almost immediately to changes in the solar heat gain, resulting in rapid fluctuations in the thermal load. In contrast, when the inertia is included, the peaks are less sharp and the curve more smooth. The delayed and dampened peaks reflect that the thermal mass within the space absorbs some of the incoming heat, releasing it gradually and

thereby reducing the instantaneous load on the HVAC system.

This comparison highlights the necessity of incorporating a transient thermal model that includes accurate estimations of the thermal capacities of bus materials, especially when integrating discrete control algorithms.

5.2 Results overview

This section provides a comprehensive overview of the findings and insights of the thesis. They are divided into two parts based on the primary objectives and identified research gaps in the literature.

5.2.1 Development of the methodology

All proposed submodels are essential to collectively achieve the primary goal of developing a comprehensive and accurate global model. The model effectively simulates the operation and energy consumption of HVAC systems and their impact on the overall energy use of electric urban buses under real-world operating conditions.

The GIS model is crucial to accurately simulate the operating conditions within an urban environment. This approach, largely absent in existing literature, represents a significant contribution of this thesis. Additionally, the GIS model is the foundation for many other developments within the study and facilitates the large-scale application of energy models that employ real open data. This is particularly relevant to accurately calculate the shading effects and view factors. Modeling solar radiation and long-wave radiative exchanges is essential and has a key impact on the thermal load in urban environments. Two shading models have been developed using geometric methods. They are both supported by validated 3D city models. The cast-based model exhibits a high accuracy, while the skyline-based model offers a more scalable solution for urban mobility applications, maintaining a similar accuracy. This model also enables the calculation of the bus route slope, which can significantly impact powertrain consumption in cities with sloping streets.

The kinematic model establishes the relationship between the simulation time and the spatial position under real-world traffic conditions using open data. The instantaneous speed is employed to determine the external convection coefficients and infiltration rates. Furthermore, it enables the consistent integration of occupancy data and the spatiotemporal context of bus stops, including the air exchanges due to

door opening and passenger flow. Moreover, this model is essential to estimate the powertrain consumption, including motor and regenerative braking, as well as the energy consumption of pneumatic and hydraulic auxiliaries.

The climatic model integrates the necessary inputs to establish heat exchanges between the bus and its environment. Differentiating the different bus surfaces is crucial due to significant variations in conductance, thermal capacity, and radiative exchanges among them.

A dynamic thermal load model has been developed and validated, demonstrating the importance of a transient approach that includes accurate thermal capacities. This approach avoids errors associated with steady-state models, which would misrepresent large fluctuations in heat gains as thermal load, adversely affecting HVAC control algorithms. The cabin model features detailed long-wave and multi-component solar radiative models, accounting for shading effects, view factors, and angular-dependent transmittance of windows on different surfaces of the vehicle. These are not common in literature and they are yet essential in the load calculation. The impact of occupancy stochasticity on thermal load has been evaluated, showing that moderate dispersion has a small impact and only high dispersion significantly affects the load. Additionally, the dispersion of passenger flow ratios has no significant effect.

Few studies in the field of mobility have employed physical HVAC models and their control mechanisms over extended simulation periods, and none have provided the level of detail of the present study, including a wide range of operating modes, the impact of frost-defrost cycles, hybridization with positive temperature coefficient (PTC) heaters, and integration of latent loads. This comprehensive approach enables an in-depth analysis of how these effects impact each HVAC system component, primary circuit variables, secondary circuit output flows, and internal performance metrics.

The battery model has been built using state-of-the-art methodologies and effectively meets the study's objectives. This research uniquely

integrates this advanced model with previous studies by employing real-world, representative parameters within an urban context.

The integration of these models results in a highly accurate, programmable, and scalable global model, composed of cutting-edge sub-models supported by extensive open data sources.

5.2.2 Application in buses of Valencia and key findings

The global model was implemented in R as a simulation tool, concluding that a one-minute time step offers a balance between accuracy and computational cost.

Results over a representative year

Three bus lines (C1, C2, and C3) from the urban fleet of València (Spain) were simulated with a one-minute time step during a representative year.

The results indicate a very minor difference in the mean daily thermal load and HVAC consumption across the three bus lines, due to their similar urban typologies and view factors. However, significant differences arise in the powertrain consumption due to the different average speeds and distances traveled, leading to notable variations in the relative impact of the HVAC equipment.

The HVAC system meets the thermal demand throughout the year and all its components works within their designated performance ranges.

On a warm summer day, the cooling demand reaches approximately 218 kWh (1.38 kWh/km for line C1). The primary driver of this demand is the cumulative sensible heat load from the cabin, which accounts for 70% to 98% of the total cooling requirement. Latent heat loads also contribute significantly, comprising over 20% of the cooling demand from June to October. In contrast, on a cold winter day, the heating demand is around 59 kWh (0.37 kWh/km for line C1). This demand

is predominantly influenced by the sensible heat load from the non-recirculated fresh airflow, which accounts for 43% to 68% of the total heating demand. Latent heat loads are negligible in winter, as they are effectively balanced between the fresh air and cabin heat loads.

Regarding the components of the sensible thermal load in a cabin, the cumulative solar load contributes yearly to 20-42% of the positive load, reaching more than 40% in summer. External infrared radiation remains relatively constant, accounting for 35-44% of the negative loads in winter and 67-91% in summer. The occupancy component is stable, and is responsible for 65-73% of the positive loads in winter and 33-45% in summer. Air changes significantly impact the heating demand, contributing to over 20% of the negative loads in winter, while conduction, convection, and internal infrared radiation account for around 40% of the negative loads in winter and 10-20% of the positive loads in summer.

The total consumption in a warm summer day is around 63.9 kWh (0.40 kWh/km in line C1) in warm summer days, with a minimum of 22.8 kWh (0.14 kWh/km in line C1) on mild-cold days and around 26.6 kWh (0.17 kWh/km in line C1) in cold winter days.

The cooling mode is on during 44.8% of the time, covering 72% of the thermal load with an average daily consumption of 63 kWh (0.40 kWh/km for line C1). The breakdown by components is 74% for the compressor, 20% of the internal fans, and 6% for the external fans. The average COP for the cooling system is 3.88, or 2.71 indicating the consumption of all auxiliaries, and an average pressure ratio of 2.69. Ventilation is employed to compensate low-intensity positive loads. This occurs during 31.2% of the time and handles 15% of the cabin load, while consuming 7% of the annual energy, with an average daily energy consumption of 0.05 kWh (0.08 kWh/km for line C1), mainly for the internal blowers. Heating modes operate during 23.9% of the time, covering 13% of the load with an average daily consumption of 36 kWh (0.23 kWh/km for line C1), or 21% of the annual consumption. The standard heating mode is the least energy demanding, with half the energy consumption of cooling. The average pressure ratio to 3.77.

In contrast, frost/defrost conditions significantly raise the energy consumption to more than double the average heating consumption and reduce the overall efficiency. The most demanding mode is heating with PTC heaters. In this mode, the consumption is three times the average heating power. The COP is of only 2, and the pressure ratio reaches more than 6. However, the annual impact of these two modes is negligible, as frost/defrost conditions are active only 2.2% of the time and the PTC mode operates just 0.1% of the time. This is nevertheless a particular result for Valencia given its mild weather.

The compressor typically operates at a minimum speed of 15 Hz, with an average on-time ratio below 57%. A maximum speed of 50 Hz is reached, but only in heating mode and in less than 0.1% of the total operational time. In cooling mode, the compressor speed does not exceed 35 Hz, with an on-time ratio below 65%. During the standard heating mode, the speed is maximum 25 Hz and the on-time ratio remains below 40%. The study suggests that the heat pump system could be downsized, and potential optimizations include increasing the capacity of the PTC heater for occasional frost and defrost conditions or incorporating thermal energy storage systems.

When assessing the overall energy consumption per bus line, line C2 demonstrated the highest average daily energy usage at 773 kWh, followed by line C3 with 571 kWh, and line C1 with 329 kWh. Variations in energy consumption among the lines are primarily attributed to the differences in the distance traveled. However, the energy consumption per kilometer remains relatively uniform across the lines, with measurements of 2.09 kWh/km for lines C1 and C2, and 2.12 kWh/km for line C3. The powertrain emerges as the predominant energy consumer, with a significant portion of its energy use mitigated through regenerative braking. The HVAC system is the second largest energy consumer, accounting annually for around 5-12% of the total energy use, followed by the consumption due to the battery charge and discharge efficiency (7%), auxiliary electrical systems and battery thermal management (1-3% each) and hydraulic and pneumatic systems (1-2% each).

The impact of the HVAC consumption on an average day varies between lines: C1 ranges from 7% to 20% (0.13–0.47 kWh/km), C2 from 3% to 10% (0.06–0.20 kWh/km), and C3 from 4% to 12% (0.08–0.27 kWh/km). The highest impact is observed on cooling-dominant days of July, while the lowest is on ventilation-dominant days of February.

Extreme weather conditions

Four scenarios have been simulated to evaluate the performance of an HVAC system along line C1 under extreme weather conditions. These scenarios involved increasing outdoor temperatures by +2.5K and +5K on the peak cooling day, and decreasing temperatures by -2.5K and -5K on the peak heating day relative to Typical Meteorological Year (TMY) data.

The results indicate a significant rise in the HVAC system's energy consumption under these extreme conditions. On the warmest days, energy consumption increased by up to 90% and 165% in the +2.5K and +5K scenarios, respectively. On the coldest days, the consumption rose by up to 40% and 181% in the -2.5K and -5K scenarios. These extreme conditions also led to higher compressor speeds, refrigerant pressures, and temperatures, which resulted in a reduced coefficient of performance (COP). In the heating scenarios, there was also a noticeable increase in the use of pre-heating components (PTC). However, the load was adequately managed by the current equipment within its operational range, except in the -5K scenario, where 1.1% of the time the load was not fully compensated.

Thermal load sensibility analysis

A sensitivity analysis was conducted to assess the impact of different parameters and conditions on the thermal load along line C1 throughout a representative year. The analysis revealed that changes in windows significantly affect both the cooling and heating demands. Specifically, changing the number of panes and their thickness can alter the cooling demand by up to 3% and heating demand by up to 17%.

As the occupancy increases, the cooling demand rises nearly proportionally, whereas the heating demand decreases. Wall insulation exhibits a minor impact on the cooling demand but has a substantial influence on the heating demand, potentially leading to a 20% reduction. The impact of air changes on the thermal load is significant, and effectively managing them with devices and control systems can substantially reduce the HVAC demand. For instance, opening windows when the bus is unoccupied can decrease the cooling demand by 23%, while using air curtains to minimize air changes can lower the heating demand by 27%.

Furthermore, the study highlights that the color and coating of the external walls plays a significant impact in the cooling demand. White walls, in particular, have the potential to reduce the cooling demand by up to 31%.

Compressor size optimization

A parametric analysis was performed for different compressor sizes, ranging from 100% (original size) to 50% of the current dimensions. The analysis identified that a compressor scaled to 75% of its original size achieved an optimal performance. This size could potentially lower the HVAC cost and, at the same time, improve the energy efficiency, while maintaining the system's capacity to meet the thermal loads. The simulation results for a representative year indicated that the 75% scaled compressor resulted in a 3% reduction in the annual energy consumption and a 4% improvement in the COP.

Additionally, the study evaluated the HVAC system's performance under extreme weather conditions to verify the scaled compressor's ability to handle peak loads. Even with ambient temperatures deviating by ± 5 K from the typical meteorological year (TMY) peak days, the 75% scaled compressor showed a satisfactory performance, with an unmet load ratio below 2%.

Chapter 6

Conclusions

6.1 General conclusions

The present thesis presents a detailed, full vehicle model to estimate the instantaneous performance during an entire representative year, in real operating conditions in urban areas. This environment is particularly complex due to radiation, shadows, traffic, variable occupancy and many more variables. By developing and validating a set of detailed submodels, the research contributes to the creation of a comprehensive global model to simulate the HVAC operations and energy consumption in electric urban buses. The major conclusions about the development of the methodology and its application are presented below.

6.1.1 Development of the methodology

- Estimating the operational conditions in real urban environments and accurately determining the HVAC energy consumption is complex, due to the influence of a wide range of factors, the nonlinear responses and the discrete domain of real control logic. Furthermore, a large volume of data is used and processed. For this reason, a work environment designed to handle massive and diverse datasets is completely necessary.

- A comprehensive set of submodels, including GIS, kinematic, climatic, thermal load, HVAC, and battery models, is required.

Their integration creates a highly accurate, programmable, and scalable global model, supported by extensive open data sources.

- The GIS model provides a 3D representation of the city, creating a realistic context based on extensive open data and facilitating the large-scale application of models. Shading significantly impacts the thermal loads. The developed approach helps obtain the street slope, which can significantly influence the powertrain consumption.
- The skyline-based shadow model is an accurate and scalable solution for urban mobility applications.
- The kinematic model correlates the simulation time with the spatial position in real-world traffic using open data. This helps to calculate external convection coefficients, infiltration rates, and the consumption of the powertrain, pneumatic, and hydraulic systems. The occupancy and bus-stop dynamics is also integrated to evaluate the associated thermal loads.
- The climatic model incorporates and processes the required inputs to simulate the heat exchanges between each bus surface.
- A transient thermal load model is essential. Steady-state models are not recommended, especially when integrated with HVAC control algorithms. The model addresses radiative exchanges using long-wave and multi-component solar models, including shading, view factors, and window transmittance.
- High occupancy stochasticity significantly affects the thermal load, whereas variations in passenger flow ratios have a minimal impact.
- The physical HVAC model, combined with control algorithms, provides a comprehensive analysis of the impact of each HVAC component, primary circuit variables, secondary circuit output flows, and the internal performance metrics across operating modes and thermal load components.

6.1.2 Application in buses of Valencia and key findings

- On warm summer days, the mean cooling power demand reaches approximately 12.1 kW, primarily driven by the sensible heat loads from the cabin, with latent heat loads also contributing significantly. On cold winter days, the mean heating power demand is around 3.3 kW, mainly influenced by the sensible heat loads from non-recirculated fresh air and with practically negligible latent heat loads.

- In summer, the cabin's sensible heat load distribution reveals that the occupancy contributes to 33-45% of the positive load, the solar load reaches 40%, and external infrared radiation dissipates more than half of the solar heat. In winter, air changes account for 20% of the negative load, external infrared radiation contributes 40%, and conduction, convection, and internal infrared radiation account for the remaining portion.

- The mean power consumption in a warm summer day is around 3.5 kW in warm summer days, with a minimum of 1.3 kW on mild-cold days and around 1.5 kW in cold winter days.

- Cooling is the predominant operational mode of HVAC system, accounting for 44.6% of the total operational time. This is followed by ventilation (31.4%) and heating (24.0%). The mean power consumption of the HVAC system is 3.5 kW for cooling, 0.4 kW for ventilation, and 2.0 kW for heating.

- The compressor is the largest energy consumer, reaching 69-75% during cooling periods, and 58-65% during ventilation periods. The internal fans use 19-38% of the total energy, with peak usage on moderately warm days. External fans account for 4-6% of the annual consumption, while PTC heaters have a minor impact, contributing to only 0.4% of the total energy use.

- The compressor COP is around 4 in cooling and standard heating modes, while the overall system COP is approximately 3. These

values decrease to 3.7 and 2.8, under frost/defrost conditions, and drop further to below 2.5 and 2.2 in PTC mode. Pressure ratios also vary according to the mode, ranging from 2.6-2.8 in cooling, 3.6-3.7 in standard heating, 3.6-6.7 under frost/defrost conditions, and up to 6.8 in PTC mode.

- The results show that the HVAC system is oversized for a typical year. The average on-time ratio is of less than 65%. The compressor can be downsized by 25%. Increasing the capacity of PTC heaters can better manage peak loads during the 2.3% of time affected by frost/defrost conditions.

- The overall energy consumption per kilometer is consistent across bus lines, averaging around 2.1 kWh/km, with daily accumulated variations driven by the differences in the powertrain consumption related to distance traveled. However, the daily accumulated HVAC consumption is similar across lines, resulting in variable relative impacts of the HVAC equipment on overall energy use.

- The powertrain is the main annual energy consumer (76–86%), followed by the HVAC system (5-12%), with a consumption of 0.24 kWh/km in line C1, 0.10 kWh/km in line C2, and 0.14 kWh/km in line C3.

- The influence of the HVAC systems on the energy consumption of urban electric buses is significantly more pronounced on routes with lower speeds and a more frequent of stops per kilometer. Under these conditions, the HVAC demands, especially in cooling mode during mild to warm summer days, can reduce the driving range by 15-20%.

- The energy consumption of the HVAC system increases significantly under extreme temperatures, rising up to 165% on extreme warm days and 181% on extreme cold days. Despite the increased energy use and reduced efficiency, the system generally manages the load, with minimal unmet load during the coldest conditions.

- To reduce the thermal load, key strategies include change the windows or the wall insulation, which can reduce the heating demand by up to 17% and 20%, respectively. The color and coating of the external walls can lower the cooling demand by up to 31%. A proper management of the air changes, such as opening windows, can reduce the cooling demand by 23%, while air curtains can lower the heating demand by 27%.

- Downscaling the standard compressor by 25% is optimal for the studied city, offering significant cost savings while maintaining improved efficiency and effectively meeting load demands.

- The potential to reduce the HVAC size suggests reconsidering the EN-14759 standard and allowing exceptions for public urban electric buses. This could optimize HVAC systems for specific cities, supporting large-scale adoption and reducing urban transport impacts.

6.2 Future work and research opportunities

The current work opens several opportunities of research which can be explored in the following fields:

- **Expanding the model scope**: Future work could involve modifying the global model by adjusting sub-models and parameters to simulate additional characteristics of different buses (e.g., 18-meter articulated buses, double-decker buses), powertrains (e.g., fuel cells, hybrids), and operational environments (e.g., bus rapid transit, shuttle buses, regional and intercity buses). Additionally, the model could be adapted to simulate other type of vehicles such as trams and trains.

- **Refinement of submodels**: The climate model can integrate satellite data to consider the impact of the urban heat island effect on temperature, as well as the urban moisture and dry island effects on humidity. Additionally, the wind intensity and direction could be introduced. The impact of rain could also be studied. The thermal model could include detailed dynamic calculations of optical parameters such as the surface reflectivity and absorptance in urban environments. More cabin air nodes could be added (e.g., distinguishing between driver and passengers), and more detailed models of convection coefficients could be introduced. The HVAC model could simulate the airflow through the ducts and evaluate the thermal comfort of passengers. Finally, the battery model could be further refined using, for example, a first-order equivalent circuit model.

- **Global experimental validation**: To enhance the reliability of the global model, extensive measurement campaigns should be conducted for experimental validation. This issue was discussed with the bus fleet company of Valencia, but no dynamic measurements were available.

- **Simulating standards testing**: Validating the model by simulating

the different testing conditions defined in the standards represents another important area of future work.

- **Inclusion of Operating Modes**: The current model can be extended to include specific operating modes such as window dehumidification and defrosting.

- **Development of data-driven methods**: A new approach can involve using the detailed model to generate and evaluate data-driven methods. These methods could be designed to be more efficient for predefined scopes, making them valuable for broader applications, including integration into control systems or large-scale deployments.

- **Techno-economic studies**: Further research should address existing knowledge gaps through techno-economical and environmental studies, including the consideration of externalized costs. Such studies would provide insights to inform effective policy-making and action plans for sustainable public transportation.

- **Design and optimization of infrastructure and operations**: The global model could also be employed in optimization studies of the infrastructure design, battery sizing, and operational planning. These studies would focus on developing cost-effective infrastructure based on energy consumption, battery capacity, and charging times, leading to more efficient and sustainable bus operations.

- **Subsystem optimization and integration of new solutions**: There is significant potential for optimizing subsystems, particularly in the area of the HVAC system. Future research could explore enhancements such as optimizing heat exchangers or using other refrigerants (e.g., R744, R290). Moreover, the use of integrated thermal strategies (e.g., waste heat recovery from electric motors, controllers, inverters, and batteries), and thermal energy storage solutions offer promising areas for future research.

6.3 Dissemination and communication of the results

6.3.1 Journal publications

The research findings in the present PhD thesis have led to the following publications:

- Joan Dídac Viana-Fons, José María Gonzálvez-Maciá, Jorge Payá. *Development and validation in a 2D-GIS environment of a 3D shadow cast vector-based model on arbitrarily orientated and tilted surfaces.* In: *Energy & Buildings* (2020), Vol. 224, p. 110258.
  DOI: https://doi.org/10.1016/j.enbuild.2020.110258.
  Impact factor: 5.9 (2020). Quartile: Q1.

- Joan Dídac Viana-Fons, Jorge Payá. *Dynamic cabin model of an urban bus in real driving conditions.* In: *Energy* (2024), Vol. 288, p. 129769.
  DOI: https://doi.org/10.1016/j.energy.2023.129769.
  Impact factor: 9.0 (2023). Quartile: Q1.

- Joan Dídac Viana-Fons, Jorge Payá. *HVAC system operation, consumption and compressor size optimization in urban buses of Mediterranean cities.* In: *Energy* (2024), Vol. 296, p. 131151.
  DOI: https://doi.org/10.1016/j.energy.2024.131151.
  Impact factor: 9.0 (2023). Quartile: Q1.

Outside the scope of this thesis, the approach to treat radiation in urban areas has had many applications, such as the analysis of the urban photovoltaic potential or the building energy demand. In this context, the author contributed to the following research publications during the development of this PhD:

- Enrique Fuster-Palop, Carlos Prades-Gil, Ximo Masip, Joan Dídac Viana-Fons, and Jorge Payá. *Innovative regression-based methodology to assess the techno-economic performance of photovoltaic installations in urban areas.* In: *Renewable and Sustainable Energy Reviews* (2021), Vol. 149, p. 111357.

DOI: https://doi.org/10.1016/J.RSER.2021.111357.
Impact factor: 16.8 (2021). Quartile: Q1.

- Enrique Fuster-Palop, Carlos Prades-Gil, Ximo Masip, Joan Dídac Viana-Fons, and Jorge Payá. *Techno-Economic Potential of Urban Photovoltaics: Comparison of Net Billing and Net Metering in a Mediterranean Municipality.* In: *Energies* (2023), Vol. 16, p. 3564.
  DOI: https://doi.org/10.3390/en16083564.
  Impact factor: 3.2 (2022). Quartile: Q2.

- Ximo Masip, Enrique Fuster-Palop, Carlos Prades-Gil, Joan Dídac Viana-Fons, Jorge Payá, and Emilio Navarro-Peris. *Case study of electric and DHW energy communities in a Mediterranean district.* In: *Renewable and Sustainable Energy Reviews* (2023), Vol. 178, p. 113234.
  DOI: https://doi.org/10.1016/j.rser.2023.113234.
  Impact factor: 15.9 (2022). Quartile: Q1.

- Carlos Prades-Gil, Joan Dídac Viana-Fons, Ximo Masip, Antonio Cazorla-Marín, and Tomás Gómez-Navarro. *An agile heating and cooling energy demand model for residential buildings. Case study in a mediterranean city residential sector.* In: *Renewable and Sustainable Energy Reviews* (2023), Vol. 175, p. 113166.
  DOI: https://doi.org/10.1016/j.rser.2023.113166.
  Impact factor: 15.9 (2022). Quartile: Q1.

- Carlos Prades-Gil, Joan Dídac Viana-Fons, Ximo Masip, Antonio Cazorla-Marín, and Tomás Gómez-Navarro. *Methodology to assess the impact of urban vegetation on the energy consumption of residential buildings. Case study in a Mediterranean city.* In: *Energy Conversion and Management: Xs* (2024), Vol. 24, p. 100706.
  DOI: https://doi.org/10.1016/j.ecmx.2024.100706.
  Impact factor: 16.3 (2023). Quartile: Q1.

6.3.2 Conferences

The author contributed to the following conferences within the context of this thesis:

- Joan Dídac Viana-Fons, José Gonzálvez-Maciá, and Jorge Payá. *Development and validation of a simplified dynamic thermal model of a vehicle's cabin.* In: *X Congreso Ibérico y VIII Congreso Iberoamericano de Ciencias y Técnicas del Frío (CYTEF 2020)* (2020).
  ISBN: 978-2-36215-043-2.
  Oral presentation

- Joan Dídac Viana-Fons, and Jorge Payá. *Methodology for the calculation of the shadow factor on roofs and facades of buildings in urban areas.* In: *XI Congreso Nacional y II Internacional de Ingeniería Termodinámica (11-CNIT)* (2019). (pp. 870-877).
  ISSN: 978-84-09-11635-5.
  Oral presentation

Outside the scope of this thesis, the author contributed to the following conferences during the development of this PhD:

- Joan Dídac Viana-Fons, and Jorge Payá. *Innovative, detailed methodology to obtain the PV potential of industrial roofs on a regional scale.* In: *XI Congreso Nacional y II Internacional de Ingeniería Termodinámica (11-CNIT)* (2019).

- Enrique Fuster-Palop, Carlos Prades-Gil, Ximo Masip, Joan Dídac Viana-Fons, and Jorge Payá. *Profitability of PV generators in urban environments considering the new Spanish regulation.* In: *X Congreso Ibérico y VIII Congreso Iberoamericano de Ciencias y Técnicas del Frío (CYTEF 2020)* (2020).

- Enrique Fuster-Palop, Carlos Prades-Gil, Ximo Masip, Joan Dídac Viana-Fons, and Jorge Payá. *Evaluation of the Solar Photovoltaic Generation Potential of a sample of residential buildings in*

the City of Valencia. In: *15th Conference on Sustainable Development of Energy, Water and Environment Systems* (2020). (pp. 288-299).

- Elisa Gimeno Gómez, Enrique Fuster-Palop, Ximo Masip, Carlos Prades-Gil, and Joan Dídac Viana-Fons. *Comunidades Energéticas como el modelo perfecto para la Transición Energética de las ciudades y la democratización de la energía. Caso práctico de la ciudad de Catarroja.* In: *XVI Congreso Nacional del Medio Ambiente (CONAMA 2022)* (2022).

- Ximo Masip, Enrique Fuster-Palop, Carlos Prades-Gil, Joan Dídac Viana-Fons, Jorge Payá, and Emilio Navarro-Peris. *Electric and thermal energy communities comparison assessment: a case study in a Mediterranean district.* In: *16th Conference on Sustainable Development of Energy, Water and Environment Systems* (2021).

- Carlos Prades-Gil, Joan Dídac Viana-Fons, Ximo Masip, Antonio Cazorla-Marín, and Tomás Gómez-Navarro. *Methodology to assess the impact of nature-based solutions on temperature in urban areas. Case study in a Mediterranean city.* In: *18th Conference on Sustainable Development of Energy, Water and Environment Systems (SDEWES)* (2023).

- Carlos Prades-Gil, Joan Dídac Viana-Fons, Ximo Masip, Antonio Cazorla-Marín, and Tomás Gómez-Navarro. *Evaluation of the heat island effect in a Mediterranean city and its impact on the thermal demand of the residential sector.* In: *17th Conference on Sustainable Development of Energy, Water and Environment Systems (SDEWES)* (2022).

- Carlos Prades-Gil, Joan Dídac Viana-Fons, Ximo Masip, Antonio Cazorla-Marín, and Tomás Gómez-Navarro. *Heating and cooling demand assessment with European standards, degree days approach and GIS-based tools. Climate change impact on demand and retrofitting benefits in Mediterranean case study.* In: *16th*

Conference on Sustainable Development of Energy, Water and Environment Systems (2021).

- Ximo Masip, Enrique Fuster-Palop, Carlos Prades-Gil, and Joan Dídac Viana-Fons. *Herramienta para la planificación como camino para la transición energética urbana.* In: *XV Congreso Nacional del Medio Ambiente (CONAMA 2020)* (2020).

- Ximo Masip, Enrique Fuster-Palop, Carlos Prades-Gil, and Joan Dídac Viana-Fons. *Herramienta para la planificación energética como camino para la transición energética urbana de las ciudades y caso de estudio aplicado.* In: *VII Congreso de Edificios de Consumo de Energía Casi Nulo (EECN 2020)* (2020).

- Ximo Masip, Enrique Fuster-Palop, Carlos Prades-Gil, and Joan Dídac Viana-Fons. *Evaluation of the Solar Photovoltaic Generation Potential of a District in the City of Valencia.* In: *15th Conference on Sustainable Development of Energy, Water and Environment Systems* (2020).

Global Bibliography

N. Abbasabadi and M. Ashayeri. Urban energy use modeling methods and tools: A review and an outlook. In: *Building and Environment* 161 (2019), 106270. https://doi.org/10.1016/j.buildenv.2019.106270 (cited on page 14).

H. Abdelaty and M. Mohamed. A Prediction Model for Battery Electric Bus Energy Consumption in Transit. In: *Energies* 14.(10) (2021). https://doi.org/10.3390/en14102824 (cited on page 11).

H. Abdelaty, A. Al-Obaidi, M. Mohamed, and H. E. Farag. Machine learning prediction models for battery-electric bus energy consumption in transit. In: *Transportation Research Part D: Transport and Environment* 96 (2021), 102868. https://doi.org/10.1016/j.trd.2021.102868 (cited on page 11).

A. A. Abulifa, A. B. C. Soh, M. K. Hassan, R. M. K. R. Ahmad, and M. A. M. Radzi. Energy Management System in Battery Electric Vehicle Based on Fuzzy Logic Control to Optimize the Energy Consumption in HVAC System. In: *International Journal of Integrated Engineering* 11.(4) (2019), 11–20. https://doi.org/10.30880/ijie.2019.11.04.002 (cited on page 92).

E. Afrasiabian, R. Douglas, and R. Best. Real-Time modelling of a two-unit baseline air conditioning system for a generic bus subjected to different levels of occupancy. In: *2020 15th International Conference on Ecological Vehicles and Renewable Energies, EVER 2020*. 2020. https://doi.org/10.1109/EVER48776.2020.9243013 (cited on page 158).

E. Afrasiabian, R. Douglas, M. Geron, and G. Cunningham. A numerical evaluation of a novel recovery fresh air heat pump concept for a generic electric bus. In: *Appl Therm Eng* 209 (2022), 118181. https://doi.org/10.1016/J.APPLTHERMALENG.2022.118181 (cited on pages 10, 18, 92, 139).

M. A. Alam, R. Kumar, D. Banoriya, A. S. Yadav, G. Goga, K. K. Saxena, D. Buddhi, and R. Mohan. Design and development of thermal comfort analysis for air-conditioned compartment. In: *International Journal on Interactive Design and Manufacturing* (2022), 1–11. https://doi.org/10.1007/S12008-022-01015-8/METRICS (cited on pages 17, 92, 139).

M. Aliahmadipour, M. Abdolzadeh, and K. Lari. Air flow simulation of HVAC system in compartment of a passenger coach. In: *Appl Therm Eng* 123 (2017), 973–990. https://doi.org/10.1016/J.APPLTHERMALENG.2017.05.086 (cited on page 92).

A. Anand and C. Deb. The potential of remote sensing and GIS in urban building energy modelling. In: *Energy and Built Environment* 5.(6) (2024), 957–969. https://doi.org/10.1016/j.enbenv.2023.07.008 (cited on page 14).

ASHRAE American Society of Heating Refrigerating and A.-C. Engineers. ASHRAE Handbook - Fundamentals. Atlanta, GA: ASHRAE, 2017 (cited on pages 8, 96, 98, 103, 170).

Asian Development Bank. Sustainable Transport Solutions: Low-Carbon Buses in the People's Republic of China. 2018. https://doi.org/10.22617/TCS189646-2 (cited on pages 7, 90, 138).

Asociación Española de Normalización (UNE). Railway applications - Air conditioning for urban, suburban and regional rolling stock (UNE-EN Standard No. 14750). 2007 (cited on pages 8, 102, 104, 113, 138, 149, 150).

Asociación Española de Normalización (UNE). Glass in building - Determination of thermal transmittance (U value) - Calculation method (UNE-EN Standard No. 673). 2011 (cited on page 96).

D. Assouline, N. Mohajeri, and J.-L. Scartezzini. Quantifying rooftop photovoltaic solar energy potential: A machine learning approach. In: *Solar Energy* 141 (2017), 278–296. https://doi.org/10.1016/j.solener.2016.11.045 (cited on page 56).

Autodesk Inc. Autodesk Revit. 2020. https://doi.org/https://www.autodesk.com/products/revit/overview (cited on page 56).

A. Avenali, G. Catalano, M. Giagnorio, and G. Matteucci. Assessing cost-effectiveness of alternative bus technologies: Evidence from US transit agencies. In: *Transportation Research Part D: Transport and Environment* 117 (2023), 103648. https://doi.org/10.1016/j.trd.2023.103648 (cited on page 4).

P. Bandi, N. P. Manelil, M. P. Maiya, S. Tiwari, A. Thangamani, and J. L. Tamalapakula. Influence of flow and thermal characteristics on thermal comfort inside an automobile cabin under the effect of solar radiation. In: *Appl Therm Eng* 203 (2022), 117946. https://doi.org/10.1016/J.APPLTHERMALENG.2021.117946 (cited on pages 17, 92, 139).

M. Bartels, H. Wei, and D. Mason. DTM generation from LIDAR data using skewness balancing. In: *Proceedings - International Conference on Pattern Recognition*. 2006, 566–569. https://doi.org/10.1109/ICPR.2006.463 (cited on page 61).

H. Basma, C. Mansour, M. Haddad, M. Nemer, and P. Stabat. Comprehensive energy modeling methodology for battery electric buses. In: *Energy* 207 (2020), 118241. https://doi.org/10.1016/J.ENERGY.2020.118241 (cited on pages 15–19, 139, 154).

H. Basma, C. Mansour, M. Haddad, M. Nemer, and P. Stabat. Energy consumption and battery sizing for different types of electric bus service. In: *Energy* 239 (2022), 122454. https://doi.org/10.1016/J.ENERGY.2021.122454 (cited on pages 15, 16, 18, 19, 21, 139, 167).

H. Basma, C. Mansour, M. Haddad, M. Nemer, and P. Stabat. A novel method for co-optimizing battery sizing and charging strategy of battery electric bus fleets: An application to the city of Paris. In:

Energy 285 (2023), 129459. https://doi.org/10.1016/j.energy.2023.129459 (cited on pages 15–18, 21, 22).

S. Bellocchi, G. L. Guizzi, M. Manno, M. Salvatori, and A. Zaccagnini. Reversible heat pump HVAC system with regenerative heat exchanger for electric vehicles: Analysis of its impact on driving range. In: *Appl Therm Eng* 129 (2018), 290–305. https://doi.org/10.1016/J.APPLTHERMALENG.2017.10.020 (cited on page 92).

D. Bickel. Robust and efficient estimation of the mode of continuous data: the mode as a viable measure of central tendency. In: *Journal of Statistical Computation and Simulation* 73 (2003), 899–912. https://doi.org/10.1080/0094965031000097809 (cited on pages 61, 62).

D. Bickel and R. Frühwirth. On a fast, robust estimator of the mode: Comparisons to other robust estimators with applications. In: *Computational Statistics and Data Analysis* 50 (2006), 3500–3530. https://doi.org/10.1016/j.csda.2005.07.011 (cited on pages 61, 67).

Y. Bie, Y. Liu, S. Li, and L. Wang. HVAC operation planning for electric bus trips based on chance-constrained programming. In: *Energy* 258 (2022), 124807. https://doi.org/10.1016/J.ENERGY.2022.124807 (cited on pages 17, 91, 139).

F. Biljecki, G. Heuvelink, H. Ledoux, and J. Stoter. Propagation of positional error in 3D GIS: estimation of the solar irradiation of building roofs. In: *International Journal of Geographical Information Science* 29 (2015), 2269–2294. https://doi.org/10.1080/13658816.2015.1073292 (cited on page 58).

F. Biljecki, H. Ledoux, and J. Stoter. An improved LOD specification for 3D building models. In: *Computers, Environment and Urban Systems* 59 (2016), 25–37. https://doi.org/10.1016/j.compenvurbsys.2016.04.005 (cited on page 58).

F. Biljecki, H. Ledoux, J. Stoter, and G. Vosselman. The variants of an LOD of a 3D building model and their influence on spatial analyses. In: *ISPRS Journal of Photogrammetry and Remote Sensing* 116

(2016), 42–54. https://doi.org/10.1016/j.isprsjprs.2016.03.003 (cited on pages 57, 58).

F. Biljecki, J. Stoter, H. Ledoux, S. Zlatanova, and A. Çöltekin. Applications of 3D city models: State of the art review. In: *ISPRS International Journal of Geo-Information* 4 (2015), 2842–2889. https://doi.org/10.3390/ijgi4042842 (cited on page 55).

R. Billen, A.-F. Cutting-Decelle, O. Marina, J.-P. de Almeida, C. M., G. Falquet, T. Leduc, C. Métral, G. Moreau, J. Perret, G. Rabin, R. S. Jose, I. Yatskiv, and S. Zlatanova. 3D City Models and urban information: Current issues and perspectives. In: *EDP Sciences* (2014), I–118. https://doi.org/10.1051/tu0801/201400001 (cited on page 55).

Bloomberg. Electric Vehicle Outlook 2024. Technical report. 2024 (cited on page 3).

M. Brito, S. Freitas, S. Guimarães, C. Catita, and P. Redweik. The importance of facades for the solar PV potential of a Mediterranean city using LiDAR data. In: *Renewable Energy* 111 (2017), 85–94. https://doi.org/10.1016/J.RENENE.2017.03.085 (cited on page 57).

M. Brito, P. Redweik, C. Catita, S. Freitas, and M. Santos. 3D Solar Potential in the Urban Environment: A Case Study in Lisbon. In: *Energies* 12 (2019), 3457. https://doi.org/10.3390/en12183457 (cited on page 57).

A. Broatch, P. Olmeda, P. Bares, and S. Aceros. Integral Thermal Management Studies in Winter Conditions with a Global Model of a Battery-Powered Electric Bus. In: *Energies (Basel)* 16.(1) (2023). https://doi.org/10.3390/en16010168 (cited on pages 15–17, 19, 21, 92, 139, 154).

C. Catita, P. Redweik, J. Pereira, and M. Brito. Extending solar potential analysis in buildings to vertical facades. In: *Computers and Geosciences* 66 (2014), 1–12. https://doi.org/10.1016/j.cageo.2014.01.002 (cited on page 57).

S. K. Chaudhry and S. P. Elumalai. The influence of school bus ventilation scenarios over in-cabin PM number concentration and air exchange rates. In: *Atmos Pollut Res* 11.(8) (2020), 1396–1407. https://doi.org/10.1016/J.APR.2020.05.021 (cited on pages 104, 117, 118, 151).

S. Chen, B. Du, Q. Li, and D. Xue. The influence of different orientations and ventilation cases on temperature distribution of the car cabin in the hot soak. In: *Case Studies in Thermal Engineering* 39 (2022), 102401. https://doi.org/10.1016/J.CSITE.2022.102401 (cited on pages 17, 92, 139).

Y. Chen, Y. Zhang, and R. Sun. Data-driven estimation of energy consumption for electric bus under real-world driving conditions. In: *Transportation Research Part D: Transport and Environment* 98 (2021), 102969. https://doi.org/10.1016/j.trd.2021.102969 (cited on page 11).

H. Cheng and K. Gupta. An historical note on finite rotations. In: *Journal of Applied Mechanics, Transactions ASME* 56 (1989), 139–145. https://doi.org/10.1115/1.3176034 (cited on page 65).

Coalition for Urban Transitions. Climate Emergency, Urban Opportunity. 2019 (cited on page 55).

M. Corazza, V. Conti, A. Genovese, F. Ortenzi, and M. P. Valentini. A Procedure to Estimate Air Conditioning Consumption of Urban Buses Related to Climate and Main Operational Characteristics. In: *World Electric Vehicle Journal 2021, Vol. 12, Page 29* 12.(1) (2021), 29. https://doi.org/10.3390/WEVJ12010029 (cited on page 115).

J. Corberan, J. Gonzalvez, P. Montes, and R. Blasco. 'ART' A Computer Code To Assist The Design Of Refrigeration and A/C Equipment. In: *International Refrigeration and Air Conditioning Conference*. https://docs.lib.purdue.edu/iracc/570. 2002 (cited on pages 139, 148).

J.-M. Corberán, S. Martínez-Ballester, J. Gonzálvez-Maciá, and C. LaBarbera. Error estimation of single phase effectiveness and LMTD methodologies when applied to heat exchangers with phase change.

In: *Journal of Physics: Conference Series* 745.(3) (2016), 032125. https://doi.org/10.1088/1742-6596/745/3/032125 (cited on pages 18, 139).

J. Corripio. insol: Solar Radiation. 2019. https://doi.org/https://cran.r-project.org/package=insol (cited on page 56).

M. Dalponte and D. A. Coomes. Tree-centric mapping of forest carbon density from airborne laser scanning and hyperspectral data. In: *Methods Ecol Evol* 7.(10) (2016), 1236–1245. https://doi.org/10.1111/2041-210X.12575 (cited on pages 15, 97, 145).

J. R. M. Delos Reyes, R. v. Parsons, and R. Hoemsen. Winter Happens: The Effect of Ambient Temperature on the Travel Range of Electric Vehicles. In: *IEEE Trans Veh Technol* 65.(6) (2016), 4016–4022. https://doi.org/10.1109/TVT.2016.2544178 (cited on page 90).

G. Desthieux, C. Carneiro, R. Camponovo, P. Ineichen, E. Morello, A. Boulmier, N. Abdennadher, S. Dervey, and C. Ellert. Solar energy potential assessment on rooftops and facades in large built environments based on lidar data, image processing, and cloud computing. Methodological background, application, and validation in geneva (solar cadaster). In: *Frontiers in Built Environment* 4 (2018), 331553. https://doi.org/10.3389/FBUIL.2018.00014/BIBTEX (cited on page 56).

D. Di Battista and R. Cipollone. High efficiency air conditioning model based analysis for the automotive sector. In: *International Journal of Refrigeration* 64 (2016), 108–122. https://doi.org/10.1016/J.IJREFRIG.2015.12.014 (cited on pages 18, 139).

M. Direk, M. S. Mert, F. Yüksel, and A. Keleşoğlu. Exergetic Investigation of a R1234yf Automotive Air Conditioning System with Internal Heat Exchanger. In: *International Journal of Thermodynamics* 21.(2) (2018), 103–109. https://doi.org/10.5541/IJOT.357232 (cited on pages 18, 139).

M. Dorman and E. Erell. A shadow: R Package for Geometric Shadow Calculations in an Urban Environment. In: *The R Journal* 11 (2019), 287. https://doi.org/10.32614/rj-2019-024 (cited on page 58).

N. Dougier, B. Celik, S.-K. Chabi-Sika, M. Sechilariu, F. Locment, and J. Emery. Modelling of Electric Bus Operation and Charging Process: Potential Contribution of Local Photovoltaic Production. In: *Applied Sciences* 13.(7) (2023), 4372. https://doi.org/10.3390/app13074372 (cited on pages 15–17, 19, 21).

S. Doulgeris, A. Zafeiriadis, N. Athanasopoulos, N. Tzivelou, M. Michali, S. Papagianni, and Z. Samaras. Evaluation of energy consumption and electric range of battery electric busses for application to public transportation. In: *Transportation Engineering* 15 (2024), 100223. https://doi.org/10.1016/J.TRENG.2023.100223 (cited on page 167).

G. Droj, L. Droj, and A.-C. Badea. GIS-Based Survey over the Public Transport Strategy: An Instrument for Economic and Sustainable Urban Traffic Planning. In: *ISPRS International Journal of Geo-Information* 11.(1) (2022). https://doi.org/10.3390/ijgi11010016 (cited on page 14).

J. A. Duffie and W. A. Beckman. Solar Engineering of Thermal Processes: Fourth Edition. Solar Engineering of Thermal Processes: Fourth Edition, 2013. https://doi.org/10.1002/9781118671603 (cited on pages 103, 107, 146).

C. Dullinger, W. Struckl, and M. Kozek. A modular thermal simulation tool for computing energy consumption of HVAC units in rail vehicles. In: *Appl Therm Eng* 78 (2015), 616–629. https://doi.org/10.1016/J.APPLTHERMALENG.2014.11.065 (cited on pages 18, 139).

Empresa Municipal de Transportes de Valencia. https://www.emtvalencia.es. 2023 (cited on pages 96, 98, 104, 105, 117, 144, 154).

Esri. Obtaining elevation information for building footprints - Help | ArcGIS Desktop. 2020. https://doi.org/https://desktop.arcgis.com/en/arcmap/latest/extensions/3d-analyst/3d-buildings-obtaining-elevation-information-for-building-footprints.htm (cited on page 61).

Esri. What is raster data? - Help | ArcGIS Desktop. 2020. https://doi.org/https://desktop.arcgis.com/en/arcmap/latest/manage-data/raster-and-images/what-is-raster-data.htm (cited on page 56).

European Automobile Manufacturers' Association. Buses - Fact sheet. 2023 (cited on page 3).

European Automobile Manufacturers' Association. Vehicles on European roads. 2024 (cited on page 3).

European Commission. Attitudes of Europeans towards Urban Mobility. Technical report. 2013 (cited on page 2).

European Commission. COM/2019/640 final - The European Green Deal. 2019 (cited on page 90).

European Commission. The Expert Group on Clean Buses - Procurement and Operation. Publications Office of the European Union, 2019 (cited on page 3).

European Commission. Transport in the European Union - Current Trends and Issues. Technical report. 2019 (cited on page 2).

European Commission. Handbook on the external costs of transport. Publications Office of the European Union, 2020. https://doi.org/doi/10.2832/51388 (cited on page 2).

European Commission. TDetermining the environmental impacts of conventional and alternatively fuelled vehicles through LCA. Publications Office of the European Union, 2020 (cited on page 3).

European Commission. COM/2021/400 final - Pathway to a Healthy Planet for All. EU Action Plan: 'Towards Zero Pollution for Air, Water and Soil'. 2021 (cited on page 2).

European Commission. COM/2021/811 final - The New EU Urban Mobility Framework. 2021 (cited on page 2).

European Commission. EU reference scenario 2020. Energy, transport and GHG emissions: trends to 2050. 2021. https://doi.org/doi/10.2833/35750 (cited on page 90).

European Commission. Regulation EU 2021/1119 of the European Parliament and of the Council of 30 June 2021 establishing the framework for achieving climate neutrality and amending Regulations (EC) No 401/2009 and EU 2018/1999 ('European Climate Law'). In: *Brussels: European Commission* (2021) (cited on page 2).

European Commission. The European pillar of social rights action plan. Publications Office of the European Union, 2021. `https://doi.org/doi/10.2767/89` (cited on page 1).

European Commission. Attitudes of Europeans towards Air Quality. Technical report. 2022 (cited on page 2).

European Commission. PE/66/2022/REV/1 - Regulation EU 2023/851 of the European Parliament and of the Council of 19 April 2023 amending Regulation EU 2019/631 as regards strengthening the CO2 emission performance standards for new passenger cars and new light commercial vehicles in line with the Union's increased climate ambition (Text with EEA relevance). 2022 (cited on page 2).

European Commission. C/2023/6783 - Commission Implementing Regulation EU 2023/2122 of 17 October 2023 amending Implementing Regulation EU 2018/2066 as regards updating the monitoring and reporting of greenhouse gas emissions pursuant to Directive 2003/87/EC of the European Parliament and of the Council. 2023 (cited on page 2).

European Commission. Proposal for amending Regulation EU 2019/1242 as regards strengthening the CO2 emission performance standards for new heavy-duty vehicles and integrating reporting obligations, and repealing Regulation EU 2018/956. 2023 (cited on page 138).

European Commission. PE/29/2024/REV/1 - Regulation EU 2024/1610 of the European Parliament and of the Council of 14 May 2024 amending Regulation EU 2019/1242 as regards strengthening the CO2 emission performance standards for new heavy-duty vehicles and integrating reporting obligations, amending Regulation EU 2018/858 and repealing Regulation EU 2018/956 (Text with EEA relevance). 2024 (cited on page 3).

European Environment Agency. Environmental noise in Europe — 2020. Technical report. 2020. https://doi.org/doi/10.2800/686249 (cited on page 2).

European Environment Agency. Transport and Environment Report 2022: Digitalisation in the Mobility System: Challenges and Opportunities. Technical report. 2022. https://doi.org/10.2800/47438 (cited on page 1).

European Environment Agency. Greenhouse gas emissions from transport in Europe. 2023 (cited on page 1).

European Environment Agency. Europe's air quality status 2024. Technical report. 2024. https://doi.org/doi/10.2800/5970 (cited on page 1).

European Environment Agency. EEA greenhouse gases. Data viewer on Total greenhouse gas emissions and removals of the EU, based on data reported by EU Member States under the EU Governance Regulation (cited on pages 1, 90).

Eurostat. Eurostat regional yearbook. Publications Office of the European Union, 2022. https://doi.org/doi/10.2785/915176 (cited on page 1).

Eurostat. Modal split of inland passenger transport. 2024. https://doi.org/10.2908/TRAN_HV_PSMOD (cited on page 3).

M. A. Fayazbakhsh and M. Bahrami. Comprehensive Modeling of Vehicle Air Conditioning Loads Using Heat Balance Method. In: *SAE Technical Papers* 2 (2013). https://doi.org/10.4271/2013-01-1507 (cited on pages 18, 139).

C. Fiori and V. Marzano. Modelling energy consumption of electric freight vehicles in urban pickup/delivery operations: analysis and estimation on a real-world dataset. In: *Transp Res D Transp Environ* 65 (2018), 658–673. https://doi.org/10.1016/J.TRD.2018.09.020 (cited on pages 12, 154).

S. Freitas, C. Catita, P. Redweik, and M. Brito. Modelling solar potential in the urban environment: State-of-the-art review. In: *Renewable and Sustainable Energy Reviews* 41 (2015), 915–931. https://doi.org/10.1016/j.rser.2014.08.060 (cited on pages 55, 56).

P. Fu and P. Rich. Design and Implementation of the Solar Analyst: an ArcView Extension for Modeling Solar Radiation at Landscape Scales. In: *19th Annual ESRI User Conference*. 1999, 1–24 (cited on page 56).

C. Gaete-Morales, H. Kramer, W. P. Schill, and A. Zerrahn. An open tool for creating battery-electric vehicle time series from empirical data, emobpy. In: *Scientific Data 2021 8:1* 8.(1) (2021), 1–18. https://doi.org/10.1038/s41597-021-00932-9 (cited on page 154).

M. Gallet, T. Massier, and T. Hamacher. Estimation of the energy demand of electric buses based on real-world data for large-scale public transport networks. In: *Appl Energy* 230 (2018), 344–356. https://doi.org/10.1016/J.APENERGY.2018.08.086 (cited on pages 15, 16, 18, 19, 21, 91, 139).

Y. Gao, S. Guo, J. Ren, Z. Zhao, A. Ehsan, and Y. Zheng. An Electric Bus Power Consumption Model and Optimization of Charging Scheduling Concerning Multi-External Factors. In: *Energies* 11.(8) (2018). https://doi.org/10.3390/en11082060 (cited on page 11).

Z. Gao, Z. Lin, T. J. LaClair, C. Liu, J.-M. Li, A. K. Birky, and J. Ward. Battery capacity and recharging needs for electric buses in city transit service. In: *Energy* 122 (2017), 588–600. https://doi.org/10.1016/J.ENERGY.2017.01.101 (cited on pages 11, 167).

J. R. García-Cascales, F. Vera-García, J. M. Corberán-Salvador, J. Gonzálvez-Maciá, and D. Fuentes-Díaz. Assessment of boiling heat transfer correlations in the modelling of fin and tube heat exchangers. In: *International Journal of Refrigeration* 30.(6) (2007), 1004–1017. https://doi.org/10.1016/J.IJREFRIG.2007.01.006 (cited on page 148).

F. Gómez, N. Tamarit, and J. Jabaloyes. Green zones, bioclimatics studies and human comfort in the future development of urban planning. In: *Landsc Urban Plan* 55.(3) (2001), 151–161. https://doi.org/10.1016/S0169-2046(01)00150-5 (cited on pages 95, 143).

H. Gong, Y. Zou, Q. Yang, J. Fan, F. Sun, and D. Goehlich. Generation of a driving cycle for battery electric vehicles: A case study of Beijing. In: *Energy* 150 (2018), 901–912. https://doi.org/10.1016/J.ENERGY.2018.02.092 (cited on pages 15, 91).

Google Inc. General Transit Feed Specification. https://developers.google.com/transit/gtfs/reference. 2022 (cited on pages 98, 146).

G. Gröger and L. Plümer. CityGML - Interoperable semantic 3D city models. In: *ISPRS Journal of Photogrammetry and Remote Sensing* 71 (2012), 12–33. https://doi.org/10.1016/j.isprsjprs.2012.04.004 (cited on pages 57, 63).

R. Günther, T. Wenzel, M. Wegner, and R. Rettig. Big data driven dynamic driving cycle development for busses in urban public transportation. In: *Transp Res D Transp Environ* 51 (2017), 276–289. https://doi.org/10.1016/J.TRD.2017.01.009 (cited on pages 15, 91).

Y. Guo, J. Guo, W. Yang, P. Zhao, Y. Zhou, R. Deng, and Z. Jin. Experimental investigation on the heating performance of a R410A vapor-injection heat pump of an electric bus in cold regions. In: *Applied Thermal Engineering* 222 (2023), 119938. https://doi.org/10.1016/j.applthermaleng.2022.119938 (cited on page 9).

R. A. Haddad, H. Basma, and C. Mansour. Modeling and control of heat pump system for battery electric buses. In: *Proceedings of the Institution of Mechanical Engineers, Part D: Journal of Automobile Engineering* 236.(14) (2022), 3201–3220. https://doi.org/10.1177/09544070211069465 (cited on pages 15–19).

X. Han, H. Zou, J. Wu, C. Tian, M. Tang, and G. Huang. Investigation on the heating performance of the heat pump with waste heat recovery for the electric bus. In: *Renew Energy* 152 (2020), 835–848.

https://doi.org/10.1016/J.RENENE.2020.01.075 (cited on pages 10, 107).

H. He, M. Yan, C. Sun, J. Peng, M. Li, and H. Jia. Predictive air-conditioner control for electric buses with passenger amount variation forecast. In: *Appl Energy* 227 (2018), 249–261. https://doi.org/10.1016/J.APENERGY.2017.08.181 (cited on pages 17, 18, 91, 139).

L. He, P. Li, Y. Zhang, H. Jing, and Z. Gu. Control strategy analysis of multistage speed compressor for vehicle air conditioning based on particle swarm optimization. In: *Case Studies in Thermal Engineering* 47 (2023), 103033. https://doi.org/10.1016/J.CSITE.2023.103033 (cited on page 140).

X. He, S. Zhang, W. Ke, Y. Zheng, B. Zhou, X. Liang, and Y. Wu. Energy consumption and well-to-wheels air pollutant emissions of battery electric buses under complex operating conditions and implications on fleet electrification. In: *Journal of Cleaner Production* 171 (2018), 714–722. https://doi.org/10.1016/j.jclepro.2017.10.017 (cited on page 11).

O. A. Hjelkrem, K. Y. Lervåg, S. Babri, C. Lu, and C. J. Södersten. A battery electric bus energy consumption model for strategic purposes: Validation of a proposed model structure with data from bus fleets in China and Norway. In: *Transp Res D Transp Environ* 94 (2021), 102804. https://doi.org/10.1016/J.TRD.2021.102804 (cited on pages 12, 15–19, 21, 105, 139).

J. Hofierka and M. Súri. The solar radiation model for Open source GIS: implementation and applications. In: *Open Source GIS - GRASS Users Conference*. 2002 (cited on page 56).

J. Hofierka and M. Zlocha. A New 3-D Solar Radiation Model for 3-D City Models. In: *Transactions in GIS* 16 (2012), 681–690. https://doi.org/10.1111/j.1467-9671.2012.01337.x (cited on pages 57, 58).

T. Huld, E. Paietta, P. Zangheri, and I. P. Pascua. Assembling Typical Meteorological Year Data Sets for Building Energy Performance Using Reanalysis and Satellite-Based Data. In: *Atmosphere 2018, Vol. 9, Page 53* 9.(2) (2018), 53. https://doi.org/10.3390/ATMOS9020053 (cited on pages 95, 144).

Instituto Geográfico Nacional. Plan Nacional de Ortofotografía Aérea. 2020. https://doi.org/https://pnoa.ign.es (cited on pages 67, 68).

International Council on Clean Transportation. Strategies for deploying zero-emission bus fleets: Route-level energy consumption and driving range analysis. 2021 (cited on page 115).

International Energy Agency. Cooling on the Move. The future of air conditioning in vehicles. https://www.iea.org/reports/cooling-on-the-move. 2019 (cited on pages 7, 90).

International Energy Agency. Global EV Outlook 2023. Paris, 2023 (cited on pages 115, 138).

J. Jabardo, W. Mamani, and M. R. Ianella. Modeling and experimental evaluation of an automotive air conditioning system with a variable capacity compressor. In: *International Journal of Refrigeration* 25.(8) (2002), 1157–1172. https://doi.org/10.1016/S0140-7007(02)00002-6 (cited on pages 18, 139).

K. Jetlund and B. Neuhäuser. Geographic Information Systems for Transportation. In: *Springer Handbook of Geographic Information*. Edited by W. Kresse and D. Danko. Cham: Springer International Publishing, 2022, 707–727. https://doi.org/10.1007/978-3-030-53125-6_26 (cited on page 14).

J. Jiang, Y. Yu, H. Min, Q. Cao, W. Sun, Z. Zhang, and C. Luo. Trip-level energy consumption prediction model for electric bus combining Markov-based speed profile generation and Gaussian processing regression. In: *Energy* 263 (2023), 125866. https://doi.org/10.1016/J.ENERGY.2022.125866 (cited on pages 17, 91, 139).

J. Karlsson and A. Roos. Modelling the angular behaviour of the total solar energy transmittance of windows. In: *Solar Energy* 69.(4) (2000), 321–329. https://doi.org/10.1016/S0038-092X(00)00083-9 (cited on page 107).

L. Kauder. NASA Technical Publication. Spacecraft Thermal Control Coatings References. Technical report. 2005 (cited on pages 96, 117).

S. Kaynak, B. Kaynak, and A. Özmen. A software tool development study for solar energy potential analysis. In: *Energy and Buildings* 162 (2018), 134–143. https://doi.org/10.1016/J.ENBUILD.2017.12.033 (cited on page 57).

H. Khayyam, J. Abawajy, and R. N. Jazar. Intelligent energy management control of vehicle air conditioning system coupled with engine. In: *Appl Therm Eng* 48 (2012), 211–224. https://doi.org/10.1016/J.APPLTHERMALENG.2012.04.050 (cited on pages 18, 139).

H. Kim, N. Hartmann, M. Zeller, R. Luise, and T. Soylu. Comparative TCO Analysis of Battery Electric and Hydrogen Fuel Cell Buses for Public Transport System in Small to Midsize Cities. In: *Energies* 14.(14) (2021). https://doi.org/10.3390/en14144384 (cited on page 3).

K. Kivekas, J. Vepsalainen, and K. Tammi. Stochastic Driving Cycle Synthesis for Analyzing the Energy Consumption of a Battery Electric Bus. In: *IEEE Access* 6 (2018), 55586–55598. https://doi.org/10.1109/ACCESS.2018.2871574 (cited on pages 12, 91).

M. Kottek, J. Grieser, C. Beck, B. Rudolf, and F. Rubel. World Map of the Köppen-Geiger climate classification updated. In: *Meteorologische Zeitschrift* 15.(3) (2006), 259–263. https://doi.org/10.1127/0941-2948/2006/0130 (cited on pages 95, 143).

A. Lajunen. Energy Efficiency and Performance of Cabin Thermal Management in Electric Vehicles. In: *SAE Technical Papers*. Volume 2017-March. March. 2017. https://doi.org/10.4271/2017-01-0192 (cited on page 92).

A. Lajunen, Y. Yang, and A. Emadi. Review of Cabin Thermal Management for Electrified Passenger Vehicles. In: *IEEE Trans Veh Technol* 69.(6) (2020), 6025–6040. https://doi.org/10.1109/TVT.2020.2988468 (cited on pages 90, 138).

F. Lan, H. Chen, J. Chen, and W. Li. Effect of urban microclimates on dynamic thermal characteristics of a vehicle cabin. In: *Case Studies in Thermal Engineering* (2023), 103162. https://doi.org/10.1016/J.CSITE.2023.103162 (cited on pages 17, 92, 139).

G. W. Larson and R. A. Shakespeare. Rendering with Radiance: The Art and Science of Lighting Visualization. Morgan Kaufman, 1998 (cited on page 56).

H. Ledoux and M. Meijers. Topologically consistent 3D city models obtained by extrusion. In: *International Journal of Geographical Information Science* 25 (2011), 557–574. https://doi.org/10.1080/13658811003623277 (cited on page 61).

D.-Y. Lee, C.-W. Cho, J.-P. Won, Y. C. Park, and M.-Y. Lee. Performance characteristics of mobile heat pump for a large passenger electric vehicle. In: *Applied Thermal Engineering* 50.(1) (2013), 660–669. https://doi.org/10.1016/j.applthermaleng.2012.07.001 (cited on page 10).

G. H. Lee and J. Y. Yoo. Performance analysis and simulation of automobile air conditioning system. In: *International Journal of Refrigeration* 23.(3) (2000), 243–254. https://doi.org/10.1016/S0140-7007(99)00047-X (cited on pages 18, 139).

J. W. Lee, E. Y. Jang, S. H. Lee, H. S. Ryou, S. Choi, and Y. Kim. Influence of the spectral solar radiation on the air flow and temperature distributions in a passenger compartment. In: *International Journal of Thermal Sciences* 75 (2014), 36–44. https://doi.org/10.1016/J.IJTHERMALSCI.2013.07.018 (cited on page 106).

T. Lee, K. H. Shin, J. Kim, D. Jung, and J. H. Kim. Design optimization of external variable displacement compressor with R1234yf for vehicle air conditioning system. In: *Appl Therm Eng* 198 (2021), 117493.

https://doi.org/10.1016/J.APPLTHERMALENG.2021.117493 (cited on page 140).

V. Lemort, G. Olivier, and C. De Pelsemaker. Thermal Energy Management in Vehicles. https://www.wiley.com/en-us/Thermal+Energy+Management+in+Vehicles-p-9781119251750. 2023, 320 (cited on pages 17, 139).

C. Li. 2.09 - GIS for Urban Energy Analysis. In: *Comprehensive Geographic Information Systems*. Edited by B. Huang. Oxford: Elsevier, 2018, 187–195. https://doi.org/10.1016/B978-0-12-409548-9.09652-4 (cited on page 14).

P. Li, Y. Zhang, K. Zhang, and M. Jiang. The effects of dynamic traffic conditions, route characteristics and environmental conditions on trip-based electricity consumption prediction of electric bus. In: *Energy* 218 (2021), 119437. https://doi.org/10.1016/J.ENERGY.2020.119437 (cited on pages 11, 15, 91, 138).

P. Li, Y. Zhang, Y. Zhang, and K. Zhang. Prediction of electric bus energy consumption with stochastic speed profile generation modelling and data driven method based on real-world big data. In: *Appl Energy* 298 (2021), 117204. https://doi.org/10.1016/J.APENERGY.2021.117204 (cited on pages 11, 15, 91, 138).

W. Li and J. Sun. Numerical simulation and analysis of transport air conditioning system integrated with passenger compartment. In: *Appl Therm Eng* 50.(1) (2013), 37–45. https://doi.org/10.1016/J.APPLTHERMALENG.2012.05.030 (cited on pages 107, 117).

J. Liang and J. Gong. A Sparse Voxel Octree-Based Framework for Computing Solar Radiation Using 3D City Models. In: *ISPRS International Journal of Geo-Information* 6 (2017), 106. https://doi.org/10.3390/ijgi6040106 (cited on page 57).

J. Liang, J. Gong, J. Zhou, A. Ibrahim, and M. Li. An open-source 3D solar radiation model integrated with a 3D Geographic Information System. In: *Environmental Modelling and Software* 64 (2015), 94–101. https://doi.org/10.1016/j.envsoft.2014.11.019 (cited on page 57).

I. Lima, V. Scalco, and R. Lamberts. Estimating the impact of urban densification on high-rise office building cooling loads in a hot and humid climate. In: *Energy and Buildings* 182 (2019), 30–44. https://doi.org/10.1016/j.enbuild.2018.10.019 (cited on page 55).

X. Liu, P. Payakkamas, M. Dijk, and J. de Kraker. GIS Models for Sustainable Urban Mobility Planning: Current Use, Future Needs and Potentials. In: *Future Transportation* 3.(1) (2023), 384–402. https://doi.org/10.3390/futuretransp3010023 (cited on page 14).

K. G. Logan, J. D. Nelson, and A. Hastings. Electric and hydrogen buses: Shifting from conventionally fuelled cars in the UK. In: *Transportation Research Part D: Transport and Environment* 85 (2020), 102350. https://doi.org/10.1016/j.trd.2020.102350 (cited on page 3).

R. Machete, A. Falcão, M. Gomes, and A. M. Rodrigues. The use of 3D GIS to analyse the influence of urban context on buildings' solar energy potential. In: *Energy and Buildings* 177 (2018), 290–302. https://doi.org/10.1016/J.ENBUILD.2018.07.064 (cited on pages 55, 56).

M. Mahmoud, R. Garnett, M. Ferguson, and P. Kanaroglou. Electric buses: A review of alternative powertrains. In: *Renewable and Sustainable Energy Reviews* 62 (2016), 673–684. https://doi.org/10.1016/j.rser.2016.05.019 (cited on page 3).

Y. Mao, J. Wang, and J. Li. Experimental and numerical study of air flow and temperature variations in an electric vehicle cabin during cooling and heating. In: *Appl Therm Eng* 137 (2018), 356–367. https://doi.org/10.1016/J.APPLTHERMALENG.2018.03.099 (cited on page 92).

R. Mastrullo, A. W. Mauro, and C. Vellucci. Refrigerant Alternatives for High Speed Train A/C Systems: Energy Savings and Environmental Emissions Evaluation under Variable Ambient Conditions. In: *Energy Procedia* 101 (2016), 280–287. https://doi.org/10.1016/J.EGYPRO.2016.11.036 (cited on pages 18, 139).

W. R. Mebane and J. S. Sekhon. Genetic Optimization Using Derivatives: The rgenoud Package for R. In: *J Stat Softw* 42.(11) (2011), 1–26. https://doi.org/10.18637/JSS.V042.I11 (cited on pages 100, 146).

F. Miguet and D. Groleau. A daylight simulation tool for urban and architectural spaces—application to transmitted direct and diffuse light through glazing. In: *Building and Environment* 37.(8) (2002), 833–843. https://doi.org/10.1016/S0360-1323(02)00049-5 (cited on page 56).

M. Mohanraj and J. D. P. Abraham. Environment friendly refrigerant options for automobile air conditioners: a review. In: *Journal of Thermal Analysis and Calorimetry* 147 (1 2022), 47–72. https://doi.org/10.1007/S10973-020-10286-W/TABLES/10 (cited on page 10).

M. Molliere. Battery-electric is now the most popular for new city buses in the EU. 2024 (cited on page 3).

J. H. Moon, J. W. Lee, C. H. Jeong, and S. H. Lee. Thermal comfort analysis in a passenger compartment considering the solar radiation effect. In: *International Journal of Thermal Sciences* 107 (2016), 77–88. https://doi.org/10.1016/J.IJTHERMALSCI.2016.03.013 (cited on page 92).

M. B. B. de Moura and A. Tribess. Climate control system improvements for better cabin environmental conditions and reduction of fuel consumption. In: *SAE Technical Papers*. 2007. https://doi.org/10.4271/2007-01-2673 (cited on pages 7, 90).

E. Mulholland. The revised CO2 standards for heavy-duty vehicles in the European Union. Technical report. 2024 (cited on page 3).

N. Muralidhar, M. Himabindu, and R. Ravikrishna. Modeling of a hybrid electric heavy duty vehicle to assess energy recovery using a thermoelectric generator. In: *Energy* 148 (2018), 1046–1059. https://doi.org/10.1016/j.energy.2018.02.023 (cited on page 10).

D. Nam, P. Lee, G. Lee, Y. Kwon, and J. Lee. Optimization of an oil charge amount on electric driven scroll compressor for eco-friendly vehicle. In: *International Journal of Refrigeration* 57 (2015), 54–61. https://doi.org/10.1016/J.IJREFRIG.2015.05.009 (cited on page 140).

E. Navarro, I. Martínez-Galvan, J. Nohales, and J. Gonzálvez-Maciá. Comparative experimental study of an open piston compressor working with R-1234yf, R-134a and R-290. In: *International Journal of Refrigeration* 36.(3) (2013), 768–775. https://doi.org/10.1016/j.ijrefrig.2012.11.017 (cited on page 10).

W. Newman, I. Sutherland, and G. Hodgman. Graphics and Reentrant Polygon Clipping. In: 1974 (cited on page 58).

D. Nicolaides, D. Cebon, and J. Miles. An Urban Charging Infrastructure for Electric Road Freight Operations: A Case Study for Cambridge UK. In: *IEEE Syst J* 13.(2) (2019), 2057–2068. https://doi.org/10.1109/JSYST.2018.2864693 (cited on page 139).

NSG Group. Pilkington catalogue (cited on pages 96, 98, 117).

M. S. Oh, J. H. Ahn, D. W. Kim, D. S. Jang, and Y. Kim. Thermal comfort and energy saving in a vehicle compartment using a localized air-conditioning system. In: *Appl Energy* 133 (2014), 14–21. https://doi.org/10.1016/J.APENERGY.2014.07.089 (cited on page 92).

T. R. Oke, G. Mills, A. Christen, and J. A. Voogt. Urban Climates. Cambridge University Press, 2017. https://doi.org/10.1017/9781139016476 (cited on pages 103, 144, 146).

X. Oregi, N. Hermoso, I. Prieto, J. Izkara, L. Mabe, and P. Sismanidis. Automatised and georeferenced energy assessment of an Antwerp district based on cadastral data. In: *Energy and Buildings* 173 (2018), 176–194. https://doi.org/10.1016/j.enbuild.2018.05.018 (cited on page 55).

C. Os'Boyle, R. Douglas, R. Best, and M. Geron. Vehicle Thermal Modelling for Improved Drive Cycle Analysis of a Generic City Bus. In: *2020 5th International Conference on Smart and Sustainable Technologies, SpliTech 2020*. 2020. https://doi.org/10.23919/SPLITECH49282.2020.9243725 (cited on pages 92, 107, 158).

S. Pili, G. Desogus, and D. Melis. A GIS tool for the calculation of solar irradiation on buildings at the urban scale, based on Italian standards. In: *Energy and Buildings* 158 (2018), 629–646. https://doi.org/10.1016/j.enbuild.2017.10.027 (cited on page 58).

A. Pisano, S. Martinez-Ballester, J. M. Corberán, F. H. Monpeán, F. I. Gómez, and J.-R. G. Cascales. A Discussion about the Methodology to Validate the Correlations of Heat Transfer Coefficients and Pressure Drop during the Condensation in a Finned-Tube Heat Exchanger. https://docs.lib.purdue.edu/iracc/1405. 2014 (cited on page 148).

P. Plötz, J. Wachsmuth, T. Gnann, F. Neuner, D. Speth, and S. Link. Net-zero-carbon transport in europe until 2050—targets, technologies and policies for a long-term eu strategy. In: *Karlsruhe: Fraunhofer Institute for Systems and Innovation Research ISI* (2021) (cited on page 2).

R. Prabakaran, D. M. Lal, and S. C. Kim. A state of art review on future low global warming potential refrigerants and performance augmentation methods for vapour compression based mobile air conditioning system. In: *Journal of Thermal Analysis and Calorimetry 2022 148:2* 148.(2) (2022), 417–449. https://doi.org/10.1007/S10973-022-11485-3 (cited on pages 96, 97, 140).

R. Prabakaran and D. Mohan Lal. A novel exergy based charge optimisation for a mobile air conditioning system: An experimental study. In: *J Therm Anal Calorim* 132.(2) (2018), 1241–1252. https://doi.org/10.1007/S10973-018-6998-0/METRICS (cited on pages 18, 139).

QGIS Development Team. Vector Data - Documentation for QGIS 3.4. 2020. https://doi.org/https://docs.qgis.org/3.4/en/docs/gentle_gis_introduction/vector_data.html (cited on page 57).

R Core Team. R: A Language and Environment for Statistical Computing. https://www.R-project.org/. 2022 (cited on pages 62, 66, 94, 143).

N. S. Raman, K. Devaprasad, B. Chen, H. A. Ingley, and P. Barooah. Model predictive control for energy-efficient HVAC operation with humidity and latent heat considerations. In: *Appl Energy* 279 (2020), 115765. https://doi.org/10.1016/J.APENERGY.2020.115765 (cited on page 151).

D. Ramsey, L. Boulon, and A. Bouscayrol. Modeling of an EV air conditioning system for energetic studies in summer. In: *2021 IEEE Vehicle Power and Propulsion Conference, VPPC 2021 - Proceedings*. 2021. https://doi.org/10.1109/VPPC53923.2021.9699119 (cited on pages 17, 92, 139).

D. Ramsey, A. Bouscayrol, and L. Boulon. Energy Consumption of a Battery Electric Vehicle in Winter Considering Preheating: Tradeoff between Improved Performance and Total Energy Consumption. In: *IEEE Vehicular Technology Magazine* 17.(3) (2022), 104–112. https://doi.org/10.1109/MVT.2022.3158043 (cited on pages 18, 92, 139).

D. Ramsey, A. Bouscayrol, L. Boulon, A. Desreveaux, and A. Vaudrey. Flexible Simulation of an Electric Vehicle to Estimate the Impact of Thermal Comfort on the Energy Consumption. In: *IEEE Transactions on Transportation Electrification* 8.(2) (2022), 2288–2298. https://doi.org/10.1109/TTE.2022.3144526 (cited on pages 18, 92, 139).

E. B. Ratts and J. S. Brown. An experimental analysis of cycling in an automotive air conditioning system. In: *Appl Therm Eng* 20.(11) (2000), 1039–1058. https://doi.org/10.1016/S1359-4311(99)00080-0 (cited on pages 18, 139).

C. Reinhart and C. C. Davila. Urban building energy modeling - A review of a nascent field. In: *Building and Environment* 97 (2016), 196–202. https://doi.org/10.1016/j.buildenv.2015.12.001 (cited on page 55).

Robert McNeel and Associates. Rhinoceros. 2019 (cited on page 56).

A. L. Rodrigues and S. R. Seixas. Battery-electric buses and their implementation barriers: Analysis and prospects for sustainability. In: *Sustainable Energy Technologies and Assessments* 51 (2022), 101896. https://doi.org/10.1016/j.seta.2021.101896 (cited on page 4).

J.-R. Roussel and D. Auty. Airborne LiDAR Data Manipulation and Visualization for Forestry Applications. https://cran.r-project.org/package=lidR. 2023 (cited on pages 15, 97, 145).

J.-R. Roussel, D. Auty, N. C. Coops, P. Tompalski, T. R. Goodbody, A. S. Meador, J.-F. Bourdon, F. de Boissieu, and A. Achim. lidR: An R package for analysis of Airborne Laser Scanning (ALS) data. In: *Remote Sensing of Environment* 251 (2020), 112061. https://doi.org/10.1016/j.rse.2020.112061 (cited on pages 15, 97, 145).

A. Saadon Al-Ogaili, A. Ramasamy, T. Juhana Tengku Hashim, A. N. Al-Masri, Y. Hoon, M. Neamah Jebur, R. Verayiah, and M. Marsadek. Estimation of the energy consumption of battery driven electric buses by integrating digital elevation and longitudinal dynamic models: Malaysia as a case study. In: *Applied Energy* 280 (2020), 115873. https://doi.org/10.1016/j.apenergy.2020.115873 (cited on pages 15, 16, 18, 19, 21).

M. Sadrani, R. Mirqasemi, A. Tirachini, and C. Antoniou. Barriers to electrification of bus systems: A fuzzy multi-criteria analysis in developed and developing countries. In: *Energy Conversion and Management* 314 (2024), 118700. https://doi.org/10.1016/j.enconman.2024.118700 (cited on page 4).

S. Sheather and M. Jones. A Reliable Data-Based Bandwidth Selection Method for Kernel Density Estimation. In: *Journal of the Royal Statistical Society. Series B (Methodological)* 53 (1991), 683–690. https://doi.org/http://www.jstor.org/stable/2345597 (cited on pages 62, 68).

Z. Shuofeng, M. R. Amini, J. Sun, and C. Mi. A Two-Layer Real-Time Optimization Control Strategy for Integrated Battery Thermal Management and HVAC System in Connected and Automated HEVs. In: *IEEE Trans Veh Technol* 70.(7) (2021), 6567–6576. https://doi.org/10.1109/TVT.2021.3085938 (cited on pages 17, 92, 139).

A. Sola, C. Corchero, J. Salom, and M. Sanmarti. Multi-domain urban-scale energy modelling tools: A review. In: *Sustainable Cities and Society* 54 (2020), 101872. https://doi.org/10.1016/j.scs.2019.101872 (cited on page 14).

Y. Song, H. Wang, Y. Ma, X. Yin, and F. Cao. Energetic, economic, environmental investigation of carbon dioxide as the refrigeration alternative in new energy bus/railway vehicles' air conditioning systems. In: *Applied Energy* 305 (2022), 117830. https://doi.org/10.1016/j.apenergy.2021.117830 (cited on page 10).

D. Srinivasan and P. Phadke. Reducing AC Power Consumption By Compressor Downsizing on a Sports Utility Vehicle. In: *International Refrigeration and Air Conditioning Conference*. https://docs.lib.purdue.edu/iracc/844. 2006 (cited on page 140).

A. Strzalka, N. Alam, E. Duminil, V. Coors, and U. Eicker. Large scale integration of photovoltaics in cities. In: *Applied Energy* 93 (2012), 413–421. https://doi.org/10.1016/j.apenergy.2011.12.033 (cited on page 58).

N. A. El-Taweel, A. Zidan, and H. E. Z. Farag. Novel Electric Bus Energy Consumption Model Based on Probabilistic Synthetic Speed Profile Integrated with HVAC. In: *IEEE Transactions on Intelligent Transportation Systems* 22.(3) (2021), 1517–1531. https://doi.

org/10.1109/TITS.2020.2971686 (cited on pages 12, 15–19, 21, 22, 91, 139).

J. Teller and S. Azar. Townscope II—A computer system to support solar access decision-making. In: *Solar Energy* 70.(3) (2001). Urban Environment, 187–200. https://doi.org/10.1016/S0038-092X(00)00097-9 (cited on page 56).

R. J. Thorne, I. B. Hovi, E. Figenbaum, D. R. Pinchasik, A. H. Amundsen, and R. Hagman. Facilitating adoption of electric buses through policy: Learnings from a trial in Norway. In: *Energy Policy* 155 (2021), 112310. https://doi.org/10.1016/j.enpol.2021.112310 (cited on page 4).

B. Torregrosa-Jaime, F. Bjurling, J. M. Corberán, F. Di Sciullo, and J. Payá. Transient thermal model of a vehicle's cabin validated under variable ambient conditions. In: *Appl Therm Eng* 75 (2015), 45–53. https://doi.org/10.1016/J.APPLTHERMALENG.2014.05.074 (cited on pages 17, 28, 92, 105, 106, 109).

B. Torregrosa-Jaime, J. Corberán, C. Vasile, C. Muller, M. Risser, and J. Payá. Sizing of a reversible magnetic heat pump for the automotive industry. In: *International Journal of Refrigeration* 37 (2014). New Developments in Magnetic Refrigeration, 156–164. https://doi.org/10.1016/j.ijrefrig.2013.06.018 (cited on page 10).

B. Torregrosa-Jaime, J. Payá, and J. Corberan. Design of efficient air-conditioning systems for electric vehicles. In: *SAE International Journal of Alternative Powertrains* 2.(2) (2013), 291–303. https://doi.org/10.4271/2013-01-0864 (cited on pages 18, 139).

E. Tosun, M. Bilgili, G. Tuccar, A. Yasar, and K. Aydin. Exergy analysis of an inter-city bus air-conditioning system. In: *International Journal of Exergy* 20.(4) (2016), 445–464. https://doi.org/10.1504/IJEX.2016.078094 (cited on pages 18, 139).

M. Tozzi, M. V. Corazza, U. Guida, and A. Musso. Testing innovations for increased energy efficiency of electric buses: Evidence from the EBSF-2 project. In: *Transportation Research Procedia* 48 (2020),

2166–2175. https://doi.org/10.1016/J.TRPRO.2020.08.273 (cited on pages 107, 150).

Trimble Inc. SketchUp. 2019. https://doi.org/https://www.sketchup.com (cited on page 56).

U.S. Department of Energy. EnergyPlusTM Version 22.1.0 - Engineering Reference. 2022 (cited on pages 102, 146, 151).

Ş. Ünal, M. T. Erdinç, and Ç. Kutlu. Optimal thermodynamic parameters of two-phase ejector refrigeration system for buses. In: *Applied Thermal Engineering* 124 (2017), 1354–1367. https://doi.org/10.1016/j.applthermaleng.2017.06.115 (cited on page 10).

United Nations. World Urbanization Prospects: The 2018 Revision. 2019. https://doi.org/10.18356/b9e995fe-en (cited on page 55).

Universitat Politècnica de Valéncia, Instituto de Ingenieria Energética, Spain. IMST-ART v4.0 - Simulation tool to assist the selection, design and optimization of refrigerator equipment and components. http://www.imst-art.com. 2022 (cited on pages 18, 148).

A. Vartholomaios. A machine learning approach to modelling solar irradiation of urban and terrain 3D models. In: *Computers, Environment and Urban Systems* 78 (2019), 101387. https://doi.org/10.1016/j.compenvurbsys.2019.101387 (cited on page 56).

D. C. Vásconez Núñez. Desarrollo de un modelo para el cálculo del consumo de climatización en vehículos de pasajeros urbanos. PhD thesis. Valencia (Spain): Universitat Politècnica de València, 2019. https://doi.org/10.4995/Thesis/10251/121133 (cited on pages 17, 92, 98, 117).

D. C. Vásconez-Núñez, J. Gonzálvez-Maciá, J. M. Corberán, and J. Payá. Development and validation of a dynamic thermal model of a minibus using TRNSYS. In: *International Journal of Vehicle Design* 77.(1–2) (2018), 87–107. https://doi.org/10.1504/IJVD.2018.098272 (cited on pages 18, 28, 139).

J. Vepsäläinen, K. Otto, A. Lajunen, and K. Tammi. Computationally efficient model for energy demand prediction of electric city bus in varying operating conditions. In: *Energy* 169 (2019), 433–443. https://doi.org/10.1016/J.ENERGY.2018.12.064 (cited on pages 7, 17, 91, 139).

J. Vepsäläinen, A. Ritari, A. Lajunen, K. Kivekäs, and K. Tammi. Energy Uncertainty Analysis of Electric Buses. In: *Energies* 11.(12) (2018). https://doi.org/10.3390/en11123267 (cited on page 11).

F. Vera-García, J. R. García-Cascales, J. M. Corberán-Salvador, J. Gonzálvez-Maciá, and D. Fuentes-Díaz. Assessment of condensation heat transfer correlations in the modelling of fin and tube heat exchangers. In: *International Journal of Refrigeration* 30.(6) (2007), 1018–1028. https://doi.org/10.1016/J.IJREFRIG.2007.01.005 (cited on page 148).

J. D. Viana-Fons, J. Gonzálvez-Maciá, and J. Payá. Development and validation in a 2D-GIS environment of a 3D shadow cast vector-based model on arbitrarily orientated and tilted surfaces. In: *Energy Build* 224 (2020). https://doi.org/10.1016/j.enbuild.2020.110258 (cited on pages 15, 145).

J. D. Viana-Fons and J. Payá. Dynamic cabin model of an urban bus in real driving conditions. In: *Energy* (2023), 129769. https://doi.org/10.1016/J.ENERGY.2023.129769 (cited on pages 140, 145, 146, 149).

A. Vulkan, I. Kloog, M. Dorman, and E. Erell. Modeling the potential for PV installation in residential buildings in dense urban areas. In: *Energy and Buildings* 169 (2018), 97–109. https://doi.org/10.1016/j.enbuild.2018.03.052 (cited on pages 58, 63).

R. Wang, J. Peethambaran, and D. Chen. LiDAR Point Clouds to 3-D Urban Models: A Review. In: *IEEE Journal of Selected Topics in Applied Earth Observations and Remote Sensing* 11 (2018), 606–627. https://doi.org/10.1109/JSTARS.2017.2781132 (cited on pages 57, 58).

K. Weiler and P. Atherton. Hidden surface removal using polygon area sorting. In: *ACM SIGGRAPH Computer Graphics* 11 (1977), 214–222. https://doi.org/10.1145/965141.563896 (cited on page 58).

M. Weisthal. Assessment of potential energy savings in Israel through climate-aware residential building design. PhD thesis. Ben Gurion University of the Negev, 2014 (cited on page 58).

World Resources Institute. Barriers to adopting electric buses. 2019 (cited on page 4).

P. Xie, L. Jin, G. Qiao, C. Lin, C. Barreneche, and Y. Ding. Thermal energy storage for electric vehicles at low temperatures: Concepts, systems, devices and materials. In: *Renewable and Sustainable Energy Reviews* 160 (2022), 112263. https://doi.org/10.1016/j.rser.2022.112263 (cited on page 10).

J. Yan, K. Zhang, C. Zhang, S. Chen, and G. Narasimhan. Automatic construction of 3-D building model from airborne LIDAR data through 2-D snake algorithm. In: *IEEE Transactions on Geoscience and Remote Sensing* 53 (2015), 3–14. https://doi.org/10.1109/TGRS.2014.2312393 (cited on page 57).

A. Yezioro and E. Shaviv. Shading: A design tool for analyzing mutual shading between buildings. In: *Solar Energy* 52.(1) (1994). Solar Buildings, 27–37. https://doi.org/10.1016/0038-092X(94)90078-G (cited on page 69).

M. Zhang. The Use and Value of Geographic Information Systems in Transportation Modeling. In: *International Encyclopedia of Transportation*. Edited by R. Vickerman. Oxford: Elsevier, 2021, 440–447. https://doi.org/10.1016/B978-0-08-102671-7.10364-1 (cited on page 14).

Z. Zhang, J. Wang, X. Feng, L. Chang, Y. Chen, and X. Wang. The solutions to electric vehicle air conditioning systems: A review. In: *Renewable and Sustainable Energy Reviews* 91 (2018), 443–463. https://doi.org/10.1016/J.RSER.2018.04.005 (cited on pages 7, 90).

Q. Zhou and U. Neumann. Fast and extensible building modeling from airborne LiDAR data. In: *GIS: Proceedings of the ACM International Symposium on Advances in Geographic Information Systems*. 2008, 43–50. https://doi.org/10.1145/1463434.1463444 (cited on page 57).